KINETICS AND MODELING OF FREE RADICAL AQUEOUS PHASE POLYMERIZATION OF ACRYLAMIDE WITH ACRYLIC ACID AT VARYING DEGREES OF IONIZATION

by

Calista Preusser

A thesis submitted to the Department of Chemical Engineering

In conformity with the requirements for

the degree of Doctor of Philosophy

Queen's University

Kingston, Ontario, Canada

(August, 2015)

Abstract

Water soluble polymers find applications in both consumer (e.g. superabsorbers in diapers, antiscalants in laundry detergent, and thickeners in shampoo) and industrial applications (e.g. antiscalants, antiflocculants and viscosity modulators in water treatment and oil drilling). Despite their industrial importance, the understanding of their kinetics have lagged behind their organic counterparts due to interaction of the monomer and polymer with the solvent, affecting the kinetics, and complicating experimental analysis such as molecular mass measurements. Additionally, the high viscosity of these systems at low monomer concentration (~5 wt%) make it difficult to take samples during polymerization reactions. Improved and specialized experimental techniques allow for the study and better understanding of these complex systems.

The work presented in this thesis focuses on the copolymerization of acrylic acid with acrylamide as a function of monomer concentration, monomer composition, temperature, and the degree of ionization of acrylic acid. Experimental monomer conversions and compositions were collected using an in-situ NMR technique developed and verified as part of this project. The in-situ NMR technique allowed for reliable data collection at monomer concentrations up to 40 wt%, covering a broader range of conditions than in previous literature, with reactivity ratios mapped over the complete range of monomer concentration and degree of ionization.

Successful modeling of the acrylamide homopolymerization included the backbiting mechanism using rate coefficients measured by our collaborators on this project and allowed for a comprehensive model valid for a range of temperatures and monomer concentrations for our and literature conversion profiles. Models of the acrylic acid and acrylamide copolymerization at non- and fully ionized conditions were also developed. However, insufficient knowledge of rate coefficients highlighted some gaps in our understanding of this copolymerization.

Acknowledgements

I would like to thank my supervisor, Robin A. Hutchinson, for his continued support and encouragement over the years. I would also like to thank him for all the amazing opportunities I have received as part of this PhD project, most notably working on this international project, spending 4 months in Slovakia, and sending me on conferences all around the world.

I would like to thank our collaborators Prof. Michael Buback, Nils Wittenberg, Hendrik Kattner, and Patrick Drawe in Göttingen (Germany), and Dr. Igor Lacík, Dr. Marek Stach, and Anna Chovancová in Bratislava (Slovakia), for their continued technical discussions, clarifying chemistry for me, and the unhindered data transfer. This work could not have been completed without the measurement of rate coefficients performed by these research groups. I am also delighted about the friendships formed that will extend past this collaboration.

I am grateful to BASF, Ludwigshafen, for their financial support, allowing this collaboration to exist. I also would like to thank Dr. Hugo Vale for being our project contact and organizing our monthly meetings facilitating the communication between the lab groups in addition to the valuable feedback and technical discussions.

I would like to thank my 4th year and summer students Danielle Austin and Otlaatla Monyatsi for helping me with the execution of the numerous experiments. In particular, I am grateful for Otlaatla who I can fully rely on, and who was able to run experiments for me while I was in Bratislava.

Lastly, I would also like to thank all my fellow lab and office mates, my friends, and my sister who have accompanied through this adventure; all the trivia nights, BBQs, Grad Club Fridays, going to concerts in Montreal and Toronto, visiting New York, Malaysia, and Thailand, more festivals, more beer, EuroCup, snowboarding and skating, sushi, all you can eat sushi, Amadeus when we had a big group, beer tasting events, cards against humanity, and of course Glühwein and the Nikolaus game.

Table of Contents

List of Figures

List of Tables

Nomenclature

Abbreviation	Description
AA	Acrylic acid
ACV	4,4’-azobis-4-cyanovaleric acid
AM	Acrylamide
BA	Butyl acrylate
BMA	Butyl methacrylate
D	Dead polymer chain
D_2O	Deuterium oxide
DiAA	Di-acrylic acid
DMAEA-Q	2-(acryloyloxyethyl)-trimethylammonium chloride
DNI	Direct numerical integration
EPR	Electron paramagnetic resonance
EVM	Error in variables method
FRP	Free radical polymerization
I	Initator
KPS	Potassium persulfate
M	Monomer
MAA	Methacrylic acid
MCR	Midchain radical
MMD	Molecular mass distributions
M_n	Molecular number weight average
M_w	Molecular weight average
MW	Molecular weight

NaCl	Sodium chloride
NaOH	Sodium hydroxide
NIR	Near infrared
NMR	Nuclear magnetic resonance
NOE	Nuclear Oberhauser effect
NVP	N-vinyl pyrrolidone
P	Polymer
PA	Propionic acid
pAA	Poly(acrylic acid)
pAM	Poly(acrylamide)
PLP	Pulsed laser polymerization
SCB	Short chain branching
SEC	Size exclusion chromatography
STY	Styrene
SP	Single pulse
SPR	Secondary propagating radical
V-50	2,2’-Azobis(2-methylpropionamidine)dihydrochloride
wt	Weight

Symbol	Units	Description
α	No units (fractional)	Degree of ionization
α_{ij}	No units (fractional)	Fraction of termination by disproportionation
f	No units (fractional)	Initiator efficiency
f_i	No units (fractional)	Monomer composition of monomer of species i
f_{i0}	No units (fractional)	Initial monomer concentration of monomer of species i
F_i^{inst}	No units (fractional)	Instantaneous copolymer composition
I	mol·L	Ionic strength
k_d	s^{-1}	Initiator decomposition rate coefficient
k_p	$L \cdot mol^{-1} \cdot s^{-1}$	Propagation rate coefficient of the secondary radical species
k_p^{cop}	$L \cdot mol^{-1} \cdot s^{-1}$	Copolymer propagation rate coefficient
k_t or $k_{t,ss}$	$L \cdot mol^{-1} \cdot s^{-1}$	Macroscopic termination rate coefficient
k_t^{cop}	$L \cdot mol^{-1} \cdot s^{-1}$	Copolymer termination rate coefficient
$k_{t,st}$	$L \cdot mol^{-1} \cdot s^{-1}$	Termination rate of secondary radical species with a midchain radical
$k_{t,tt}$	$L \cdot mol^{-1} \cdot s^{-1}$	Termination rate of two midchain radical species
k_{bb}	s^{-1}	Backbiting rate coefficient
$k_{p,tert}$	$L \cdot mol^{-1} \cdot s^{-1}$	Propagation rate coefficient of the midchain radical
k_{tr}	$L \cdot mol^{-1} \cdot s^{-1}$	Transfer to monomer rate coefficient
pK_a	No units	Dissociation coefficient
r_i	No units	Reactivity ratio of monomer species i
s_i	No units	Radical ratios
t	s	Time
w’	No units (fractional)	weight fraction
x	No units (fractional)	Molar monomer conversion

Chapter 1

Introduction

Synthetic polymers, often formed by free radical polymerization (FRP), are important products in our everyday lives, with a multitude of industrial and consumer applications. FRP offers fast rates of polymerization for most vinyl monomers over a wide temperature range.[1] Copolymerization of two or more different monomers offers a convenient method to create polymers with property characteristics between those of the corresponding homopolymers.

An important class of polymers is water soluble polymers, where both the starting monomer and the resulting polymer are soluble in water. Applications of these polymers include cosmetics (e.g. shampoos and hair gel), superabsorbers (e.g. diapers), and water treatment (e.g. laundry detergents and oil drilling).[2,3] Although water soluble polymers are omnipresent, understanding of the kinetics of these systems has somewhat lagged behind that of organic systems. One major difference in water soluble monomers, compared to their organic counterparts, is that rate coefficients, in addition to temperature, are often a function of monomer concentration and pH resulting from monomer-solvent interactions. With improved experimental laser techniques such as pulsed laser polymerization (PLP) reliable rate data can be collected when used in combination with size exclusion chromatography (SEC),[4,5] near infrared (NIR),[6] or electron paramagnetic resonance (EPR).[7,8] As a result, rate coefficients have been measured for water soluble monomers such as methacrylic acid (MAA),[9] acrylic acid (AA),[10] acrylamide (AM),[11,12] and N-vinylpyrrolidone (NVP).[13] For the homopolymerization of NVP[14] and MAA[15,16] these determined rate coefficients data have been used to develop mechanistic models that accurately predict conversion rate profiles and molecular weight for various initial monomer and initiator concentrations and temperature for both batch and semibatch operation. However, these systems are straightforward, in the sense that the kinetics are described by the standard radical

polymerization mechanism of initiation, propagation, termination, and chain transfer. It is now understood, as will be described in this thesis, that the kinetics of other important water soluble monomers such as AA and AM are further complicated by the formation of midchain radicals (MCR).

This work focuses on the free radical copolymerization of AA and AM in aqueous solution as a function of monomer composition, monomer concentration, degree of ionization of AA, and temperature. Experimental monomer conversions and compositions were collected using an in-situ NMR technique developed and verified as part of this project. The in-situ NMR technique allowed for reliable data collection at monomer concentrations up to 40 wt%, higher than previously studied in the scientific literature. The expanded experimental space has allowed for systematic observations of how monomer concentration and degree of ionization affects the drift in monomer composition with conversion. From this, a generalized representation for reactivity ratios varying with initial reaction conditions was developed, contributing to the understanding emerging from other recent work performed on the copolymerization of AM with charged monomers.

Relevant rate coefficients were measured as part of this ongoing collaboration by the groups of Prof. Buback (University of Göttingen) and Dr. Lacík (Polymer Institute of the Slovak Academy of Sciences) and incorporated in kinetic models developed using Predici to represent not only copolymer compositions, but also polymerization rates and polymer molecular weights. Models are presented for the AM homopolymerization, the copolymerization of non-ionized AA and AM, and the copolymerization of fully ionized AA and AM, with rate coefficients implemented as a function of monomer concentration and with the backbiting mechanism for both monomers included. The predictions of these models are compared to the experimental data set, and it is demonstrated that the observed trends of faster conversion profiles with increasing monomer concentration can only be explained by the occurrence of backbiting in the system. While our understanding of rate coefficients for the copolymerization is not yet completed, the model

developed for the AM homopolymerization is validated over a wide range of monomer concentrations and temperatures using both the batch data acquired using the in-situ NMR technique as well as other data reported in the literature.

Chapter 2

Literature Review

2.1 Mechanisms of Free Radical Homopolymerization

Water soluble polymers such as poly(acrylic acid) (pAA), poly(acrylamide) (pAM), poly(methacrylic acid), and poly(N-vinyl-pyrrolidone) are used in a variety of applications including cosmetics, water treatment, antiflocculants, pharmaceuticals, textiles, and paper processing.[2] These polymers are generally produced using FRP, with the basic reaction mechanisms summarized in Table 2.1. The subscripts n and m denote the chain length of the polymerizing chains, P, and the dead polymer chains, D. The initiator decomposes into two radical species with an efficiency, *f*, generally between 0.4 and 0.9.[1] A polymerizing chain is formed when an initiator radical initiates a monomer unit, forming a chain-end radical species and continues to propagate as denoted by the rate coefficient k_p. Two polymerizing chains can terminate, $k_{t,ss}$, by either forming one (termination by combination) or two (termination by disproportionation) polymer chains, where α_{ss} is the fraction of termination by disproportionation and $(1 - \alpha_{ss})$ is the fraction of termination by combination. The subscripts "ss" for the termination rate coefficients signify chain end radicals and in the case of AA and AM, these are secondary propagating radicals (SPR). Dead polymer chains can also be formed when a polymerizing chain abstracts a weakly bonded hydrogen from a monomer unit (k_{tr}). In our work it is assumed that transfer to solvent (water) is negligible.

Table 2.1 Mechanisms of free radical polymerization.[1]

Initiator Decomposition	$\mathrm{I} \xrightarrow{k_\mathrm{d}} 2f\mathrm{I}^{\mathrm{rad}}$
Chain Initiation	$\mathrm{I}^{\mathrm{rad}} + \mathrm{M} \xrightarrow{k_\mathrm{p}} \mathrm{P}_1$
Chain Propagation	$\mathrm{P}_\mathrm{n} + \mathrm{M} \xrightarrow{k_\mathrm{p}} \mathrm{P}_{\mathrm{n+1}}$
Chain Termination	
By Combination	$\mathrm{P}_\mathrm{n} + \mathrm{P}_\mathrm{m} \xrightarrow{(1-\alpha_{\mathrm{ss}})k_{\mathrm{t,ss}}} \mathrm{D}_{\mathrm{n+m}}$
By Disproportionation	$\mathrm{P}_\mathrm{n} + \mathrm{P}_\mathrm{m} \xrightarrow{\alpha_{\mathrm{ss}}k_{\mathrm{t,ss}}} \mathrm{D}_\mathrm{n} + \mathrm{D}_\mathrm{m}$
Chain Transfer	
To Monomer	$\mathrm{P}_\mathrm{n} + \mathrm{M} \xrightarrow{k_\mathrm{tr}} \mathrm{D}_\mathrm{n} + \mathrm{P}_1$

These mechanisms can be used to form an expression for the rate of monomer consumption in a constant volume batch reactor by applying the quasi-steady-state-hypothesis on the total radical concentration:

$$R_p = -\frac{d[\mathrm{M}]}{dt} = k_\mathrm{p}[\mathrm{M}]\left(\frac{2fk_\mathrm{d}[\mathrm{I}]}{k_{\mathrm{t,ss}}}\right)^{1/2} \qquad 2.1$$

Substituting in the definition of monomer conversion $[\mathrm{M}]=[\mathrm{M}]_0(1-x)$, with $[\mathrm{M}]_0$ being the initial monomer concentration and x the conversion, the rate of conversion is:

$$\frac{dx}{dt} = k_\mathrm{p}(1-x)\left(\frac{2fk_\mathrm{d}[\mathrm{I}]}{k_{\mathrm{t,ss}}}\right)^{1/2} \qquad 2.2$$

It can be observed from Equation 2.2 that the monomer concentration should have no effect on the rate of conversion. While this has been observed for monomers in organic solvents in the absence of complicating side reactions,[17] this relationship seldom holds for water soluble systems such as MAA,[15] AA,[18] AM,[19,20] and NVP.[14] In all of these cases, the initial rate of conversion is affected by the monomer concentration, as the rate coefficients for many of the reactions steps

in aqueous solution, in particular k_p and $k_{t,ss}$, show a dependency on monomer concentration and degree of ionization, or pH. Thus, the rate coefficients in Table 2.1 become functions of these variables, as will be discussed in more detail later in this chapter. For NVP[14] and MAA[15,16] the deviations in behavior from Equation 2.2 – an increased rate of conversion with decreasing monomer concentration – were successfully modeled with rate coefficients implemented as a function of monomer concentration, based upon the measurements made by specialized pulsed-laser kinetic experiments that demonstrate that both the propagation and termination rate coefficients decrease with increasing monomer concentration.

In contrast to NVP and MAA, for the batch homopolymerizations of both AA and AM an increase in the conversion rates with increasing monomer concentration is observed.[18,19,21–24] As this finding is contrary to the trends observed in the propagation and termination rate coefficients, additional mechanisms must be influencing the rate. For AA this increase in the conversion rate with increasing monomer concentration has recently been modeled by implementing backbiting into the kinetic scheme, based on numerous independent experimental observations.[21] As documented in this thesis, it is now understood that backbiting plays an important role in the polymerization of AM, as well.[25]

The concept of intramolecular chain transfer, or backbiting, was first introduced in 1953 by Roedel[26] to explain changes in the physical properties of poly(ethylene) with synthesis temperature. It is now well-known that the mechanism is also important for acrylates.[27] The associated reaction steps relating to backbiting are summarized in Table 2.2. Midchain radicals (MCR) are formed when the chain-end propagating radical (denoted as SPR, for secondary propagating radical) curls back on itself to form a cyclic structure, generally a 6-membered ring, and abstracts a hydrogen atom from the polymer backbone (with rate coefficient k_{bb}).[8,26,27] A monomer unit can add to the MCR with a rate coefficient of $k_{p,tert}$. Since the MCR is less reactive than the SPR, the rate coefficient $k_{p,tert}$ is much lower than k_p, such that from a kinetic standpoint

the MCR can be regarded as a radical sink and can therefore be easily observed with EPR.[27] The midchain radical can also undergo termination reactions with another MCR, $k_{t,tt}$, or with an SPR, $k_{t,st}$. The fraction of termination by combination and disproportionation is represented by $(1 - \alpha_{st})$ or $(1 - \alpha_{tt})$ and α_{st} or α_{tt}, respectively.

Table 2.2 Mechanisms associated with backbiting reactions.[8]

Backbiting	$P_n \xrightarrow{k_{bb}} MCR_n$
Propagation of MCR	$MCR_n + M \xrightarrow{k_{p,tert}} P_{n+1}$
Chain Termination	
Cross termination of SPR and MCR	
	$MCR_n + P_m \xrightarrow{(1-\alpha_{st})k_{t,st}} D_{n+m} / \xrightarrow{\alpha_{st}k_{t,st}} D_n + D_m$
Termination of 2 MCRs	
	$MCR_n + MCR_m \xrightarrow{(1-\alpha_{tt})k_{t,tt}} D_{n+m} / \xrightarrow{\alpha_{tt}k_{t,tt}} D_n + D_m$

2.1.1 Discussion of the Propagation Rate Coefficients of AA and AM

Experimental pulsed-laser polymerization (PLP)[4,28] techniques have been applied to obtain reliable estimates of FRP rate coefficients in aqueous solution that are difficult to extract from conventional continuously-initiated reactions. Propagation rate coefficients, k_p, are estimated with PLP coupled with off-line measurement of polymer molecular weights (typically by SEC) to measure the chain growth that has occurred during the dark periods between the laser pulses.[5] As discussed in the previous section, the propagation rate coefficients of water soluble monomers are often a function of monomer concentration as measured with PLP-SEC for monomers including AA,[10,29,30] AM,[11,12,31] MAA [32–34] and NVP.[13] In Figure 2.1 the k_p of AA and AM are plotted at 40 °C as a function of monomer concentration in aqueous solution from 3 to 40 wt%. AA exhibits

a more pronounced effect of monomer concentration, with k_p decreasing by a factor of 2.6 between 5 to 40 wt%, while the propagation of AM decreases by a factor of 1.7 in the same monomer concentration range. This decrease in k_p with increasing monomer concentration has been attributed to the influence of competitive hydrogen bonding between the reacting monomer unit and side groups of the monomer and the solvent on the transition state.[10,33–36] When the effect of solvent is studied, it is observed that the k_p in solvents less polar than water are closer to the bulk monomer values for both AA[36] and AM.[35] Not only are AA and AM more soluble in water, but the hydrogen bonding between the monomer and water lowers the energy in the transition state structure for the monomer addition to the radical, making the reaction proceed more quickly as confirmed by theoretical studies.[37,38] Experimental studies in which AA was polymerized in the presence of its saturated analogue, propionic acid, showed a decrease in k_p similar to that with only AA present,[10] which further supports the theory that hydrogen bonding is the culprit for the decrease in k_p with increasing monomer concentration. For AA, it was postulated that the presence of dimers influenced k_p; however, modeling of these systems indicated that the presence of dimer alone could not explain the decrease in k_p with increasing monomer concentration.[10]

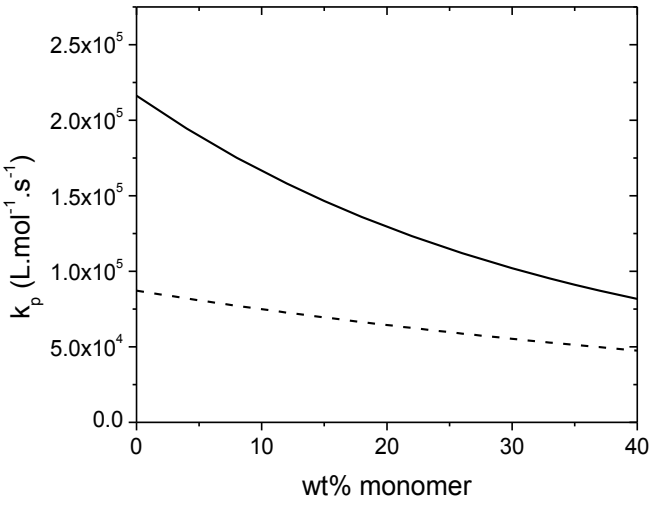

Figure 2.1 Comparison of the chain-end propagation rate coefficient of AA (solid line)[10] and AM (dashed line)[12] as a function of monomer concentration at 40 °C, as measured by PLP-SEC.

In order to provide reliable estimates of rate coefficients at known (controlled) monomer concentrations, PLP-SEC experiments are run only to low conversion. Since the propagation rate coefficient is a function of monomer concentration, the effect of monomer conversion has been studied for MAA[33] and NVP[13] by introducing a specified amount of given homopolymer with known molecular weight into the system and then running the reaction such that the conversion of the monomer is kept low in order to maintain the validity of the PLP-SEC analysis. It was observed that the presence of polymer has little effect on k_p and as a result the propagation rate coefficient will change with monomer conversion. This effect was successfully modeled for MAA[15,16] and NVP.[14] Analogous studies for AA and AM have not been completed to date and it is assumed that AA and AM behave the same way as MAA and NVP with conversion.

The degree of ionization can also affect the polymerization kinetics of acidic water soluble monomers such as AA[29] and MAA,[34,39] for which the hydroxyl group is easily ionizable with the addition of a strong base. In contrast, the rate coefficients for AM[12] and NVP[13] remain unchanged

(within experimental error) with pH. The pH of the acidic systems can be determined by the Henderson-Hasselbalch equation:

$$\mathrm{pH} = \mathrm{p}K_\mathrm{a} + \log\left(\frac{[\mathrm{A}^-]}{[\mathrm{HA}]}\right) \qquad 2.3$$

Here pK_a is the dissociation coefficient for the acid, $[\mathrm{A}^-]$ is the concentration of ionized molecules and [HA] is the concentration of non-ionized molecules. A more useful parameter to define is the degree of ionization, α, which is defined as:

$$\alpha = \frac{[\mathrm{A}^-]}{[\mathrm{HA}] + [\mathrm{A}^-]} \qquad 2.4$$

For weak acids such as AA and MAA one can assume that all of the molecules are ionized with addition of a strong base such as NaOH and thus the degree of ionization can be rewritten as:

$$\alpha = \frac{[\mathrm{NaOH}]}{[\mathrm{AA}]} \qquad 2.5$$

where [AA] is the concentration of AA before the addition of NaOH. By definition, the degree of ionization is bounded from 0 to 1. For AA, k_p decreases by a factor of 10 as α increases from 0 to 1, as illustrated in Figure 2.2 for 6 ºC and 5 to 6 wt% monomer concentration. A broader range of conditions has been studied for MAA as shown in Figure 2.3. A diminished effect of monomer concentration is experienced with increasing degree of ionization. The same is believed to be true for AA concentration, with further experimental verification ongoing in Bratislava.

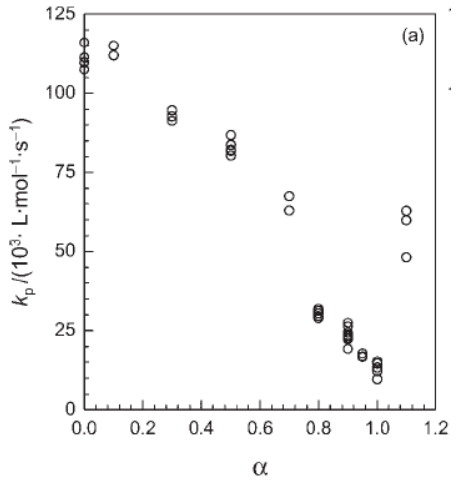

Figure 2.2 Propagation rate coefficient of AA, k_p^{AA}, as a function of degree of ionization, α, for [AA] = 0.69 mol·L^{-1} (~5 wt%) and 6 °C.[29] **Reprinted with permission from Macromolecules. Copyright 2009 American Chemical Society.**

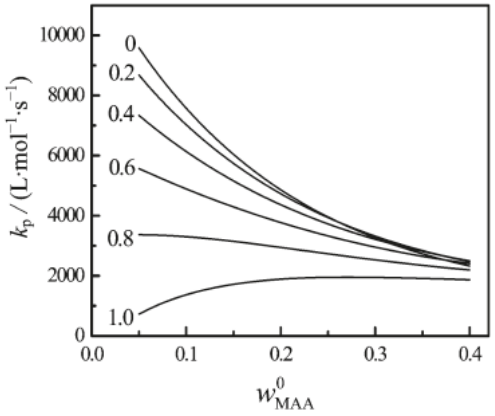

Figure 2.3 Effect of monomer weight fraction in aqueous solution and degree of ionization (labeled in the graph) on the propagation rate coefficient at 50 °C for MAA.[34] **Reprinted with permission from Macromolecular Chemistry and Physics. Copyright 2004, Wiley-VCH Verlag GmbH & Co. KGaA.**

Although the influence of backbiting in the polymerization of secondary radicals such as AA,[7,8,21] AM,[25] and butyl acrylate (BA)[40] complicates their study, it is still possible to measure the rate coefficients associated with backbiting using single pulse-PLP-EPR (SP-PLP-EPR) as well as PLP-SEC with varying frequency.[25,41,42] Supported by experimental data, backbiting is assumed

to be independent of monomer concentration as it is a unimolecular reaction, while the rate coefficient for the addition to the MCR is assumed to be a function of monomer concentration and implemented as $k_{p,tert}/k_p$.[21]

Figure 2.4 compares the backbiting rate coefficients for AA and AM, which controls the level of short chain branches (SCB) found in the system according to the competition between backbiting and chain growth:[43]

$$\% \text{ SCB} = \frac{k_{bb}}{k_p[\text{M}] + k_{bb}} * 100\ \% \qquad 2.6$$

Equation 2.6 highlights the relative effect of monomer concentration on the branching levels. A systematic study on the branching levels as a function of temperature and monomer concentration of AA homopolymerization confirmed this relationship using ^{13}C NMR measurements.[21] Branching levels are influenced by adjusting monomer concentration and temperature, with branching levels dropping from 1.1 to 0.6 % as the monomer concentration was increased from 10 to 20 wt% at 70 ^{o}C.[21] For AM, the low backbiting rate coefficient leads to branching levels below the detection limit of ^{13}C NMR, even for polymerizations run at 90 ^{o}C.

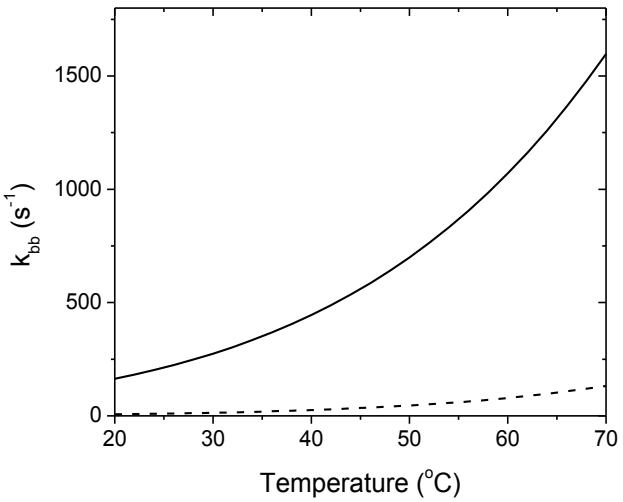

Figure 2.4 The backbiting rate coefficient, k_{bb}, for AA[21] (solid line) and AM[25] (dashed line) plotted as a function of temperature.

2.1.2 Discussion of the Termination Rate Coefficient of AA and AM

Similar to the propagation rate coefficients, the termination rate coefficients are a function of monomer concentration and pH, as studied using SP-PLP-EPR[7,8] and SP-PLP-NIR.[6] The termination rate coefficients are a function of initial monomer concentration, decreasing by a factor of 6.5 from 10 to 50 wt% monomer in aqueous solution for non-ionized AA. This variation is similar to that reported for NVP[44] which decreases by a factor of 5 between 20 wt% and bulk. The termination rate coefficient for AM was measured at the University of Göttingen as part of this collaboration and it was found that there is a decrease by a factor of 1.4 in $k_{t,ss}$ from 25 to 45 wt%.[25]

2.2 Copolymerization of AA and AM

Copolymerization reactions are commonly performed in order to obtain properties intermediate between those of the two homopolymers. The copolymerization mechanism now must consider cross- rate coefficients. Four potential propagation steps for the copolymerization of AA and AM are outlined in Table 2.3.

Table 2.3 Propagation steps defined by the terminal model.[45]

$P_n^{AA} + AA \xrightarrow{k_p^{AA}} P_{n+1}^{AA}$
$P_n^{AA} + AM \xrightarrow{k_p^{AA\cdot AM}} P_{n+1}^{AM}$
$P_n^{AM} + AM \xrightarrow{k_p^{AM}} P_{n+1}^{AM}$
$P_n^{AM} + AA \xrightarrow{k_p^{AM\cdot AA}} P_{n+1}^{AA}$

Using these four propagation steps, the instantaneous copolymer composition is described by the Mayo-Lewis equation, or, terminal model,[45] as written in terms of AM copolymer composition for the AA/AM copolymerization:

$$F_{AM} = \frac{r_{\mathrm{AM}} f_{\mathrm{AM}}^2 + f_{\mathrm{AM}} f_{\mathrm{AA}}}{r_{\mathrm{AM}} f_{\mathrm{AM}}^2 + 2 f_{\mathrm{AM}} f_{\mathrm{AA}} + r_{\mathrm{AA}} f_{\mathrm{AA}}^2} \quad 2.7$$

where f_{AM} refers to the monomer composition, given by f_{AM}=[AM]/([AM]+[AA]) with $f_{\mathrm{AA}} = 1 - f_{\mathrm{AM}}$, and $r_{\mathrm{AA}}=k_p^{\mathrm{AA}}/k_p^{\mathrm{AA\cdot AM}}$ and $r_{\mathrm{AM}}=k_p^{\mathrm{AM}}/k_p^{\mathrm{AM\cdot AA}}$ are the reactivity ratios. More complex copolymerization models exist in the literature, but for the copolymerization of AA and AM the terminal model has successfully been used to describe copolymer composition.[36,46–48]

The general methodology to determine reactivity ratios in the literature is to run experiments at different monomer compositions to low conversion (less than 10 % conversion) and determine the resulting copolymer composition.[36,46,47] With online measurements and an increase in computing power over the years, it is becoming more commonplace to collect monomer or copolymer composition data over a range of conversions.[23,48–52] Reactivity ratios are estimated from Equation 2.7 using different parameter estimation methods, including the Kelen-Tüdös method,[46] an integrated form of the Mayo-Lewis equation,[53] or by evaluating the differential change in monomer composition with conversion.[23,48–52] By evaluating the monomer composition drift with a direct numerical integration method (DNI), the error structure can be significantly reduced relative to other methods for determining reactivity ratios.[54]

Online measurements are advantageous as monomer composition can be tracked as a function of conversion over the entire course of the experiment. To estimate reactivity ratios from such a data set at least two methods can be employed: the Meyer-Lowry method[55] and direct numerical integration.[54]

The Meyer-Lowry model is the integrated form of the terminal model, written here in terms of monomer AM:

$$x = \left(\frac{f_{\mathrm{AM}}}{f_{\mathrm{AM0}}}\right)^{\alpha} \left(\frac{f_{\mathrm{AA}}}{f_{AA0}}\right)^{\beta} \left(\frac{f_{\mathrm{AM0}} - \delta}{f_{AM} - \delta}\right)^{\gamma} \quad 2.8$$

with $\alpha = r_{\mathrm{AA}}/(1\text{-}r_{\mathrm{AA}})$, $\beta = r_{\mathrm{AM}}/(1\text{-}r_{\mathrm{AM}})$, $\gamma = (1\text{-}r_{\mathrm{AA}}r_{\mathrm{AM}})/(1\text{-}r_{\mathrm{AM}})(1\text{-}r_{\mathrm{AA}})$, $\delta = (1\text{-}r_{\mathrm{AA}})/(2\text{-}r_{\mathrm{AA}}\text{-}r_{\mathrm{AM}})$.[55] Certain conditions, such as $r_{\mathrm{AA}} \neq 1$, $r_{\mathrm{AM}} \neq 1$, $r_{\mathrm{AA}} + r_{\mathrm{AM}} \neq 2$, must be met, which leads to restrictions

and instability of this equation. An alternate method of solving for the reactivity ratios is to use a differential form of the terminal model which has the following form in terms of AM:

$$\frac{df_{\mathrm{AM}}}{dx} = \frac{f_{\mathrm{AM}} - F_{\mathrm{AM}}}{1 - x} \qquad 2.9$$

The copolymer composition F_{AM} is defined as in equation 2.7 with initial condition $f_{\mathrm{AM}} = f_{\mathrm{AM0}}$ at $x = 0$. Although this method is more computationally intensive, no transformations are necessary and the error structure is somewhat reduced compared to the Meyer-Lowry model.[54]

The reactivity ratios for the AA/AM copolymerization determined in the literature are quite scattered, as illustrated by Figure 2.5.[36,46–48,50,53] Overall it was found from experiments run at low monomer concentration (4 wt% monomer or less) that the reactivity ratios are a function of the system pH, with the change in reactivity ratios being reflective of the change in the propagation rate coefficient of AA.[46] Similar observations were made for the copolymerization of AM and MAA at different pH values.[36,53] The solvent effect extends to the copolymerization system and different reactivity ratios are calculated in different solvents.[36] Thus, as with the homopolymerization of AA, the copolymerization is affected by the reaction environment.

From the literature data as a whole it is difficult to extract which reactivity ratios are reliable (Figure 2.5). Error is introduced by examining different monomer composition ranges; work explicitly utilizing the Tidwell-Mortimer criterion where only two "optimal" monomer compositions are determined (f_{AM0} = 0.1 and 0.46 for the AA/AM copolymerization)[50,51] or other work looking at only two monomer compositions (f_{AM0} = 0.5 and 0.7)[48] may not provide a reliable range of monomer compositions to accurately describe the copolymerization as a whole. In the latest publication by Rianhizhad et al., where the Tidwell-Mortimer criterion is always used to determine the two monomer compositions studied, the "optimal" monomer compositions are re-evaluated, leading to new monomer compositions used in the reactivity ratio estimation and yielding new and different reactivity ratios, even with the new "optimal" conditions generally being f_{AM0} = 0.5.[52] As will be shown in a subsequent chapter (Chapter 6), the range of monomer

compositions used to estimate reactivity ratios greatly influences the estimated reactivity ratios and therefore their accuracy in predicting monomer composition drift with conversion.

For ionized conditions, an effect of the monomer concentration on the reactivity ratios is also evident,[51,52] contributing to the scatter in the reported reactivity ratios. Generally, monomer concentration is not considered an important variable and therefore is only recently being considered by other research groups. Monomer concentration has always been an important variable in our work, resulting in its incorporation in the experimental design for all degrees of ionization studied in this work.[23]

In recent years the effect of the ionic strength – i.e., the total concentration of charged species – on copolymer composition has been examined as a variable manipulated separately from the comonomer composition.[49,51] This interest developed as a result of Losada and Wandrey's 2009 paper that reported a systematic variation in the reactivity ratios with monomer concentration for the copolymerization of AM with 1,3-bis(*N*,*N*,*N*-trimethylammonium)-2-propylmethacrylate dichloride, a monomer holding two permanent charges.[56] This effect of monomer concentration and ionic strength was also observed in the copolymerization of AM with 2-(acryloyloxyethyl)-trimethylammonium chloride (DMAEA-Q), a cationic monomer with one permanent charge.[57] Therefore, it is not surprising that the same is observed for the copolymerization of AM with AA, with the added complexity that AA can be partially ionized.

Paril et al. ran experiments for the AA/AM system at two ionic strengths at a degree of ionization of 0.2, and keeping the ionic strength constant by varying the monomer concentration and composition.[49] The estimated reactivity ratios were different for the two ionic strengths considered leading to the conclusion that the ionic strength has an effect on the reactivity ratios,[49] although it should be noted that other effects such as the total monomer concentration were not considered. In contrast, Riahinezhad et al.[51] studied the effect of ionic strength by adding sodium chloride salt (NaCl) to fully ionized AA and AM copolymerization. The incorporation of charged

AA was found to increase with the addition of salt, supporting the idea that a higher concentration of ionic species will screen the negative charges, making it easier for AA to incorporate into the polymerizing chain. The conversion rates also seem to be very strongly affected by the monomer composition even at high salt concentrations (1.288 $mol \cdot L^{-1}$).[51] For experiments run at the same initial monomer composition, the added salt led to an increase in the monomer conversion rate.[51] For fully ionized AA an increase in the polymerization rate was observed as excess salt was added,[22] the same behavior as was observed for the copolymerization of fully ionized AA and AM.

The work presented for this PhD thesis expands the range of conditions examined experimentally in previous literature, systematically examining the effect of ionic strength and monomer concentration on the reactivity ratios at different degrees of ionization. Overall we find that the change in the reactivity ratios is not a function of the ionic strength alone, but rather a function of the degree of ionization of the AA and the overall monomer concentration.

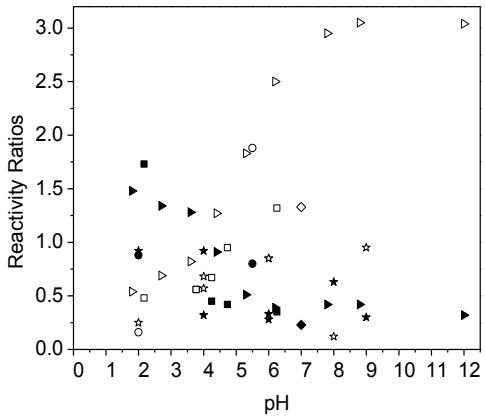

Figure 2.5 Reactivity ratios for r_{AA} (full symbols) and r_{AM} (empty symbols) as a function of pH from (▲,△)[36], (▶,▷)[46], (■,□)[47], (●,○)[48], (★,☆)[53], (♦,◊).[50]

2.3 Modeling Work of Water Soluble Polymerizations to Date in the Literature

Recently a full kinetic model for the AA homopolymerization including rate coefficients that are functions of monomer concentrations and backbiting was developed and published as part of this collaboration.[21] The resulting model is valid for a range of monomer concentrations and temperatures and forms the basis for the AA rate coefficients used in this work. The model presented in the paper also considers the addition of chain transfer agent, which affects the molecular mass of the resulting polymer.

Prior to the AA model developed by Wittenberg et al.,[21] a model for semi-batch homopolymerization of AA was developed in 2011 by Minari et al.[58] As reliable data for the termination and backbiting rate coefficients were not available at the time of this publication, these rate coefficients were estimated using an optimization routine.[58] Comparing the values to k_{bb} and $k_{p,tert}$, the estimated values are in reasonable agreement with the coefficients measured by Barth for 10 wt% AA.[8] This model however did not introduce a k_p dependency on temperature or monomer concentration as it is assumed that the concentration is kept sufficiently low at 2 wt% monomer in water during semi-batch operation and the temperature remains at 60 ºC for all experiments; in addition, a single termination rate coefficient was used to describe termination involving both MCR and SPR species.[58]

Models to represent the homopolymerization of AM had also been developed in the literature prior to the model presented as part of this thesis. Difficulties arose in trying to represent the influence of monomer concentration on the rate of AM polymerization, as reaction orders between 1.24 to 1.49 were found experimentally,[19,20,59,60] greater than the expected value of 1. The higher reaction order was first described in terms of the cage effect on initiation[19] and later the rate coefficients k_p and k_t were thought to be diffusion controlled.[24,61] Although these models did not represent k_p as a function of monomer concentration, the efforts were successful in describing individual data sets,[19,24] but were unable to provide a consistent representation of the complete set

of available experimental data. For example, with the cage effect implemented into the reaction scheme, the resulting model was able to predict a reaction order between 1.0 and 1.5 dependent on the initial monomer concentration to fit experimental conversion data collected between 2 and 16 wt% AM,[19] but a single model was not able to successfully simulate the conversion profiles between 5 and 24 wt% AM.[24] The model developed and presented in Chapter 4 includes rate coefficients as a function of monomer concentration and includes the backbiting mechanism, creating a model that is valid over a range of temperatures and monomer concentrations, and can successfully model the conversion profiles in the published literature.

No attempts have been made in the literature to model conversion profiles of the copolymerization of AA and AM. Rintoul and Wandrey developed a representation of reactivity ratios as a function of pH[62] by treating the system as a terpolymerization of non-ionized AA, ionized AA, and AM. The reactivity ratios were predicted reasonably well, and took the differences in the pK_a between the monomer and the polymer into account, where the equilibrium is shifted towards AA units in the monomer phase being more charged relative to the polymer chain.[29,34]

As mentioned previously, modeling of the water soluble systems has been successfully completed for batch and semibatch polymerization of NVP,[14] non-ionized MAA,[15,16] and, most recently, non-ionized AA[21,58] by accounting for the dependency of rate coefficients on monomer concentration and conversion. The goal of this work is to extend this methodology to the copolymerization of AA and AM. As backbiting is observed for both of the AA and AM systems, these side reactions are also incorporated in the model. It is worth noting that, to the best of my knowledge, this is the first time that these side reactions have been modeled for a system where both monomers undergo backbiting.

Chapter 3

An In-Situ NMR Study of Free Radical Copolymerization Kinetics of Acrylamide and Non-Ionized Acrylic Acid in Aqueous Solution

This chapter was published in Macromolecular Symposia, **2013**, 333, 122 – 137. The formatting was edited to match that of the thesis.

3.1 Summary

An in-situ NMR technique has been developed to study the aqueous phase copolymerization of non-ionized acrylic acid (AA) and acrylamide (AM) under near-isothermal conditions at much higher monomer contents than previously reported in the literature. The composition data obtained over the entire conversion range provides a precise estimate of monomer reactivity ratios not available from low conversion data. The set of experiments, with initial monomer content in aqueous solution varied between 5 and 40%, were well-fit over the complete conversion range by $r_{AA} = 1.24 \pm 0.02$, and $r_{AM} = 0.55 \pm 0.01$. It was found that the rate of monomer conversion increases with increasing monomer concentration, a trend contrary to the known decrease in the AA and AM chain-end propagation rate coefficients.

3.2 Introduction

Water soluble polymers are an important family of products with diverse applications in personal-care (e.g., thickening agents for shampoos, hair gel, and other cosmetics, anti-flocculants in laundry detergents) and industrial (e.g., water treatment facilities, antiscalants in oil drilling) markets. Despite their commercial importance, the kinetics of these radical polymerizations are still not well understood. This paper will discuss the copolymerization of acrylic acid (AA) and acrylamide (AM) using an in-situ NMR technique at various monomer concentrations and

monomer compositions, with the goal of improving the understanding of this complex system over a broader range of operating conditions.

Experimental pulsed-laser polymerization (PLP)[4,28] techniques have been applied to obtain reliable estimates of rate coefficients difficult to extract from conventional continuously-initiated reactions for radical polymerization in aqueous solution. Propagation rate coefficients, k_p, are estimated using PLP in combination with size exclusion chromatography (SEC) to measure chain growth that occurs during the dark periods between the laser pulses.[5] The PLP-SEC technique has been applied to the study of water soluble monomers including AA,[10,29,30] AM,[11,12,31] methacrylic acid (MAA)[32–34] and N-vinylpyrrolidone (NVP).[13] For all systems, the value of k_p increases as the monomer concentration is lowered, a result attributed to the reduced barrier to rotational motion in the transition state structure upon replacing monomer units with H_2O.[10,13,32,35] These theories have been confirmed by computational studies for AA[37] and AM.[38]

Similar to k_p, the termination rate coefficients, k_t, of AA,[8] NVP[44] and MAA[6,63] exhibit a dependency on the initial monomer concentration even at low conversion in aqueous solution, as measured using single pulse-PLP-electron paramagnetic resonance (SP-PLP-EPR)[8] and SP-PLP-near-infrared spectroscopy (NIR).[6] Studies with NVP[14] and MAA[15] demonstrate that conversion profiles and molecular-weight data from continuously-initiated batch and semibatch polymerizations are well-represented using the concentration-dependent k_t and k_p values measured using PLP techniques. The modeling work for the MAA system has recently been extended to include the chain-length dependence of k_t measured using the SP-PLP-EPR technique,[63] which is especially important for systems with high levels of added chain-transfer agent.[16]

Intramolecular transfer to polymer, also referred to as backbiting, is a major side reaction that occurs during the polymerization of acrylates such as butyl acrylate (BA),[40] and also AA in aqueous solution.[8] Backbiting reactions occur when the polymerizing chain end curls back on itself to form a six-membered ring and abstracts a hydrogen atom from the polymer backbone with

rate coefficient k_{bb}. A short-chain branch is formed when a monomer unit adds to the resulting midchain radical; as the rate coefficient for this monomer addition, $k_{p,tert}$, is significantly smaller than $k_{p,}$ the formation of midchain radicals leads to a reduction in the overall rate of conversion. The net effect of backbiting is an apparent reaction order of greater than unity when the variation of overall polymerization rate with respect to monomer concentration is examined. The rate coefficients for the backbiting reactions have been measured using SP-PLP-EPR[7,8,40] as well as PLP-SEC with varying frequency.[41] For AA k_{bb} and $k_{p,tert}$ are also a function of monomer concentration, decreasing as monomer concentration in aqueous solution increases in a similar manner to k_p.[40]

The ultimate objective of this work is to develop an understanding of the copolymerization of AA and AM over a broad range of reaction conditions utilizing the rate coefficients measured using PLP techniques. In order to attain this goal, polymerization behavior at monomer concentrations higher than currently published in the literature are investigated. Conventional experimental methods using batch reactors that require mixing and sample collection are problematic, as the solution viscosity even at low monomer concentrations (~7 wt%) increases rapidly with monomer conversion.[19] Therefore the monomer concentrations in the literature are maintained below 5 wt% as a rule[20,64,65] to ensure good mixing of the reaction solution and isothermal operation. Limited data for AM homopolymerization is available to a maximum of 20 wt%,[19,24] and for AA a maximum of 30 wt% has been studied.[18] For AA/AM copolymerization, however, the monomer concentrations investigated are much lower, at less than 4 wt%.[46–48] Significantly higher monomer contents are utilized in industrial copolymerization to increase reactor productivity. At these higher concentrations, the variation of k_p with concentration, as well as the possible variation of diffusion-controlled k_t with conversion, may lead to rates of polymerization and comonomer incorporation that differ from behavior observed at low monomer concentration.

Several experimental methods of tracking monomer conversion on-line have been applied to water soluble polymerizations, including near-IR spectroscopy,[15,16] light scattering,[48,65] and NMR.[18,20,66] Due to the experimental constraints, namely the high monomer concentration, a method which requires a larger reaction volume and therefore mechanical mixing was not considered. The advantage of the in-situ NMR method is that monomer composition can be tracked in addition to the overall monomer conversion. In the literature in-situ NMR experiments for AA and AM homopolymerizations were successfully reported,[18,20,66] and these studies form the basis of the technique applied to AA/AM copolymerization. The group of Mahdavian has studied AM homopolymerization in aqueous solution[20] as well as various copolymerization in organic solution.[67–70] Three criteria for running in-situ NMR experiments were reported:[20] 1) a reaction rate that is less than the scanning rate, 2) solubility of the polymer in the solvent, and 3) distinguishable monomer/ polymer peaks so that monomer composition and conversion can be determined. A fourth criterion, namely that isothermal conditions are maintained, should be added. As will be shown, these criteria are fulfilled for the copolymerization of AA and AM.

In this work, experimental procedures have been developed to study the isothermal batch copolymerization of non-ionized AA and AM. Monomer conversion profiles are presented from a set of experiments completed at 40 °C over a broad range of monomer concentrations and comonomer compositions. The data collected are used to estimate reactivity ratios and to develop an improved mechanistic understanding of the system.

3.3 Experimental Section

The monomers acrylic acid (99%, Sigma Aldrich) and electrophoresis grade acrylamide (99+%, Sigma Aldrich) were used as received. Deuterated water (D_2O) (99.9%, Cambridge Isotope Laboratories Inc.) and 2,2-azobis(2-methylpropionamidine)dihydrochloride (V-50) (97%, Sigma Aldrich) were also used as is. Poly(acrylic acid) (pAA) (Sigma Aldrich) at an average molecular

weight of 1800 $g \cdot mol^{-1}$ was purchased and used without purification for development of the NMR procedures.

Stock solutions of monomer and initiator were prepared separately ahead of time, with the initiator stock solution of 4 wt% V-50 in D_2O made fresh weekly. The solutions were mixed at the appropriate ratios on the day of the experiment to the desired total monomer concentration and composition. The solutions were purged with nitrogen for 15 minutes to ensure complete mixing and solvation of the monomer in the D_2O, transferred to labeled NMR tubes and stored under refrigeration until polymerization. It was difficult to fully isolate the reaction mixture from air when transferring the solution to the 5 mm NMR tubes. However, a study by Cutié et al.[66] showed that while purging with nitrogen for the AA system reduces the inhibition time, it does not have an effect on the shape of the monomer conversion profile. Since the reaction mixture sits in the NMR machine for at least 4 minutes before the first scan is taken, an inhibition time is vital in order to ensure that a complete conversion profile is obtained. The inhibition times at 40 °C are between 15 minutes and 1 hour, depending on the AA content in the reaction mixture. The start time of the experiment is calculated by fitting the linear portion of the conversion profile and solving for the x-intercept.

The polymerizations are conducted using a Bruker 500 with TopSpin as the interface and a BVT3000 heating element. The NMR sample chamber is first increased to 40 °C using a flow rate of heated air of 535 $L \cdot h^{-1}$, and allowed to equilibrate for 20 minutes. The NMR tube containing the reaction mixture is then placed into the machine and allowed to heat for 4 minutes, at which time the instrument is shimmed and tuned to reduce the signal to noise ratio and obtain sharp peaks. Since peak positions and peak quality are temperature sensitive, it is necessary to perform the tuning and shimming when the reaction mixture has reached the reaction temperature. No changes are made to the standard ^1H NMR settings on the spectrometer (3.17 s acquisition time, 1 s relaxation delay, 6 μs dead time, 48.4 μs dwell time). Subsequent analysis showed good agreement

between measured NMR monomer composition and conversion with values determined by alternate laboratory methods, indicating sufficient relaxation times. The first scan is taken approximately eight minutes after insertion of the NMR tube, and subsequent scans every two minutes afterwards until full conversion, with the total number of spectra collected ranging between 40 and 80.

3.4 Data Analysis

The NMR spectra were processed using the NMR software MestReNova 6.0. The spectra used for the following discussion were taken from a representative non-ionized experiment run at 40 ºC with an initial AA monomer mole fraction (f_{AA0}) of 0.7, 20 wt% monomer and 0.217 wt% V-50 in D2O. Figure 3.1 shows the ^{1}H NMR spectrum of the monomer solution and the peak assignment of the hydrogen atoms for AA and AM. Note that the exact positions of the peaks shift slightly relative to each other with monomer composition, overall monomer concentration and temperature; however, the overall shape and ordering of the peaks remains the same.

The monomer fractional molar composition can be calculated from the integrated area of the monomer peaks according to

$$f_{\mathrm{AM}} = \frac{\text{Area AM}}{\text{Area AM} + \text{ Area AA}} \qquad 3.1$$

Since one of the AA peaks overlap with an AM peak as can be seen in Figure 3.1, the peaks between 5.72 and 5.74 ppm for AM and between 5.90 and 5.92 ppm for AA were used. In order to test the validity of the measurement, the NMR values were compared to the "lab-measured" composition, as calculated by the measured masses of the reaction ingredients. As seen in Figure 3.2, the agreement is excellent. Based on 42 runs, the average relative error between the two values is 2%, with the absolute error ranging between 0 and 4%.

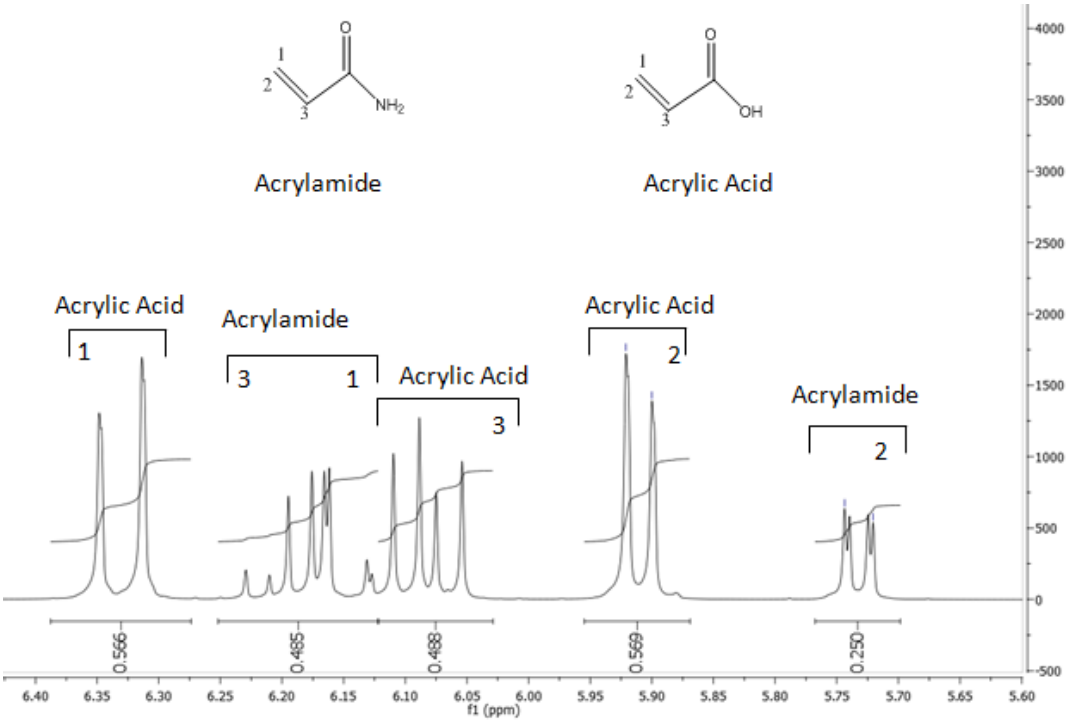

Figure 3.1 ^{1}H NMR peaks assignments for AA and AM monomer with f_{AA0} = 0.7 and 20 wt% monomer in D_2O with 0.217 wt% initiator at 40 °C.

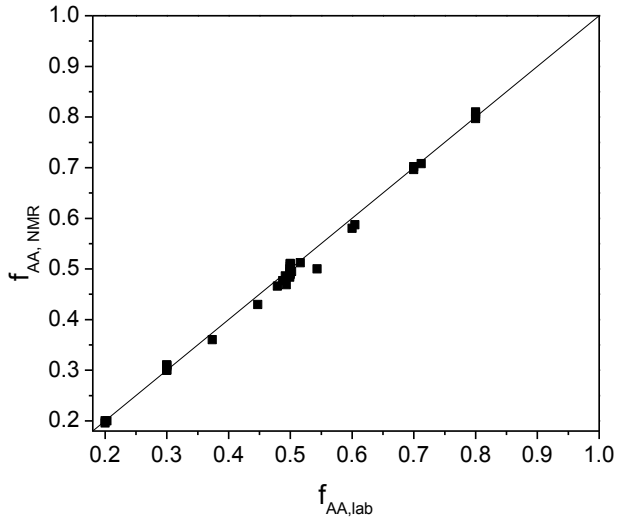

Figure 3.2 Molar monomer composition of AA in the AA/AM mixture calculated in the lab compared to the monomer composition measured with NMR.

The AA and AM repeat units on the polymer backbones are similar and can therefore not be differentiated on the ^{1}H NMR spectra. The chemical shifts of the backbone hydrogen atoms are more shielded than those on the monomeric units; as can be observed in Figure 3.3, the CH peak is located between 2.59 and 2.09 ppm, while the CH_2 peak is between 2.07 and 1.16 ppm. The sharp peak at 1.46 ppm has been assigned to the methyl groups on the initiator, V-50. Although this peak is prominent on the spectra, the initiator levels cannot be directly measured due to the overlap with the CH_2 peak. However, by overlapping the spectra at different conversions in this region, a qualitative observation of the relative consumption of initiator can be made by comparing peak intensities. For this set of experiments, the intensity of the initiator peak is constant over the polymerization time of 1-2 h, as the half-life of V-50 at 40 °C is 100 h.

The fractional conversion of monomer is calculated using the following equation:

$$x = \frac{\text{Area polymer}}{\text{Area polymer} + \text{Area monomer}} \qquad 3.2$$

As with Equation 3.1, the areas of the polymer and monomer peaks are scaled to one hydrogen. The conversion measurements were verified by simulating specific conversions by adding pAA to monomer/D_2O mixtures. The agreement between the 'conversion' measured in the lab and that calculated from the NMR spectra is presented in Figure 3.4. The average relative error between the calculated monomer conversions is 6%, with the absolute error between 0 and 3% based on 13 data points.

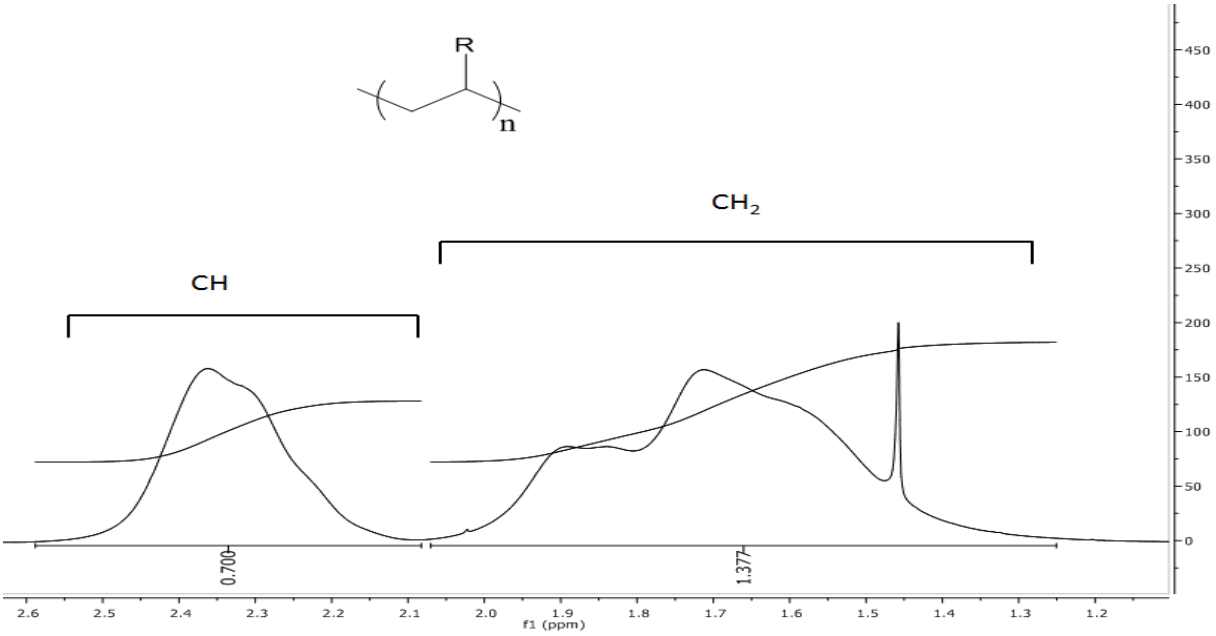

Figure 3.3 ^{1}H NMR peaks assignments for the polymer backbone with f_{AA0} = 0.7 and 20 wt% monomer in D_2O with 0.217 wt% initiator at 40 °C at 92 % conversion.

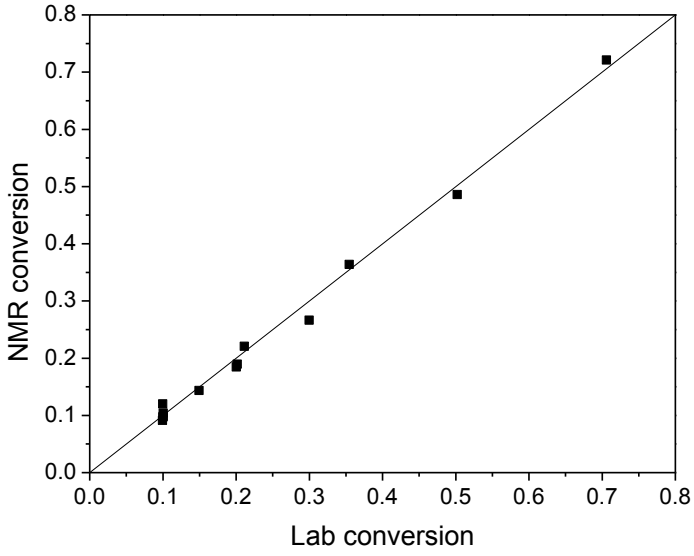

Figure 3.4 Monomer conversion calculated in the lab compared to the monomer conversion measured with NMR.

Figure 3.5 shows the evolution of the NMR spectra collected over the course of an experiment. The solvent peak is locked at 4.7 ppm and taken as the reference peak for the integration in the analysis. One can clearly see with increasing time the disappearance of the monomer peaks between 5.5 to 6.5 ppm and the appearance and growth of the polymer peaks between 1.5 to 3.0 ppm.

Small peaks from diacrylic acid (DiAA) are observed between 4.37 to 4.31 ppm and 2.74 to 2.68 ppm, with each dimer peak representing two hydrogen atoms. These conclusions were confirmed with 2D NMR. DiAA is formed very slowly over time by a Michael addition reaction that is promoted with increasing temperature and humidity.[71] The fraction of DiAA in the acrylic acid can be calculated according to the following equation:

$$\% \, DiAA = \frac{Area \; DiAA}{\frac{Area \; DiAA}{2} + \; Area \; AA} * 100 \qquad 3.3$$

Correcting for the consumption of two AA molecules to form a single DiAA molecule, the value represents the fraction of AA molecules in DiAA form. DiAA has a much lower reactivity than AA monomer and accumulates in the system with increasing conversion during polymerization. The DiAA level is monitored from reaction to reaction using the NMR spectra, and a fresh batch of monomer is purchased when it reaches 5%.

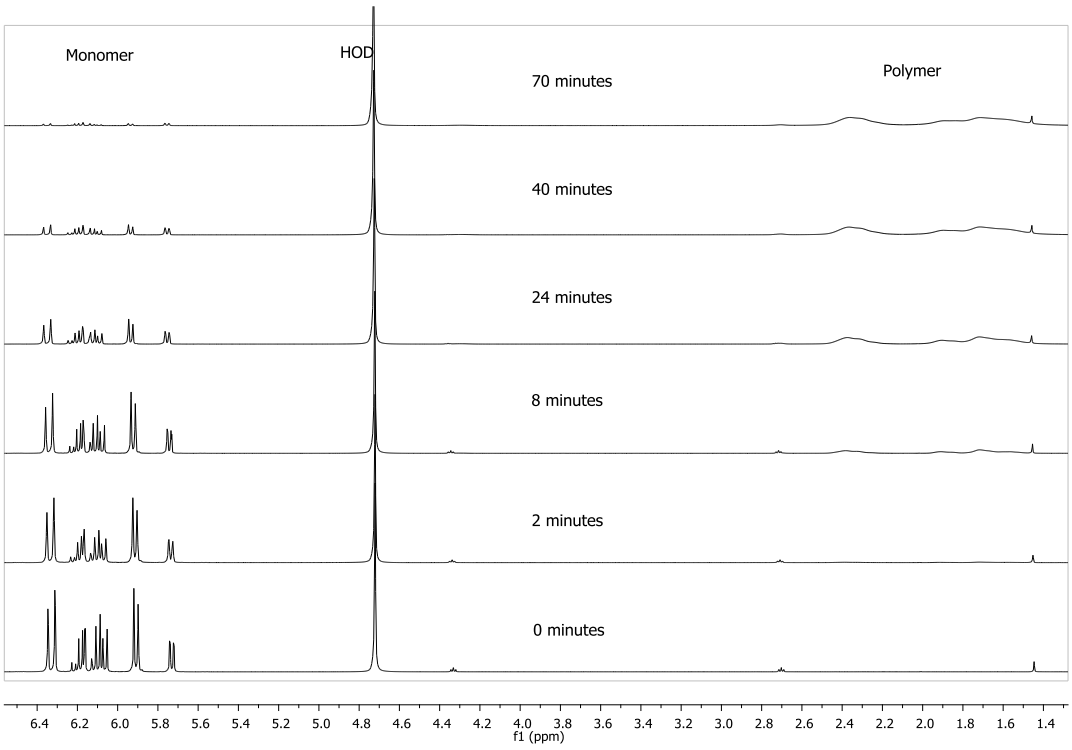

Figure 3.5 Evolution of the ^{1}H NMR spectra from low to high conversion for an experiment run with f_{AA0} = 0.7 and 20 wt% monomer in D_2O with 0.217 wt% initiator at 40 °C.

The experiments were run in randomized order and re-runs were periodically performed, with an example of the reproducibility shown in Figure 3.6. The monomer conversion profiles shown were from repeat experiments run during a period of over a month, with all of the reactions performed using different initiator stock solutions. The effect of varying initiator concentration on the monomer conversion rates was also examined and shown to give the expected behavior, in agreement with previous AA[18] and AM[19,20] homopolymerization studies.

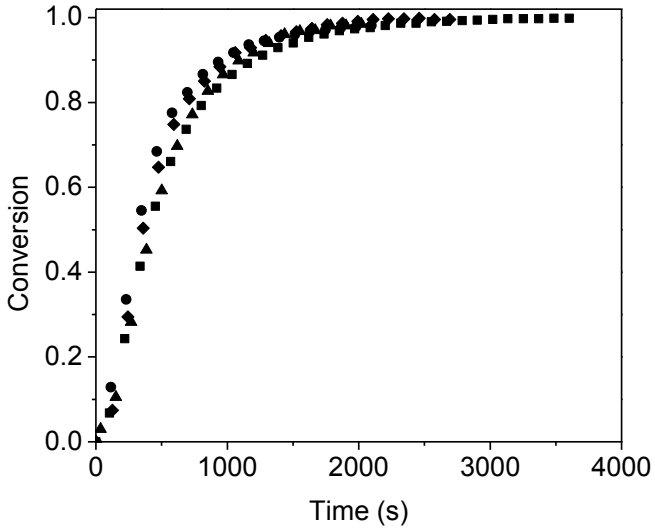

Figure 3.6 Comparison of monomer conversion profiles for AM homopolymerization at 40 °C, 40 wt% initial monomer in D_2O, and 0.217 wt% V-50 for four experiments conducted over the period of one month with different initiator stock solutions.

3.4.1 Exotherm experienced during the polymerization

Due to the small reaction volume and the experimental NMR setup, it is impossible to directly measure the temperature of the reaction mixture. Instead, the measured temperature is of the air flowing through the cavity in which the NMR tube resides. The reaction mixture in the 5 mm inner diameter NMR tube is generally filled to a height of about 3 cm, which corresponds to approximately 0.7 g of reaction mixture. The amount of heat released by the exothermic reaction increases with increased monomer concentration and thus good heat removal is essential. Therefore it is important that the air flow rate is at least 535 $L \cdot h^{-1}$ at 40 °C; for higher temperatures a faster flow rate is advised. In order to monitor the extent of exotherm, the temperature of the reaction mixture can be inferred from the movement of the chemical shifts of the monomer peaks. In previous studies, the distance between the methylene and hydroxyl peaks in ethylene glycol has been used as an NMR thermometer, with the peak separation increasing by a chemical shift of 0.01 $ppm \cdot °C^{-1}$.[72] For systems with D_2O solvent, however, the OH groups are not visible due to the fast

exchange of hydrogen with D_2O.[73] In the course of this investigation, it was determined that the position of monomer peaks were also sensitive to temperature and therefore systematic experiments were conducted by placing monomer/polymer mixtures of different monomer compositions and conversions without initiator into the NMR at 40 ºC and then increasing the temperature to 50 °C in 1 °C interval steps, allowing the samples to equilibrate for 10 minutes after each step. As observed in Figure 3.7, the monomer peak position shifts by 0.01 ppm with every degree increase. Studies were conducted at different monomer compositions, conversions, and concentration, all showing the same trend.

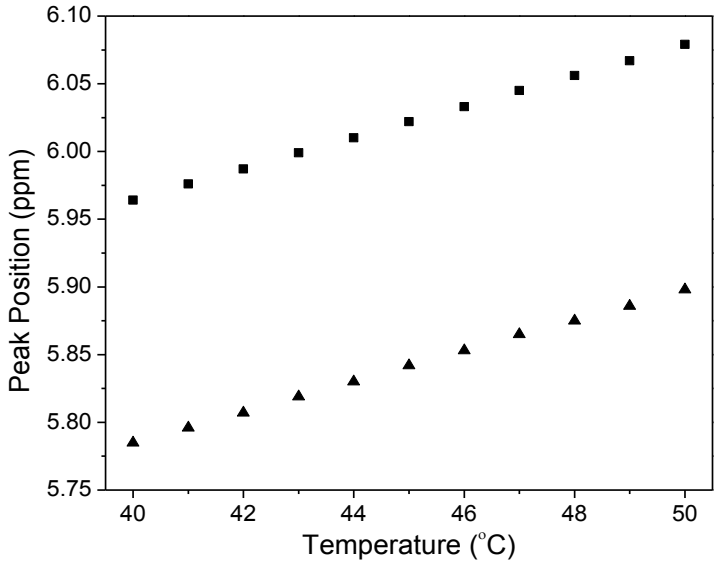

Figure 3.7 AA (■) and AM (▲) monomer peak positions with 20 wt% monomer and f_{AA} = 0.5 as a function of temperature with no polymer or initiator present in the sample.

To complicate the issue, however, a shift in monomer peaks is also observed with the presence of polymer, and therefore only a maximum temperature increase can be inferred. Figure 3.8 plots the shift in the peak position relative to the peak position at 0 % conversion as a function of conversion for polymerizations run at 5, 20, and 40 wt% monomer and initial f_{AM0} = 0.5. Neglecting any peak shifts with the appearance of polymer and assuming a 0.01 ppm shift·°C^{-1},

the maximum temperature increase varies between 1.5 and 3.5 °C. However, as the maximum rate of polymerization occurs at the start of the batch reaction, it can safely be assumed that the increase in polymer conversion contributes significantly to the movement of the peak position, and that the actual temperature increase is lower.

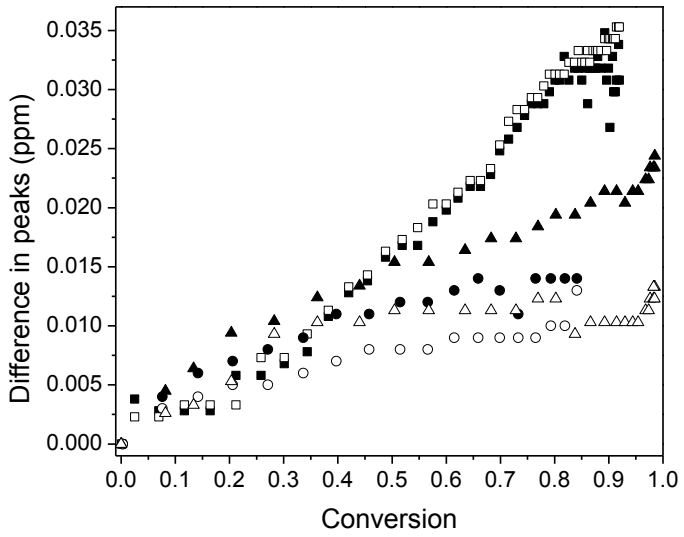

Figure 3.8 Shift in the AA (filled symbols) and AM (empty symbols) monomer peak positions for experiments run at 5 (●,○), 20 (■, □), and 40 (▲, Δ) wt% initial monomer concentration, f_{AA0} = 0.5, and 0.217 wt% V-50 at 40 °C. The difference in peak position is relative to the initial peak position at 0 % conversion.

3.5 Results and Discussion

3.5.1 Overall Monomer Conversion

Experiments were conducted with non-ionized monomer and initial compositions of f_{AM0} = 0.0, 0.3, 0.5, 0.8, and 1.0 at initial monomer concentrations of 5, 20, and 40 wt% in D_2O at 40 °C and 0.217 wt% V-50. Figure 3.9 demonstrates the influence of the initial monomer concentration on the measured monomer conversion profiles, while Figure 3.10 shows the effect of monomer composition. Figure 3.11 plots the initial rate of monomer conversion for all experiments, dx/dt, as estimated from the linear portion of the profiles between 0 and 40% conversion.

For all monomer compositions in Figure 3.9, including AA and AM homopolymerizations, the rate of monomer conversion increases with increasing monomer content. In most cases, the conversion profiles for 20 and 40 wt% monomer overlap, and are significantly faster than the profile measured with 5 wt% monomer. The faster rates for the 20 and 40 wt% experiments occur from the start of the polymerization, as seen by the initial rates of conversion in Figure 3.11. These results are in agreement with the previous AM[19,20,24] and AA[18,66] batch homopolymerization studies, and are indicative of an apparent reaction order with respect to monomer of greater than unity. The expected rate of monomer conversion (x) for FRP in a batch reactor is:

$$\frac{dx}{dt} = k_{\mathrm{p}}(1-x)\sqrt{\frac{2fk_{\mathrm{d}}[I]}{k_{\mathrm{t}}}} \qquad 3.4$$

assuming the reaction is first order with respect to monomer concentration and also with respect to radical concentration. This relationship indicates that the absolute monomer concentration should have no effect on the initial rate of conversion, contrary to the observed trends in Figure 3.9 and 3.11. It is necessary to systematically examine possible explanations for the experimental deviations from expected behavior, starting with the propagation rate coefficient.

Published PLP-SEC data for AA and AM indicate a decrease in k_{p} with increasing monomer concentration,[10,12] as summarized in Figure 3.12. Assuming constant values for k_{d} (initiator decomposition), k_{t} (bimolecular radical termination), f (initiator efficiency) and [I] (initiator concentration), one would therefore expect a decrease in the rate of conversion with increasing monomer concentration. This expected behavior has been observed in aqueous batch solution polymerizations of other water soluble monomers such as MAA[15] and NVP,[14] with the increased rate of conversion observed at lower monomer concentrations well represented by models that account for the influence of concentration on k_{p}. However, for both AA and AM (as well as for their copolymerization), dx/dt increases with monomer concentration even though PLP-SEC studies indicate a decrease in k_{p}. Thus, the observed increase in the rate of conversion cannot be

explained by k_p (indeed, is contrary to expected behavior), and must result either from changes in k_t or side reactions (backbiting) that influence the rate of monomer conversion significantly.

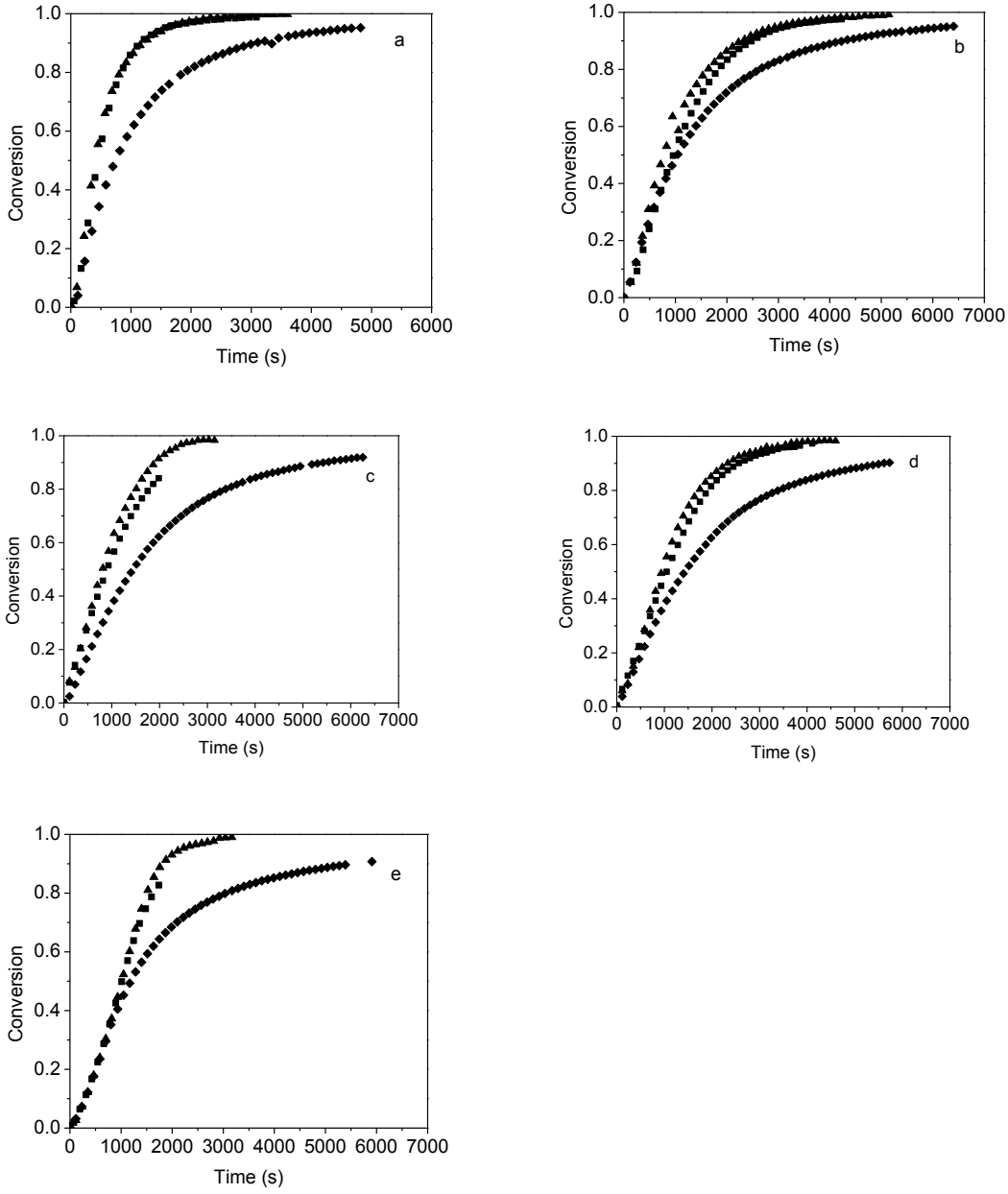

Figure 3.9 Monomer conversion vs. time profiles comparing different initial monomer concentrations of 5 (♦), 20 (■), and 40 (▲) wt% for AA/AM batch copolymerization at 40 °C and 0.217 wt% V-50 for f_{AA0} = 0.0 (a), 0.2 (b), 0.5 (c), 0.7 (d), and 1.0 (e).

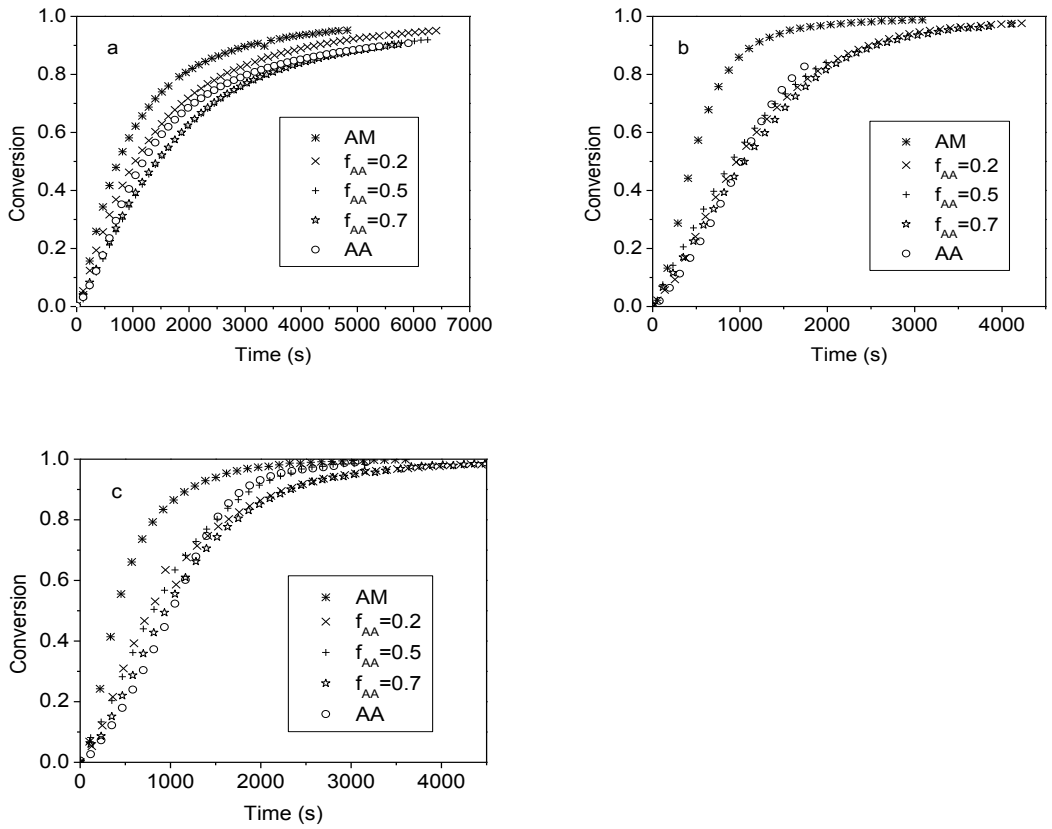

Figure 3.10 Monomer conversion vs. time profiles for AA/AM batch copolymerization at 40°C and 0.217 wt% V-50 for 5 (a), 20 (b), and 40 (c) wt% monomer in D_2O with varying initial monomer compositions of f_{AA0} = 0.0, 0.2, 0.5, 0.7, and 1.0, as indicated in the figure legend.

As seen in Equation 3.4, the rate of monomer conversion is also a function of k_t. Studies on monomers in aqueous solution such as AA,[8] MAA,[6] and NVP[44] have found that termination rate coefficients decrease with increasing monomer concentration. SP-PLP-EPR data on AA[8] show a decrease in the termination rate coefficient of two monomeric radicals at low conversion, $k_t^{1,1}$, by a factor of 6.5 as the monomer concentration increases from 10 to 50 wt%. (The termination rate for two polymer chains of length i is calculated by multiplying $k_t^{1,1}$ by a correction factor,[74] but the effect of monomer concentration on $k_t^{i,i}$ can be assumed to be the same.) By assuming that $(2fk_d[I])^{1/2}$ is constant, then the rate of conversion is proportional to $k_p/(k_t^{1,1})^{1/2}$. Using the available

PLP-measured rate coefficients presented in Table 1, this ratio decreases from 2.6 to 2.4 as monomer concentration is increased from 10 to 50 wt% at 40 °C. Thus, even with a decrease in the termination rate coefficient, the rate of AA conversion is still expected to decrease slightly with increasing monomer concentration, contrary to the 35% increase observed experimentally between 5 and 40 wt% (see Figure 3.11).

Up to date data on the termination rate coefficient for AM are few. In a paper by Seabrook et al,[75] k_t is reported to be on the order of 10^7 $L \cdot mol^{-1} \cdot s^{-1}$ for monomer concentrations of less than 1 wt% in aqueous solution at 50 °C. More recently, Schrooten has used the SP-PLP-NIR technique to measure a k_t on the order of 10^8 $L \cdot mol^{-1} \cdot s^{-1}$ at 40 °C,[76] with the value decreasing as initial weight fraction of AM is increased from 20 to 50 wt%. This latter determination is more in line with the value required to fit the conversion rate profile for 5 wt% AM (Figure 3.9a); using the most recent PLP-SEC k_p data[12] a k_t value of 2.5×10^8 $L \cdot mol^{-1} \cdot s^{-1}$ is required. However, in order to explain the increase in rate of conversion observed at the higher monomer levels of 20 and 40 wt%, a decrease in the k_t value by an order of magnitude would be required. This large shift may be plausible, as the k_t for NVP was found to decreases by over half an order of magnitude between 20 wt% and bulk.[44] More data and subsequent mechanistic modeling are required to develop a complete understanding of the termination rate coefficient of AM. (Further consideration of this point is presented in the following chapter, based upon recent SP-PLP-EPR measurements.)

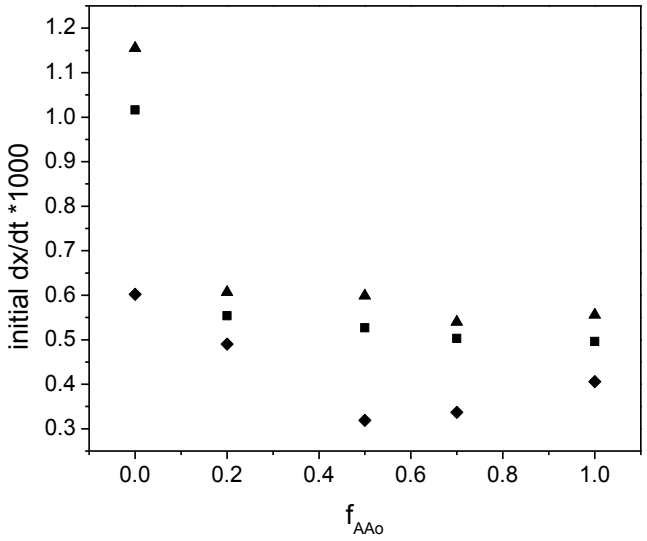

Figure 3.11 Initial rate of monomer conversion, d*x*/d*t*, as a function of initial monomer composition for AA/AM batch copolymerization at 40 °C and 0.217 wt% V-50 with initial monomer concentrations of 5 (♦), 20 (■), and 40(▲) wt% in D_2O.

Table 3.1 Estimated individual and lumped rate coefficients for polymerization of non-ionized acrylic acid (AA) at 40 ºC, with 10 and 50 wt% AA in aqueous solution.

Rate coefficient	10 wt% AA	50 wt% AA	Ref
k_p ($L \cdot mol^{-1} \cdot s^{-1}$)	1.76×10^5	6.46×10^4	[10]
$k_t^{1,1}$ ($L \cdot mol^{-1} \cdot s^{-1}$)	4.57×10^9	7.08×10^8	[8]
$k_p/\sqrt{(k_t^{1,1})}$ $(L \cdot mol^{-1} \cdot s^{-1})^{1/2}$	2.6	2.4	
k_p^t ($L \cdot mol^{-1} \cdot s^{-1}$)	87.5	24.5	[8]
k_{bb} (s^{-1})	423.6	199	[8]
k_p^{avg} ($L \cdot mol^{-1} \cdot s^{-1}$)	3.95×10^4	2.98×10^4	
$k_p^{avg}/\sqrt{(k_t^{1,1})}$ $(L \cdot mol^{-1} \cdot s^{-1})^{1/2}$	0.58	1.12	

The above analysis indicates that it is difficult to explain the increasing rate of conversion observed with increasing monomer content observed experimentally by consideration of the recent PLP k_p and k_t data. Equation 4 is derived assuming that no side-reactions occur during

polymerization. However, evidence has emerged that AA undergoes intramolecular chain transfer (backbiting), as summarized in the recent work of Barth et al.[8] As well documented for acrylates, these reactions decrease the overall observed propagation rate from the chain-end k_p value to yield an average propagation rate of:[41]

$$k_p^{avg} = k_p - \frac{k_p - k_{p,tert}}{1 + \frac{k_{p,tert}[M]}{k_{bb}}} \quad 3.5$$

Using the rate coefficients from Barth et al.[8] summarized in Table 1, the values of $(k_p^{avg}/k_t^{1,1})^{1/2}$ are 0.58 and 1.12 at 10 and 50 wt%, respectively. Thus, when the effect of backbiting on rate is accounted for, the predicted shifts in rate of conversion for AA are in agreement with the trends observed experimentally. Very recently, evidence of mid-chain radical formation, albeit at much lower rates, has been found for AM using the SP-PLP-EPR technique.[25] Backbiting in the AM homopolymerization system, along with a monomer concentration dependent termination rate coefficient, could combine to explain the increase in conversion rate with increasing monomer concentration in the AM homopolymerizations.

The analysis of the homopropagation rates of conversion for AA and AM can be extended to the copolymerization system. As shown in Figure 3.9 and 3.11, the initial rates of conversion for copolymerization are very similar to those for AA homopolymerization (but lower than for AM homopolymerization), independent of the monomer composition. It is likely that backbiting occurs with any amount of AA in the monomer mixture, leading to the same decrease in the initial rate of conversion at 5 wt% monomer relative to 20 and 40 wt% as observed in the homopolymerizations. Work is ongoing to measure the extent of short chain branch formation as a function of monomer composition and concentration using ^{13}C NMR. These data along with estimates of monomer reactivity ratios (see below) will be combined with k_p and k_t results from PLP to provide the kinetic coefficients necessary to model the set of conversion profiles obtained in this study.

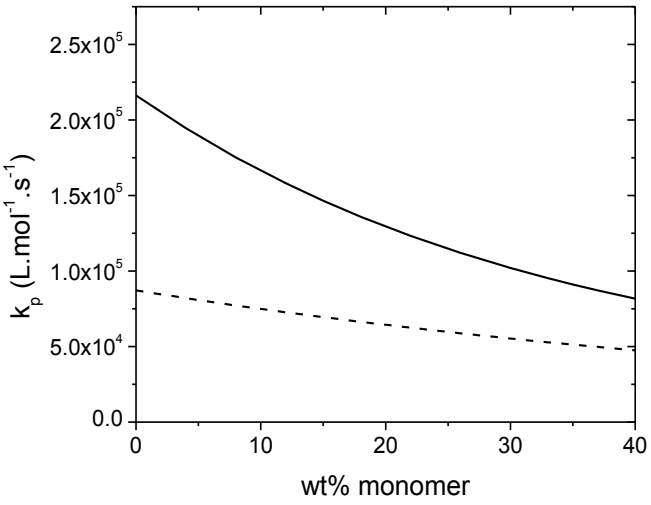

Figure 3.12 Comparison of the chain-end propagation rate coefficient of AA (solid line)[10] and AM (dashed line)[12] as a function of monomer concentration at 40 °C, as estimated by PLP-SEC.

3.5.2 Copolymer Composition

In addition to the overall conversion profiles discussed above, the NMR experiments are used to track how monomer composition changes over the course of the batch experiment. Monomer composition is plotted as a function of conversion for the entire set of experiments in Figure 3.13. At all compositions examined (f_{AM0} = 0.3, 0.5 and 0.8), the monomer mixture becomes enriched in AM as the polymerization proceeds due to the preferential incorporation of AA into the copolymer. It is interesting to note that the composition drift is independent of the initial monomer concentration. The result suggests that the monomer reactivity ratios are independent of total monomer concentration. While commonly found for copolymerization in organic solution,[77] this result is not necessarily expected for AA/AM aqueous-phase copolymerization as the homopropagation rate coefficient of AA is a stronger function of monomer concentration than AM: as shown in Figure 3.12, the ratio of k_p^{AA} to k_p^{AM} increases from 1.6 at 40 wt% monomer to 2.6 at 5 wt%. With reactivity ratios defined according to the terminal model ($r_{AA} = k_p^{AA}/k_p^{AA\cdot AM}$ and r_{AM}

= $k_p^{AM}/k_p^{AM \cdot AA}$), the data suggest that cross-propagation rate coefficients vary in the same fashion as the homopropagation values, such that r_{AA} and r_{AM} are invariant with monomer concentration.

The AA/AM reactivity ratios reported in the literature are determined using copolymer compositions measured in low conversion (<10%) experiments fit to the terminal model (TM),[36,46–48] where the instantaneous mole fraction of AM incorporated into the polymer (F_{AM}) is described by the Mayo-Lewis equation:[45]

$$F_{AM} = \frac{r_{AM} f_{AM}^2 + f_{AM} f_{AA}}{r_{AM} f_{AM}^2 + 2 f_{AM} f_{AA} + r_{AA} f_{AA}^2} \quad 3.6$$

In order to fit the NMR data from this work using the same methodology, it is necessary to estimate F_{AM} from the consumption of monomer and the overall monomer conversion:

$$F_{AM}^{cum} = \frac{f_{AM0} - f_{AM}(1-x)}{x} \quad 3.7$$

Figure 3.14 plots the copolymer compositions estimated at conversions of 5 and 10%. The best-fit reactivity ratios, estimated using non-linear parameter estimation tools in Predici, are r_{AA} = 1.27 ± 0.26, and r_{AM} = 0.54 ± 0.21. It is evident that significant uncertainty is introduced by the calculation of copolymer composition from the small change in monomer composition that occurs over the first 10% of monomer conversion.

To take advantage of the complete range of composition vs conversion data measured using the NMR technique (Figure 3.13), the reactivity ratios were also estimated using the integrated form of the Mayo-Lewis equation as derived by Meyer and Lowry,[55] as well as the differential form of the balances coupled with direct numerical integration (DNI).[54] The DNI method relates overall monomer conversion, monomer composition, and the reactivity ratios according to:

$$\frac{df_{AM}}{dx} = \frac{f_{AM} - F_{AM}}{1-x} \quad 3.8$$

Here x is the total monomer conversion and F_{AM} is calculated using Equation 3.6. While slightly more computationally intensive (the differential equation is solved as part of the parameter estimation methodology), the DNI methodology is preferred as it avoids using any transformations

and has a reduced error structure.[54] The reactivity ratios estimated using the DNI method are r_{AA} = 1.24 ± 0.02 and r_{AM} = 0.55 ± 0.01; values estimated using the integrated Meyer-Lowry form of the equation are in excellent agreement, at 1.23 ± 0.02 and 0.58 ± 0.01 for r_{AA} and r_{AM}, respectively. Both estimates are in good agreement with those estimated using low conversion data (r_{AA} = 1.27 ± 0.26, and r_{AM} = 0.54 ± 0.21), but have a much lower associated error, as reflected by the reported 95% confidence intervals. The estimates provide a very good description of the drift in f_{AM} with overall conversion, as shown by the curves plotted in Figure 3.13. In addition, they are in reasonable agreement with the reactivity ratios of 1.48 and 0.54 for r_{AA} and r_{AM} reported by Rintoul and Wandrey[46] for experiments conducted with 4 wt% monomer. Work is ongoing to determine the reactivity ratios from polymerizations conducted at other experimental conditions. (Since this publication, this work has been completed and will be discussed in Chapter 5.)

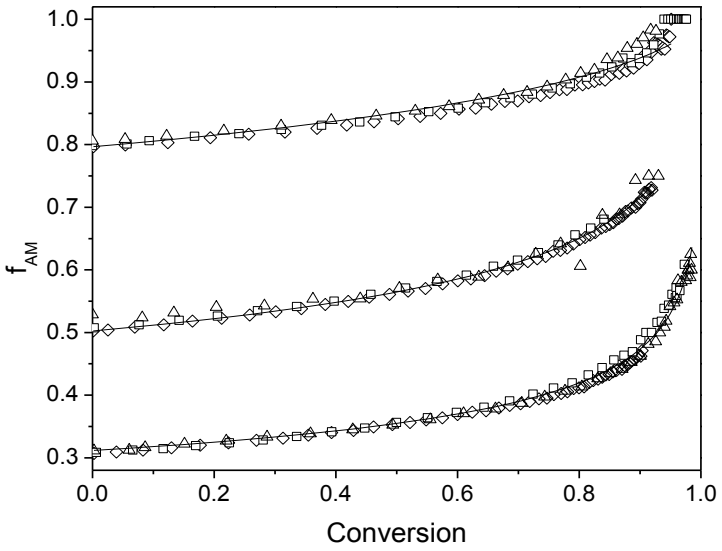

Figure 3.13 Monomer composition as a function of conversion for all experiments at f_{AA0} = 0.2, 0.5, and 0.7 with initial monomer concentration of 5 (◊), 20 (□), and 40(△) wt% and 0.217 wt% V-50 at 40 °C, and the resulting fit (solid line) calculated with reactivity ratios r_{AA} = 1.24 ± 0.02 and r_{AM} = 0.55 ± 0.01, as estimated using the DNI method.

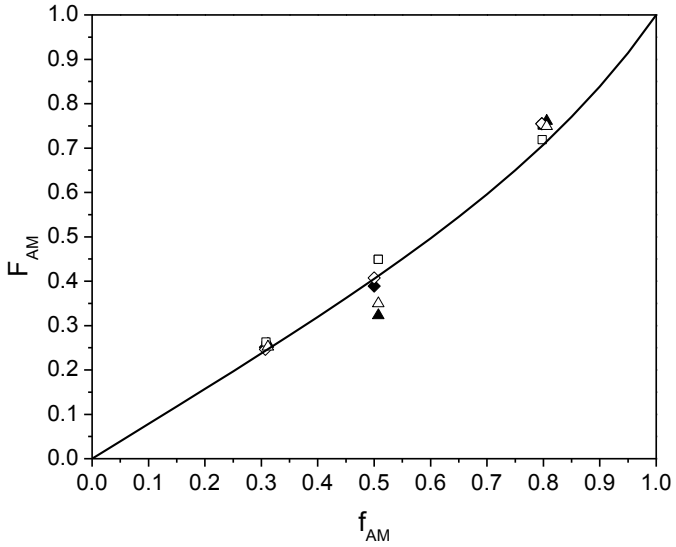

Figure 3.14 Cumulative copolymer composition estimated at 5 (filled symbols) and 10 (empty symbols) % monomer conversion as a function of monomer composition with initial monomer concentration of 5 (♦,◊), 20 (■,□), and 40(▲,△) wt%, and the best fit (solid line) calculated from the combined dataset with r_{AA} = 1.27 ± 0.26, and r_{AM} = 0.54 ± 0.21.

3.6 Conclusion

The radical copolymerization of non-ionized AA with AM in aqueous solution was investigated at 40 ºC using an NMR in-situ technique. The experimental methodology allows the study of monomer concentrations significantly higher than reported in the literature under near-isothermal conditions while simultaneously tracking changes in co-monomer composition and overall monomer conversion. The composition data obtained over the entire conversion range provide a more precise estimate of monomer reactivity ratios than values estimated from low conversion data. The complete set of experiments, with initial monomer content in aqueous solution varied between 5 and 40%, were well-fit over the complete conversion range by r_{AA} = 1.24 ± 0.02, and r_{AM} = 0.55 ± 0.01, in good agreement with values reported in the literature for more dilute systems.

It was found that the rate of monomer conversion increases with increasing monomer concentration, a trend contrary to the known decrease in the AA and AM chain-end propagation rate coefficients with increasing monomer concentration. It is hypothesized that backbiting reactions, which exert a larger effect on polymerization rate as monomer concentration is lowered, significantly slow the conversion rate for both the AA and AA/AM polymerizations. Work is underway to measure the polymer molecular weights (using size exclusion chromatography) and branching levels (using ^{13}C NMR) of the samples obtained in the study, as well as applying the NMR technique to study copolymerization over a broader range of experimental conditions.

Chapter 4

Kinetics and Modeling of Acrylamide Free Radical Homopolymerization

4.1 Introduction

Water soluble polymers are used in a variety of applications including cosmetics, pharmaceuticals, water treatment, mining, oil sands, textiles, and paper processing.[2] High molecular weight (>1×10^6 Da) polyacrylamide (pAM) and its copolymers are commonly used as flocculants due to their ability to bind to various charged particles in aqueous solution. In addition to use as flocculants for mining and textile industries, they are finding some applications in treatment of oil sand tailing ponds in western Canada, with research ongoing in this area due to the complexity of the finely dispersed clays and residual bitumen make-up of the settling ponds.[3] Although acrylamide (AM) radical polymerization has been the subject of scientific study since the 1970's,[19] it is only recently that a more complete understanding of the kinetic complexities of the polymerization system has been realized.[12,25]

Measurement of the individual rate coefficients for radical polymerization of water soluble monomers are notoriously challenging due to high viscosity and a pH and monomer concentration dependency on the rate coefficients.[78,79] As a result, the studies in the literature are often limited to measuring the batch conversion profiles at low monomer concentration to deduce the ratio of $k_p/k_t^{1/2}$ from the well-known expression for polymerization rate written assuming the IUPAC convention for termination ($r_{\mathrm{term}} = 2k_t[P]^2$, where $[P]$ is the total polymer radical concentration):

$$R_p = -\frac{d[M]}{dt} = k_p[M]\left(\frac{fk_d[I]}{k_t}\right)^{1/2} \qquad 4.1$$

While the rate of polymerization is expected to be first order with respect to monomer concentration (Equation 4.1), studies with AM yield a reaction order between 1.24 to 1.49.[19,20,59,60] The higher

reaction order was first described in terms of the cage effect on initiator efficiency (f),[19] and later by diffusion-controlled rate coefficients for propagation (k_p) and termination (k_t).[24,61] However, these explanations were unable to provide a consistent representation of the available experimental data. For example, with the cage effect implemented into the reaction scheme, the resulting model was able to predict a reaction order between 1.0 and 1.5 dependent on the initial monomer concentration to fit experimental conversion data collected between 2 and 16 wt% AM,[19] but a single model was not able to successfully simulate the conversion profiles between 5 and 24 wt% AM.[24] Recent studies at the University of Göttingen using specialized pulsed-laser techniques show no significant evidence of a gel effect, with the termination rate coefficient remaining constant as a function of monomer conversion.[25]

Given the recent application of pulsed-laser experimental techniques to the study of the polymerization kinetics of water-soluble monomers in aqueous phase, it is worthwhile to revisit modeling of the polymerization behavior of this important monomer. None of the AM models in the literature incorporate a propagation rate coefficient (k_p) that is a function of monomer concentration, although it is now known that k_p values for non-ionized water soluble monomers show this dependency. This behavior has been measured by pulsed-laser polymerization (PLP) coupled with analysis of the resulting polymer molar mass distribution (MMD) by size exclusion chromatography (SEC) (the PLP-SEC technique) for monomers including acrylic acid (AA),[10,29,30] methacrylic acid (MAA),[32–34] and N-vinyl pyrrolidone (NVP).[13] The decrease in k_p with increasing monomer concentration has been attributed to competitive hydrogen bonding between the reacting monomer unit and side groups of the monomer and the solvent in the transition state.[10,33–36] Hydrogen bonding between the monomer and water lowers the internal rotational mobility in the transition state structure for propagation, making the reaction proceed more quickly, as confirmed by theoretical studies.[38] The first PLP-SEC study of AM was done in 2005 by the research group of Gilbert over a narrow range of conditions, between 10 and 30 °C and 2 and 20

wt% AM in aqueous solution.[11] These experimental conditions have been expanded by Lacík's research group to a broader temperature range (5 to 70 °C) for similar monomer concentrations (3 to 30 wt% AM),[12] with the estimated k_p data in the two lab groups being within 10 to 30 % relative error. These new experimental data were used to develop the expression used to represent the propagation rate coefficient as a function of temperature and monomer concentration for the model implemented in this study.

Backbiting, also known as the 1,5 hydrogen transfer reaction, is a side reaction commonly observed during polymerization of vinyl monomers that form secondary carbon-centered chain-end radicals such as butyl acrylate (BA)[40,41,80] and AA.[8,21,42] The propagating chain-end radical curls back on itself via a temporary 6 membered ring and transfers the radical onto the polymer backbone by abstracting a H-atom to form a mid-chain radical (MCR). As the MCR is a tertiary radical that is less reactive than the secondary propagating chain end radical,[27] the overall polymerization rate is decreased; the competition between the first-order backbiting reaction with the second order propagation reaction leads to an apparent reaction order of greater than unity with respect to monomer concentration,[23,27] as has been observed experimentally for AM. The presence of MCRs has recently been observed by electron paramagnetic resonance (EPR) spectroscopy, thus confirming (for the first time) the occurrence of backbiting during acrylamide polymerization. Furthermore, the rate coefficients relevant to backbiting, monomer addition to the MCR, and radical-radical termination have been estimated by analysis of the time-resolved EPR spectra measured after application of a single laser pulse (the SP-PLP-EPR technique) over a range of monomer concentrations and temperatures by Kattner and Buback.[25]

The model developed in this work uses these new mechanistic insights developed for AM polymerization kinetics and the rate coefficients measured by the PLP investigations described above. The predictions of the model, implemented in Predici,[81] are compared to experimental monomer conversion and polymer MW data collected from recent isothermal batch experiments

followed in-situ using NMR spectroscopy[23] as well as previously published data in the literature.[19,24] The resulting model captures the experimental trends over a range of initial monomer concentrations and temperatures collected using various experimental methods from different lab groups.

4.2 Experimental

4.2.1 Materials Used

Electrophoresis grade acrylamide monomer (99+%, Sigma Aldrich), deuterated water (D_2O) (99.9%, Cambridge Isotope Laboratories Inc.) and 2,2-azobis(2-methylpropionamide)dihydrochloride initiator (V-50) (97%, Sigma Aldrich) were used as received.

Stock solutions of monomer and initiator were prepared separately and purged for 15 minutes with nitrogen. The initiator stock solutions of 4 wt% V-50 in D_2O were made fresh weekly. The solutions were mixed at the appropriate ratios on the day of the experiment to the desired total monomer concentration, transferred to conventional 5 mm labeled NMR tubes and set in the fridge until polymerization.

4.2.2 Measurement of Conversion Profiles

As part of this cooperation, data was collected at 4 laboratories by 4 individuals, with labs in Kingston, Bratislava and Zürich using the in-situ NMR method as developed in reference,[23] where the conversion is determined by dividing the area of the polymer peak by the total area of the polymer and monomer peaks. The lab in Göttingen using an in-situ NIR method with an experimental setup described in reference [16]. Figure 4.1 shows superb reproducibility of the data between the lab groups.

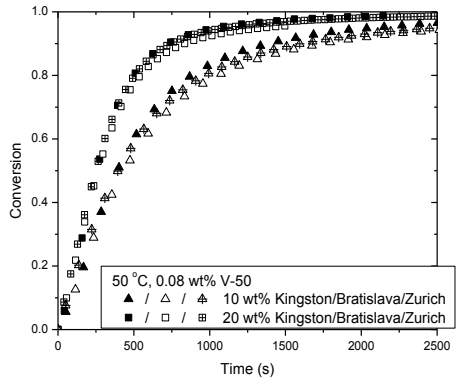

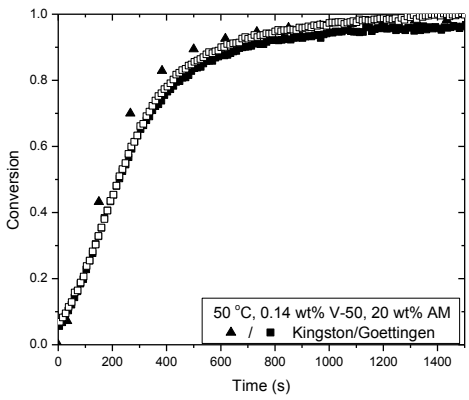

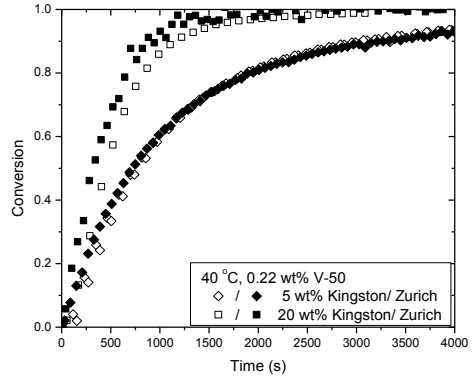

Figure 4.1 Acrylamide monomer conversion profiles obtained by batch radical polymerizations in aqueous solution conducted in different labs at a range of temperatures, initiator content, and monomer concentrations. The experimental conditions and lab (Kingston, Bratislava, Zürich, and Göttingen) are indicated in the plot legends.

4.2.3 SEC Analysis

Aqueous phase SEC was performed on the high conversion batch polymer samples collected at the end of the in-situ experiments using the SEC equipment and procedures described for SEC analysis of polyacrylic acid in reference [32]. The eluent used was 0.1 M Na_2HPO_4 at pH 9 at flow rate 0.5 mL·min^{-1}. The polymer samples were dissolved for 48 hours at mild stirring and

run at concentrations 1 mg·mL^{-1}. The autosampler injected 100 μL per sample and each sample was injected twice. The Suprema columns at 100 Å, 1000 Å, 3000 Å and 10000 Å were maintained at 60 °C. A direct calibration to pAM standards between M_p values of 2950 to 6 500 000 Da were used (American Standards Corporation). For MALLS calibration pullulan of 113 000 g·mol^{-1} was used as in isorefractive scatterer. The dn/dc values for pullulan and pAM are 0.136 mL·g^{-1} and 0.132 mL·g^{-1}, respectively.

4.2.4 Experimental Data Collected

Batch polymerizations were conducted at various temperatures, initiator (V-50) concentrations and AM concentrations in aqueous solution with the resulting conversion profiles plotted in Figure 4.1 to 4.4. The data collected at 40 °C has already been published in reference[23]. The expected rate of conversion for FRP in a batch reactor is:

$$\frac{dx}{dt} = k_{\mathrm{p}}(1-x)\sqrt{\frac{f k_{\mathrm{d}}[I]}{k_{\mathrm{t}}}} \qquad 4.2$$

where k_d is the first order rate coefficient for initiator decomposition and f is the initiator efficiency; Equation 4.2 written assuming the IUPAC convention for termination. The conversion rate is expected to be independent of monomer concentration, a result that is not observed experimentally; as shown in Figure 4.1, the conversion rates increase with increasing monomer concentration at constant temperature and initiator concentration, a result also found in previous literature.[19,24] Using the newly developed knowledge of AM kinetics developed by the PLP studies,[25] this increase can be attributed to changes in the propagation and termination rate coefficients with monomer concentration, and to the occurrence of backbiting reactions,[23] as confirmed by the modeling work discussed below.

4.3 Reaction Mechanism and Discussion of Fit to Experimental Data

The reaction mechanism used in the AM model is summarized in Table 4.1. The initiation, propagation, transfer to monomer, and termination reactions of secondary chain-end propagating radicals (SPR, denoted by P_n in Table 4.1) all follow the conventional free radical polymerization mechanism,[1] while the additional reaction steps are all related to the formation of midchain radicals (Q_n) by backbiting and their consumption by termination or monomer addition.[27] Reaction mechanisms as in Table 4.1 have successfully been used to model butyl acrylate and acrylic acid polymerizations.[21,80,82,83] It should be noted that no evidence of ß-scission reactions have been observed for AM at the experimental conditions studied.

Table 4.1 Reaction Mechanism used in the AM model.

Initiation	$\mathrm{I} \xrightarrow{k_\mathrm{d}} 2f\mathrm{I}^{\mathrm{rad}}$
	$\mathrm{I}^{\mathrm{rad}} + \mathrm{AM} \xrightarrow{k_\mathrm{p}} \mathrm{P}_1$
Chain Propagation	$\mathrm{P}_\mathrm{n} + \mathrm{AM} \xrightarrow{k_\mathrm{p}} \mathrm{P}_{\mathrm{n+1}}$
Transfer to Monomer	$\mathrm{P}_\mathrm{n} + \mathrm{AM} \xrightarrow{k_\mathrm{tr}} \mathrm{D}_\mathrm{n} + \mathrm{P}_1$
Termination SPR-SPR	$\mathrm{P}_\mathrm{n} + \mathrm{P}_\mathrm{m} \xrightarrow{(1-\alpha_{\mathrm{ss}})k_{\mathrm{t,ss}}} \mathrm{D}_{\mathrm{n+m}} \,/\, \xrightarrow{\alpha_{\mathrm{ss}}k_{\mathrm{t,ss}}} \mathrm{D}_\mathrm{n} + \mathrm{D}_\mathrm{m}$
Reactions related to Backbiting	
Backbiting	$\mathrm{P}_\mathrm{n} \xrightarrow{k_{\mathrm{bb}}} \mathrm{Q}_\mathrm{n}$
Addition to MCR	$\mathrm{Q}_\mathrm{n} + \mathrm{AM} \xrightarrow{k_{\mathrm{p,tert}}} \mathrm{P}_{\mathrm{n+1}}$
Cross Termination MCR-SPR	$\mathrm{P}_\mathrm{n} + \mathrm{Q}_\mathrm{m} \xrightarrow{(1-\alpha_{\mathrm{st}})k_{\mathrm{t,st}}} \mathrm{D}_{\mathrm{n+m}} \,/\, \xrightarrow{\alpha_{\mathrm{st}}k_{\mathrm{t,st}}} \mathrm{D}_\mathrm{n} + \mathrm{D}_\mathrm{m}$
Termination MCR-MCR	$\mathrm{Q}_\mathrm{n} + \mathrm{Q}_\mathrm{m} \xrightarrow{(1-\alpha_{\mathrm{tt}})k_{\mathrm{t,tt}}} \mathrm{D}_{\mathrm{n+m}} \,/\, \xrightarrow{\alpha_{\mathrm{tt}}k_{\mathrm{t,tt}}} \mathrm{D}_\mathrm{n} + \mathrm{D}_\mathrm{m}$

The rate coefficients pertaining to the AM homopolymerization reactions are tabulated in Table 4.2. With the exception of the initiation and transfer to monomer rate coefficients, all rate coefficients were measured by our collaborators at the Polymer Institute at the Slovak Academy of Sciences and at the University of Göttingen.

The propagation rate coefficient, k_p, was measured using PLP-SEC for various monomer concentrations (3 to 20 wt%) between 5 and 70 °C.[12] The data from Dr. Lacík's research group covers a broader temperature range, thus providing more data for the expression of the rate propagation rate coefficient as a function of temperature and monomer concentration compared to the data measured by Seabrook et al.[11] As with other water soluble monomers, the propagation rate coefficient is expressed as a function of monomer concentration as well as temperature. The expression is a function of the mass fraction of AM on a polymer free basis, w'_M, as studies on AA,[10] MAA,[33] and NVP[13] have shown that the value of k_p is independent of the presence of polymer. This results in the propagation rate coefficient increasing with monomer conversion as the monomer concentration decreases in a batch polymerization.

For many monomers, including acrylates and acrylic acid, it has been found that the activation energy for chain-termination follows that of the fluidity, η^{-1}, of the monomer-solvent mixture, as both processes are controlled by segmental diffusion.[74] The activation energy was determined by measuring the fluidity at different temperatures and monomer concentrations and yielding $E_A/R = (1991+1477w'_{M0})$(K), where w'_{M0} is the initial weight fraction of AM in water;[25] the dependence on monomer concentration has been verified using SP-PLP-EPR data collected at 10 and 20 wt% AM at −5 °C.[25] The termination rate is modeled in a similar manner as was done in previous modeling efforts for NVP[14] and AA,[21] and assuming that the influence of fluidity is the same for SPR-SPR ($k_{t,ss}$), SPR-MCR ($k_{t,st}$), and MCR-MCR ($k_{t,tt}$) termination.

The SP-PLP-EPR technique measures the termination rate coefficient as a function of radical chain-length. To facilitate the modeling of the very high MW polymer produced in batch

polymerizations, an averaged chain-length independent value is used. The pre-exponential factor for the termination rate coefficient was developed in several steps based upon SP-PLP-EPR data collected at 10 wt% AM and −5 °C. The pre-exponential factor for the termination rate coefficient for the monomeric radicals in the short chain length regime (k_t^0) was determined to be 1.1×10^{11} $L\cdot mol^{-1}\cdot s^{-1}$. The following relationship is used to extrapolate this expression to higher chain lengths for termination of two chain-end radicals ($k_{t,ss}$):[74]

$$k_{t,ss}(i,i) = k_t^0 i^{-\alpha_1} \qquad 4.3$$

where i is the chain length and α_1 is the composite model parameter capturing the effect of chain length on termination of longer radicals, determined to be 0.15 for AM.[25] For radicals of significant length, the chain-length dependency quickly levels out, as can be seen by the ratios calculated for chain lengths of 100, 1000, and 10000: $k_{t,ss}(100)/k_t^0 = 0.5$, $k_{t,ss}(1000)/k_t^0 = 0.35$, $k_{t,ss}(10000)/k_t^0 = 0.25$. To simplify the model implementation for representing the production of high-MW pAM, a constant value for $k_{t,ss}$ was used, with a pre-exponential factor of 2×10^{10} $L\cdot mol^{-1}\cdot s^{-1}$, a factor of five lower than the pre-exponential of k_t^0.

The cross termination rate coefficient of the MCR and SPRs, $k_{t,st}$, has also been estimated at 10 and 20 wt% AM and found to vary with monomer concentration in the same manner as $k_{t,ss}$.[25] Therefore this cross termination is implemented as a ratio of $k_{t,st}/k_{t,ss}$ at a constant value of 0.27.[25] No evidence of MCR homotermination was found from the SP-PLP-EPR data,[25] however for completeness this reaction step is included in the model and set to the low ratio of $k_{t,tt}/k_{t,ss} = 0.01$.

The mode of termination of chain-end radicals was set predominantly to termination by combination. Note that this is contrary to the previous work of Hamielec and coworkers,[19,24] who base their assumption on older MMD measurements. Seabrook, on the other hand, state that termination is by combination. As an analysis of the MMDs produced in this study did not provide a definitive answer, we follow the recommendations by Moad and Solomon that secondary radicals generally terminate by combination, while tertiary radicals undergo a higher fraction of

disproportionation.[84] Termination by combination is generally assumed for similar secondary radical structures formed from styrene,[83] butyl acrylate,[85] acrylic acid,[21] and ethyl acetate.[86] The fractions for disproportionation were adopted from the butyl acrylate model from Nikitin et al. to be $\alpha_{ss} = 0.1$, $\alpha_{st} = 0.7$, and $\alpha_{tt} = 0.9$.[85]

The rate coefficient for backbiting, k_{bb}, is taken from reference[25] for the combined fit of the measured SP-PLP-EPR radical profiles at 10 and 20 wt% AM, with the Arrhenius parameters summarized in Table 4.2. While the individual fits for k_{bb} at 10 and 20 wt% SP-PLP-EPR 40 °C differed by 16%, it was assumed that this is within experimental error such that k_{bb} is independent of monomer concentration, an assumption also used for modeling of AA polymerization.[21]

The rate coefficient for monomer addition to the tertiary radical, $k_{p,tert}$, was estimated from the SP-PLP-EPR study to have $A = 1.47\times10^6$ L·mol^{-1}·s^{-1} and $E_A/R = 3601$ K at both 10 and 20 wt% monomer.[25] The expected difference in the rate coefficient between 10 and 20 wt% is 6% assuming that $k_{p,tert}$ varies in a similar manner as k_p.[21,25] As this expected variation is within the experimental error, it has been assumed that k_p and $k_{p,tert}$ have the same dependence on monomer concentration, as done previously for modeling of AA. The expression for the ratio of $k_{p,tert}/k_p$ in Table 4.2 is thus obtained by dividing the two expressions of the rate coefficients.

Table 4.2 Rate coefficients used to model AM aqueous-phase batch polymerization.

Rate Expression	Values*	Ref
Initiation:		
$k_{\mathrm{d}}(\mathrm{s}^{-1}) = 9.24\times10^{14}\exp\left(-\frac{14\,915}{T/\mathrm{K}}\right)$	2×10^{-6}	[87]
Initiator efficiency: 0.8		
Chain Propagation:		
$k_{\mathrm{p}}(\mathrm{L}\cdot\mathrm{mol}^{-1}\cdot\mathrm{s}^{-1}) = k_{\mathrm{p,max}}\exp[-w'_{\mathrm{M}}(0.0016(T/\mathrm{K}^{-1}) + 1.015)]$	6.4×10^{4}	[12], this work
$k_{\mathrm{p,max}}(\mathrm{L}\cdot\mathrm{mol}^{-1}\cdot\mathrm{s}^{-1}) = 9.5\times10^{7}\exp\left(-\frac{2189}{T/\mathrm{K}}\right)$	8.7×10^{4}	
Transfer to Monomer:		
$C_{\mathrm{tr}} = \frac{k_{\mathrm{tr}}}{k_{\mathrm{p}}} = 0.00118\exp\left(-\frac{1002}{T/\mathrm{K}}\right)$	4.8×10^{-5}	This work
Termination SPR-SPR:		
$k_{\mathrm{t,ss}}(\mathrm{L}\cdot\mathrm{mol}^{-1}\cdot\mathrm{s}^{-1}) = 2\times10^{10}\exp\left(-\frac{(1991 + 1477w'_{\mathrm{M0}})}{T/\mathrm{K}}\right)$	1.3×10^{7}	[25], This work
$\alpha_{\mathrm{s,s}} = 0.1$		
Reactions Related to Backbiting:		
Backbiting		
$k_{\mathrm{bb}}\,(\mathrm{s}^{-1}) = 3.7\times10^{9}\exp\left(-\frac{5874}{T/\mathrm{K}}\right)$	26	[25]
Addition to MCR		
$k_{\mathrm{p,tert}}(\mathrm{L}\cdot\mathrm{mol}^{-1}\cdot\mathrm{s}^{-1}) = 0.0155\exp\left(-\frac{1412}{T/\mathrm{K}}\right)k_{\mathrm{p}}$	11	[25]
Cross Termination MCR-SPR		
$k_{\mathrm{t,st}}(\mathrm{L}\cdot\mathrm{mol}^{-1}\cdot\mathrm{s}^{-1}) = 0.27k_{\mathrm{t,ss}}$	3.5×10^{6}	[25]
$\alpha_{\mathrm{s,t}} = 0.7$		
Termination MCR-MCR		
$k_{\mathrm{t,tt}}(\mathrm{L}\cdot\mathrm{mol}^{-1}\cdot\mathrm{s}^{-1}) = 0.01k_{\mathrm{t,ss}}$	1.3×10^{5}	This work
$\alpha_{\mathrm{t,t}} = 0.9$		
Density		
$\rho_{AM/H2O}(\mathrm{g}\cdot\mathrm{mL}^{-1}) = (-0.0002T^{2}(^{\circ}C^{-2}) + 0.0087T(^{\circ}C^{-1}) - 0.2493){w'_{\mathrm{M}}}^{2} + (6\times10^{-5}T^{2}(^{\circ}C^{-2}) - 0.0023T(^{\circ}C^{-1}) - 0.1382)w'_{\mathrm{M}} + (-6\times10^{-6}T^{2}(^{\circ}C^{-2}) + 0.0003T(^{\circ}C^{-1}) - 1.0048)$	1.0028	[12]

*evaluated at 40 °C and 20 wt% monomer

4.3.1 Fit of the Model to the Measured Conversion Profiles

Figure 4.2, Figure 4.3, and Figure 4.4 compare the simulated monomer conversion profiles to batch polymerizations with varying initial AM content and conversions measured by in-situ NMR at 40, 50 and 70 ^{o}C, respectively. Repeat runs are shown on the plots to demonstrate the experimental variability for experiments conducted at the same condition. Overall, the fit of the model to the experimental data is good, with the only notable deviation seen for the experiment conducted at 20 wt% AM at 50 ^{o}C (Figure 4.3) in the region between 50 and 90 % conversion. Comparing the fit at these conditions to the variability of repeat runs (Figure 4.2), it is uncertain whether this is a model deficiency or whether the agreement is within experimental variability; a more complete analysis is presented later. The fact the data is fit at 40 wt% monomer indicates that the model does not lose its validity at high monomer concentrations. Overall, the current model predicts the overwhelming majority of the data using the parameters measured as reported in the previous section. This is also true for experiments with varying initiator concentration at constant temperature and initial AM content, as shown in Appendix A.

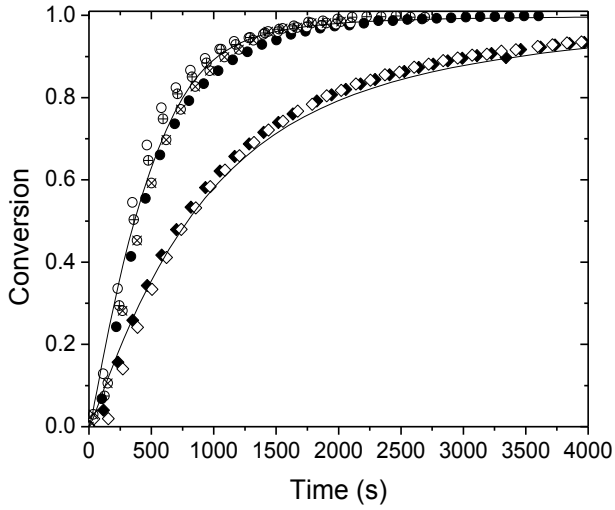

Figure 4.2 Experimental batch monomer conversion data (symbols) and predictions (lines) at 40 ^{o}C, 0.22 wt% V-50 for two experiments at 5 (♦), and four experiments at 40 (●) wt% AM.

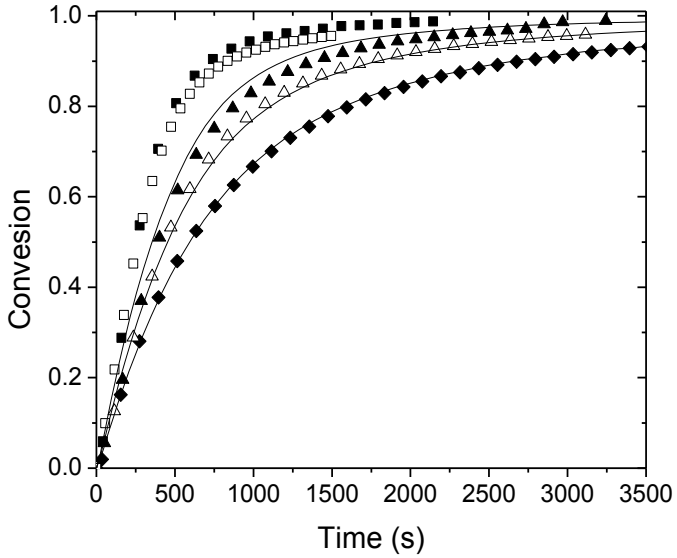

Figure 4.3 Experimental batch monomer conversion data (symbols) and predictions (lines) at 50 ºC, 0.08 wt% V-50 for 5 (♦), 10 (▲), and 20 (■) wt% AM.

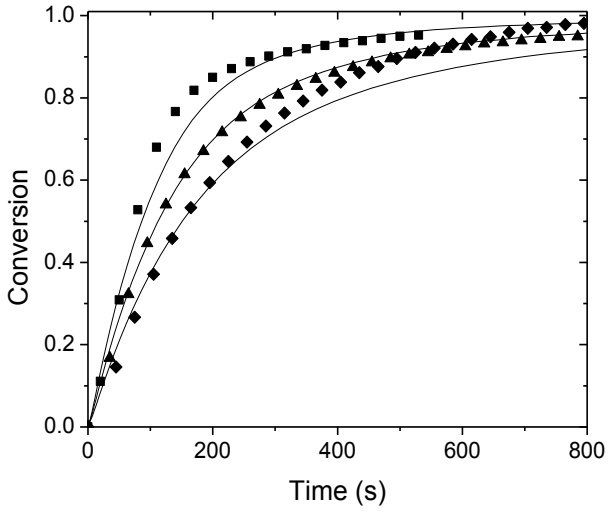

Figure 4.4 Experimental batch monomer conversion data (symbols) and predictions (lines) at 70 ºC, 0.08 wt% V-50 for 5 (♦), 10 (▲), and 20 (■) wt% AM.

4.3.2 Fit of the Model to the Measured Molecular Mass Data

Table 4.3 compares the measured and predicted values of polymer weight average (M_w) molar masses and dispersities (PDI) of the MMDs measured by SEC, with the model fit of the M_w also visualized in Figure 4.5. These fits were obtained after using the data to estimate the importance of transfer to monomer by adjusting the C_{tr} ratio between 1×10^{-5} and 7×10^{-5} and comparing the resulting predicted value at 95 % conversion to the measured M_w value. The best-fit rate coefficient for each experiment was chosen based on the minimum value of the sum of least squares of the relative error ($SSE=\Sigma((M_{w,meas} - M_{w,pred})/M_{w,meas})^2$). The estimates showed no dependence on monomer concentration, and the variation with temperature was used to develop the Arrhenius fit summarized in Table 4.2. The resulting set of predicted M_w values yielded the lowest sum of least squares of the relative error for all of the experiments combined; Figure 4.5 compares the measured and predicted M_w values using a parity plot. Repeat injections were performed to ensure reproducibility of the M_w measurements. Data points represent the average value of the M_w measurements.

The model provides a reasonable representation of the effect of temperature and initial monomer content on polymer MWs. Figure 4.6, Figure 4.7, and Figure 4.8 compare the MMDs of the high conversion pAM samples synthesized at 40, 50, and 70 ^oC, respectively, for different monomer concentrations. The M_w are higher for increasing initial monomer concentrations as expected, but are strongly affected by temperature due to the higher radical flux at 70 ^oC vs 40 ^oC. Thus low temperatures and high initial monomer concentrations yield the highest M_w polymer. However, the predicted MMD, especially at higher temperatures, are broader than the experimental ones, as also seen in the higher PDI values (Table 4.3). The PDI values reported in other literature has been assumed to be 2,[19,24] reported to be below 2,[65] and to be on the order of 3,[88] indicating the difficulty in obtaining reliable values.

The model-predicted PDI at 5 wt% AM is significantly larger than those at 20 and 40 wt%, especially at higher temperatures. This broadening is a result of the backbiting reaction, which increases in importance relative to chain-growth with increased temperature and decreased monomer concentration. The final amount of short chain branches (the structure that results from monomer addition to the MCR formed by backbiting) in the polymer is predicted to be quite low: 0.1, 0.05 and 0.03 % (branches per monomer repeat unit in the polymer) for 5, 20, and 40 wt% AM, respectively at 40 ºC. Even at 90 ºC the predicted % SCB (0.6 % at 5 wt% AM) is below the detection limit of ^{13}C NMR, which is most likely why backbiting reactions were not associated with AM in the past. For polymers derived from AA[21] and BA,[89] the quarternary carbon peak can be observed using ^{13}C NMR, as the rate coefficients associated with backbiting are greater for these monomers compared to AM.[8,40] As discussed in the following section, even this relatively low amount of backbiting affects the AM conversion profiles significantly, leading to the observation that it is necessary to include the mechanism in the model in order to obtain the correct trends in the monomer conversion profiles (i.e., increasing polymerization rate with increasing initial monomer concentration), something not possible with the model developed by Kim and Hamielec.[24]

Table 4.3 Comparison of the measured and predicted weight-average molar mass (M_w) and dispersity (PDI) values of high-conversion polymer produced by aqueous-phase batch polymerization of acrylamide.

			Measured Values		Predicted Values	
Initial wt% AM	**Initial wt% V-50**	**Temp (°C)**	**M_w (avg) (kg·mol^{-1})**	**PDI**	**M_w (kg·mol^{-1})**	**PDI**
5	0.22	40	5.30×10^2	3.1	1.17×10^3	3.7
20	0.22	40	2.54×10^3	2.6	2.36×10^3	2.2
40	0.22	40	3.23×10^3	2.7	2.72×10^3	2.0
5	0.08	50	3.76×10^3	2.9	9.79×10^2	3.7
10	0.08	50	2.30×10^3	2.9	1.57×10^3	2.7
10	0.14	50	1.45×10^3	3.5	1.45×10^3	2.9
20	0.08	50	1.90×10^3	2.7	2.08×10^3	2.2
5	0.08	70	5.54×10^2	3.8	3.79×10^2	4.9
10	0.08	70	1.12×10^3	4.3	7.73×10^2	3.7
20	0.08	70	1.74×10^3	3.9	1.28×10^3	2.6

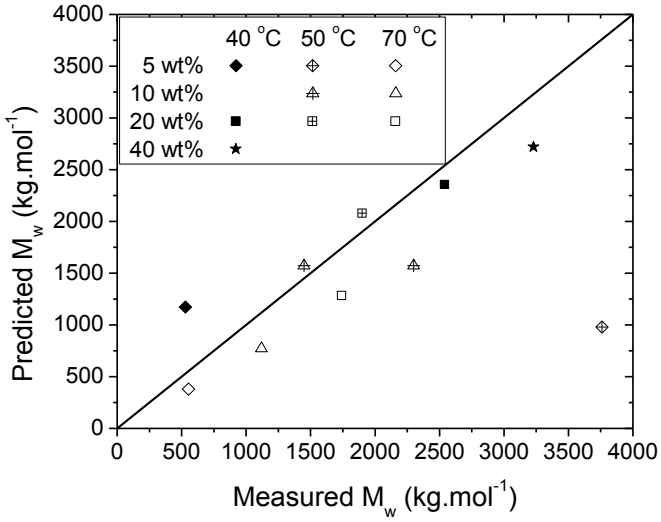

Figure 4.5 Comparison of the measured and predicted polymer weight-average molar mass (M_w) values for AM polymerization taken to high conversion at 40, 50, and 70 ºC at various monomer concentrations, as indicated in the legend.

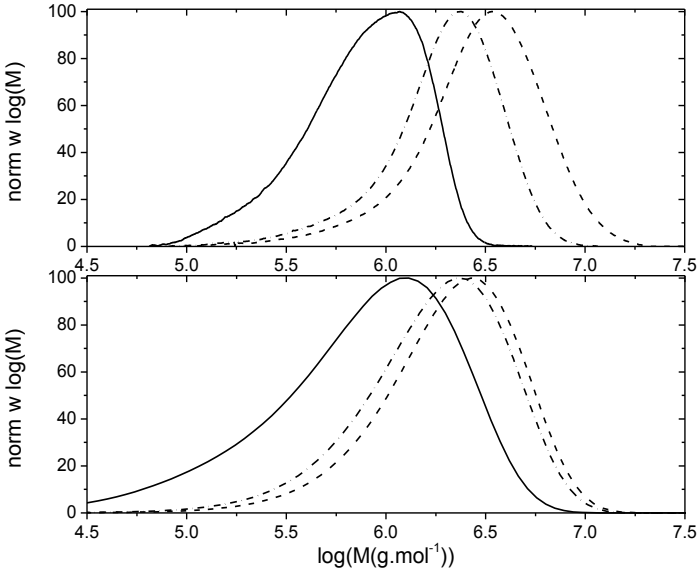

Figure 4.6 Measured (top) and simulated (bottom) pAM MMDs produced at 40 ºC with 0.22 wt% V-50 and initial monomer contents of 5 (solid line), 20 (dash-dotted line), and 40 (dashed line) wt% AM in aqueous solution.

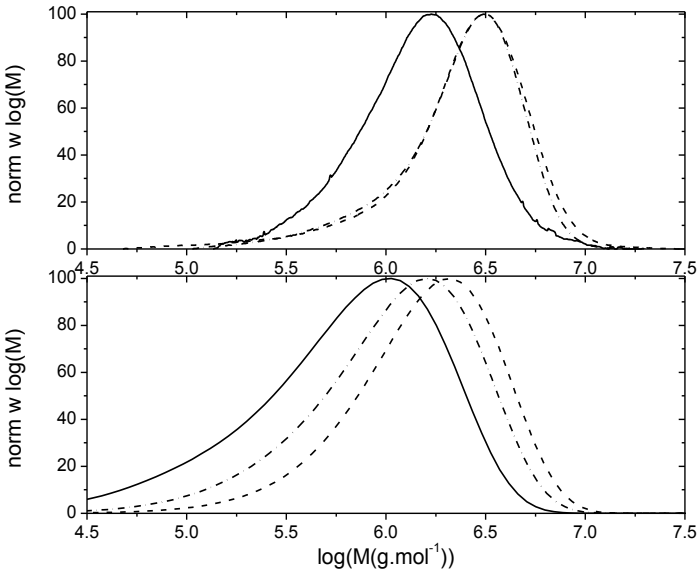

Figure 4.7 Measured (top) and simulated (bottom) pAM MMDs produced at 50 ºC with 0.082 wt% V-50 and initial monomer contents of 5 (solid line), 10 (dash-dotted line), 20 (dashed line) wt% AM in aqueous solution.

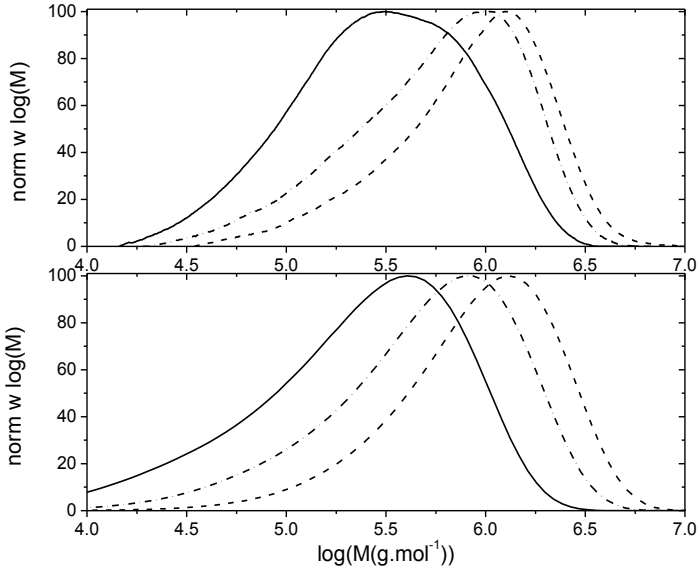

Figure 4.8 Measured (top) and simulated (bottom) pAM MMDs produced at 70 ºC and 0.082 wt% V-50 and initial monomer contents of 5 (solid line), 10 (dash-dotted line), 20 (dashed line) wt% AM in aqueous solution.

4.3.3 Sensitivity of the Model to Backbiting and Transfer to Monomer Reactions

The relative importance of backbiting and transfer to monomer reactions were studied by separately deactivating the mechanisms in the model and comparing the resulting simulated conversion profiles and high-conversion polymer MMDs to those of the full model. When the backbiting reaction is deactivated, the rate of monomer conversion is increased (Figure 4.9a), especially at low initial monomer concentrations, as no MCR species are formed. Although the conversion profiles show some sensitivity to the initial monomer concentration due to its influence on k_p and k_t, the influence is small relative to that of backbiting. It is evident that the backbiting reaction is instrumental in slowing the predicted conversion rate. Thus, it can be concluded that the inclusion of the backbiting reaction is necessary in order to adequately represent the experimental conversion profiles. The influence of backbiting on polymer MMDs mirrors that of its influence on rate. With lower initial monomer concentration, there is a lower polymerization rate and thus a corresponding decrease in the MMD. Thus, for the experiments with 5 wt% initial AM content, the simulations indicate that backbiting lowers M_w from 1.8 to 1.1×10^6 Da, while there is very little influence with 40 wt% initial AM (Figure 4.9b). It is also found that the backbiting mechanism broadens the distribution; in its absence, the predicted PDI values are much closer to 2. The influence of backbiting on PDI increases with decreasing monomer concentration, as the reaction increases in importance relative to chain growth.

As expected, deactivating the chain transfer to monomer reaction in the model with backbiting now included, has no influence on the simulated conversion profiles (not shown). Figure 4.10, however, illustrates the importance of the reaction to polymer MMDs. In the absence of transfer, the predicted M_w values increase significantly, especially at high monomer concentration; the predicted M_w value is greater by almost a factor of 20 at 40 ^oC and 40 wt% compared to the full model. From this, it can be concluded that transfer to monomer is an important reaction that limits the attainable M_w of pAM.

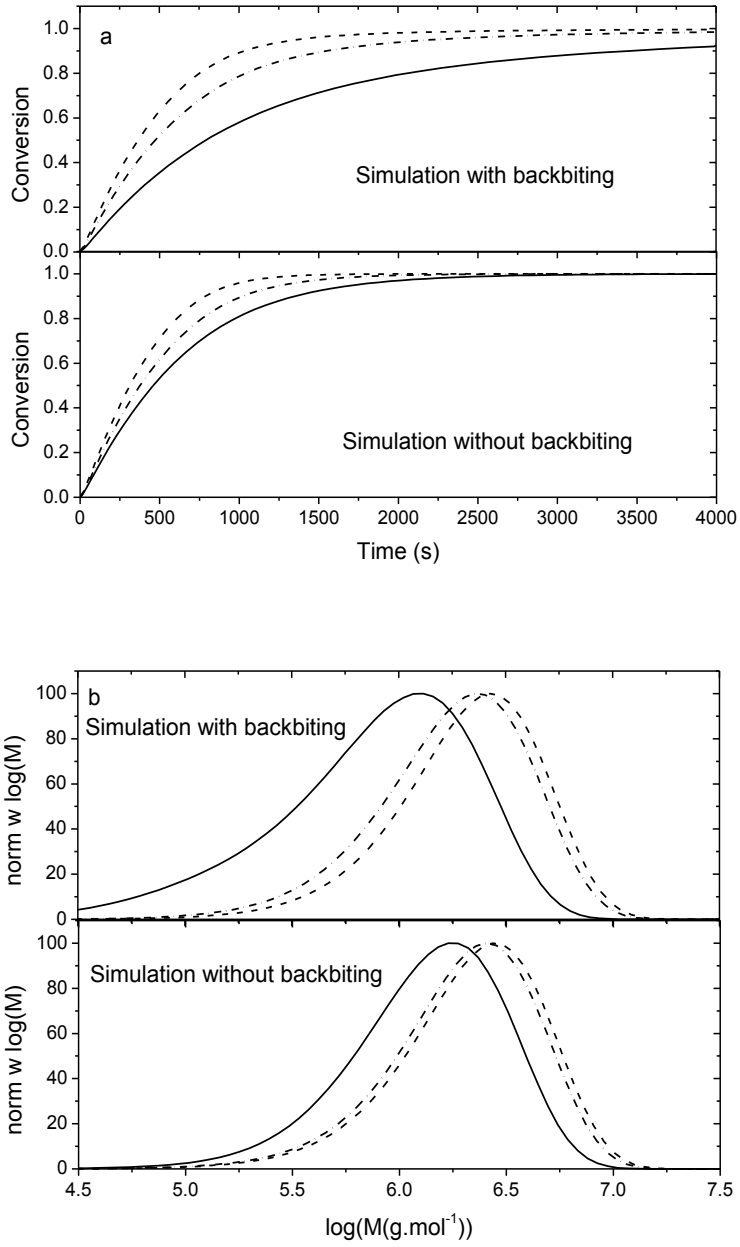

Figure 4.9 Comparison of the simulated conversion (a) and MMD (b) profiles with (top) and without (bottom) the presence of backbiting reactions at 40 ºC and 0.22 wt% V-50 at 5 (solid line), 20 (dash-dotted line), and 40 (dashed line) wt% AM.

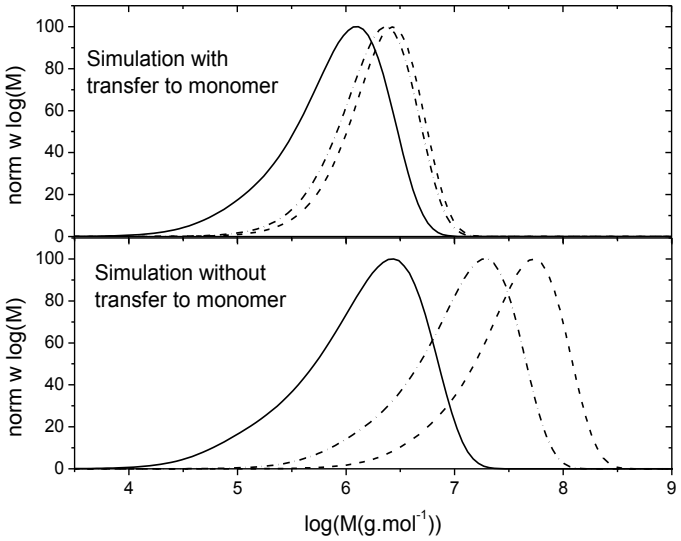

Figure 4.10 Comparison of the simulated MMD profiles with (top) and without (bottom) the presence of transfer to monomer at 40 ºC, 0.22 wt% V-50 at 5 (solid line), 20 (dash-dotted line), and 40 (dashed line) wt% AM.

4.3.4 Fit of the Model to Data Published in the Literature

In order to test the general performance of the model over a broader range of conditions, a comparison to literature data was also performed. The data was taken from Ishige and Hamielec (1973),[19] with the AM conversion measured by a combination of SEC and gravimetry, and Kim and Hamielec (1984),[24] where the conversion was measured using SEC. The model was amended to include the decomposition of 4,4'-azobis-4-cyanovaleric acid (ACV)[19] and potassium persulphate (KPS),[24] with the decomposition rates[90] outlined in Table 4.4, and initiator efficiency maintained at 0.8.

Table 4.4 Initiator decomposition of ACV and KPS.

Initiator	Rate Expression	Ref
ACV	$k_{\mathrm{d}}(\mathrm{s}^{-1}) = 8.96 \times 10^{16} \exp\left(-\frac{17\,080}{T/\mathrm{K}}\right)$	[90]
KPS	$k_{\mathrm{d}}(\mathrm{s}^{-1}) = 1.17 \times 10^{16} \exp\left(-\frac{7\,500}{T/\mathrm{K}}\right)$	[90]

The published conversion data in the two cited references are in a similar temperature range as the data collected as part of this work, between 40 and 70 °C, with lower monomer concentrations, ranging from 2 to 24 wt%. The initiator concentration is much lower compared to the ones used in this work, leading to reaction times on the order of several hours. Excellent fit of the model to the conversion profiles is shown in Figure 4.11 and Figure 4.13. Fits to all of the experimental data published in these papers can be found in Appendix A. As discussed previously, Hamielec and coworkers used several different model variants in an attempt to describe their experimental data, while the understanding captured in our representation provides an excellent fit over all conditions.

The predicted values of polymer average MW values (number-average M_n as well as M_w) as a function of time, plotted in Figure 4.12, underestimate the experimental values reported by Ishige and Hamielec by a factor between 1.5 and 3. In that work, the MW values were predominantly estimated by two different viscosity correlations, with the estimates themselves differing by a factor of 2.[19] However, both experimental estimates are higher than the predicted values based upon the C_{tr} rate coefficient estimated from our experimental M_w results. Although some attempts were made by Ishige and Hamielec to further verify the M_w values, none were sufficient to completely independently determine both M_n and M_w and for some analysis and in their model a PDI of 2 was assumed.[19] The M_w values published in the later work by Kim and Hamielec were determined using low-angle laser light scanning photometry at a wavelength of

632.8 nm and a dn/dc value of 0.1829 in water.[24] Our model predictions also underestimate these published M_w values by a factor between 2 and 4, the error increasing along with initial monomer concentration (Figure 4.13).

Although the model does not quantitatively predict the MW of this earlier published data, the relative trends with temperature, monomer concentrations, and initiator concentrations are captured. There are three possible explanations for the mismatch. Firstly, the M_w data sets can be matched by decreasing the chain transfer to monomer rate coefficient by a factor of 2 from its current value of 4.8×10^{-5} (Table 4.2); a constant C_{tr} value of 2.5×10^{-5} yields satisfactory prediction of the M_w for both studies from the Hamielec group; this value can thus be used as a lower bound of the transfer coefficient. Alternatively, the initiator efficiency, *f*, could be decreased to values of 0.5 and 0.2 for ACV and KPS, respectively, as suggested in reference [24]. By doing so, however, the fit to the M_w data is improved at the expense of the fit of the model to the conversion profiles. The third explanation is that the experimental methods used in the previous efforts, discussed above, led to an overestimation of polymer MWs.

The ability of the model to adequately predict the conversion profiles measured in the literature as well as data measured for this work validates the set of mechanisms and kinetic coefficients determined by PLP studies. Due to the difficulty in measuring high molecular weight water soluble polymers, the biggest uncertainty in the model is the transfer coefficient, C_{tr}, with the upper and lower bounds determined using available data. Despite the uncertainty in this rate coefficient, the predicted trends in M_w with temperature, monomer and initiator concentration match what is found experimentally.

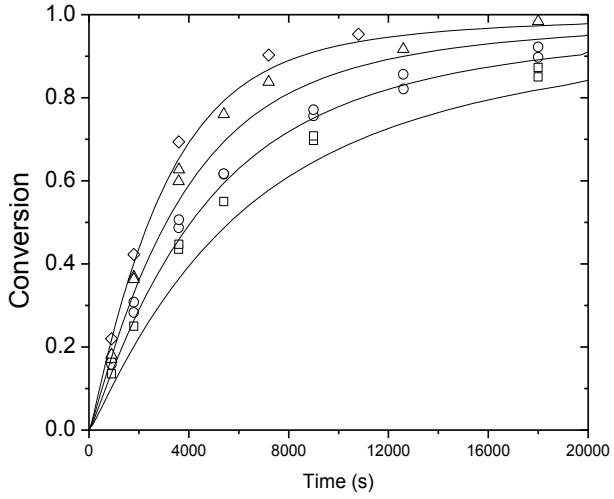

Figure 4.11 Experimental data from Ref [19] plotted against model predictions (lines) for the conversion profiles at 50 ºC and 0.02 wt% ACV at 2 (0.282 mol·L^{-1}) (□), 4 (0.563 mol·L^{-1}) (○), 8 (1.126 mol·L^{-1}) (Δ), and 16 (2.252 mol·L^{-1}) (◊) wt% AM in aqueous solution.

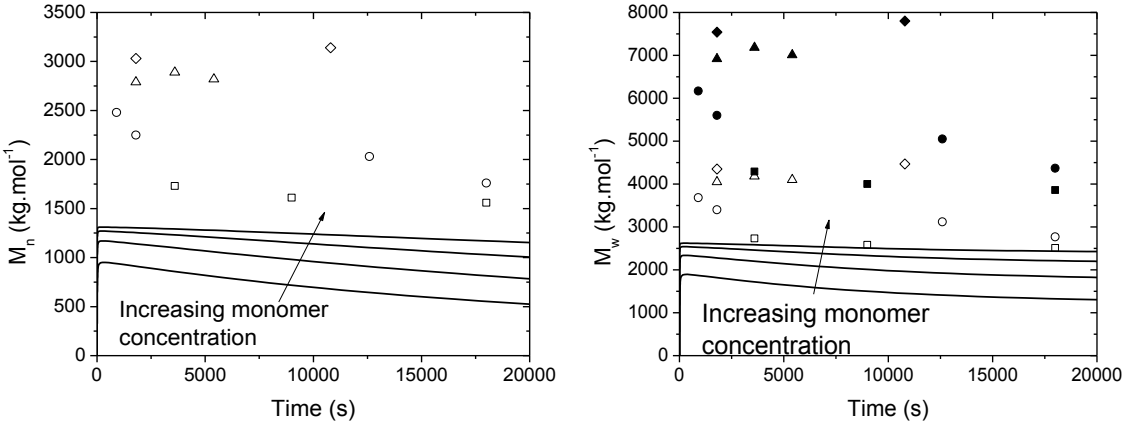

Figure 4.12 Experimental M_n (left) and M_w (right) data from Ref [19] plotted against model predictions. Experimental conditions and symbols as indicated in Figure 11, with open and closed symbols in b) indicating experimental M_w values estimated using two different assumptions.

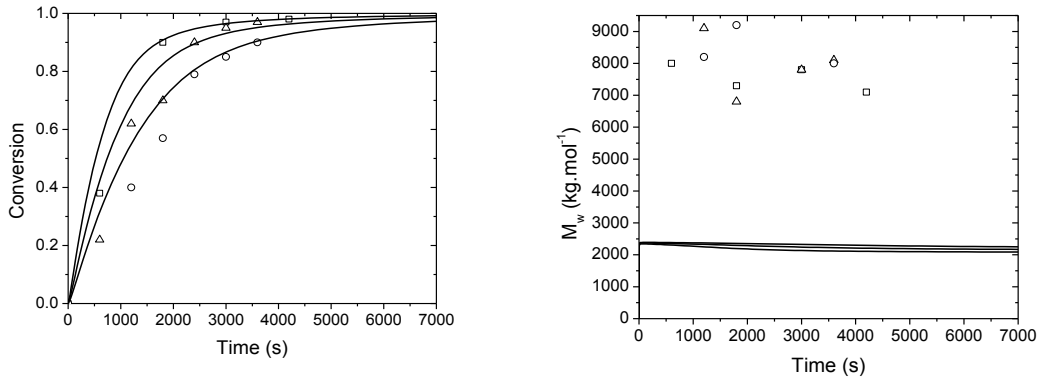

Figure 4.13 Experimental data (points) from Ref [24] plotted against model predictions (lines) for the batch conversion profiles (left plot) and polymer M_w values (right plot) obtained at 60 ºC and 24.2 wt% (3.4 mol·L^{-1}) AM in aqueous solution with 5.2×10^{-4} (□), 2.6×10^{-4} (Δ), and 1.3×10^{-4} (○) mol·L^{-1} KPS.

4.4 Evaluation of the Model

To better examine the quality of the fit to the conversion profiles the standard error of the estimate, which is analogous to the standard deviation of the fit, was calculated for every experiment run as part of this study as well as those taken from the literature[19,24] according to the following equation, with *y* indicating the experimental and *y*' the estimated value at a specific time point and *N* being the number of data points collected for the specific experiment:

$$\sigma_{\text{est}} = \sqrt{\frac{\sum_{N=1}^{N}(y - y')^2}{N}} \qquad 4.4$$

A total of 41 experiments were analyzed, with 68 % of those having σ_{est} less than 0.05, 83 % having an σ_{est} less than 0.10, and 98 % having σ_{est} less than 0.15. The standard errors were found to be independent of monomer concentration and temperature, as shown in Appendix A. The experiments with the highest error were generally run at lower initiator concentrations, especially for the KPS used by Kim and Hamielec. This may be due to the difficulty in obtaining reliable rate

data at conditions with lower radical generation rates, or might be an indication of a slight mismatch in the assumed value of KPS initiator decomposition rate. Considering that over 80 % of the experiments are well predicted without systematic variations, it can be concluded that the model, by accounting for the effect of monomer concentration on propagation kinetics and by including backbiting, adequately predicts conversion profiles over a broad range of conditions.

4.5 Conclusions

A kinetic model for the radical homopolymerization of AM in aqueous solution was successfully developed to explain the trends in batch monomer conversion profiles and polymer MWs as a function of temperature, monomer concentration, and initiator content. Based on recent PLP studies, the propagation and termination rate coefficients were expressed as a function of monomer concentration and temperature. In addition, the formation (via backbiting) and reaction of midchain radicals has been introduced to the model, based upon their detection by the SP-PLP-EPR technique. Although MCR formation during AM polymerization does not result in detectable branching levels by ^{13}C NMR, the mechanism captures the increase in conversion rate with increasing monomer concentration found experimentally, something that previous models in the literature were unable to accomplish. Difficulties in measuring molecular masses over one million Da result in scatter and inconsistencies between our experimental data and those published in the literature, leading to a transfer coefficient with an upper and lower bound. However, overall, the trends with monomer concentration and temperature in the measured M_w are also well captured in the model. The model developed in this chapter will serve as a basis to model the copolymerization of both non-ionized AA and ionized AA with AM.

Chapter 5

Kinetics and Modeling of Free Radical Non-Ionized AA and AM Copolymerization

5.1 Introduction

Successful models for batch monomer conversion profiles for monomer concentrations up to 40 wt% and temperatures between 40 and 70 °C for both non-ionized AA[21] and AM (Chapter 4) have been developed using independently measured rate coefficients for propagation, termination, and backbiting reactions. The progression of this work is to now model the copolymerization of non-ionized AA and AM over a range of monomer concentrations, compositions, and temperatures. In addition to the batch monomer conversion and composition data collected at 40 °C using an in-situ NMR technique,[23] data was collected at 70 °C at various monomer concentrations (5, 10, 20 wt%) and monomer compositions (f_{AM0} = 0.3, 0.5, 0.8) to verify the monomer concentration and composition changes with temperature.

As with all water soluble polymerization, the interactions between the monomer and the solvent must be considered in the model development for NVP,[14] MAA, [15,16] and AA[21,58] by implementing the rate coefficients as a function of the monomer concentration, as estimated by PLP-SEC experiments.[10,13,29,30,32–34] Additional complexity is introduced in the copolymer system as now the co-monomer must also be considered when discussing solvent/ solute interactions. AA is a weak acid with a pK_a of 4.37 [29] and remains in its non-ionized form when the weak base AM, predicted pK_a of 15.35,[91] is introduced as a co-monomer. Overall it is assumed that hydrogen bonding between the solvent, water, and the monomer still occurs. As will be shown later in this chapter, the AA and AM monomer interact with each other via hydrogen bonding as well, which may explain the increase in the copolymer propagation rate coefficient at intermediate co-monomer

compositions. Hydrogen bonding, or complexation, between pAA and pAM homo- and copolymers under non-reactive conditions have been studied in the literature as a function of temperature,[92] molar mass,[93] and copolymer composition[94] using a variety of experimental methods including viscosity and potentiometry,[92] measurement of a critical pH,[93] and using pyrene labeled polymers.[94] All studies suggest complexation between the carboxylic acid and amide groups. These complexes increase the rigidity of the polymer chains; chain stiffness increases with increasing molar mass,[93,95] decreasing temperature,[92] and increases at intermediate copolymer compositions (i.e. from $F_{AM} = 0.92$ to $F_{AM} = 0.57$) in the copolymer.[94] Although the final polymer properties are not the focus of this work, it is important to acknowledge the polymer interactions as the complexation of the side groups may explain the discrepancy between the simulation results and experimental data at 40 °C and the satisfactory fit at 70 °C, as discussed later in this chapter.

Prior to this work, rate coefficients relating to this copolymerization had not been measured and published in the scientific literature. Therefore, as part of this collaboration, the copolymer propagation rate was measured at Bratislava, and viscosity measurements were performed on co-monomer mixtures at various monomer compositions and concentrations in an attempt to understand the copolymer termination rate coefficient in Göttingen. The resulting observations are incorporated in the kinetic model. However, several of the rate coefficients, namely the termination, transfer to monomer, and backbiting related rate coefficients, remain unknown and assumptions as to their interactions are based on work done in the published literature. Different treatments of the termination rate are considered, including the geometric mean,[83,96–98] the Atherton North treatment which considers a linear change in the termination rate coefficient based on monomer composition,[99] and the Fukuda treatment which considers the copolymer termination rate coefficient to be inversely proportional to the friction coefficient.[100] As both monomers are known to undergo backbiting reactions, treatments to include the backbiting rate coefficient and the probability of the identity of the antepenultimate unit were considered. Cross-rate coefficients

needed for backbiting, addition to the MCR, and transfer to monomer were approximated, assuming the same relative reactivity for the addition of co-monomer as for the propagation step, assuming the terminal model. The sensitivity of the overall model fit to the unknown rate coefficients is examined as part of this chapter.

5.2 Experimental

5.2.1 Measurement of Monomer Conversion and Composition Profiles

The monomers, AA (99%, Sigma Aldrich) and AM (99+%, Sigma Aldrich), D_2O (99.9%, Cambridge Isotope Laboratories Inc.), and V-50 initiator (97%, Sigma Aldrich) were bought and used without further purification. The preparation of the reaction solutions remained the same as discussed in our previous work.[23] The collection of the conversion and monomer compositions remained the same, with the exception that fewer scans were used to obtain each NMR spectra due to the faster conversion rate at 70 ^oC relative to 40 ^oC. Additionally, the time between each spectra acquisition was decreased to 50 seconds, compared to the 120 seconds used at 40 ^oC in order to measure more data points during the polymerization. No decrease in the quality of the spectra was observed as the number of scans per spectra was decreased.

5.2.2 Molecular Mass Measurements

SEC measurements were conducted in Bratislava where the conditions developed and verified as part of the collaboration of this project. The same set-up was used for the MW analysis as described in Chapter 4. The dn/dc values used for pAA and pAM were 0.141 and 0.132 $mL \cdot g^{-1}$, respectively. The reported Mw values were obtained by applying a composition averaged calibration.

5.3 Copolymerization Data at 70 ^oC

Monomer conversion and composition were collected using the in-situ NMR method at 70 ^oC, with 5, 10, and 20 wt% monomer in D_2O and monomer compositions of f_{AM0} = 0.3, 0.5, and

0.8, with the results plotted in Figure 5.1 and Figure 5.2. The monomer composition in Figure 5.1 show that the consumption of monomer as a function of conversion remains independent of monomer concentration at higher temperatures and that the reactivity ratios remain constant in the given temperature range with $r_{AA} = 1.24$ and $r_{AM} = 0.55$, as determined for the data at 40 ^{o}C (Chapter 3).[23]

Consistent with the water soluble copolymerization of AA and AM at 40 ^{o}C, the rate of conversion increases with increasing monomer concentration and is relatively independent of the monomer composition. As the primary goal of the experiments at higher temperatures was to examine for a temperature dependency on the reactivity ratios, conversion profiles of the homopolymerizations at the same initiator concentrations were not collected. Figure 5.1 plots the conversion profiles of the copolymerization experiments at 70 ^{o}C, as well as the predictions of the AA and AM homopolymerizations, using the models previously discussed. The model predictions of the AA and AM homopolymerizations are very close to each other, something that was not observed at 40 ^{o}C. Additionally, at 70 ^{o}C the experimental copolymer conversion profiles are faster than the predictions for both of the homopolymerizations.

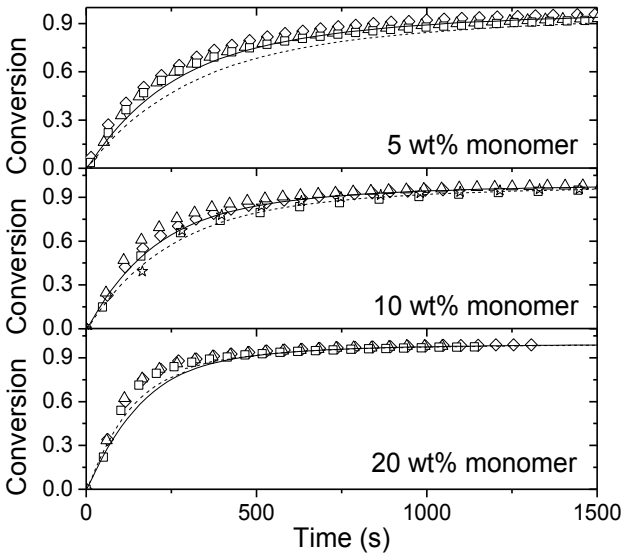

Figure 5.1 Experimental batch conversion profiles collected at 70 ºC and 0.04 wt% V-50 with total monomer content of 5 (top), 10 (middle) and 20 (bottom) wt%, and initial f_{AM0} of 0.8 (◊), 0.5 (Δ), and 0.3 (◊). The lines are model predictions for the homopolymerization of AA (solid line) and AM (dashed line) at the same experimental conditions.

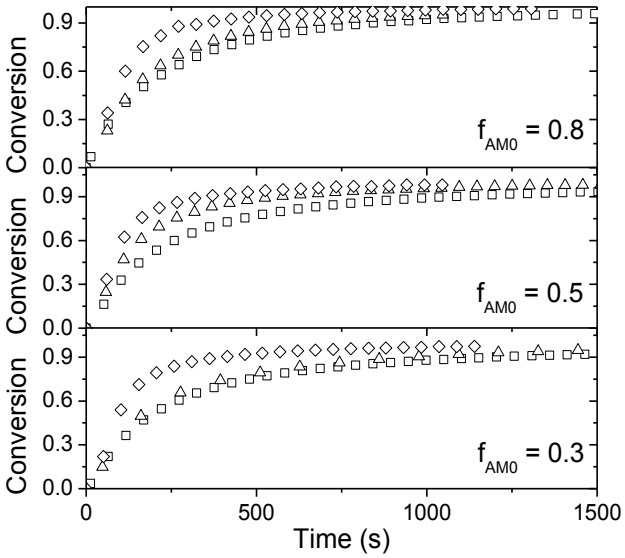

Figure 5.2 Experimental batch conversion profiles collected at 70 ºC and 0.04 wt% V-50 with initial f_{AM0} of 0.8 (top), 0.5 (middle), and 0.3 (bottom) and total monomer content of 5 (□), 10 (Δ) and 20 (◊) wt%.

The faster conversion rate overall as well as relative to the homopolymerizations model predictions led us to examine the claim of isothermal conditions. Previous work had shown that NMR peak positions shift at a rate of 0.01 ppm/ ^{o}C, however the peaks also shift in the presence and growth of the polymer peak.[23] Due to the compounding effects of temperature and polymer, a maximum exotherm can only be estimated.[23] The change in the peak positions of AA and AM relative to their position at no conversion were plotted for 40 and 70 ^{o}C for experiments run at 5 wt% and monomer compositions of f_{AM0} = 0.5 in Figure 5.3. For the experiment at 70 ^{o}C in Figure 5.3, the shape of the peak shift with monomer conversion reaches a maximum at 30 % conversion, which could be an indication of an exotherm. However, the difference in ppm relative to no conversion indicates that this exotherm is less than 2 ^{o}C and subsides towards higher monomer conversions. The discrepancy in the difference in ppm at high conversion between the experiments run at 40 and at 70 ^{o}C is likely related to the difference in the molecular weight of the polymer produced during the reaction. In light of this comparison of the data at 40 and 70 ^{o}C, it is possible that at 40 ^{o}C isothermal conditions are in fact achieved as the difference in the ppm steadily increases with monomer conversion. At 70 ^{o}C then the conclusion can be made that a small exotherm is observed at low (less than 50 %) conversions but then the sample returns back to the reaction temperature. It is assumed that this is true for all monomer concentrations at 70 ^{o}C; this analysis could not be done at the higher monomer concentrations as the peak positions at 0 % conversion are not available. Another indication that near isothermal conditions are maintained at 70 ^{o}C is by considering the good model fit of the AM homopolymerization at this temperature with twice the initiator content (0.08 wt%, see Figure 4.4). Since no exotherm was considered for the homopolymerization at a faster conversion rate, it is unlikely that the copolymerization would suffer from an exotherm. Therefore, near isothermal conditions are assumed for the data collected at both 40 and 70 ^{o}C.

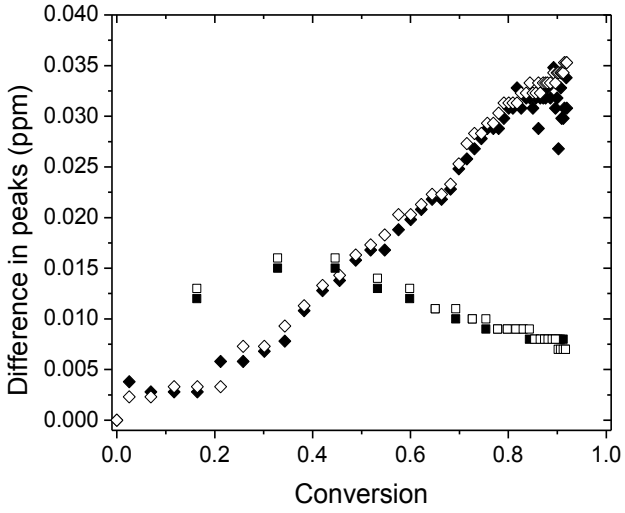

Figure 5.3 Shift in the AA (filled symbols) and AM (empty symbols) monomer peak positions for experiments run at 5 wt% monomer and f_{AM0} = 0.5 at 40 ºC and 0.22 wt% V-50 (♦, ◊) and 70 ºC and 0.04 wt% V-50 (■, □). The difference in peak position is relative to the initial peak position at 0 % conversion.

The monomer composition drift with conversion at 70 ºC is plotted in Figure 5.4 for various initial monomer concentrations and compositions. As was observed for the copolymerization at 40 ºC, the monomer composition drift is independent of monomer concentration between 5 and 20 wt% monomer. When the data collected at 70 ºC is compared to the data at 40 ºC (Figure 5.4), it can be observed that the reactivity ratios are independent of temperature between 40 and 70 ºC and the reactivity ratios estimated in Chapter 3 will be used for all future work for the copolymerization of non-ionized AA and AM.

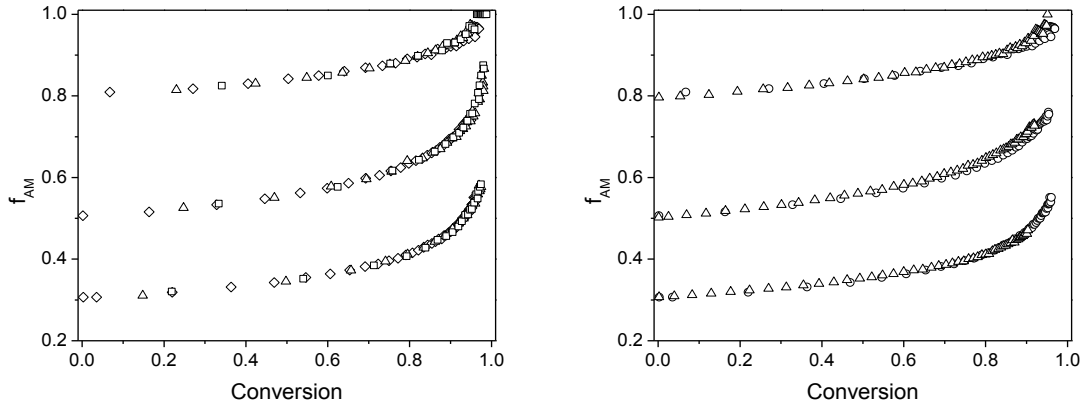

Figure 5.4 Experimental monomer composition as a function of conversion at 70 ºC and 0.04 wt% V-50 at monomer concentrations of 5 (◇), 10 (△), 20 (□) (left plot), and a comparison of the data collected at 5 wt% at 40 ºC and 0.2 wt% V-50 (△) and 70 ºC and 0.04 wt% V-50 (○) (right plot).

5.4 Estimation of Copolymer Propagation Rate Coefficient

The work discussed in this section was performed in close collaboration with PISAS, where I participated in the experimental design of the PLP-SEC study, running PLP experiments and preparing the SEC samples during my four month scientific visit to Slovakia in 2013. Water soluble polymers are notoriously difficult to analyze using SEC and with the absence of AA/AM copolymer standards, the SEC methodology had to be verified for this copolymer. The expertise in this area remains in Bratislava and therefore my discussion focuses on the fitting of the propagation rate coefficient to the terminal and penultimate model and the discussion of the final results.

The principle behind PLP-SEC experiments is to measure the rate of monomer addition, k_p, by measuring the polymer chain growth occurring in between the laser pulses according to

$$L_i = ik_p[\mathrm{M}]t_0 \qquad 5.1$$

Where L_i refers to the units of monomer, or the chain length, for each pulse *i*, and with [M] being the total monomer concentration, and t_o referring to the flash interval or the inverse of the laser frequency. Assuming that chain growth predominantly only occurs for one pulse interval, Equation 5.1can be solved for $i = 1$ and rearranged:

$$k_p = \frac{L_1}{[M]t_0} \tag{5.2}$$

where

$$L_1 = \#\ units\ of\ monomer = \frac{MW_1}{MW_{MP}} \tag{5.3}$$

with MW_{i1} referring to the molecular weight of the first inflection point and MW_{MP} the average molecular weight of the monomer units in the copolymer, which is a function of the copolymer composition, *F*, assuming negligible composition drift at low conversion and terminal kinetics. Thus,

$$MW_{MP} = F_{AM}MW_{AM} + F_{AA}MW_{AA} \tag{5.4}$$

For the AA and AM copolymerization it was shown previously that the copolymer composition can be described by the terminal model with $r_{AA} = 1.24$ and $r_{AM} = 0.55$:[23]

$$F_{AM} = \frac{r_{AM}f_{AM}^2 + f_{AM}f_{AA}}{r_{AM}f_{AM}^2 + 2f_{AM}f_{AA} + r_{AA}f_{AA}^2} \tag{5.5}$$

and $F_{AA} = 1 - F_{AM}$. The initial monomer concentration term can be rewritten in terms of the composition averaged molecular mass of the monomer MW_M, mass fraction of monomer mixture, w'_M, total density of the reaction solution, ρ_T:

$$[M] = \frac{\rho_T * w'_M}{MW_M} \tag{5.6}$$

Adjusting the monomer concentration to the average of the total conversion of the PLP experiment, the copolymer propagation rate coefficient can be estimated as follows, with *x* being the monomer conversion obtained at the end of the PLP experiment:

$$k_{\mathrm{p}}^{\mathrm{cop}} = \frac{\frac{MW_1}{MW_{\mathrm{MP}}}}{\frac{\rho_{\mathrm{T}} * w'_{\mathrm{M}}}{MW_{\mathrm{M}}}(1 - 0.5x)t_0} \qquad 5.7$$

The conversion is divided in half, representing the average conversion between the beginning and end of the experiment. This equation was used to estimate the propagation rate coefficient at various temperatures, monomer compositions, and concentrations. As the propagation rate coefficients of both monomers in this system are known to be functions of monomer concentration, the experimental design included various experiments to study the effect of monomer concentration. PLP-SEC experiments were conducted at various temperatures (20 to 60 °C in 20 °C increments), monomer compositions (f_{AM} = 0.1 to 0.9 in increments of 0.2), and concentrations (10 and 30 wt%), with results shown as the symbols in Figure 5.5. The experimental data show an increase of the propagation rate coefficient at intermediate co-monomer compositions at all of the temperatures (Figure 5.5a) and a decrease with increasing monomer concentration (Figure 5.5b). My contribution to this work was to fit these data points to the terminal and penultimate model, required for the implementation of the representation into the mechanistic model.

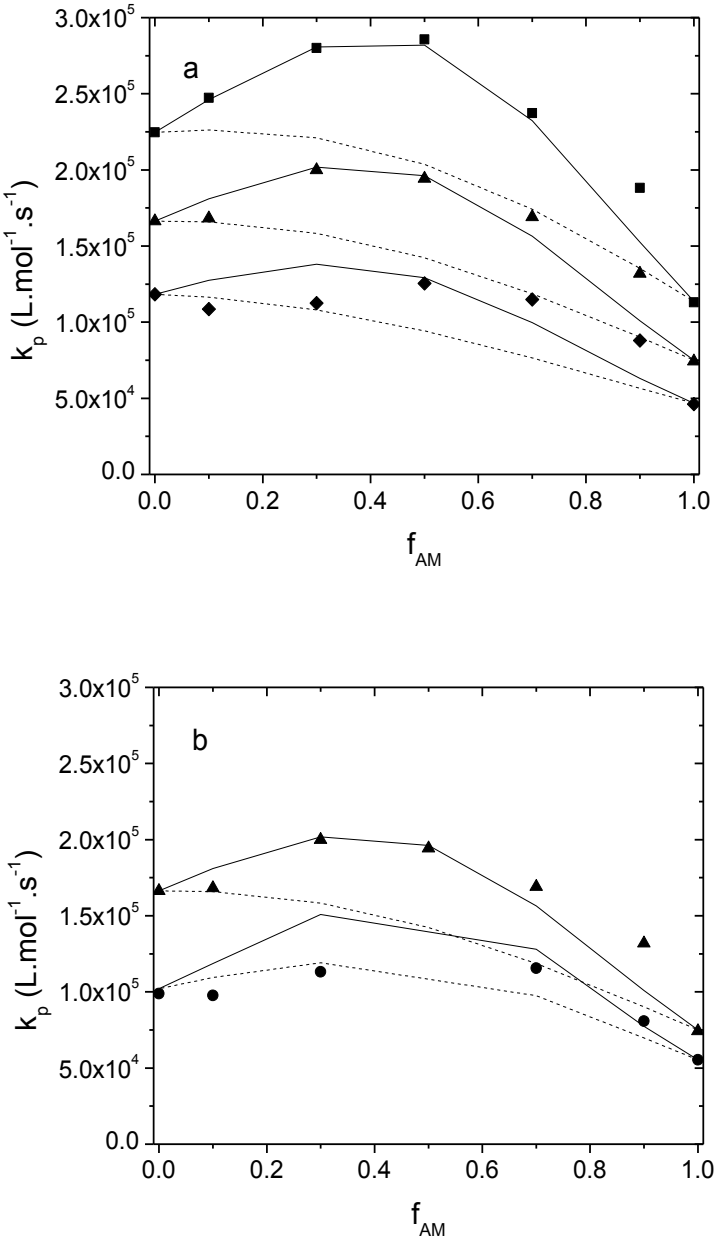

Figure 5.5 Copolymer propagation rate coefficient (k_p^{cop}) as determined by PLP-SEC (symbols) and predicted using the terminal (dashed line) and penultimate model (solid line) plotted as a function of monomer composition at 10 wt% monomer (a) for temperatures of 20 (♦), 40 (▲), and 60 (■) ºC, and at 40 ºC (b) for 10 (▲) and 30 (●) wt% monomer.

For copolymer systems, the simplest model that describes the addition of the monomer units to the growing polymer chain is the terminal model;[45] the same model used to estimate the reactivity ratios from the monomer composition in this work.[23] In this model, the identity of the terminal unit dictates the rate of the addition of the monomer and leads to four possible propagation steps, as summarized in Table 5.1.[45]

Table 5.1 Propagation steps defined by the terminal model.

$P_n^{AA} + AA \xrightarrow{k_p^{AA}} P_{n+1}^{AA}$
$P_n^{AA} + AM \xrightarrow{k_p^{AA\cdot AM}} P_{n+1}^{AM}$
$P_n^{AM} + AM \xrightarrow{k_p^{AM}} P_{n+1}^{AM}$
$P_n^{AM} + AA \xrightarrow{k_p^{AM\cdot AA}} P_{n+1}^{AA}$

Using the reactivity ratios ($r_{AA} = k_p^{AA}/k_p^{AA\cdot AM}$ and $r_{AM} = k_p^{AM}/k_p^{AM\cdot AA}$) and the homopropagation rate coefficients of the monomer, a propagation rate coefficient for the copolymer is defined as:[100]

$$k_p^{\text{cop,term}} = \frac{r_{AA}f_{AA}^2 + 2f_{AA}f_{AM} + r_{AM}f_{AM}^2}{\frac{r_{AA}f_{AA}}{k_p^{AA}} + \frac{r_{AM}f_{AM}}{k_p^{AM}}} \qquad 5.8$$

For some copolymerization systems both the terminal and the penultimate unit on the polymerizing chain affect the addition of monomer. Eight possible propagation steps are defined for the penultimate model, as specified in Table 5.2.[101]

Table 5.2 Propagation steps defined by the penultimate model.

$P_n^{AA\cdot AA} + AA \xrightarrow{k_p^{AA}} P_{n+1}^{AA\cdot AA}$	$P_n^{AA\cdot AM} + AM \xrightarrow{k_p^{AA\cdot AM\cdot AM}} P_{n+1}^{AM\cdot AM}$
$P_n^{AM\cdot AA} + AA \xrightarrow{k_p^{AM\cdot AA\cdot AA}} P_{n+1}^{AA\cdot AA}$	$P_n^{AM\cdot AM} + AM \xrightarrow{k_p^{AM}} P_{n+1}^{AM\cdot AM}$
$P_n^{AA\cdot AA} + AM \xrightarrow{k_p^{AA\cdot AA\cdot AM}} P_{n+1}^{AA\cdot AM}$	$P_n^{AA\cdot AM} + AA \xrightarrow{k_p^{AA\cdot AM\cdot AA}} P_{n+1}^{AM\cdot AA}$
$P_n^{AM\cdot AA} + AM \xrightarrow{k_p^{AM\cdot AA\cdot AM}} P_{n+1}^{AA\cdot AM}$	$P_n^{AM\cdot AM} + AA \xrightarrow{k_p^{AM\cdot AM\cdot AA}} P_{n+1}^{AM\cdot AA}$

Many copolymerization systems, such as STY/BMA (styrene/ butyl methacrylate) exhibit penultimate effects in the copolymer propagation rate coefficient, but not in the copolymer composition.[102] For these cases, $r_{ij} = r_{ii}$: for the copolymerization of AA and AM, the reactivity ratios $r_{AA} = k_p^{AA}/k_p^{AA\cdot AA\cdot AM} = k_p^{AM\cdot AA\cdot AA}/k_p^{AM\cdot AA\cdot AM}$ and $r_{AM} = k_p^{AM}/k_p^{AM\cdot AM\cdot AA} = k_p^{AA\cdot AM\cdot AM}/k_p^{AA\cdot AM\cdot AA}$ are estimated from copolymer composition, as discussed earlier. It is only the radical ratios, defined as $s_{AA} = k_p^{AM\cdot AA\cdot AA}/k_p^{AA}$ and $s_{AM} = k_p^{AA\cdot AM\cdot AM}/k_p^{AM}$ that must be estimated from the copolymer propagation rate data.

The overall copolymer propagation rate coefficient is defined as:[100]

$$k_p^{cop,pen} = \frac{r_{AA}f_{AA}^2 + 2f_{AA}f_{AM} + r_{AM}f_{AM}^2}{\frac{r_{AA}f_{AA}}{k_p^{AA}} + \frac{r_{AM}f_{AM}}{k_p^{AM}}}$$

$$\overline{k_p^{AA}} = \frac{k_p^{AA}[r_{AA}f_{AA} + f_{AM}]}{r_{AA}f_{AA} + \frac{f_{AM}}{s_{AA}}} \qquad 5.9$$

$$\overline{k_p^{AM}} = \frac{k_p^{AM}[r_{AM}f_{AM} + f_{AA}]}{r_{AM}f_{AM} + \frac{f_{AA}}{s_{AM}}}$$

In Figure 5.5 the predicted propagation rate coefficient as calculated by the terminal (dashed lines) and the penultimate model with $s_{AA} = 4.0$ and $s_{AM} = 1.5$ (solid lines) are shown. It is evident that the terminal model is insufficient to describe the measured propagation rate data, as it does not capture the increase in the rate coefficient at the intermediate monomer compositions and therefore the penultimate model must be implemented to represent the data.

The homopropagation rate coefficients used in Equations 5.8 and 5.9 are calculated on a co-monomer free basis, following an experimental investigation that indicated the propagation rate coefficients do not significantly change in the presence of the saturated analogue of the co-monomer. Table 5.3 shows the measured propagation rate coefficient of AM in the presence of the saturated analogue of AA, propionic acid (PA). Although not tabulated here, the results for AA polymerized in the presence of propionamide, the saturated analogue of AM, give the equivalent conclusions. This finding is somewhat surprising, as the measurement of AA,[10] MAA,[33] and NVP[13] homopropagation rate coefficients in the presence of their saturated analogue showed a decrease in the measured coefficient, a result confirmed by theoretical studies.[37,38,103] For the measurement of the homopropagation rate coefficient in the presence of the saturated analogue of the co-monomer however, little change in the measured rate coefficient is observed, as shown in the tabulated results.

Table 5.3 k_p values of AM measured in the presence of propionic acid (PA) at 20 °C.

wt % AM	wt% PA	k_p (L·mol^{-1}·s^{-1})
5	0	50 000
5	5	54 300
5	5	60 400
10	0	46 000
15	0	42 500
15	15	39 000
15	15	37 900
30	0	34 500

5.5 Model Development

The copolymerization model follows the same format as the AA[21] and AM (Chapter 4) models; the reaction mechanisms comprise of conventional free radical kinetics[1] and backbiting reactions.[27] As discussed previously, the rate coefficients for the homopolymerizations and the copolymer propagation rate coefficient are known. All other copolymer rate coefficients are based on treatments found elsewhere in the literature,[83,96,102] with additional assumptions required as this model considers two monomers that undergo backbiting reactions. The complete reaction mechanism used for the copolymerization of non-ionized AA and AM is summarized in Table 5.4. The rate coefficients for the AA and AM homopolymerizations and copolymer ratios are outlined in Table 5.5.

Table 5.4 Set of reaction steps for the free radical copolymerization of non-ionized acrylic acid (AA) and acrylamide (AM)

Initiation	
$\mathrm{I} \xrightarrow{k_\mathrm{d}} 2f\mathrm{I}^{\mathrm{rad}}$	
$\mathrm{I}^{\mathrm{rad}} + \mathrm{AM} \xrightarrow{k_\mathrm{p}^{\mathrm{AM}}} \mathrm{P}_1^{\mathrm{AM}}$	$\mathrm{I}^{\mathrm{rad}} + AA \xrightarrow{k_\mathrm{p}^{\mathrm{AA}}} P_1^{\mathrm{AA}}$
Chain Propagation	
$\mathrm{P}_\mathrm{n}^{\mathrm{AA\cdot AA}} + \mathrm{AA} \xrightarrow{k_\mathrm{p}^{\mathrm{AA}}} \mathrm{P}_{\mathrm{n+1}}^{\mathrm{AA\cdot AA}}$	$\mathrm{P}_\mathrm{n}^{\mathrm{AA\cdot AM}} + \mathrm{AM} \xrightarrow{k_\mathrm{p}^{\mathrm{AA\cdot AM\cdot AM}}} \mathrm{P}_{\mathrm{n+1}}^{\mathrm{AM\cdot AM}}$
$\mathrm{P}_\mathrm{n}^{\mathrm{AM\cdot AA}} + \mathrm{AA} \xrightarrow{k_\mathrm{p}^{\mathrm{AM\cdot AA\cdot AA}}} \mathrm{P}_{\mathrm{n+1}}^{\mathrm{AA\cdot AA}}$	$\mathrm{P}_\mathrm{n}^{\mathrm{AM\cdot AM}} + \mathrm{AM} \xrightarrow{k_\mathrm{p}^{\mathrm{AM}}} \mathrm{P}_{\mathrm{n+1}}^{\mathrm{AM\cdot AM}}$
$\mathrm{P}_\mathrm{n}^{\mathrm{AA\cdot AA}} + \mathrm{AM} \xrightarrow{k_\mathrm{p}^{\mathrm{AA\cdot AA\cdot AM}}} \mathrm{P}_{\mathrm{n+1}}^{\mathrm{AA\cdot AM}}$	$\mathrm{P}_\mathrm{n}^{\mathrm{AA\cdot AM}} + \mathrm{AA} \xrightarrow{k_\mathrm{p}^{\mathrm{AA\cdot AM\cdot AA}}} \mathrm{P}_{\mathrm{n+1}}^{\mathrm{AM\cdot AA}}$
$\mathrm{P}_\mathrm{n}^{\mathrm{AM\cdot AA}} + \mathrm{AM} \xrightarrow{k_\mathrm{p}^{\mathrm{AM\cdot AA\cdot AM}}} \mathrm{P}_{\mathrm{n+1}}^{\mathrm{AA\cdot AM}}$	$\mathrm{P}_\mathrm{n}^{\mathrm{AM\cdot AM}} + \mathrm{AA} \xrightarrow{k_\mathrm{p}^{\mathrm{AM\cdot AM\cdot AA}}} \mathrm{P}_{\mathrm{n+1}}^{\mathrm{AM\cdot AA}}$
Transfer to Monomer	
$\mathrm{P}_\mathrm{n}^{\mathrm{AM}} + \mathrm{AM} \xrightarrow{k_\mathrm{tr}^{\mathrm{AM}}} \mathrm{D}_\mathrm{n} + \mathrm{P}_1^{\mathrm{AM}}$	$\mathrm{P}_\mathrm{n}^{\mathrm{AA}} + \mathrm{AA} \xrightarrow{k_\mathrm{tr}^{\mathrm{AA}}} \mathrm{D}_\mathrm{n} + \mathrm{P}_1^{\mathrm{AA}}$
$\mathrm{P}_\mathrm{n}^{\mathrm{AM}} + \mathrm{AA} \xrightarrow{k_\mathrm{tr}^{\mathrm{AM\cdot AA}}} \mathrm{D}_\mathrm{n} + \mathrm{P}_1^{\mathrm{AA}}$	$\mathrm{P}_\mathrm{n}^{\mathrm{AA}} + \mathrm{AM} \xrightarrow{k_\mathrm{tr}^{\mathrm{AA\cdot AM}}} \mathrm{D}_\mathrm{n} + \mathrm{P}_1^{\mathrm{AM}}$

Termination SPR-SPR

$$P_n^{AM} + P_m^{AM} \xrightarrow{(1-\alpha_{ss})k_{t,ss}^{cop}} D_{n+m} \,/\, \xrightarrow{\alpha_{ss}k_{t,ss}^{cop}} D_n + D_m$$

$$P_n^{AA} + P_m^{AA} \xrightarrow{(1-\alpha_{ss})k_{t,ss}^{cop}} D_{n+m} \,/\, \xrightarrow{\alpha_{ss}k_{t,ss}^{cop}} D_n + D_m$$

$$P_n^{AA} + P_m^{AM} \xrightarrow{(1-\alpha_{ss})k_{t,ss}^{cop}} D_{n+m} \,/\, \xrightarrow{k_{t,ss}^{cop}} D_n + D_m$$

Backbiting

$$P_n^{AM} \xrightarrow{F_{AM}k_{bb}^{AM}} Q_n^{AM} \qquad P_n^{AA} \xrightarrow{(1-F_{AM})k_{bb}^{AA}} Q_n^{AA}$$

$$P_n^{AM} \xrightarrow{(1-F_{AM})k_{bb}^{AM\cdot AA}} Q_n^{AA} \qquad P_n^{AA} \xrightarrow{F_{AM}k_{bb}^{AA\cdot AM}} Q_n^{AM}$$

Addition to MCR

$$Q_n^{AM} + AM \xrightarrow{k_{p,tert}^{AM}} P_{n+1}^{AM} \qquad Q_n^{AA} + AA \xrightarrow{k_{p,tert}^{AA}} P_{n+1}^{AA}$$

$$Q_n^{AM} + AA \xrightarrow{k_{p,tert}^{AM\cdot AA}} P_{n+1}^{AA} \qquad Q_n^{AA} + AM \xrightarrow{k_{p,tert}^{AA\cdot AM}} P_{n+1}^{AM}$$

Cross Termination MCR-SPR

$$P_n^{AM} + Q_m^{AM} \xrightarrow{(1-\alpha_{st})k_{t,st}^{cop}} D_{n+m} \,/\, \xrightarrow{\alpha_{st}k_{t,st}^{cop}} D_n + D_m$$

$$P_n^{AA} + Q_m^{AA} \xrightarrow{(1-\alpha_{st})k_{t,st}^{cop}} D_{n+m} \,/\, \xrightarrow{\alpha_{st}k_{t,st}^{cop}} D_n + D_m$$

$$P_n^{AM} + Q_m^{AA} \xrightarrow{(1-\alpha_{st})k_{t,st}^{cop}} D_{n+m} \,/\, \xrightarrow{\alpha_{st}k_{t,st}^{cop}} D_n + D_m$$

$$P_n^{AA} + Q_m^{AM} \xrightarrow{(1-\alpha_{st})k_{t,st}^{cop}} D_{n+m} \,/\, \xrightarrow{\alpha_{st}k_{t,st}^{cop}} D_n + D_m$$

Termination MCR-MCR

$$Q_n^{AM} + Q_m^{AM} \xrightarrow{(1-\alpha_{tt})k_{t,tt}^{cop}} D_{n+m} \,/\, \xrightarrow{\alpha_{tt}k_{t,tt}^{cop}} D_n + D_m$$

$$Q_n^{AA} + Q_m^{AA} \xrightarrow{(1-\alpha_{tt})k_{t,tt}^{cop}} D_{n+m} \,/\, \xrightarrow{\alpha_{tt}k_{t,tt}^{cop}} D_n + D_m$$

$$Q_n^{AA} + Q_m^{AM} \xrightarrow{(1-\alpha_{tt})k_{t,tt}^{cop}} D_{n+m} \,/\, \xrightarrow{\alpha_{tt}k_{t,tt}^{cop}} D_n + D_m$$

Table 5.5 Rate coefficients used in the model for the copolymerization of non-ionized AA and AM.

Rate Expression	Values*	Ref
Initiation:		
$k_{\mathrm{d}}(\mathrm{s}^{-1}) = 9.24\times10^{14}\exp\left(-\frac{14\,915}{T/\mathrm{K}}\right)$	2×10^{-6}	[87]
$f = 0.8$		
Chain Propagation:		
$k_{\mathrm{p}}^{\mathrm{AM}}(\mathrm{L}\cdot\mathrm{mol}^{-1}\cdot\mathrm{s}^{-1}) = k_{\mathrm{p,max}}^{\mathrm{AM}}\exp[-w'_{\mathrm{AM}}(0.0016(T/\mathrm{K}^{-1}) + 1.015)]$	6.4×10^{4}	[12], this work
$k_{\mathrm{p,max}}^{\mathrm{AM}}(\mathrm{L}\cdot\mathrm{mol}^{-1}\cdot\mathrm{s}^{-1}) = 9.5\times10^{7}\exp\left(-\frac{2189}{T/\mathrm{K}}\right)$	8.7×10^{4}	
$k_{\mathrm{p}}^{\mathrm{AA}}(\mathrm{L}\cdot\mathrm{mol}^{-1}\cdot\mathrm{s}^{-1}) = 3.2\times10^{7}\exp\left(-\frac{1564}{T/\mathrm{K}}\right)(0.11 + 0.89\exp(-3w'_{\mathrm{AA}}))$	1.3×10^{5}	[21]
$r_{\mathrm{AA}} = 1.24$, $r_{\mathrm{AM}} = 0.55$, $s_{\mathrm{AA}} = 4.0$, $s_{\mathrm{AM}} = 1.5$		[23], this work
Transfer to Monomer:		
$C_{\mathrm{tr}}^{\mathrm{AM}} = \frac{k_{\mathrm{tr}}^{\mathrm{AM}}}{k_{\mathrm{p}}^{\mathrm{AM}}} = 0.00118\exp\left(-\frac{1002}{T/\mathrm{K}}\right)$	4.8×10^{-5}	This work
$C_{\mathrm{tr}}^{\mathrm{AA}} = \frac{k_{\mathrm{tr}}^{\mathrm{AA}}}{k_{\mathrm{p}}^{\mathrm{AA}}} = 7.5\times10^{-5}$	7.5×10^{-5}	[21]
Termination SPR-SPR:		
$k_{\mathrm{t,ss}}^{\mathrm{AM}}(\mathrm{L}\cdot\mathrm{mol}^{-1}\cdot\mathrm{s}^{-1}) = 2\times10^{10}\exp\left(-\frac{(1991 + 1477w'_{\mathrm{Mo}})}{T/\mathrm{K}}\right)$	1.3×10^{7}	[25], This work
$k_{\mathrm{t,ss}}^{\mathrm{AA}}(\mathrm{L}\cdot\mathrm{mol}^{-1}\cdot\mathrm{s}^{-1}) = 1.5\times10^{10}\exp\left(-\frac{1858}{T/\mathrm{K}}\right)\varphi_{\mathrm{AA}}$	4.7×10^{7}	[21]
$\varphi_{\mathrm{AA}} = 1.56 - 1.77w'_{\mathrm{Mo}} - 1.2(w'_{\mathrm{Mo}})^2 + 2.43(w'_{\mathrm{Mo}})^3$		[21]
$k_{\mathrm{t,ss}}^{\mathrm{cop}}(\mathrm{L}\cdot\mathrm{mol}^{-1}\cdot\mathrm{s}^{-1}) = \left(k_{\mathrm{t,ss}}^{\mathrm{AA}}k_{\mathrm{t,ss}}^{\mathrm{AM}}\right)^{1/2}$	2.5×10^{7}	This work
$\alpha_{\mathrm{ss}} = 0.1$		
Backbiting		
$k_{\mathrm{bb}}^{\mathrm{AM}}(\mathrm{s}^{-1}) = 3.7\times10^{9}\exp\left(-\frac{5881}{T/\mathrm{K}}\right)$	26	[25]
$k_{\mathrm{bb}}^{\mathrm{AA}}(\mathrm{s}^{-1}) = 9.94\times10^{8}\exp\left(-\frac{4576}{T/\mathrm{K}}\right)$	4.4×10^{2}	[21]
Addition to MCR		
$k_{\mathrm{p,tert}}^{\mathrm{AM}}(\mathrm{L}\cdot\mathrm{mol}^{-1}\cdot\mathrm{s}^{-1}) = 0.0155\exp\left(-\frac{1412}{T/\mathrm{K}}\right)k_{\mathrm{p}}^{\mathrm{AM}}$	11	[25]
$k_{\mathrm{p,tert}}^{\mathrm{AA}}(\mathrm{L}\cdot\mathrm{mol}^{-1}\cdot\mathrm{s}^{-1}) = 0.755\exp\left(-\frac{2464}{T/\mathrm{K}}\right)k_{\mathrm{p}}^{\mathrm{AA}}$	37	[21]

Cross Termination MCR-SPR		
$k_{\mathrm{t,st}}^{\mathrm{cop}}(\mathrm{L}\cdot\mathrm{mol}^{-1}\cdot\mathrm{s}^{-1}) = 0.3k_{\mathrm{t,ss}}^{\mathrm{cop}}$ $\alpha_{\mathrm{st}} = 0.7$	7.4×10^{6}	This work
Termination MCR-MCR		
$k_{\mathrm{t,tt}}^{\mathrm{cop}}(\mathrm{L}\cdot\mathrm{mol}^{-1}\cdot\mathrm{s}^{-1}) = 0.01k_{\mathrm{t,ss}}^{\mathrm{cop}}$ $\alpha_{\mathrm{tt}} = 0.9$	2.5×10^{5}	This work
Density		
$\rho_{\mathrm{AM}}(\mathrm{g}\cdot\mathrm{mL}^{-1}) = 1.0854 - 2.4663\times10^{-3}T(^{\circ}C^{-1}) + 1.3154\times10^{-5}T^{2}(^{\circ}C^{-2})$	1.008	[12]
$\rho_{\mathrm{AA}}(\mathrm{g}\cdot\mathrm{mL}^{-1}) = 1.0731 - 1.0826\times10^{-3}T(^{\circ}C^{-1}) - 7.2379\times10^{-7}T(^{\circ}C^{-2})$	1.029	[21]
$\rho_{\mathrm{H2O}}(\mathrm{g}\cdot\mathrm{mL}^{-1}) = 0.9999 - 2.3109\times10^{-5}T(^{\circ}C^{-1}) - 5.44807\times10^{-6}T(^{\circ}C^{-2})$	0.992	[21]

*evaluated at 40 °C and 20 wt% monomer
w' refers to monomer concentration of AA, AM or total monomer concentration on a polymer free basis

The penultimate propagation kinetics are implemented by using the fraction of P_{ij} to determine the amount of each radical type, and thus tracking in the model only the terminal radicals:[83,102]

$$\mathrm{P}^{\mathrm{AA\cdot AA}} = P_{\mathrm{AA\cdot AA}}\mathrm{P}^{\mathrm{AA}} \qquad \mathrm{P}^{\mathrm{AM\cdot AM}} = P_{\mathrm{AM\cdot AM}}\mathrm{P}^{\mathrm{AM}}$$
$$\mathrm{P}^{\mathrm{AM\cdot AA}} = P_{\mathrm{AM\cdot AA}}\mathrm{P}^{\mathrm{AA}} \qquad \mathrm{P}^{\mathrm{AA\cdot AM}} = P_{\mathrm{AA\cdot AM}}\mathrm{P}^{\mathrm{AM}} \tag{5.10}$$

From the definition one can see that $P_{\mathrm{AA\cdot AM}} + P_{\mathrm{AM\cdot AM}} = 1$ and $P_{\mathrm{AM\cdot AA}} + P_{\mathrm{AA\cdot AA}} = 1$. In the model, the probabilities are calculated using the following equations by applying the long chain hypothesis and the steady state assumption to the radical balances:[83,102]

$$P_{\mathrm{AA\cdot AA}} = \frac{k_{\mathrm{p}}^{\mathrm{AM\cdot AA\cdot AA}}[\mathrm{AA}]}{k_{\mathrm{p}}^{\mathrm{AM\cdot AA\cdot AA}}[\mathrm{AA}] + k_{\mathrm{p}}^{\mathrm{AA\cdot AA\cdot AM}}[\mathrm{AM}]}$$
$$P_{\mathrm{AM\cdot AM}} = \frac{k_{\mathrm{p}}^{\mathrm{AA\cdot AM\cdot AM}}[\mathrm{AM}]}{k_{\mathrm{p}}^{\mathrm{AA\cdot AM\cdot AM}}[\mathrm{AM}] + k_{\mathrm{p}}^{\mathrm{AM\cdot AM\cdot AA}}[\mathrm{AA}]} \tag{5.11}$$

Only the SPR propagation steps are considered to be affected by the penultimate monomer unit, while all other rate coefficients are dependent on the terminal unit. The cross-rate coefficients

for the transfer to monomer, backbiting, and addition of monomer to the MCR are assumed to have the same relative propensity to react as the propagation steps according to the terminal model (X = tr, bb, or p,tert):[96]

$$\frac{k_{\mathrm{X}}^{\mathrm{AA{\cdot}AA}}}{k_{\mathrm{X}}^{\mathrm{AM{\cdot}AA}}} = \frac{k_{\mathrm{p}}^{\mathrm{AA}}}{k_{\mathrm{p}}^{\mathrm{AM{\cdot}AA}}}$$

$$\frac{k_{\mathrm{X}}^{\mathrm{AM{\cdot}AM}}}{k_{\mathrm{X}}^{\mathrm{AA{\cdot}AM}}} = \frac{k_{\mathrm{p}}^{\mathrm{AM}}}{k_{\mathrm{p}}^{\mathrm{AA{\cdot}AM}}} \qquad 5.12$$

Models of the copolymerization of STY/BA consider the backbiting of a single monomer, BA, with the rate of the backbiting being a function of the probability of the three final monomer units being either BA-STY-BA or BA-BA-BA, and assuming that a BA unit can only abstract a hydrogen from another BA unit.[83] A similar approach was taken for the BMA/BA copolymerization.[96] As both AA and AM are known to undergo backbiting, it is necessary to include four backbiting steps in the model, as outlined in Table 5.4. To the best of our knowledge, this is the first copolymerization model that considers this complexity. The cross-backbiting steps are implemented using the same treatment as in Equation 5.12, making this rate coefficient a function of monomer concentration. This treatment may not describe the cross-backbiting rate coefficient accurately, as backbiting is a unimolecular reaction and therefore thought to be independent of the monomer concentration. This treatment does, however, take the relative abstractability of the hydrogen from an AA unit compared to an AM unit in the antepenultimate position into consideration, with AA in the antepenultimate position more readily forming MCRs. In addition to the rate coefficients, a probability, defined as the instantaneous copolymer composition, is introduced to determine the identity of the antepenultimate unit.

Little is known about the termination mechanism for this copolymerization. Measurements show that the viscosity (Figure 5.6) is independent of the monomer composition but varies with total monomer concentration, consistent with the treatment that the termination rate coefficient is

a function of the total monomer concentration. Additionally, it is observed that the viscosity of the monomers AA and AM are very similar to the comonomer mixtures, indicating a similar effect with monomer concentration as the homomonomer mixtures. Therefore the termination rate coefficient is calculated based on the initial weight fraction of the total monomer in water (w'_M). The chain length dependency of the AA termination rate coefficient considered in reference[21] was removed, as this level of complexity is not required for this copolymerization model in the absence of chain transfer agent. The resulting predictions of the AA homopolymerization model are equivalent to those presented in reference.[21]

The copolymer termination coefficient is calculated assuming the geometric mean; other termination treatments are considered and discussed later.

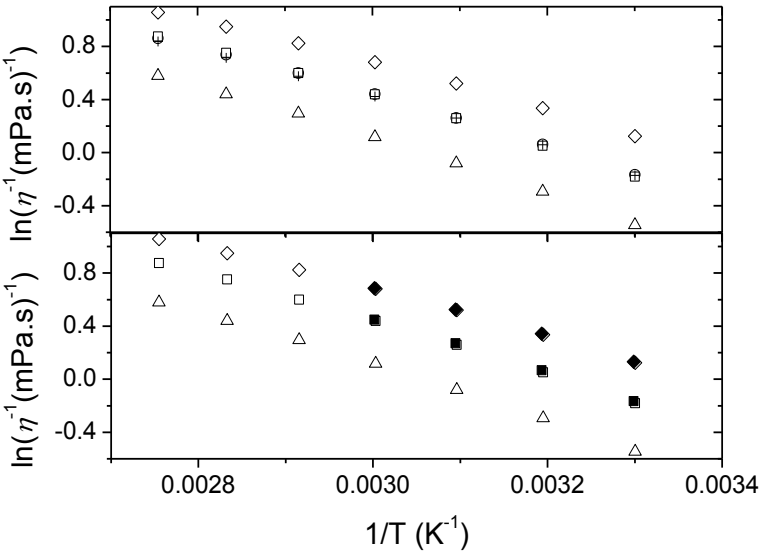

Figure 5.6 Viscosity measurements plotted as a function of temperature at f_{AM} = 0.5 and 5 (◊), 20 (□), and 40 (Δ) wt% monomer, with measurements at 20 wt% monomer and f_{AM} = 0.3 (○) and f_{AM} = 0.8 (+) (top), and plotted with AM at 5 (♦) and 20 (■) wt% monomer (bottom).[25]

Using the reaction mechanism and rate coefficients discussed, a model in Predici was implemented. The predicted conversion profiles, corresponding to experiments at 40 and 70 ^{o}C are shown in Figure 5.7 and Figure 5.8, respectively, grouped according to monomer composition.

At 70 ^{o}C the predicted conversion profiles are close to the experimentally measured data, with some room for improvement at 20 wt% monomer. This same observation cannot be made for the data at 40 ^{o}C, as the measured conversion copolymer conversion profiles are close to the AA homopolymerization rate, with a significant reduction in the predicted conversion rate needed in order to match the experimental data. From a kinetic standpoint, assuming that the chain end propagation rate coefficient is correct, a higher rate of termination, more backbiting, or slower addition to the MCR is required to slow the conversion profiles down appropriately. As will be demonstrated in the following sections, no changes to the rate coefficients can satisfactorily model the conversion rates at both 40 and 70 ^{o}C. If the kinetic model cannot capture the trends in the conversion rates, then other effects are likely causing a reduction in the observed conversion rate at 40 ^{o}C. One possible explanation is the complexation reactions between the amide and carboxylic groups on the formed polymer chain. As the hydrogen bonding is stronger at lower temperatures[92] and higher molar masses,[93] the polymer chains are more rigid at 40 ^{o}C, leading to the observed reduction in the conversion rate. The complexation argument is consistent with the model fit at 70 ^{o}C, as the extent of complexation decreases with increasing temperature.[92] At this point in time we are unsure of the exact mechanism by which the kinetics are affected by the complexation, an uncertainty that could be examined by additional experiments as outlined in the further work section.

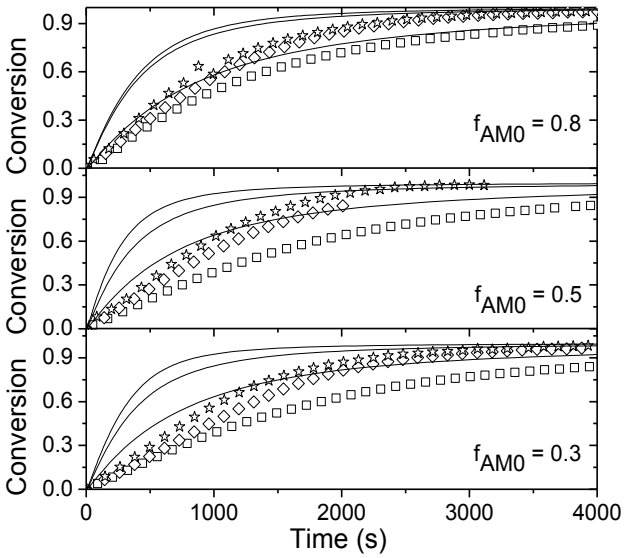

Figure 5.7 Copolymer conversion profiles measured (symbols) and predicted (lines) at 40 ºC and 0.2 wt% V-50 with monomer concentrations of 5 (□), 20 (◇), 40 wt% (☆) in aqueous solution at initial monomer compositions f_{AM0} = 0.8 (top), 0.5 (middle), and 0.3 (bottom).

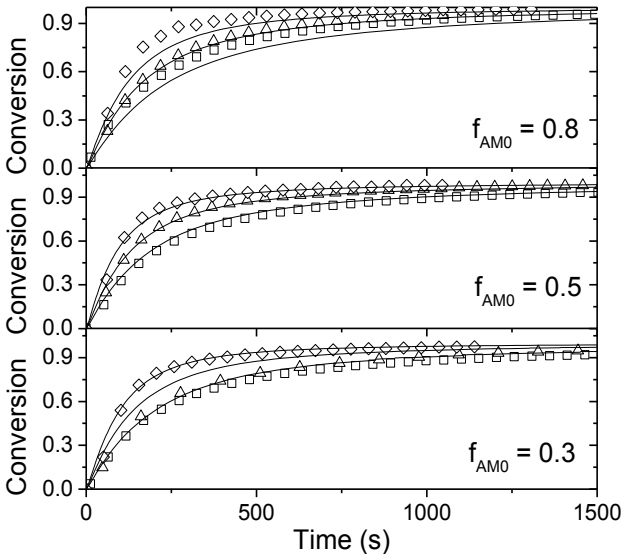

Figure 5.8 Copolymer conversion profiles measured (symbols) and predictions (lines) at 70 ºC and 0.04 wt% V-50 with monomer concentrations of 5 (□), 10 (△), 20 wt% (◇) in aqueous solution at initial monomer compositions f_{AM0} = 0.8 (top), 0.5 (middle), and 0.3 (bottom).

5.5.1 Sensitivity of the Termination Rate Coefficient

The model implemented uses the geometric mean for the copolymer termination rate coefficient; however, other treatments of copolymer termination have been described in the literature. Atherton and North introduced a diffusion controlled instantaneous copolymer composition averaged termination rate coefficient in 1962:[99]

$$k_{t,ss}^{cop} = k_{t,ss}^{AM} F_{AM}^{inst} + k_{t,ss}^{AA} F_{AA}^{inst} \qquad 5.13$$

Alternatively, one can consider the rate coefficient to be inversely proportional to the friction coefficient, leading to an expression proposed by Fukuda in 1992:[100]

$$\frac{1}{k_{t,ss}^{cop}} = \frac{F_{AM}^{inst}}{k_{t,ss}^{AM}} + \frac{F_{AA}^{inst}}{k_{t,ss}^{AA}} \qquad 5.14$$

Figure 5.9 plots the termination rate coefficient as a function of monomer composition at 10 wt% monomer and 40 ºC calculated by these different treatments. The termination rate coefficient as calculated by the geometric mean is independent of monomer composition, consistent with the viscosity data (Figure 5.6). The Atherton-North and Fukuda treatments, however, show an effect of the monomer composition on the calculated termination rate coefficient. Figure 5.10 compares the influence of the different types of termination on monomer conversion profiles for f_{AM0} = 0.5 at 40 and 70 ºC. It can be observed that the various treatments have little effect on the predicted conversion profiles. This result can be understood by looking at the relative rate coefficents: the calculated difference in k_t^{cop} for the Atherton-North method from the geometric mean is an increase in 48 % at f_{AM0} = 0.5, which translates into a 15 % decrease in $(k_t^{cop})^{-1/2}$ and thus reaction rate. For the Fukuda, a decrease of 33 % for the rate coefficient, and a 6 % increase in the rate is expected relative to the geometric mean.

In order to be consistent with the observations from the measured viscosity of monomer solutions at various monomer concentrations and compositions, the geometric mean will be used in the model for this copolymerization.

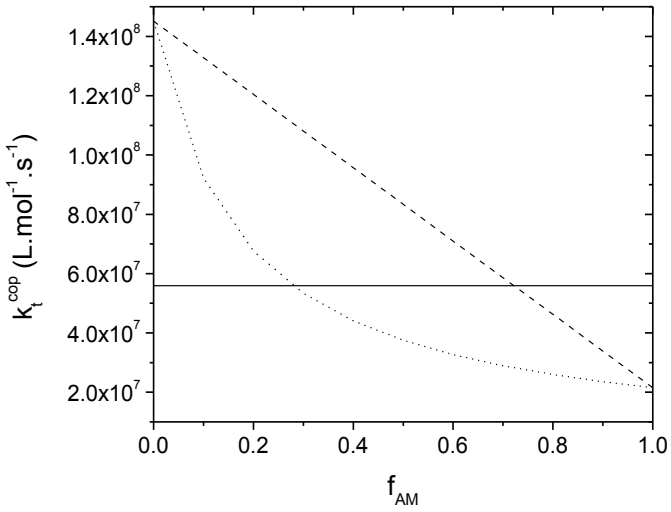

Figure 5.9 Calculated termination rate coefficient at 40 ºC and 10 wt% monomer for the geometric mean (solid line), Atherton North (dashed line), and Fukuda treatment (dotted line) as a function of monomer composition.

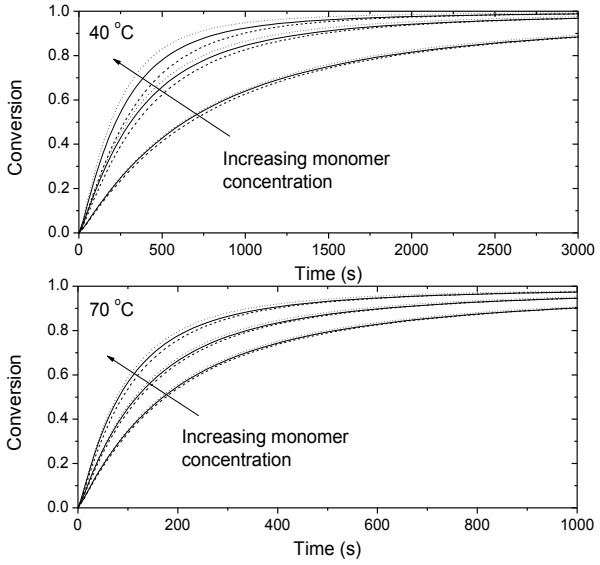

Figure 5.10 Predicted conversion profiles for f_{AM0} = 0.5 at 40 ºC and 0.2 wt% V-50 (top) at 5, 20, and 40 wt% monomer and 70 ºC and 0.04 wt% V-50 (bottom) at 5, 10, and 20 wt% monomer with the copolymer termination rate coefficient calculated using the geometric mean (solid lines), Atherton North (dashed lines), and Fukuda method (dotted lines).

A simple strategy to decrease the predicted conversion rates to match the experimental data at 40 °C is to increase the termination rate coefficient to the value of AA for all SPR termination steps; the resulting conversion profiles are plotted in Figure 5.11 and Figure 5.12. The increase in the termination rate coefficient (from 2.5×10^7 $L\cdot mol^{-1}\cdot s^{-1}$ for the copolymerization) to 4.7×10^7 $L\cdot mol^{-1}\cdot s^{-1}$ for all rate SPR termination at 20 wt% monomer yields conversion rates that are visibly slower, leading to a mismatch of the data at 70 °C, while only slightly improving the fit of the conversion profiles at 40 °C.

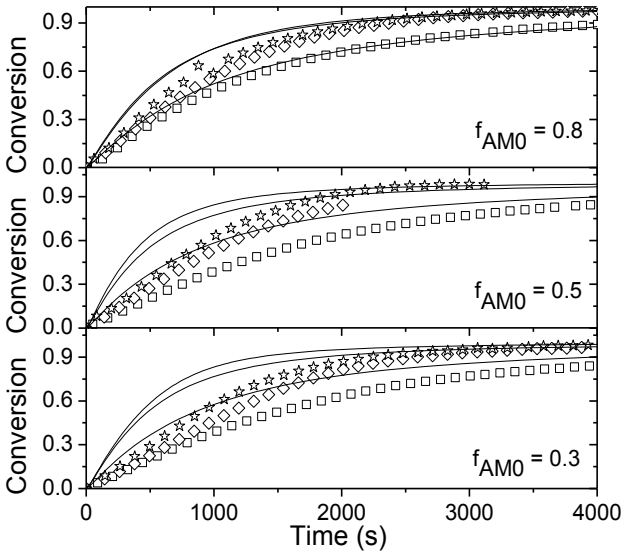

Figure 5.11 Copolymer conversion profiles measured (symbols) and predictions with the AA termination rate coefficient (solid line) at 40 °C and 0.2 wt% V-50 with monomer concentrations of 5 (□), 20 (◇), 40 wt% (☆) in aqueous solution at initial monomer composition f_{AM0} = 0.8 (top), 0.5 (middle), and 0.3 (bottom).

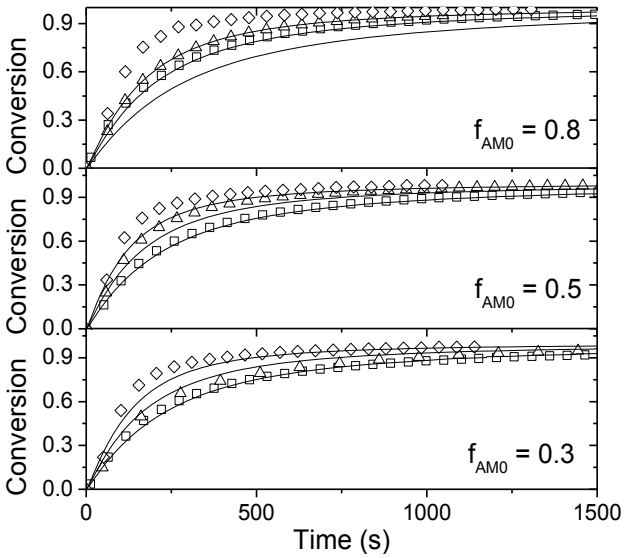

Figure 5.12 Copolymer conversion profiles measured (symbols) and predictions with the AA termination rate coefficient (lines) at 70 °C and 0.04 wt% V-50 with monomer concentrations of 5 (□), 10 (△), 20 wt% (◇) in aqueous solution at initial monomer composition f_{AM0} = 0.8 (top), 0.5 (middle), and 0.3 (bottom).

5.5.2 Sensitivity of the Rate Coefficients Related to MCRs

Very little is known about the nature of the backbiting rate coefficients for this copolymerization system. In fact, the backbiting rate coefficient has not directly been measured for any copolymer system. Rate coefficients for BA-STY and BA-BMA copolymerizations were based on ^{13}C NMR data indicating a reduction in the backbiting rate coefficient if the penultimate unit was a STY and assuming that BA will only abstract a hydrogen from a BA unit in the antepenultimate unit.[83] This assumption led to model predictions that matched the measured conversion and M_w profiles. As part of this work, a similar approach was taken to determine the relative amount of backbiting in the AA/AM copolymer system. Samples were polymerized at 10 wt% monomer at 90 °C to ensure the highest possible amount of backbiting at a concentration sufficient for ^{13}C NMR. The ^{13}C experiments were run an inverse gated pulse program and a sufficient relaxation delay to ensure no NOE (Nuclear Oberhauser Effect). All samples were run

with similar number of scans. Figure 5.13 plots the region from 29 to 50 ppm on a ^{13}C spectra for an AA and a f_{AM} = 0.5 sample polymerized at 90 ºC and 10 wt% monomer. The region between 41 and 43 ppm denote the CH peak on the polymer backbone, while the region from 32 to 36.5 ppm signified the CH_2 peak on the polymer backbone. The CH and CH_2 peaks adjacent to the quarternary carbon can be seen for the AA sample between the CH and CH_2 peaks of the polymer backbone. The quarternary carbon peak can be found between 47 and 48 ppm. The peak assignments are in agreement with literature values for AA[21,104] as well as other acrylates such as BA.[89,105] Due to the similarity of the AA and AM chemical structure, the peaks of the backbone and any quarternary carbon peaks lose in overall intensity due to the peak overlap of all the AA/AM monomer unit configurations, resulting in the quarternary carbon peak becoming greatly reduced in size relative to the AA quarternary carbon peak. Therefore ^{13}C cannot be used to measure the extent of backbiting in the copolymerization, leaving no clues on the backbiting rate coefficient. Additionally, the model predictions of backbiting for the AA homopolymerization at 90 ºC and 10 wt% is 2.52 % SCB, much greater than the predicted 0.68 % SCB for the copolymerization at f_{AM0} of 0.8 at the same temperature and monomer concentration, a value which is below the sensitivity of ^{13}C NMR. Based on the increase in conversion rate of the copolymer system with increasing monomer concentration and the presence of backbiting in both AA and AM homopolymerizations, the backbiting reactions will remain in the kinetic scheme with the treatment of these rate coefficients relying on previous knowledge and reasonable assumptions.

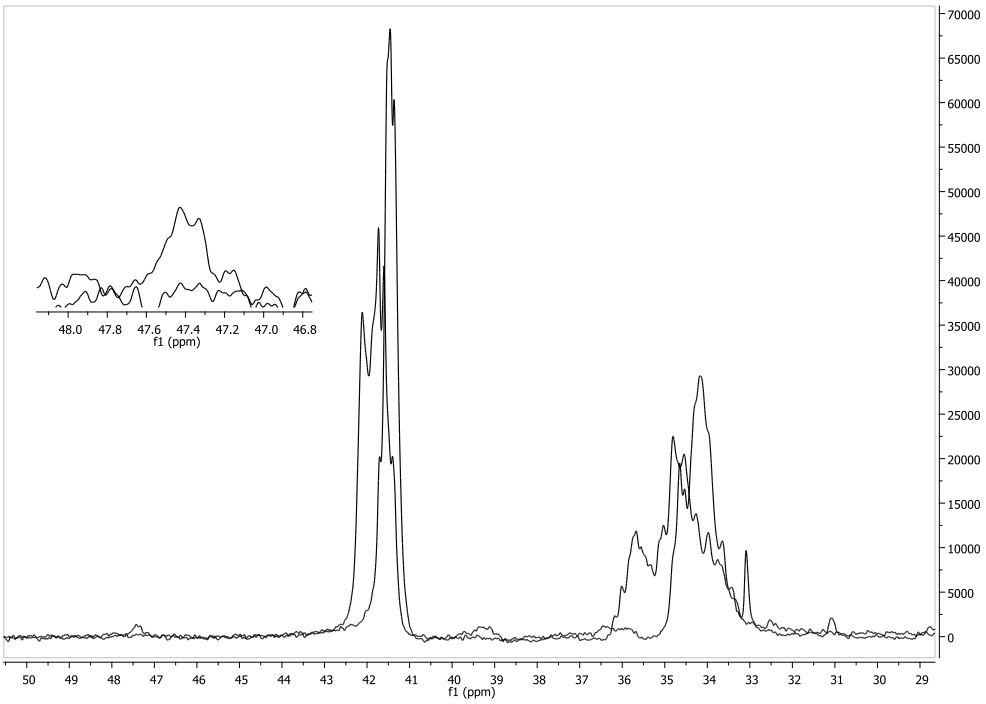

Figure 5.13 ^{13}C NMR of samples polymerized at 10 wt% and 90 ^{o}C of AA and of copolymer with f_{AM0} = 0.8. The taller peaks are from the AA sample, while the shorter peaks are of the copolymer.

In order to decrease the rate of the predicted conversion profiles at 40 ^{o}C to better match experiment, another tactic is to increase the backbiting rate coefficient. Model predictions are plotted in Figure 5.14 and Figure 5.15 for simulations run with this rate coefficient set to the value for AA for all backbiting reaction steps, and the remaining rate coefficients set to base case values. The resulting conversion profiles are not sufficiently decreased to match the conversion rates at 40 ^{o}C while the fit at 70 ^{o}C is compromised at all conditions.

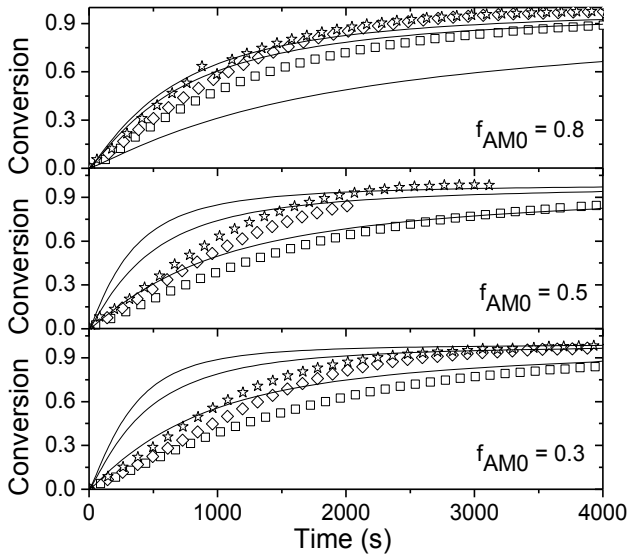

Figure 5.14 Copolymer conversion profiles measured (symbols) and predictions with the backbiting coefficient for AA (lines) at 40 ºC and 0.2 wt% V-50 with monomer concentrations of 5 (□), 20 (◇), 40 wt% (☆) in aqueous solution at initial monomer composition f_{AM0} = 0.8 (top), 0.5 (middle), and 0.3 (bottom).

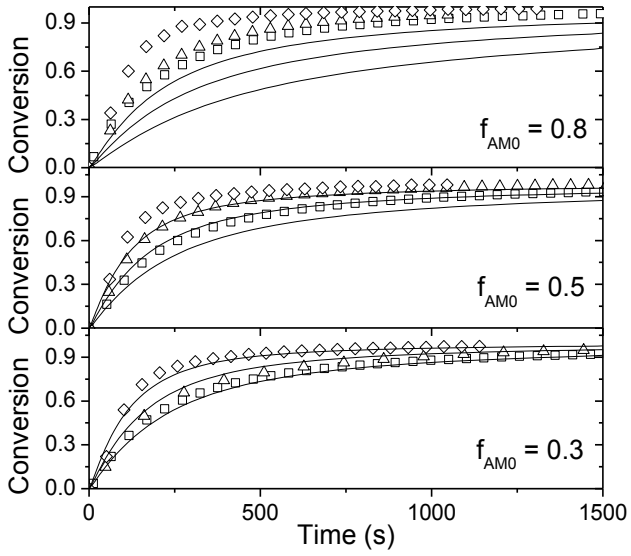

Figure 5.15 Copolymer conversion profiles measured (symbols) and predictions with the backbiting coefficient for AA (lines) at 70 ºC and 0.04 wt% V-50 with monomer concentrations of 5 (□), 10 (△), 20 wt% (◇) in aqueous solution at initial monomer composition f_{AM0} = 0.8 (top), 0.5 (middle), and 0.3 (bottom).

The third rate coefficient that can be adjusted to affect reaction rate is that for addition of monomer to the MCR, $k_{p,tert}$. Lowering this rate coefficient makes the MCRs dormant for a longer period, effectively lowering the overall conversion rate. Thus, all $k_{p,tert}$ values were decreased to that of AM, with the predictions compared to experiment in Figure 5.16 and Figure 5.17. It can be seen that decreasing this rate coefficient has a much larger effect compared to increasing the backbiting and termination rate coefficients. At 40 °C the predicted conversion profiles are closer to the experimental data; however, at 70 °C the predictions are much slower than the experimental data, as expected. Thus, any treatment proposed to fit the model at 40 °C is not consistent with a good fit at 70 °C. Therefore the argument of complexation polymerization affecting the kinetics at the lower temperature remains the most probable explanation of the poor fit at 40 °C.

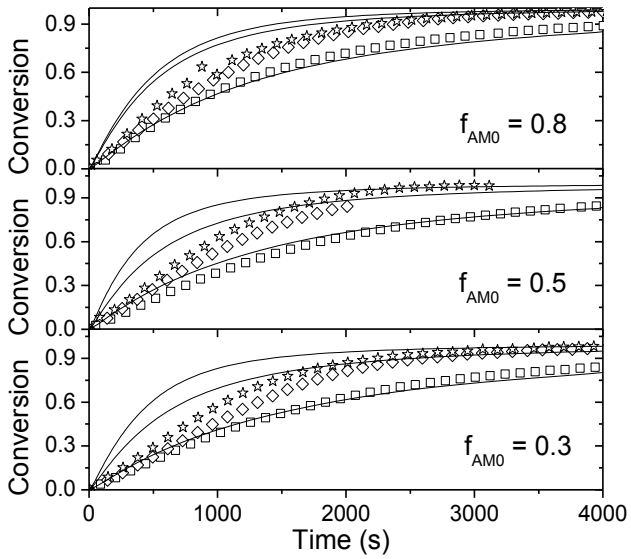

Figure 5.16 Copolymer conversion profiles measured (symbols) and predictions with the addition of monomer to the MCR rate coefficient for AM (lines) at 40 °C and 0.2 wt% V-50 with monomer concentrations of 5 (□), 20 (◇), 40 wt% (☆) in aqueous solution at initial monomer compostion f_{AM0} = 0.8 (top), 0.5 (middle), and 0.3 (bottom).

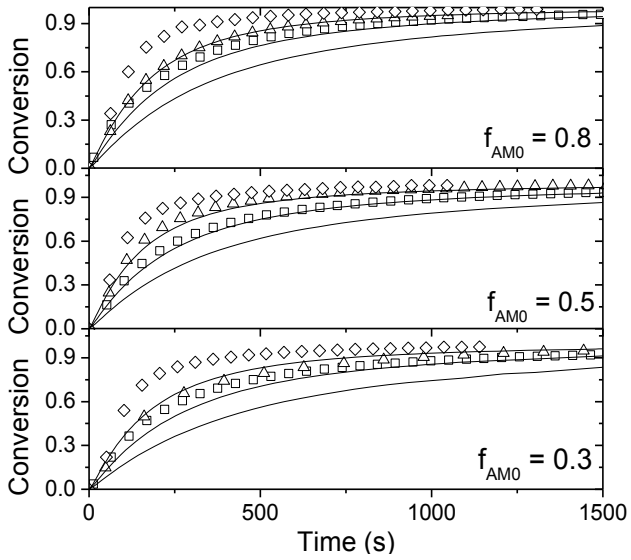

Figure 5.17 Copolymer conversion profiles measured (symbols) and predictions with the addition of monomer to the MCR rate coefficient for AM (lines) at 70 °C and 0.04 wt% V-50 with monomer concentrations of 5 (□), 10 (△), 20 wt% (◇) in aqueous solution at initial monomer compostion f_{AM0} = 0.8 (top), 0.5 (middle), and 0.3 (bottom).

5.5.3 Molecular Weight Predictions

The measured and predicted final polymer weight-average molar masses, M_w, are compared for experiments run at 40 (Figure 5.18) and 70 (Figure 5.19) °C for various monomer concentrations and compositions. Despite the poor prediction of conversion profiles at 40 °C, the Mw predictions are in reasonable agreement with experimental measurements. Data at 70 °C is more limited, but suggests that perhaps cross transfer occurs at a lower rate than currently implemented in the model.

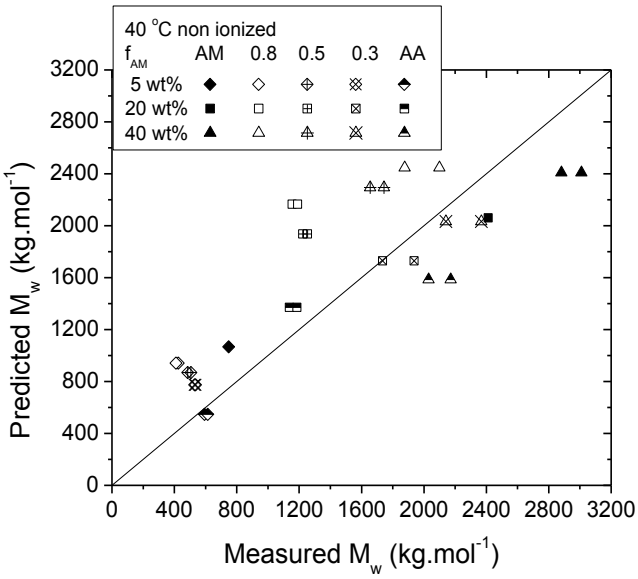

Figure 5.18 Comparison of the measured and predicted polymer weight-average molar mass (M_w) values for AA and AM copolymerization taken to high conversion at 40 ºC for various monomer concentrations and concentrations, as indicated in the legend.

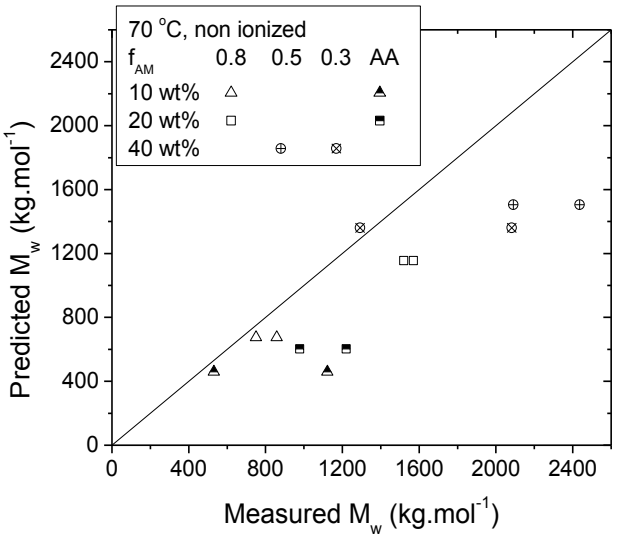

Figure 5.19 Comparison of the measured and predicted polymer weight-average molar mass (M_w) values for AA and AM copolymerization taken to high conversion at 70 ºC for various monomer concentrations and concentrations, as indicated in the legend.

5.6 Conclusion and Recommendations for Future Work

A model for the copolymerization of non-ionized AA and AM that includes the effect of monomer concentration, composition, and temperature on rate coefficients was developed based on known rate coefficients for the AA and AM homopolymerizations and measured copolymer compositions and propagation rate data. As the copolymerization rate coefficients for termination, transfer to monomer and backbiting are unknown, literature treatments were extended to describe a system for which both monomers are known to undergo backbiting reactions. The model predictions were compared to batch polymerization data collected at 40 and 70 ^{o}C. The model fit the measured conversion profiles well at 70 ^{o}C, and overpredicted that data at 40 ^{o}C. A sensitivity analysis of the rate coefficients did not yield a model capable of predicting the copolymerization at both 40 and 70 ^{o}C. Therefore we hypothesize that in addition to the monomer-solvent interaction captured in the rate coefficients, complexation between the formed polymer chains leads to a decrease in the copolymerization conversion rate at 40 ^{o}C, since literature studies have found that these interactions, which lead to a more rigid polymer structre, are much stronger at lower temperatures and at higher polymer molecular weights. Although the precise mechanism of how the polymer rigidity affects the polymerization kinetics is unknown, the following set of experiments may provide some insight into clarifying the interactions and testing this hypothesis. The proposed additional experiments are as follows:

- Run non-ionized copolymerization experiments at intermediate temperatures between 40 and 70 ^{o}C and compare the results to model predictions. The intermediate monomer compositions and the monomer concentrations should be kept the same as previously reported, with emphasis on the conversion profiles at 5 and 20 wt% monomer. The deviation in the model prediction from the experimental data should decrease systematically with increasing temperature.

Additionally, experiments could be run at lower temperatures to observe a stronger deviation from the model predictions.

- Polymerizations in the presence of salt (NaCl) could also be run with experiments at 40 ^{o}C. The additional salt will shield the charges on the polymer side groups, increasing the polymer flexibility, and thus also the conversion rate. Similar experiments have been conducted for partially and fully ionized AA homo- and copolymerizations with AM.[22,51]
- If possible, PLP-SEC experiments in the presence of formed copolymer should be run, similar to reactions performed with MAA.[33] Perhaps homopolymerizations of AA and AM in the presence of the homopolymer of the opposite identity could give an indication as to complexation reactions that would occur. Experiments of this nature would be a proof of concept, as there also must be interactions on the polymer chain formed during the copolymerizations.

Chapter 6

Kinetics and Modeling of Fully Ionized Acrylic Acid and Acrylamide Free Radical Copolymerization in Aqueous Solution

6.1 Introduction

This chapter focuses exclusively on the copolymerization of fully ionized AA and AM, while the following chapter will discuss the copolymerization at different degrees of ionization. AA is a weak acid with a pK_a of 4.37[29] and therefore is easily ionized by strong bases, NaOH in our work. The degree of ionization, α, is defined as follows

$$\alpha = \frac{[A^-]}{[HA] + [A^-]} = \frac{[\mathrm{NaOH}]}{[\mathrm{AA}]} \qquad 6.1$$

where AA represents the total concentration of AA, both ionized and non-ionized. From the definition, the degree of ionization spans from 0 to 1. The pH of the system can be calculated using the Henderson-Hasselbalch equation

$$\mathrm{pH} = \mathrm{p}K_a + \log\left(\frac{[A^-]}{[HA]}\right) \qquad 6.2$$

and substituting the definition of alpha into the equation yields:

$$\mathrm{pH} = \mathrm{p}K_a + \log\left(\frac{\alpha}{1-\alpha}\right) \qquad 6.3$$

Figure 6.1 plots the pH of AA in water for different degrees of ionization. From this equation a pH value of 6.4 is calculated for α equal to 0.99, a pH of 7.3 at 0.999, and a pH of 8.4 at 0.9999. This sensitivity of the pH at near fully ionized conditions is not surprising, a small change in the concentration of NaOH will lead to large changes in the measured pH near the equivalence point and is the reason a range of pH values is cited as fully ionized in the literature.[46,48–51,53]

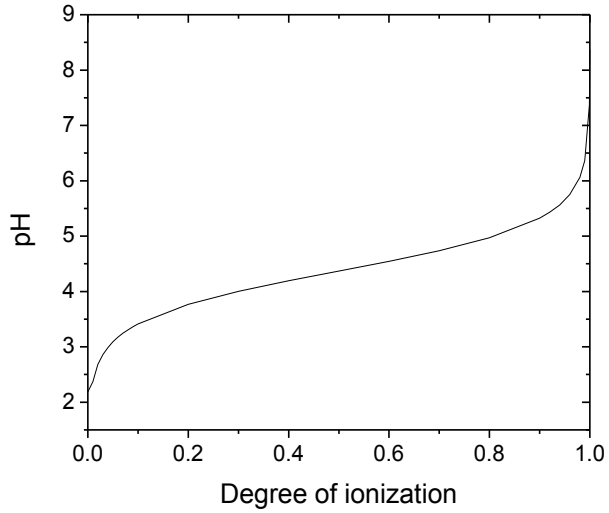

Figure 6.1 Calculated pH as a function of the degree of ionization of AA with a pK_a of 4.37.[29]

The propagation rate coefficient of AM was shown to be independent of the system pH and it is assumed that all other rate coefficients of AM are also independent of the system pH, with values the same as outlined in the AM homopolymerization (Chapter 4) and non-ionized AA/AM copolymerization model (Chapter 5). However, the treatment of AA homopolymerization kinetics needs to be modified to account for the influence of ionization. Fully ionized AA holds a negative charge on the carboxylic acid group, reducing the rate coefficients relative to the non-ionized conditions and causing the polymer chain to become more rigid. This work systematically studies the effect of the monomer concentration on the conversion profiles and the reactivity ratios, as the rate coefficients are known to be a function of monomer concentration at all degrees of ionization of AA.

Propagation rate coefficients for fully ionized AA are available only at 6 wt% monomer, at which concentration was shown that this rate coefficient is about 10 times lower than the value for non-ionized conditions at 6 ^{o}C.[29] Due to the low termination rate coefficient of fully ionized AA, propagation rate data using the PLP-SEC method cannot be measured at temperatures and

monomer concentrations relevant to this model.[106] Therefore the effect of the monomer concentration is modeled according to fully ionized MAA behavior, as it was found that MAA and AA exhibit similar changes in the propagation rate coefficient with monomer concentration at non-ionized conditions.[34] Figure 6.2 from reference [34] shows the effect of monomer concentration on the propagation rate coefficient of MAA at different degrees of ionization, with the monomer concentration having less of an influence as the degree of ionization increases. In fact, at fully ionized conditions, the rate coefficient of MAA increases with monomer concentration. Some values for the termination, backbiting, and addition to mid chain radical rate coefficient have been reported in the literature.[7] However, the work by Barth and Buback assumes the termination of the mid chain radicals to be negligible compared to the other rate coefficients, affecting the estimates of all rate coefficients, in particular k_{bb} and $k_{p,tert}$.[7] In the modeling work it is assumed that termination of the mid chain radical occurs, as has been considered in all the work for AA and AM in previous chapters.

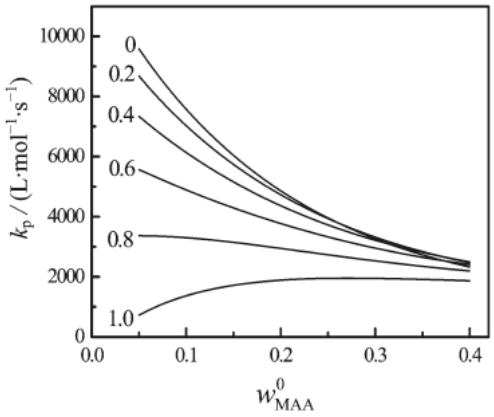

Figure 6.2 Effect of monomer weight fraction and degree of ionization (labeled in the graph) on the propagation rate coefficient at 50 °C for MAA in aqueous solution.[34] Reprinted with permission from Macromolecular Chemistry and Physics. Copyright 2004, Wiley-VCH Verlag GmbH & Co. KGaA.

Estimates of the other rate coefficients for fully ionized AA are even less well understood; those used in the copolymerization model developed in this thesis follow the work of Wittenberg, where the treatments were developed based on known changes in the viscosity and polymer chain flexibility as a function of the degree of ionization.[107] The expressions for the rate coefficients are discussed in the following sections and the sensitivity of the model to the backbiting rate coefficient, poorly understood for the ionized system, is explored. The decreased rate coefficients at fully ionized conditions relative to the ones at non-ionized conditions are attributed to the negative charges on the monomer and polymer repelling each other.[29,34] When fully ionized AA is polymerized in the presence of species that form complexes with the Na^+, the polymerization is effectively suppressed.[22] On the other hand, when fully ionized AA is polymerized with excess NaCl, an increase in the conversion rate is observed with the conversion rate profile of non-ionized AA fully recovered with the addition of 6 times the molar amount of NaCl relative to AA.[22] These homopolymerization studies demonstrate the significant influence of the charged species on polymerization kinetics.

For copolymerization, the interactions of charged AA units with AM must also be considered. Studies on unreactive polymer chains of pAA and pAM indicate that when the AA units are fully ionized on the polymer backbone, there is little to no complexation between the AM and charged AA side groups.[108–110] This is in contrast to the non-ionized pAA and pAM interactions, where complexation between the side groups leads to more rigid polymer structures[92–94,108] that likely affects the copolymerization kinetics of non-ionized AA and AM, as discussed in the previous chapter.

Due to the complexity, the available literature studies of AM with ionized AA focus mainly on copolymer composition as a function of pH,[36,46–51,53,111] with recently targeted experiments studying the effect of ionic strength.[49,51] As summarized in Table 6.1, however, the reported sets of reactivity ratios are very scattered at pH values between 6.2 and 8.8, conditions that can be

considered fully ionized. The range in the reported reactivity ratios is large, with the only consistent observation being that fully ionized AA is less reactive than AM. Reactivity ratios were estimated with the Kelen-Tüdös method,[46] the integrated form of the Mayo-Lewis equation,[53] as well as using an error in variables (EVM) and direct numerical integration (DNI) method.[48,50] No consistency was seen in data collected at the same monomer concentrations.[46,48,50,53] For the data collected at 0.4 mol·L^{-1} at different pH values, one can see that even though the AA is fully ionized, the reactivity ratio of AM changes considerably.

Table 6.1 Reported literature reactivity ratios and selected reaction conditions for AA and AM ionized with NaOH.

r_{AM}	r_{AA}	pH	Monomer concentration (mol·L^{-1})	Ref.
2.50	0.39	6.2	0.4	[46]
2.95	0.42	7.8	0.4	[46]
3.05	0.42	8.8	0.4	[46]
1.88	0.80	7.3	0.47	[48]
1.33	0.23	7	1	[50]
0.63	0.12	8	1	[53]

An interesting feature of copolymerization of charged monomers with AM, is that the drift in monomer composition as a function of conversion is a function of total monomer concentration and ionic strength.[50,51,56,57] This effect has been explained by the influence that the charges in the system have on the rate coefficients, in particular the propagation rate coefficients,[50,51,56,57] a hypothesis validated by running polymerizations in the presence of additional salt (NaCl).[51,57] With the addition of salt, the charges on the polymer chain and monomers are electrostatically shielded, leading to more flexible chains and allowing for easier incorporation of the ionized monomer species.[51,57] The resulting conversion and monomer composition profiles changed in such a way that indicated the ionic strength of the total reaction mixture dictates the relative

monomer consumption. Work done for ionized AA homopolymerizations with a variety of bases and salt additions led to similar conclusions about the effect of ionic strength.[22] Cuccato et al. is the only work to our knowledge that attempts to describe the combined effect of monomer concentration and ionic strength on monomer composition as a function of conversion, df_A/dx for copolymerization of AM with the fixed charge cationic monomer 2-(acryloyloxyethyl)-trimethylammonium chloride (DMAEA-Q).[57] The change in monomer composition as a function of conversion, written in terms of AM and consistent with our previous work (Chapter 3), is

$$\frac{df_{\mathrm{AM}}}{dx} = \frac{f_{\mathrm{AM}} - F_{\mathrm{AM}}}{1 - x} \qquad 6.4$$

with

$$F_{\mathrm{AM}} = \frac{r_{\mathrm{AM}} f_{\mathrm{AM}}^2 + f_{\mathrm{AM}} f_{\mathrm{AA}}}{r_{\mathrm{AM}} f_{\mathrm{AM}}^2 + 2 f_{\mathrm{AM}} f_{AA} + r_{\mathrm{AA}} f_{\mathrm{AA}}^2} \qquad 6.5$$

and $r_{AA} = k_p^{AA}/k_p^{AA\cdot AM}$ and $r_{AM} = k_p^{AM}/k_p^{AM\cdot AA}$. The work in reference [57] focuses mainly on simulating df_A/dx, so Equation 6.4 is extended to include the electrostatic effect of the charged monomer on the rate coefficients and backbiting reactions of the AM.[57] However, branching levels for AA and AM are low and monomer composition is thus controlled by the propagation rate coefficients, as also found for the copolymerization of BA with ST[83] and BMA.[96] Thus, the approach taken in this work is to represent the reactivity ratios using an empirical relationship based on the initial total monomer weight fraction. Future experimental and modeling work of copolymerizations with charged species both in our and other lab groups will allow a more complete understanding of these interesting systems and help to better explain the observed effects.

This chapter presents experimental data and a kinetic model for the copolymerization of fully ionized AA with AM. Experimental data was collected at 50 °C at various monomer compositions (f_{AM0} = 0.3, 0.5, 0.7) and monomer concentrations (5, 10, 20, and 30 wt%). The kinetic model was developed using rate coefficients of AM previously discussed (Chapter 4) and rate

coefficients of fully ionized AA summarized by Nils Wittenberg in his PhD thesis.[107] Reactivity ratios were developed as a function of initial weight fraction total monomer to represent the experimentally observed drift in monomer composition with conversion. It is shown that the experimental batch monomer conversion and composition profiles and final polymer molecular weights are reasonably represented by the model at lower monomer concentrations, with systematic deviations found at higher monomer levels.

6.2 Experimental Section

The monomers, AA (99%, Sigma Aldrich) and AM (99+%, Sigma Aldrich), D_2O (99.9%, Cambridge Isotope Laboratories Inc.), and V-50 initiator (97%, Sigma Aldrich) were bought and used without further purification. Fully ionized AA stock solution was made by titrating non-ionized AA with a mixture of NaOH and D_2O, the solvent used for the ^1H NMR experiments. The equivalence point was reached at a pH of 7.9 and checked the following day to ensure consistency between measurements and pH meter calibrations. Stock solutions of fully ionized AA in D_2O were preferred over adding NaOH to each experimental reaction solution, as the amounts needed for the individual NMR experiments are small, between 0.018 to 0.3 g fully ionized AA. The titration yielded stock solutions of approximately 30 wt% fully ionized AA in D_2O. The sodium ion was considered in the mass calculations of the ionized AA required for recipe formulations, even though the sodium dissociates in solution. This assumption was validated when solutions at different degrees of ionization and monomer compositions yielded good agreement between the expected and experimentally measured monomer composition with ^1H NMR, as demonstrated in Figure 6.3 for fully ionized conditions.

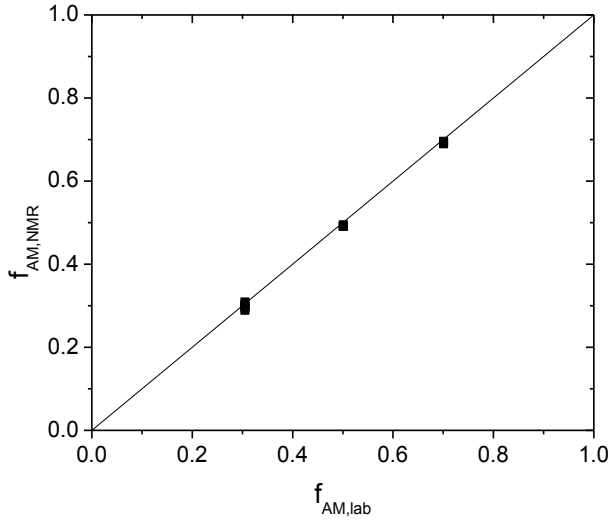

Figure 6.3 Parity plot of the monomer composition (mol fraction of AM) as calculated in the lab compared to the monomer composition measured with NMR. Excellent agreement is indicated by overlapping data points.

The same in-situ NMR methodology as described in reference [23] is used, however the monomer peaks had to be reassigned on the ^{1}H NMR spectra as the negative charge on the fully ionized AA results in a change in the magnetic environment relative to that of non-ionized AA. This essentially leads to the reversal of the AA and AM monomer peak positions relative to the non-ionized peak positions as seen in Figure 6.4. All equations for the calculation of monomer composition and conversion remain the same.[23]

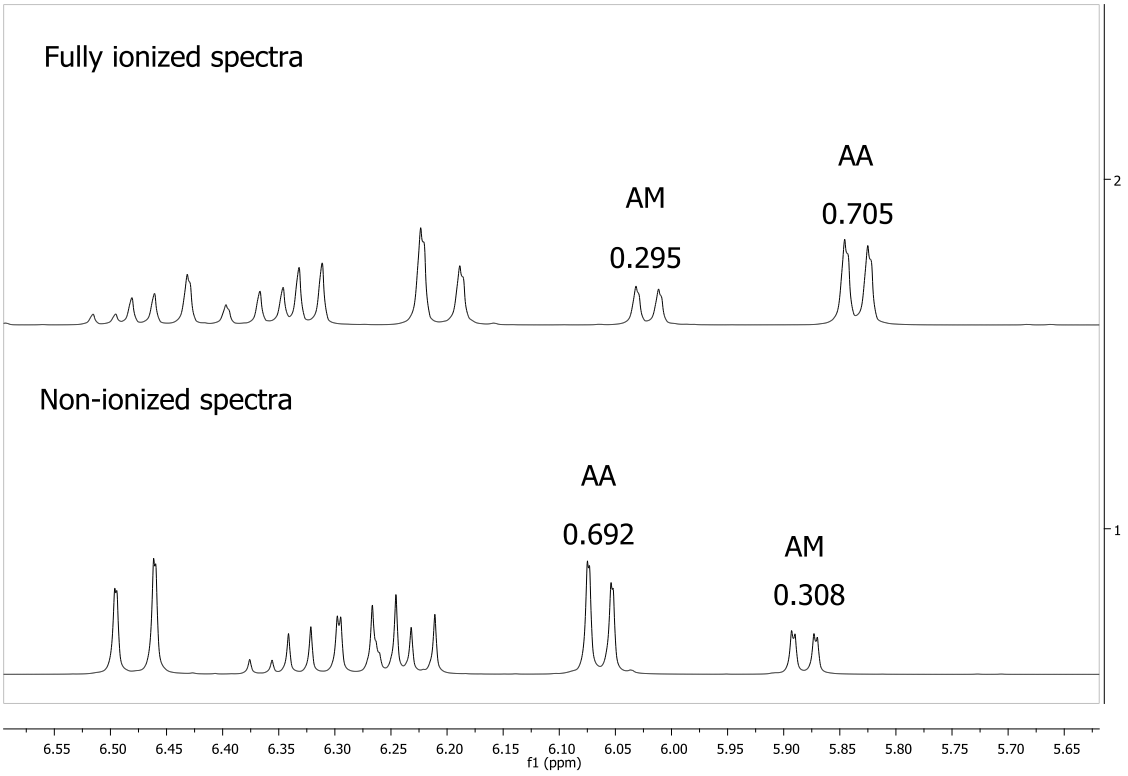

Figure 6.4 Comparison of fully ionized (top) and non-ionized (bottom) monomer peaks at f_{AM} = 0.3 and 5 wt% monomer. Only the monomer peaks used in the integration for the monomer composition and conversion calculation are labeled.

6.3 Experimental Results

6.3.1 Effect of Monomer Concentration on the Monomer Composition

The intent of the experimental design was to take advantage of the capabilities of the in-situ NMR technique in order to expand the range of monomer concentration over that of the previous literature,[46,48–51,53] approaching conditions more relevant to industry. Monomer concentration was increased to 30 wt% monomer (3.7 mol·L^{-1}), with the drift in monomer composition as a function of conversion measured at three initial monomer compositions. Figure 6.5 plots the monomer composition as a function of conversion at various initial monomer compositions and concentrations for experiments at 50 ºC with 0.2 wt% V-50. (The experiment run

at 20 wt% monomer has an initial monomer composition of f_{AM0} = 0.72, slightly higher than the other experiments performed at initial monomer composition f_{AM0} = 0.7.) It is clear that the drift in monomer composition is a function of the initial monomer concentration, suggesting that the system reactivity ratios are a function of the initial conditions of the system. Such an effect of the monomer concentration on the monomer compositions profiles has been observed in the literature for this system,[51] as well as for the copolymerization of AM with a quarternary ammonium salt (DMAEA-Q), a monomer that carries a permanent positive charge.[57] The change in the monomer composition drift with monomer concentration is attributed to the ionic strength of the system: the higher the monomer concentration, the more charged species are in the system to screen the charges, leading to a greater incorporation of the charged species into the copolymer, as indicated by the slower relative consumption of AM.

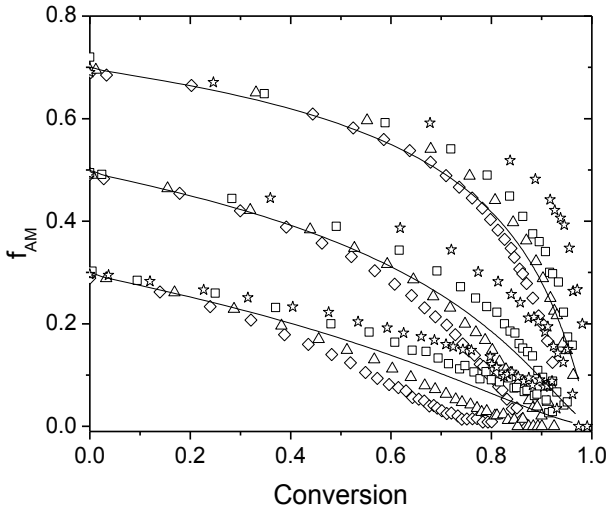

Figure 6.5 Experimental monomer composition as a function of conversion measured at 50 ºC, 0.2 wt% V-50 at 5 (◇), 10 (△), 20 (□), and 30 initial wt% monomer (☆) in aqueous solution. The lines indicate the predicted drift in monomer composition as a function of conversion calculated using the best-fit global reactivity ratios (r_{AM} = 2.15 and r_{AA} = 0.4), as estimated by non-linear parameter estimation using the entire data set.

In order to obtain the best possible representation of the monomer composition data, the reactivity ratios were fit with a variety of assumptions using the non-linear parameter estimation capabilities of Predici. First, the reactivity ratios were fit globally yielding one set of reactivity ratios independent of monomer concentration with r_{AA} = 0.4 and r_{AM} = 2.15. While a single set of reactivity ratios were sufficient to describe the copolymerization of non-ionized AA with AM (Chapter 3 and Chapter 5), such is not the case for the ionized copolymerization; the corresponding prediction of the monomer composition as a function of conversion clearly cannot capture the effect of monomer composition (Figure 6.5). Next, separate values of the reactivity ratios were estimated for each initial weight fraction of monomer (w'_{M0} = 0.05, 0.1, 0.2 and 0.3), assuming that the value stayed constant with conversion. As shown in Figure 6.6, the estimated values vary systematically with w'_{M0}, as reasonably captured by a linear fit that provides a description of the data that can be easily implemented in a model.

$$r_{AA} = 0.13 + 1.27w'_{M0} \qquad 6.6$$

$$r_{AM} = 2.07 - 1.37w'_{M0}$$

The resulting fit of the monomer composition drift as a function of conversion data is very good, as seen in Figure 6.7. The variation in the reactivity ratios with the initial monomer weight fraction highlights the sensitivity of estimated reactivity ratios to the quality of the experimental data, which explains the high scatter of the reactivity ratios in the published literature. For experiments with added salt, it is likely that the total initial weight fraction of monomer and salt would have to be accounted for in the above equations. Further experimental studies would validate or disprove this claim.

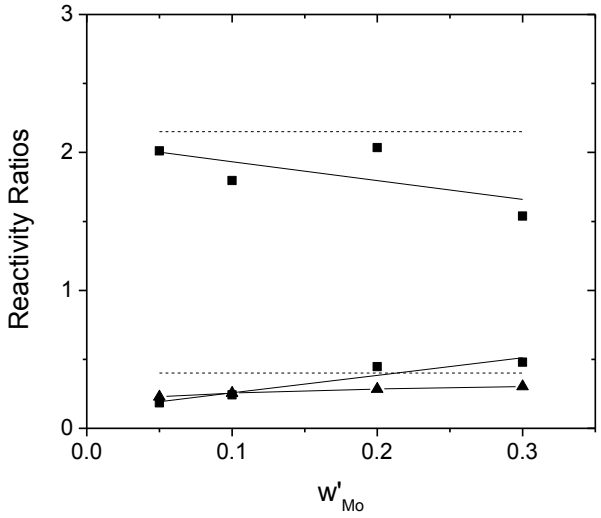

Figure 6.6 Reactivity ratios as predicted by the global fit to the combined data set (dashed line); estimates obtained at each initial monomer concentration (■) and the corresponding linear fit by Equation 6.6 (solid line), and the initial fully ionized AA concentration fit (Equation 6.8,-▲-). The r_{AM} values are at the top of the figure, while the r_{AA} values are at the bottom of the figure.

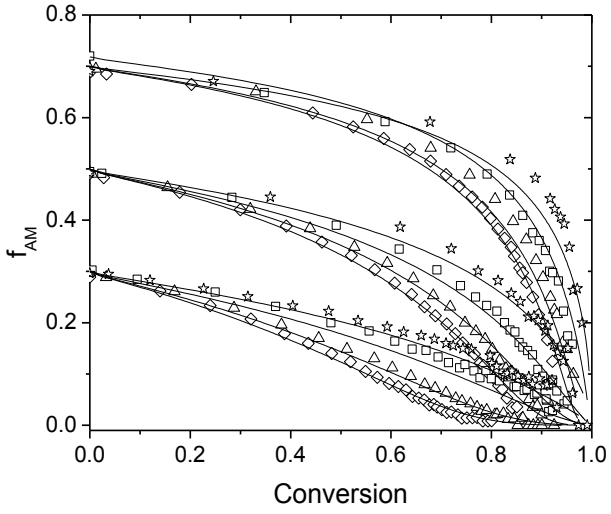

Figure 6.7 Experimental monomer composition as a function of conversion measured at 50 ºC, 0.2 wt% V-50 at 5 (◇), 10 (△), 20 (□), and 30 wt% monomer (☆). The predicted monomer compositions (lines) as a function of conversion are calculated using reactivity ratios that vary with the total initial monomer concentration (Equation 6.6).

Lastly, the reactivity ratios were fit incorporating the initial molar concentration of fully ionized AA as a measure of ionic strength, based on the work by Cuccato et al. discussed in the introduction to the chapter.[57] The reactivity ratios follow the format

$$r = A[\text{ionized AA}]_o^b \qquad 6.7$$

where A and b are constants and $[\text{ionized AA}]_o$ is the initial molar concentration of fully ionized AA. In an attempt to follow the approach used by Cuccato et al., the reactivity ratios were estimated as follows:

$$r_{AA} = 0.4[\text{ionized AA}]_0^{0.16} \qquad 6.8$$

$$r_{AM} = 2.15$$

When the three parameters were estimated in Predici, A and $r_{AM,}$ were close to those of the global fit values, and b was estimated to be close to 0 and with a confidence interval passing through zero. As a result, the r values estimated from the global fit were used, and b was estimated to a value of 0.16 by Predici. A comparison of the estimated reactivity ratios using Equation 6.8 can be found in Figure 6.6. The effect of monomer concentration on r_{AA} is quite small, leading to poorly predicted monomer composition drifts, as shown in Figure 6.8. The poor predictive value of the reactivity ratios are a result of the concentration of fully ionized AA being a function of both monomer composition and concentration. For example, at f_{AM0} = 0.7 and 10 wt% monomer, $[\text{ionized AA}]_0$ is 0.038 mol·L^{-1}, similar to the value for f_{AM0} = 0.3 at 5 wt%, which is 0.040 mol·L^{-1}, leading to the same reactivity ratios with Equation 6.8.

For this copolymerization it is known that both reactivity ratios are a function of the degree of ionization following the change in the propagation rate coefficient of AA.[46] For a fit capturing the entire range of degree of ionization, which will be discussed in the following chapter, it is reasonable to have both reactivity ratios changing with monomer concentration. Therefore the reactivity ratios that are a function of the initial total weight fraction as described in Equation 6.6 will be used in the modeling efforts.

Our work considers the total initial weight fraction of monomer in the implementation of the reactivity ratios, while the work by Cuccato implements backbiting and rate coefficients dependent on ionic strength. Further work into modeling monomer conversion and composition of copolymerizations with charged species will show which method is more useful. The empirical methodology presented here is easily implemented into any modeling framework, and it based on experimentally measured composition over a range of conditions. However the robustness of this method still must be validated, especially when moving to conditions at different temperatures and varying ionic strengths by the addition of salt.

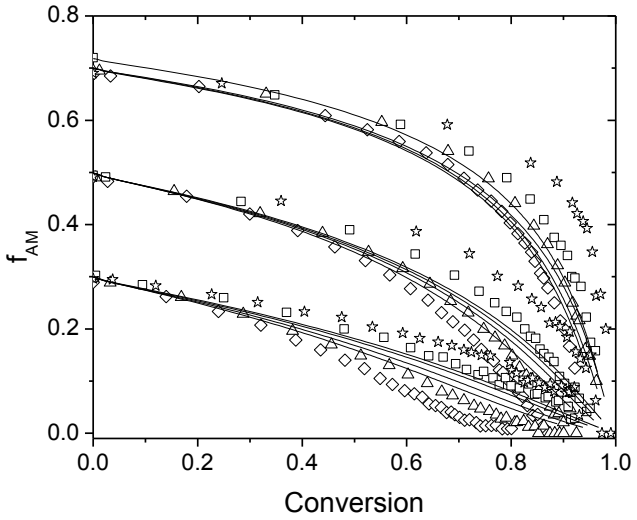

Figure 6.8 Experimental monomer composition as a function of conversion measured at 50 ºC, 0.2 wt% V-50 at 5 (◇), 10 (△), 20 (□), and 30 wt% monomer (☆). The predicted monomer composition as a function of conversion using the total initial fully ionized AA concentration fit (Equation 6.8) is graphed using solid lines.

6.3.2 Understanding the Scatter in the Literature Reactivity Ratios

For anyone working with the copolymerization of AA and AM, it is a well-known fact that the reported reactivity ratios are very scattered, especially for fully ionized conditions.[46,48–51,53] Therefore this section aims to investigate the source of these discrepancies and to evaluate whether

reactivity ratios in the literature provide a reasonable prediction of the composition drift of our NMR data, which covers a wider range of concentrations than considered in the literature.

The data from Paril et al. was measured at 60 °C and 0.47 mol·L^{-1} (3.7 wt% monomer) using ACV as initiator.[48] Experimental data in reference [48] is available for f_{AM0} = 0.7 in graphical format and was read from the plot in 0.1 increments in conversion. As the monomer composition presented in reference [48] is very scattered, one average value was read for each conversion and compared to our NMR data in Figure 6.9. At the initial condition (x = 0.0), the monomer composition measured ranged within ±0.01, while at high conversion (x = 0.8) the confidence interval increases to ±0.04. The monomer composition drift measured by Paril et al. follows the same trend as we found for all initial monomer contents until a conversion of 40 % and then follows the drift of our high monomer concentration (20 and 30 wt% monomer) experiments, despite their low monomer concentration of 3.7 wt% monomer. The experimental method used is termed ACOMP (automatic continuous online monitoring of polymerization reactions), which relies on the continuous removal of sample from the reaction mixture with a pump in order to obtain the monomer composition and conversion using light scattering and UV detection.[48] While routinely used by this group, the rate of monomer removal or the size of the reaction vessel is not specified;[48,49,65,112] the only information given is that typically 5 mL of the total reaction solution is removed.[65] If the sample removed is not homogenous due to higher viscosity, this may explain some of the mismatch observed at higher conversions.

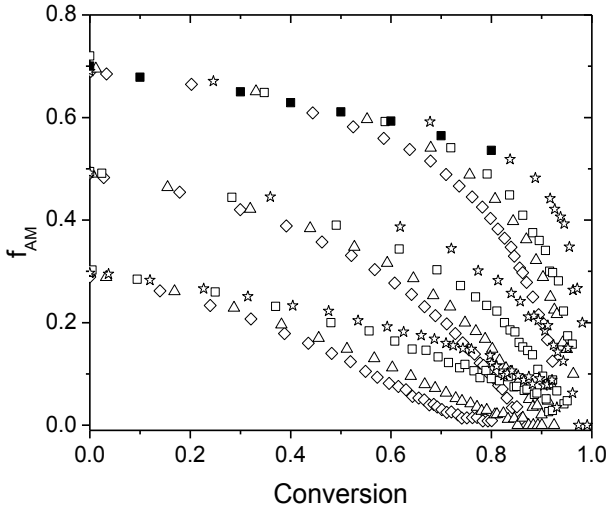

Figure 6.9 Comparison of experimental monomer composition as a function of conversion data measured as part of this work at 50 ºC, 0.2 wt% V-505 (◇), 10 (△), 20 (□), and 30 wt% monomer (☆). Experimental literature data collected at 60 ºC, 8.9 x 10^{-3} mol·L^{-1} ACV, f_{AM0} = 0.7 and 3.7 wt% monomer (■).[48]

The reactivity ratios were estimated to be 1.88 and 0.8 for r_{AM} and r_{AA}, respectively, using monomer composition as a function of conversion data collected at seven initial monomer compositions.[48] The resulting simulation of monomer composition is plotted against our data in Figure 6.10. It is seen that the predicted drift matches our experimental results only at low conversions, with the high conversion behavior best matched for f_{AM0}=0.7 and 30 wt% monomer, far from the conditions of their experimental study (3.4 wt% monomer).

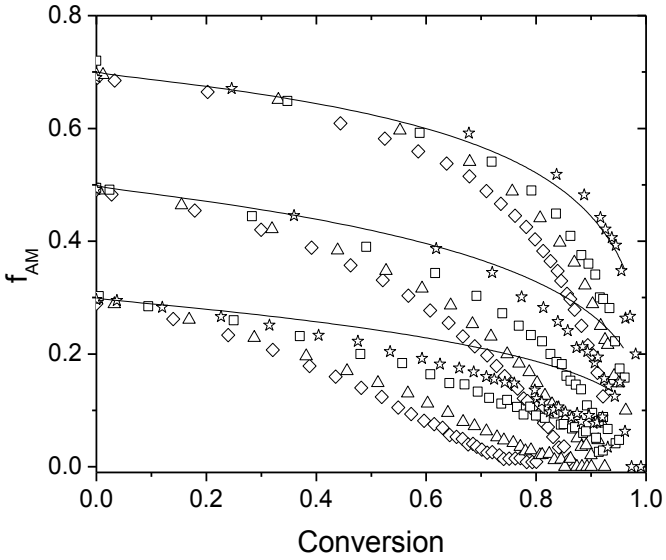

Figure 6.10 Experimental monomer composition as a function of conversion measured at 50 ºC, 0.2 wt% V-50 at 5 (◇), 10 (△), 20 (□), and 30 wt% monomer (☆). The predicted monomer composition as a function of conversion using the reactivity ratios from reference [48] (r_{AM} = 1.88 and r_{AA} = 0.8) is graphed with the solid line.

Another set of experimental data was tabulated by Riahinezhad et al.[50] in terms of monomer conversion and copolymer composition. The monomer composition was calculated by re-arranging and solving the equation of the cumulative copolymer composition

$$F_{\mathrm{AM}}^{\mathrm{cum}} = \frac{f_{\mathrm{AM0}} - f_{\mathrm{AM}}(1-x)}{x} \qquad 6.9$$

where x is the total conversion. Figure 6.11 compares the data collected as part of our work and the data collected at initial monomer compositions of f_{AM0} = 0.1 and 0.46 at 40 ºC, 4×10^{-3} mol·L^{-1} ACV (4,4'-azo-bis(4-cyano valeric acid)) and at 1 mol·L^{-1} monomer (7.2 wt% monomer). The elemental analysis used to determine the copolymer composition yields a higher level of scatter[50] than the NMR data. This scatter in the copolymer composition leads to monomer compositions that are negative for low monomer compositions (Figure 6.11). Nevertheless, the agreement between the two techniques is very satisfying, even at high conversions, and gives confidence in the data

collected from both lab groups. The estimated reactivity ratios of r_{AM} = 1.33 and r_{AA} = 0.23[50] are used to predict the monomer composition drift with conversion and compared to our experimental NMR data in Figure 6.12. The monomer composition drift at 10 wt% is reasonably well fit for f_{AM0} = 0.3 and 0.5, similar to the monomer compositions used to estimate the reactivity ratios.[50] However, for f_{AM0} = 0.7 the monomer composition drift at 10 wt% monomer is not accurately captured, a result perhaps of not studying a sufficient initial monomer composition range to estimate the reactivity ratios. Therefore the reactivity ratios estimated in reference [50] give good predictions of monomer composition drift at monomer concentrations of ~10 wt% and for AA rich monomer compositions. In a subsequent publication by this group the effect of monomer concentration was also studied (3.5 to 10.8 wt% monomer) at full degree of ionization.[52] A similar effect of the monomer concentration was observed as found in our study, however, the highest f_{AM0} content remained below 0.6, leading to similar observations of a poor fit of our data collected at high AM contents.[52]

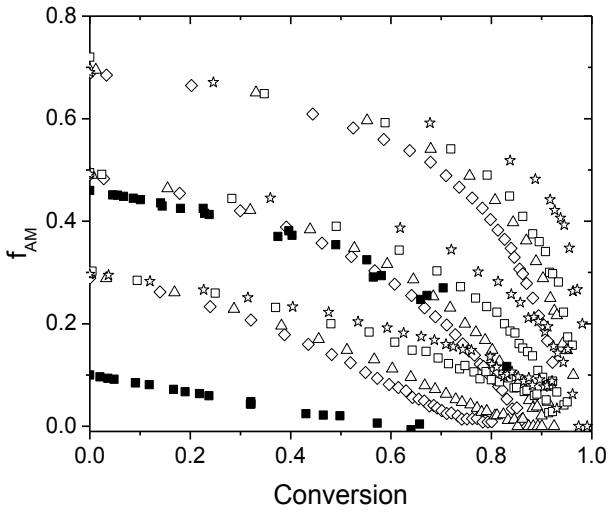

Figure 6.11 Comparison of experimental monomer composition as a function of conversion data measured as part of this work at 50 ºC, 0.2 wt% V-50, 5 (◇), 10 (△), 20 (□), and 30 wt% monomer (☆). Experimental literature data collected at 40 ºC, 4 x 10^{-3} mol·L^{-1} ACV, and 7.2 wt% monomer (■).[50]

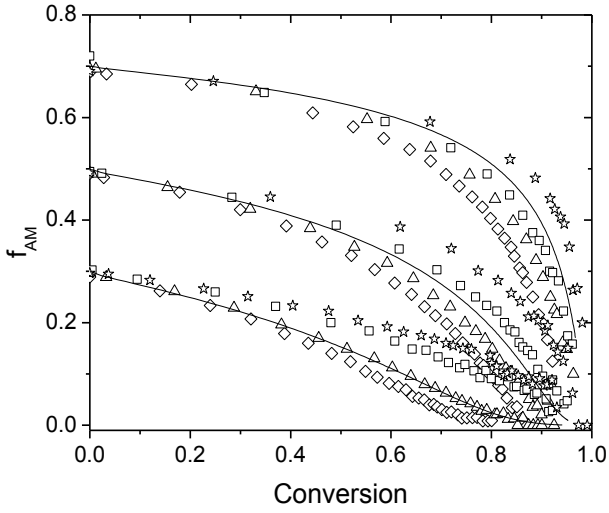

Figure 6.12 Experimental monomer composition as a function of conversion measured at 50 °C, 0.2 wt% V-50 at 5 (◇), 10 (△), 20 (□), and 30 wt% monomer (☆). The predicted monomer composition as a function of conversion using the reactivity ratios from reference [50] (r_{AM} = 1.33 and r_{AA} = 0.23) is graphed with the solid line.

The experimental data used in the reactivity ratio estimation in the work of Ponratnam and Kapur is tabulated, yet limited.[53] Here, one data point per experiment run at initial monomer compositions f_{AM0} = 0.2557, 0.2906, 0.5029, 0.5912 and 0.7159 is available for experiments conducted at 30 °C, 2.5×10^{-3} mol·L^{-1} potassium persulfate-sodium dithionite as initiator, and 1 mol·L^{-1} monomer (7.2 wt% monomer).[53] The cumulative copolymer compositions were experimentally determined using the Kjeldahl method, a process involving several steps to determine the nitrogen content by liberating and capturing it from the sample. The monomer composition was calculated using Equation 6.9 and the resulting comparison to the NMR data can be found in Figure 6.13. Even with the limited available data at the similar initial monomer composition (f_{AM0} = 0.3 and 0.5), it appears that the experimental composition drift reflect the trends of the NMR data collected at higher monomer concentrations (20 and 30 wt% monomer). Reactivity ratios of r_{AM} = 0.63 and r_{AA} = 0.12[53] were estimated and the resulting monomer

composition drift predictions are plotted in Figure 6.14 with the NMR data. The predictions of the monomer composition drift compare well with our data at 10 wt% monomer and f_{AM0} = 0.3, however this is not the case at f_{AM0} = 0.5 and 0.7.

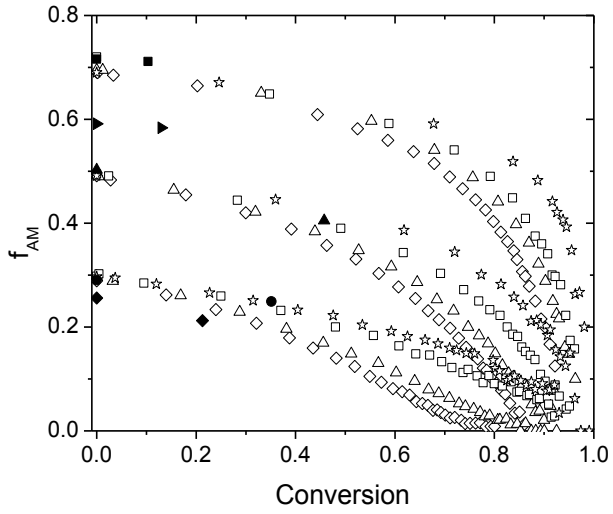

Figure 6.13 Comparison of experimental monomer composition as a function of conversion data measured as part of this work at 50 ºC, 0.2 wt% V-50, 5 (◇), 10 (△), 20 (□), and 30 wt% monomer (☆). Experimental literature data collected at 30 ºC, 2.5 x 10^{-3} mol·L^{-1} potassium persulfate-sodium dithionite, 7.2 wt% monomer and f_{AM0} = 0.2557 (♦), 0.2906 (●), 0.5029 (▲), 0.5912 (►), and 0.7159 (■).[53]

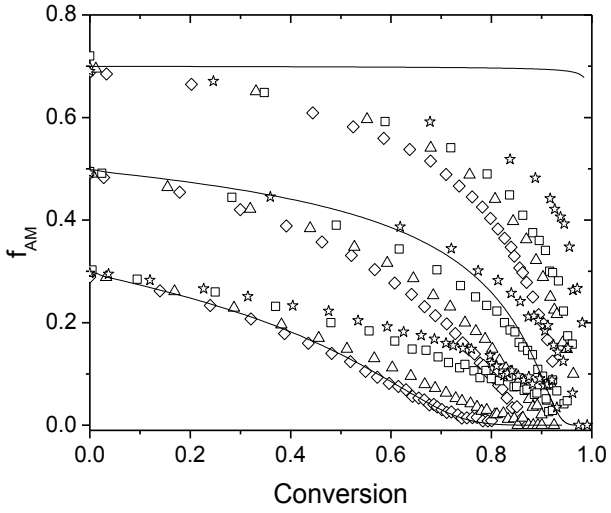

Figure 6.14 Experimental monomer composition as a function of conversion measured at 50 ºC, 0.2 wt% V-50 at 5 (◇), 10 (△), 20 (□), and 30 wt% monomer (☆). The predicted monomer composition as a function of conversion using the reactivity ratios from reference [53] (r_{AM} = 0.63 and r_{AA} = 0.12) is graphed with the solid line.

No experimental data at the relevant pH from Rintoul and Wandrey's work[46] were available to compare to data measured in our work. As a result, only the fit of the monomer composition as a function of conversion calculated using the reactivity ratios they estimated from low conversion experiments at a pH value of 7.8 and an initial monomer content of 3 wt% can be compared to our data (Figure 6.15). The predicted monomer composition drift is close to our measured data at low monomer concentrations (5 and 10 wt%), the conditions at which these reactivity ratios were determined.

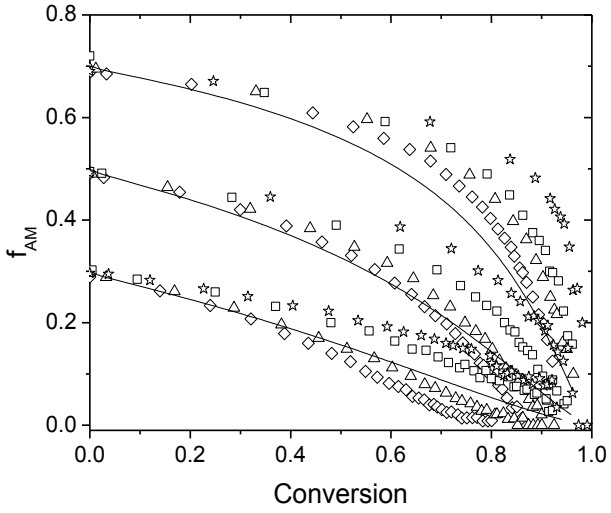

Figure 6.15 Experimental monomer composition as a function of conversion measured at 50 ºC, 0.2 wt% V-50 at 5 (◇), 10 (△), 20 (□), and 30 wt% monomer (☆). The predicted monomer composition as a function of conversion using the reactivity ratios from reference [46] at a pH of 7.8 (r_{AM} = 2.95 and r_{AA} = 0.42) is graphed with the solid line.

Unsurprisingly, the scattered reactivity ratios in the literature are the result of scatter in the experimental data. Data between lab groups is not consistent for the same initial monomer compositions, with the exception of the data measured by Riahinezhad and our NMR data at 10 wt% monomer and the predictions of composition drift at low monomer concentrations using reactivity ratios estimated from low conversion data by Rintoul and Wandrey at low monomer concentrations. The scatter in the reactivity ratios are a testament to the difficulty analyzing water soluble polymers, and in particular this system. With the systematic approach taken in our work to measure the monomer composition drift as a function of monomer composition over a wide range of monomer compositions and monomer concentrations for the full conversion range, we were able to illuminate some of the shortcomings in the experimental design in the literature. Most importantly, a large range of monomer composition is needed for accurate representation of the monomer composition drift. Secondly, the reactivity ratios are a function of initial monomer

concentration at fully ionized conditions, as shown by this work, and the recent work by Riahinezhad et al.[50] By going to high monomer concentrations (30 wt%), we provide a comprehensive examination of this system not available in the previous literature. As a result, we were able to determine a representation of reactivity ratios valid over a range of monomer compositions and concentrations.

6.3.3 Monomer Conversion Profiles

Figure 6.16 plots the monomer conversion profiles for varying initial monomer compositions at constant initial monomer concentration, while Figure 6.17 plots the same information grouped at constant monomer composition. A pronounced monomer composition effect is observed (Figure 6.16) at all monomer concentrations, unlike the data collected at non-ionized conditions (Chapter 3 and 5) where the conversion profiles are almost independent of monomer composition. A monomer concentration effect is visible (Figure 6.17): the slower conversion rates at lowered monomer concentrations is consistent with all of the previous data presented, indicating that backbiting also influences this copolymerization.

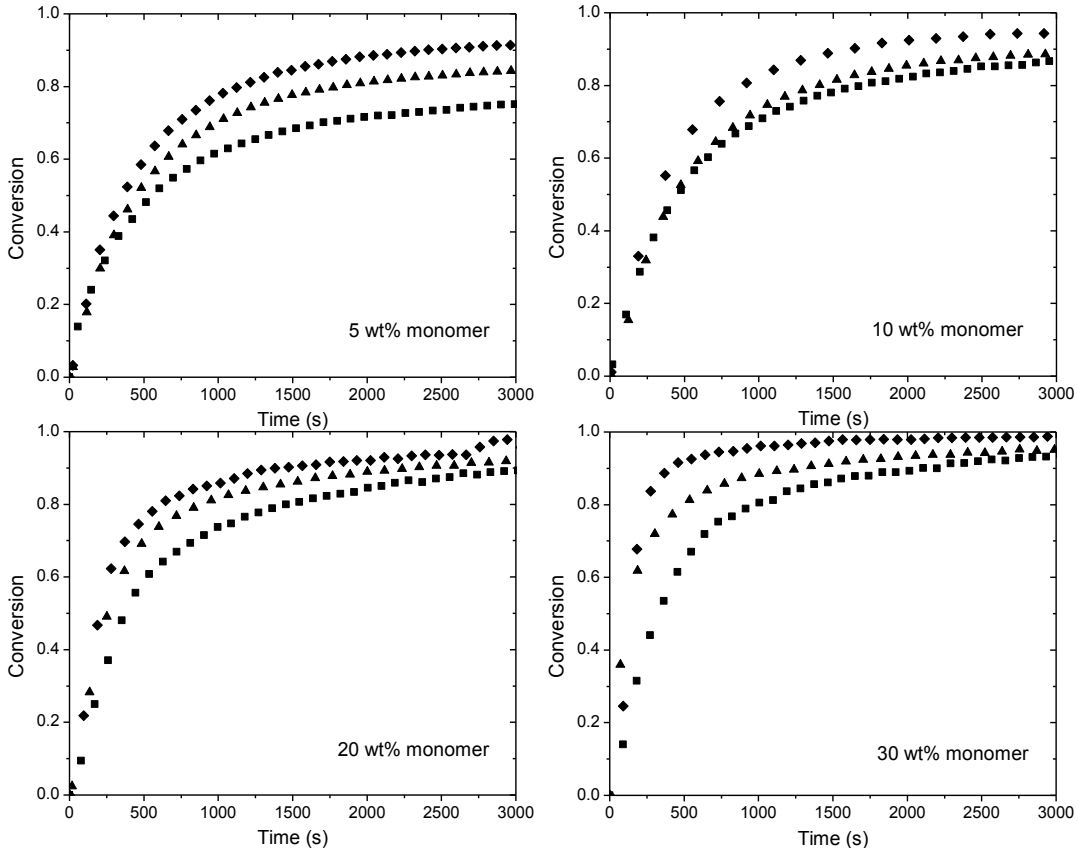

Figure 6.16 Experimental batch monomer conversion profiles of fully ionized AA and AM at 50 ºC, 0.2 wt% V-50, at 5 (top left), 10 (top right), 20 (bottom left) and 30 wt% monomer (bottom right) in aqueous solution for initial monomer compositions of f_{AM0} = 0.3 (■), 0.5 (▲), and 0.7 (♦).

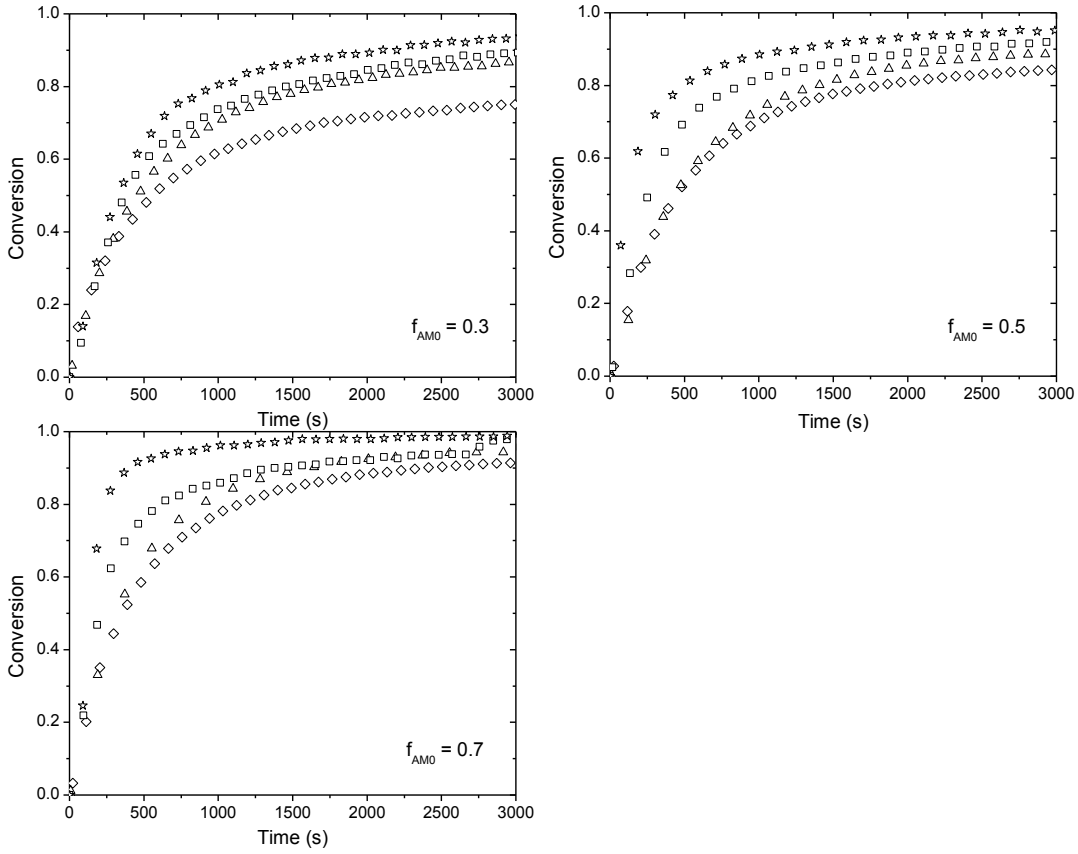

Figure 6.17 Experimental batch monomer conversion profiles of fully ionized AA and AM at 50 °C, 0.2 wt% V-50, at f_{AM0} = 0.3 (top left), 0.5 (top right), and 0.7 (bottom left) for initial monomer concentration of 5 (◇), 10 (△), 20 (□), and 30 wt% (☆) in aqueous solution.

6.4 Model Development

Table 6.2 outlines the reaction steps considered while Table 6.3 summarizes rate coefficients necessary for the model implementation. The reaction steps are the same as for the non-ionized model, with the exception that the cross-propagation rate coefficients are described by the terminal model as no copolymer propagation rate data is currently available. While the rate coefficients of AM are measured and validated, there is uncertainty in all rate coefficients for fully ionized AA. It is assumed that the influence of monomer concentration on the propagation rate coefficient follows the same functional form as that for MAA.[34] The activation energy and pre-

exponential factor were adapted from non-ionized conditions using the functional form employed to represent MAA propagation as a function of ionization,[34] using also the propagation rate coefficient of the fully ionized AA collected at 6 °C.[29] It was assumed that the monomer addition to the AA-based MCR is affected by monomer concentration and degree of ionization in the same way as the SPR propagation rate coefficient.[107] The pre-exponential term of the termination rate coefficient was reduced by a factor of 12 relative to the non-ionized system, following the increase in the measured viscosity of fully ionized AA.[107] The backbiting rate coefficient, thought to be a function of the flexibility of the polymer chain, was implemented as a function of ionic strength to mimic this effect.[107] This effect is combined with the non-ionized backbiting rate coefficient to yield the expression in Table 6.3. For the copolymerization the AM units were also considered to affect the polymer backbone flexibility, an effect captured by using the instantaneous copolymer composition (F_{AA}^{inst}). The term I in the backbiting rate coefficient refers to the sum of the charges in the system given by:

$$I = \frac{1}{2}\sum c_i z_i^2 \qquad 6.10$$

where c is the concentration of ion i, and z is the charge of species i. As all charged species have one charge each, Equation 6.10 reduces to I = [AA], the ionic strength.

The same general treatments for the description of copolymer termination, cross transfer to monomer and cross backbiting is used as described for the non-ionized copolymerization model.

Table 6.2 Set of reaction steps considered for the copolymerization of fully ionized AA and AM.

Initiation	
$$I \xrightarrow{k_d} 2f I^{rad}$$	
$$I^{rad} + AM \xrightarrow{k_p^{AM}} P_1^{AM}$$	$$I^{rad} + AA \xrightarrow{k_p^{AA}} P_1^{AA}$$
Chain Propagation	
$$P_n^{AA} + AA \xrightarrow{k_p^{AA}} P_{n+1}^{AA}$$	$$P_n^{AM} + AM \xrightarrow{k_p^{AM}} P_{n+1}^{AM}$$
$$P_n^{AA} + AM \xrightarrow{k_p^{AA\cdot AM}} P_{n+1}^{AM}$$	$$P_n^{AM} + AA \xrightarrow{k_p^{AM\cdot AA}} P_{n+1}^{AA}$$
Transfer to Monomer	
$$P_n^{AM} + AM \xrightarrow{k_{tr}^{AM}} D_n + P_1^{AM}$$	$$P_n^{AA} + AA \xrightarrow{k_{tr}^{AA}} D_n + P_1^{AA}$$
$$P_n^{AM} + AA \xrightarrow{k_{tr}^{AM\cdot AA}} D_n + P_1^{AA}$$	$$P_n^{AA} + AM \xrightarrow{k_{tr}^{AA\cdot AM}} D_n + P_1^{AM}$$
Termination SPR-SPR	
$$P_n^{AM} + P_m^{AM} \xrightarrow{(1-\alpha_{ss})k_{t,ss}^{cop}} D_{n+m} \,/\, \xrightarrow{\alpha_{ss}k_{t,ss}^{cop}} D_n + D_m$$	
$$P_n^{AA} + P_m^{AA} \xrightarrow{(1-\alpha_{ss})k_{t,ss}^{cop}} D_{n+m} \,/\, \xrightarrow{\alpha_{ss}k_{t,ss}^{cop}} D_n + D_m$$	
$$P_n^{AA} + P_m^{AM} \xrightarrow{(1-\alpha_{ss})k_{t,ss}^{cop}} D_{n+m} \,/\, \xrightarrow{k_{t,ss}^{cop}} D_n + D_m$$	
Backbiting	
$$P_n^{AM} \xrightarrow{F_{AM}^{inst}k_{bb}^{AM}} Q_n^{AM}$$	$$P_n^{AA} \xrightarrow{(1-F_{AM}^{inst})k_{bb}^{AA}} Q_n^{AA}$$
$$P_n^{AM} \xrightarrow{(1-F_{AM}^{inst})k_{bb}^{AM\cdot AA}} Q_n^{AA}$$	$$P_n^{AA} \xrightarrow{F_{AM}^{inst}k_{bb}^{AA\cdot AM}} Q_n^{AM}$$
Addition to MCR	
$$Q_n^{AM} + AM \xrightarrow{k_{p,tert}^{AM}} P_{n+1}^{AM}$$	$$Q_n^{AA} + AA \xrightarrow{k_{p,tert}^{AA}} P_{n+1}^{AA}$$
$$Q_n^{AM} + AA \xrightarrow{k_{p,tert}^{AM\cdot AA}} P_{n+1}^{AA}$$	$$Q_n^{AA} + AM \xrightarrow{k_{p,tert}^{AA\cdot AM}} P_{n+1}^{AM}$$

Cross Termination MCR-SPR

$$P_n^{AM} + Q_m^{AM} \xrightarrow{(1-\alpha_{st})k_{t,st}^{cop}} D_{n+m} \,/\, \xrightarrow{\alpha_{st}k_{t,st}^{cop}} D_n + D_m$$

$$P_n^{AA} + Q_m^{AA} \xrightarrow{(1-\alpha_{st})k_{t,st}^{cop}} D_{n+m} \,/\, \xrightarrow{\alpha_{st}k_{t,st}^{cop}} D_n + D_m$$

$$P_n^{AM} + Q_m^{AA} \xrightarrow{(1-\alpha_{st})k_{t,st}^{cop}} D_{n+m} \,/\, \xrightarrow{\alpha_{st}k_{t,st}^{cop}} D_n + D_m$$

$$P_n^{AA} + Q_m^{AM} \xrightarrow{(1-\alpha_{st})k_{t,st}^{cop}} D_{n+m} \,/\, \xrightarrow{\alpha_{st}k_{t,st}^{cop}} D_n + D_m$$

Termination MCR-MCR

$$Q_n^{AM} + Q_m^{AM} \xrightarrow{(1-\alpha_{tt})k_{t,tt}^{cop}} D_{n+m} \,/\, \xrightarrow{\alpha_{tt}k_{t,tt}^{cop}} D_n + D_m$$

$$Q_n^{AA} + Q_m^{AA} \xrightarrow{(1-\alpha_{tt})k_{t,tt}^{cop}} D_{n+m} \,/\, \xrightarrow{\alpha_{tt}k_{t,tt}^{cop}} D_n + D_m$$

$$Q_n^{AA} + Q_m^{AM} \xrightarrow{(1-\alpha_{tt})k_{t,tt}^{cop}} D_{n+m} \,/\, \xrightarrow{\alpha_{tt}k_{t,tt}^{cop}} D_n + D_m$$

Table 6.3 Rate expressions used in the model for the copolymerization of fully ionized AA and AM.

Rate Expression	Values*	Ref
Initiation:		
$k_d(s^{-1}) = 9.24\times10^{14}\exp\left(-\frac{14\,915}{T/K}\right)$	8.7×10^{-6}	[87]
Initiator efficiency: 0.8		
Chain Propagation:		
$k_p^{AM}(L\cdot mol^{-1}\cdot s^{-1})$ $= k_{p,max}^{AM}\exp[-w'_{AM}(0.0016(T/K^{-1}) + 1.015)]$	8.0×10^4	[12], this work
$k_{p,max}^{AM}(L\cdot mol^{-1}\cdot s^{-1}) = 9.5\times10^7\exp\left(-\frac{2189}{T/K}\right)$	1.1×10^5	

$k_{\mathrm{p}}^{\mathrm{AA}}(\mathrm{L}\cdot\mathrm{mol}^{-1}\cdot\mathrm{s}^{-1})$		[107]
$= 1.97\times10^{7}\exp\left(-\frac{1395}{T/\mathrm{K}}\right)(0.16 + 0.84\exp(-3.7w'_{\mathrm{AA}}))(1.6w'_{\mathrm{AA}} + 0.04)$	5.3×10^{4}	
$r_{AA} = 0.13 + 1.27w'_{Mo}$	0.38	This work
$r_{AM} = 2.07 - 1.37w'_{Mo}$	1.8	
Transfer to Monomer:		
$C_{\mathrm{tr}}^{\mathrm{AM}} = \frac{k_{\mathrm{tr}}^{\mathrm{AM}}}{k_{\mathrm{p}}^{\mathrm{AM}}} = 0.00118\exp\left(-\frac{1002}{T/\mathrm{K}}\right)$	5.3×10^{-5}	This work
$C_{\mathrm{tr}}^{\mathrm{AA}} = \frac{k_{\mathrm{tr}}^{\mathrm{AA}}}{k_{\mathrm{p}}^{\mathrm{AA}}} = 7.5\times10^{-5}$	7.5×10^{-5}	[21]
Termination SPR-SPR:		
$k_{\mathrm{t,ss}}^{\mathrm{AM}}(\mathrm{L}\cdot\mathrm{mol}^{-1}\cdot\mathrm{s}^{-1}) = 2\times10^{10}\exp\left(-\frac{(1991 + 1477w'_{\mathrm{Mo}})}{T/\mathrm{K}}\right)$	1.7×10^{7}	[25], This work
$k_{\mathrm{t,ss}}^{\mathrm{AA}}(\mathrm{L}\cdot\mathrm{mol}^{-1}\cdot\mathrm{s}^{-1}) = 1.5\times10^{10}\exp\left(-\frac{1858}{T/\mathrm{K}}\right)\varphi_{\mathrm{AA}}$	1.3×10^{7}	[107]
$\varphi_{\mathrm{AA}} = 1.56 - 1.77w'_{\mathrm{Mo}} - 1.2(w'_{\mathrm{Mo}})^2 + 2.43(w'_{\mathrm{Mo}})^3$		[21]
$k_{\mathrm{t,ss}}^{\mathrm{cop}}(\mathrm{L}\cdot\mathrm{mol}^{-1}\cdot\mathrm{s}^{-1}) = \left(k_{\mathrm{t,ss}}^{\mathrm{AA}}k_{\mathrm{t,ss}}^{\mathrm{AM}}\right)^{1/2}$	1.5×10^{7}	This work
$\alpha_{\mathrm{ss}} = 0.1$		This work
Backbiting		
$k_{\mathrm{bb}}^{\mathrm{AM}}(\mathrm{s}^{-1}) = 3.7\times10^{9}\exp\left(-\frac{5881}{T/\mathrm{K}}\right)$	46	[25]
$k_{\mathrm{bb}}^{\mathrm{AA}}(\mathrm{s}^{-1}) = \frac{1.35\times10^{9}\exp\left(-\frac{5020}{T/\mathrm{K}}\right)}{\left(12 + 19.5\sqrt{\frac{F_{\mathrm{AA}}^{\mathrm{inst}}}{I}}\right)^{0.43}}$	65	[107], this work

Addition to MCR		
$k_{\mathrm{p,tert}}^{\mathrm{AM}}(\mathrm{L}\cdot\mathrm{mol}^{-1}\cdot\mathrm{s}^{-1}) = 0.0155\exp\left(-\frac{1412}{T/\mathrm{K}}\right)k_{\mathrm{p}}^{\mathrm{AM}}$	19	[25]
$k_{\mathrm{p,tert}}^{\mathrm{AA}}(\mathrm{L}\cdot\mathrm{mol}^{-1}\cdot\mathrm{s}^{-1}) = 1.5\exp\left(-\frac{2315}{T/\mathrm{K}}\right)k_{\mathrm{p}}^{\mathrm{AA}}$	48	[21]
Cross Termination MCR-SPR		
$k_{\mathrm{t,st}}^{\mathrm{cop}}(\mathrm{L}\cdot\mathrm{mol}^{-1}\cdot\mathrm{s}^{-1}) = 0.3k_{\mathrm{t,ss}}^{\mathrm{cop}}$ $\alpha_{\mathrm{st}} = 0.7$	4.4×10^{6}	This work
Termination MCR-MCR		
$k_{\mathrm{t,tt}}^{\mathrm{cop}}(\mathrm{L}\cdot\mathrm{mol}^{-1}\cdot\mathrm{s}^{-1}) = 0.01k_{\mathrm{t,ss}}^{\mathrm{cop}}$ $\alpha_{\mathrm{tt}} = 0.9$	1.45×10^{5}	This work
Density		
$\rho_{\mathrm{AM}}(\mathrm{g}\cdot\mathrm{mL}^{-1}) = 1.0854 - 2.4663\times10^{-3}T(^{\circ}C^{-1}) + 1.3154\times10^{-5}T^{2}(^{\circ}C^{-2})$	0.995	[12]
$\rho_{\mathrm{AA}}(\mathrm{g}\cdot\mathrm{mL}^{-1}) = 1.0731 - 1.0826\times10^{-3}T(^{\circ}C^{-1}) - 7.2379\times10^{-7}T^{2}(^{\circ}C^{-2})$	1.017	[107]
$\rho_{\mathrm{H2O}}(\mathrm{g}\cdot\mathrm{mL}^{-1}) = 0.9999 - 2.3109\times10^{-5}T(^{\circ}C^{-1}) - 5.44807\times10^{-6}T^{2}(^{\circ}C^{-2})$	0.984	[21]

*evaluated at 50 °C and 20 wt% monomer and $f_{\mathrm{AM}} = 0.5$
w' refers to monomer concentration of AA, AM or total monomer concentration on a polymer free basis

6.4.1 Model fit to monomer conversion profiles

The comparison of the model predictions to the experimental data, without any fitting of individual parameters other than the reactivity ratios described earlier, is shown in Figure 6.18. As the monomer mixture is enriched towards AM, the fit of the conversion profiles is improved. However, as the monomer concentration increases, the simulated initial conversion rate becomes independent of the monomer composition, in contrast to the experimental findings. This result can be explained by the convergence of the propagation rate coefficients with increasing monomer concentration: at 50 ^{o}C and 5 wt% monomer k_p^{AM}/k_p^{AA} is 3.7, while this values decreases to 1.5 and 1.14 at 20 and 30 wt% monomer respectively. As the representation of the termination rate coefficient is composition independent (as seen in Table 6.3, the estimated value for ionized AA is very similar to that of AM), and the backbiting rate coefficients for the two monomers are also of similar magnitude, it is evident why the initial conversion rates are very similar at high monomer concentration, with differences becoming apparent only at higher conversions. A better fit of the conversion profiles therefore would benefit from experimentally determined rate coefficients for fully ionized AA, especially for the propagation and backbiting rate coefficients.

Figure 6.19 compares the measured and estimated M_w values for this copolymerization. The general trends in M_w with monomer concentration and composition are captured by the model, even with the large scatter in the experimental data.

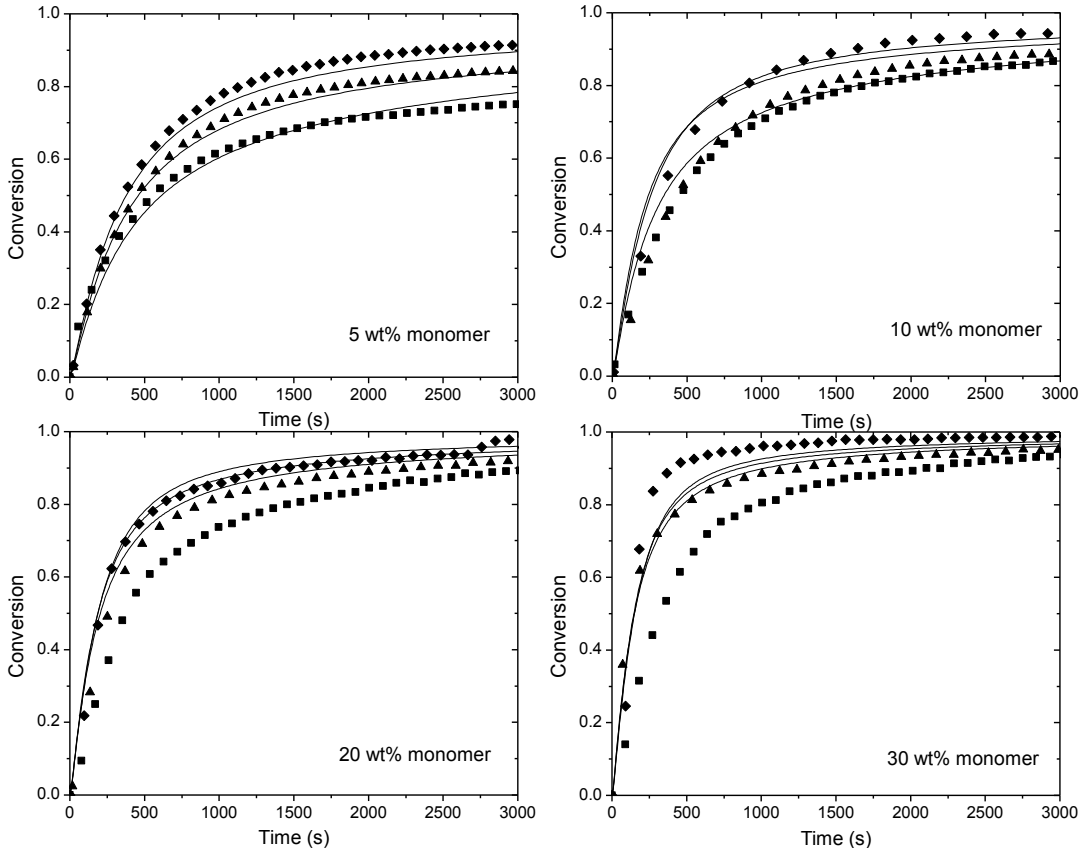

Figure 6.18 Experimental batch monomer conversion profiles of fully ionized AA and AM at 50 ºC, 0.2 wt% V-50, at 5 (top left), 10 (top right), 20 (bottom left) and 30 wt% monomer (bottom right) for initial monomer compositions of f_{AM0} = 0.3 (■), 0.5 (▲), and 0.7 (♦). Model predictions are plotted as solid lines.

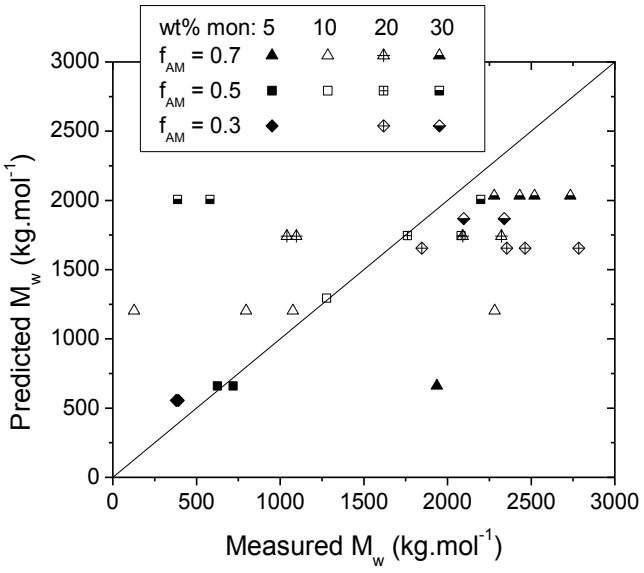

Figure 6.19 Comparison of measured M_w and predicted M_w for samples polymerized at 50 °C and 0.2 wt% V-50. Monomer compositions and concentrations are indicated in the figure legend. Experimental data points at one predicted value indicate experimental scatter.

6.4.2 Sensitivity of the Backbiting Rate Coefficient

An expression for the backbiting rate coefficient and addition to the resulting MCR for fully ionized AA can be found in the literature.[7] However, these rate coefficients were estimated assuming that the MCRs do not participate in termination reactions, and that brings into question the reported values and the reason why Wittenberg developed the expressions used in the current models.[107] For completeness, and in order to examine the sensitivity of the simulated conversion profiles their values, the published expressions were substituted into the model for 20 wt% fully ionized AA as follows:[7]

$$k_{\mathrm{bb}}^{\mathrm{AA}}(s^{-1}) = 2.2 \cdot 10^{6} \exp\left(-\frac{3090}{T} K\right)$$
$$k_{\mathrm{p,tert}}^{\mathrm{AA}}(L.mol^{-1}.s^{-1}) = 6.4 \cdot 10^{4} \exp\left(-\frac{2712}{T} K\right) \qquad 6.11$$

The calculated rate coefficient for backbiting of fully ionized AA (154 s^{-1}) is more than twice that estimated using the expression in Table 6.3 (60 s^{-1}) at 20 wt% fully ionized AA and 50 °C.

The higher backbiting rate coefficient leads to much slower predicted conversion profiles that do not match the copolymerization data well, especially at 5 wt% monomer, as shown in Figure 6.20. The predicted % SCB using the rate coefficients above, 1.18% (at f_{AM0} = 0.5, 50 ^{o}C for 90 % conversion) is more than three times higher than the value of 0.32% calculated using the expressions from Table 6.3. The difference in the predicted values is striking. Considering that we experimentally measured 1.23 % SCB for fully ionized AA homopolymerization at 90 ^{o}C and 10 wt%, and that the branching level should decrease significantly in the presence of AM due to its lower susceptibility to H-atom abstraction, it is concluded that the variable backbiting rate coefficient in Table 6.3 gives a more reasonable prediction of % SCB.

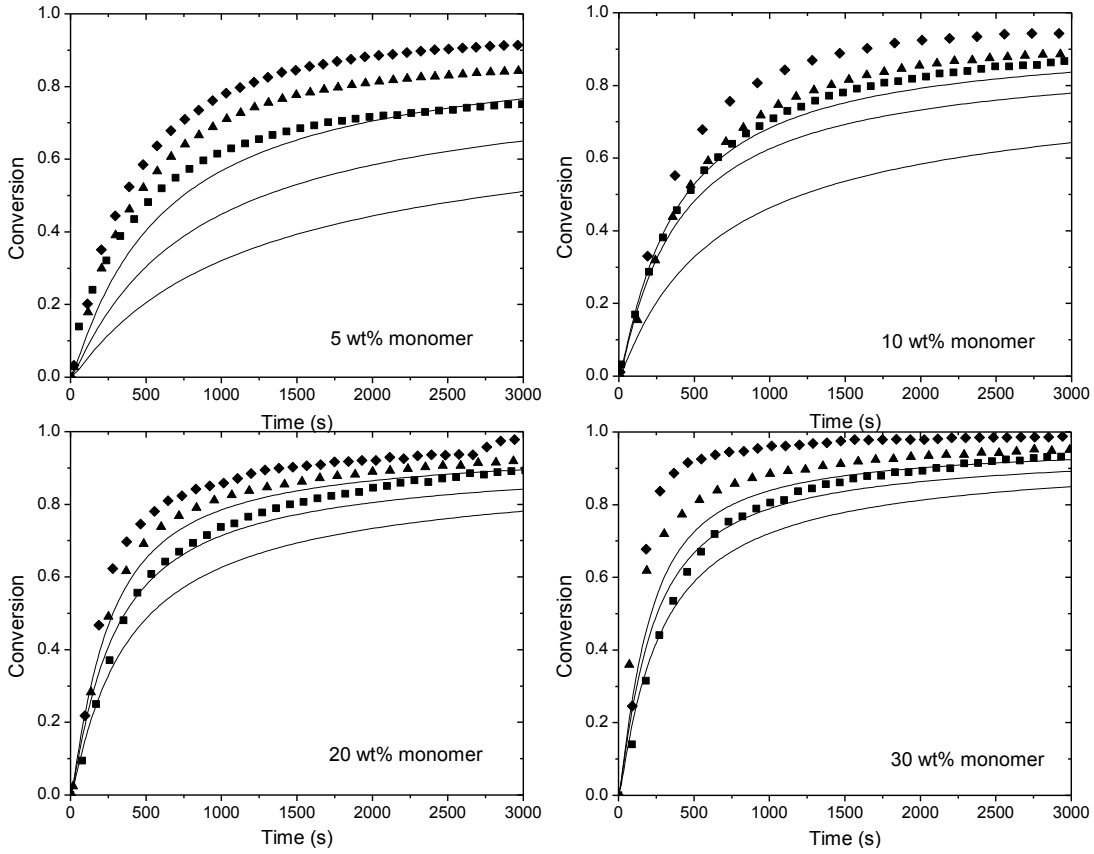

Figure 6.20 Experimental batch monomer conversion profiles of fully ionized AA and AM at 50 ºC, 0.2 wt% V-50, at 5 (top left), 10 (top right), 20 (bottom left) and 30 wt% monomer (bottom right) for initial monomer compositions of f_{AM0} = 0.3 (■), 0.5 (▲), and 0.7 (♦). Model predictions using the backbiting rate coefficients reported in reference [7] are plotted as solid lines.

6.5 Conclusions and Recommendations for Future Work

Experimental data was measured and a kinetic model was developed to represent the copolymerization of fully ionized AA and AM at 50 ºC over a broad range of monomer concentrations (5, 10, 20, and 30 wt%) and initial monomer compositions (f_{AM0} = 0.3, 0.5, and 0.7). The reactivity ratios were fit as a function of total initial monomer concentration on a weight fraction basis in order to represent the observed differences in composition drift with conversion

with varying initial monomer concentration. This empirical model relies on known experimental conditions and can be easily used to predict monomer composition drift and reactivity ratios.

The kinetic model has the same structure and set of mechanisms as the non-ionized copolymerization model, with the exception that the propagation rate coefficient is represented by the terminal model as no copolymer propagation rate data is available at this time. The AM rate coefficients, assumed to be independent of pH, are unchanged from the homopolymerization model, while the rate coefficients for fully ionized AA were adopted from Nils Wittenberg's thesis. The backbiting rate coefficient is implemented as a function of the ionic strength and instantaneous copolymer composition to account for the change in the chain flexibility at different conditions. Although this representation is based on theoretical consideration and has not been experimentally verified, the variable backbiting rate coefficient yields improved agreement with the experimental data. Measurements of rate coefficients for this copolymerization using the SP-PLP-SEC and PLP-SEC technique would give insight into the validity of the current treatment.

While the range of monomer concentrations examined experimentally is significantly expanded over previous studies, the data was only collected at a single temperature, 50 ^{o}C. In order to validate the model at different conditions, it is imperative to collect data at other temperatures. Although no effect of temperature on reactivity ratios was found for the copolymerization of AM with non-ionized AA, the same should be checked for the fully ionized system. Additionally, experiments at low monomer concentrations with added salt to match the ionic strength of higher monomer concentrations should be run, to verify if the change in the monomer composition with conversion is controlled by ionic strength, as observed in the copolymerization of other charged monomers with AM.

Chapter 7

Experimental Study of the Free Radical Copolymerization of Partially Ionized Acrylic Acid and Acrylamide

7.1 Introduction

This chapter aims to deepen the discussion and understanding of the copolymerization of ionized AA with AM. The experimental design explores the effect of monomer concentration (5 – 40 wt% monomer), degree of ionization of AA (α = 0, 0.3, 0.5, 0.7, 1.0), and the total concentration of ions (ionic strength), on the monomer composition drift and conversion profiles, thereby elaborating experimental conditions in the literature and providing a more comprehensive picture of this copolymerization system.

This chapter discusses the degree of ionization, α, frequently, thus it is important to reiterate that AA is a weak acid with a pK_a value 4.37[29] which is readily ionized by the addition of a strong base, NaOH in this work. The degree of ionization is defined as

$$\alpha = \frac{[A^-]}{[HA] + [A^-]} = \frac{[NaOH]}{[AA]} \qquad 7.1$$

where AA represents the total concentration of AA, both ionized and non-ionized. The pH can be related to the degree of ionization by substituting its definition into the Henderson-Hasselbalch equation:

$$\text{pH} = \text{p}K_a + \log\left(\frac{\alpha}{1-\alpha}\right) \qquad 7.2$$

The rate coefficients of AA are strongly affected by the system pH due to the negative charges in the monomer and polymer,[29] leading to conversion profiles that are functions of system pH or the degree of ionization.[18,22] The rate coefficients of AM, however, are thought to be independent of pH, as propagation rate measurements showed no change in system pH.[12]

Several lab groups have systematically estimated reactivity ratios for this system as a function of degree of ionization,[36,46–53] with the most complete study being from Rintoul and Wandrey.[46] Reactivity ratios from reference [46] are plotted in Figure 7.1 along with the propagation rate coefficient of AA at different pH values.[29] The change in both reactivity ratios follows the trend of the change in the propagation rate coefficient of AA, leading to the logical and generally accepted hypothesis that the ionization of the AA monomer influences its addition rate to both AA and AM radicals thus controlling the change in both reactivity ratios with pH.[36,46–51,53] Recent work on the copolymerization of ionized AA with AM has shown that reactivity ratio can further be influenced by total monomer concentration and ionic strength of the system (Chapter 6).[49,51] An increase in the ionic strength, either by increased total monomer concentration or by the addition of NaCl, leads to an increased incorporation of the charged monomer into the copolymer chain, the result of increased electrostatic screening of the charges on the incorporated (including radical chain-end) and un-reacted monomer units. Similar observations and conclusions have been made for the copolymerization of AM with permanently charged monomers,[56,57] as well as AA homopolymerization studies with varying amounts of counterions present.[22]

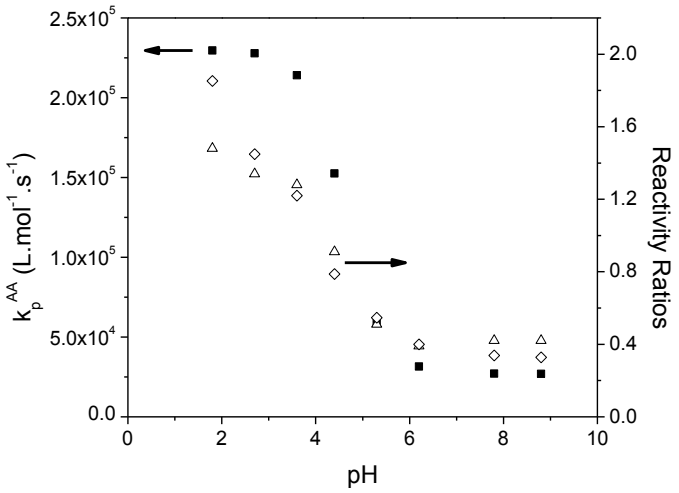

Figure 7.1. The variation in propagation rate coefficient, k_p, of AA at 6wt% monomer and 6 ºC[29] as a function of pH (■) compared to the corresponding variation in the reactivity ratios r_{AA} (△) and $1/r_{AM}$ (◇).[46]

The experimental work discussed in this thesis has so far focused on the effect of monomer concentration on the monomer composition drift and conversion profiles for the limiting conditions of fully (Chapter 6) and non-ionized (Chapter 3 and Chapter 5) AA copolymerization with AM. This chapter focuses on the effect of monomer concentration and composition of partially ionized AA and AM and examines the relative effect of the ionic strength on the conversion and monomer composition profiles. A set of reactivity ratios that are a function of total initial monomer concentration and degree of ionization are developed to explain the entire reaction space studied.

Earlier this year (2015), Rianhinezhad et al. published work similar to that presented in this chapter, where the effect of monomer concentration (3.5, 8.0 and 10.7 wt% monomer; 0.5, 1.0 and 1.5 mol·L^{-1}) and degree of ionization (α = 0.059, 0.86 and 0.998; pH = 3, 5, 7) on the reactivity ratios was studied, with the system adjusted to constant ionic strength by adding NaCl.[52] Not only does our work consider a broader experimental range in terms of monomer concentration (5 to 40 wt% monomer) and degrees of ionization (α = 0, 0.3, 0.5, 0.7, and 1.0), we also make no attempt

to artificially adjust the ionic strength by adding NaCl. Although the results by Rianhinezhad et al. give insights into this system for constant ionic strength and constant degree of ionization, our work focuses on copolymerization conditions more relevant to industry and provides a usable expression to determine reactivity ratios from initial polymerization conditions. Overall trends in the effect of monomer concentration and pH are in very good agreement between bodies of work, however the reactivity ratios themselves cannot be compared with each other as the experimental conditions are not equivalent.

7.2 Experimental

The monomers, AA (99%, Sigma Aldrich) and AM (99+%, Sigma Aldrich), D_2O (99.9%, Cambridge Isotope Laboratories Inc.), and V-50 initiator (97%, Sigma Aldrich) were bought and used without further purification. Fully ionized AA stock solution was made by titrating non-ionized AA with a mixture of NaOH and D_2O, the solvent used for the ^1H NMR experiments. The equivalence point was reached at a pH of 7.9 and checked the following day ensuring consistency between measurements and pH meter calibrations. Stock solutions of fully ionized AA in D_2O were preferred over adding NaOH to each experimental reaction solution, as the amounts needed for the NMR experiments are between 0.018 to 0.3 g ionized AA. The titration yielded stock solutions of approximately 30 wt% fully ionized AA in D_2O. The sodium ion was considered in the mass calculations of the ionized AA required for recipe formulations, even though the sodium dissociates in solution. This assumption was validated when solutions at different degrees of ionization and monomer compositions yielded good agreement between the expected and experimentally measured monomer composition with ^1H NMR as demonstrated in Figure 7.2. The degree of ionization was experimentally adjusted with the addition of non-ionized AA to the desired degree of ionization.

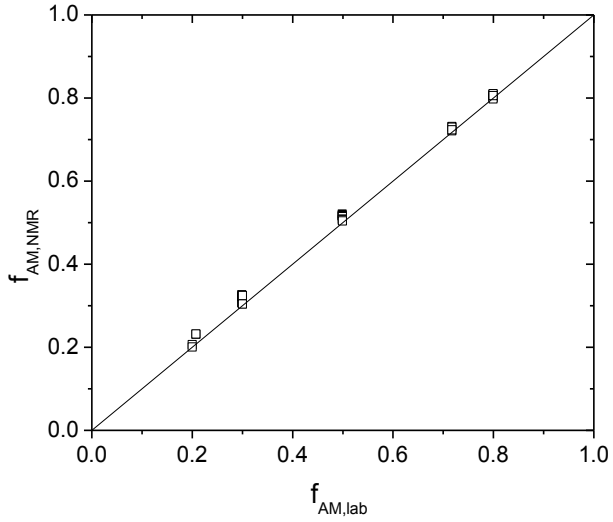

Figure 7.2 Parity plot of the monomer composition (mol fraction of AM) as calculated in the lab compared to the monomer compositions measured by NMR at degree of ionization α = 0.3 (■) and 0.7 (□). Data points at α = 0.5 are not available due to monomer peak overlap. Excellent agreement is indicated by overlapping data points at different degrees of ionization.

The monomer conversion and composition were experimentally determined by the in-situ NMR technique described in previous chapters. Due to the fast exchange between charged and uncharged AA, the monomer peaks of AA always appear as one peak on the spectra. The pH of the reaction mixture has an effect on the peak positions, as observed for the AA peaks at different degrees of ionization.[18] The monomer peak positions in Figure 7.3 vary with the degree of ionization; at fully ionized conditions the AA and the AM monomer peaks are in opposite positions relative to the non-ionized case. Although the monomer peaks shift with pH, it is impossible to reliably correlate the degree of ionization with peak positions during polymerization as the peaks also shift with temperature and monomer concentration.[23] Therefore only qualitative observations can be made about how the degree of ionization changes with monomer conversion.

The reversal of the AA and AM peak positions at fully and non-ionized conditions unfortunately leads to peak overlap of the monomer peaks at intermediate degrees of ionization,

with the overlap dependent on monomer content and conversion. For a degree of ionization of 0.5, the monomer peaks overlap until a monomer conversion of 40 %, as illustrated in Figure 7.4. For alpha of 0.3 the opposite is observed; the monomer peaks are separate until a monomer conversion of approximately 60 % is reached, and overlap for the remainder of the reaction. When the monomer peaks overlap, it is impossible to determine the instantaneous monomer composition and only the overall conversion can be measured. The cumulative copolymer composition cannot be determined by examining the polymer peaks by ^{1}H NMR for this copolymerization at any experimental condition, as the backbone structure of the two monomer units are essentially identical and are only differentiated by their respective side groups.

The change in the monomer peak overlap with conversion is an indication that the degree of ionization of the AA monomer increases with conversion. This was proposed by Lacík et al. based on the lower pK_a of the polymer relative to the AA monomer.[29] The charge distribution between the monomer and polymer is dictated by chemical equilibrium, meaning that as the polymer chain grows, more hydrogen atoms will associate with the carboxylic acid groups on the polymer chain compared to the monomer, effectively leading to the pAA having a lower degree of ionization relative to the monomer. Additionally, as the polymer chain grows, the pK_a of the chain will change as a function of M_w,[113] leading a continuous change in the charge distribution on the polymer and in the monomer. Of course, the maximum number of charged sites in the overall system is dictated by the initial degree of ionization of the monomer and corresponds to the final degree of ionization of the polymer. For experiments at degree of ionization α = 0.3, this explains the peak overlap occurring at higher conversions, and the peak separation of experiments run at α = 0.5 at higher conversions.

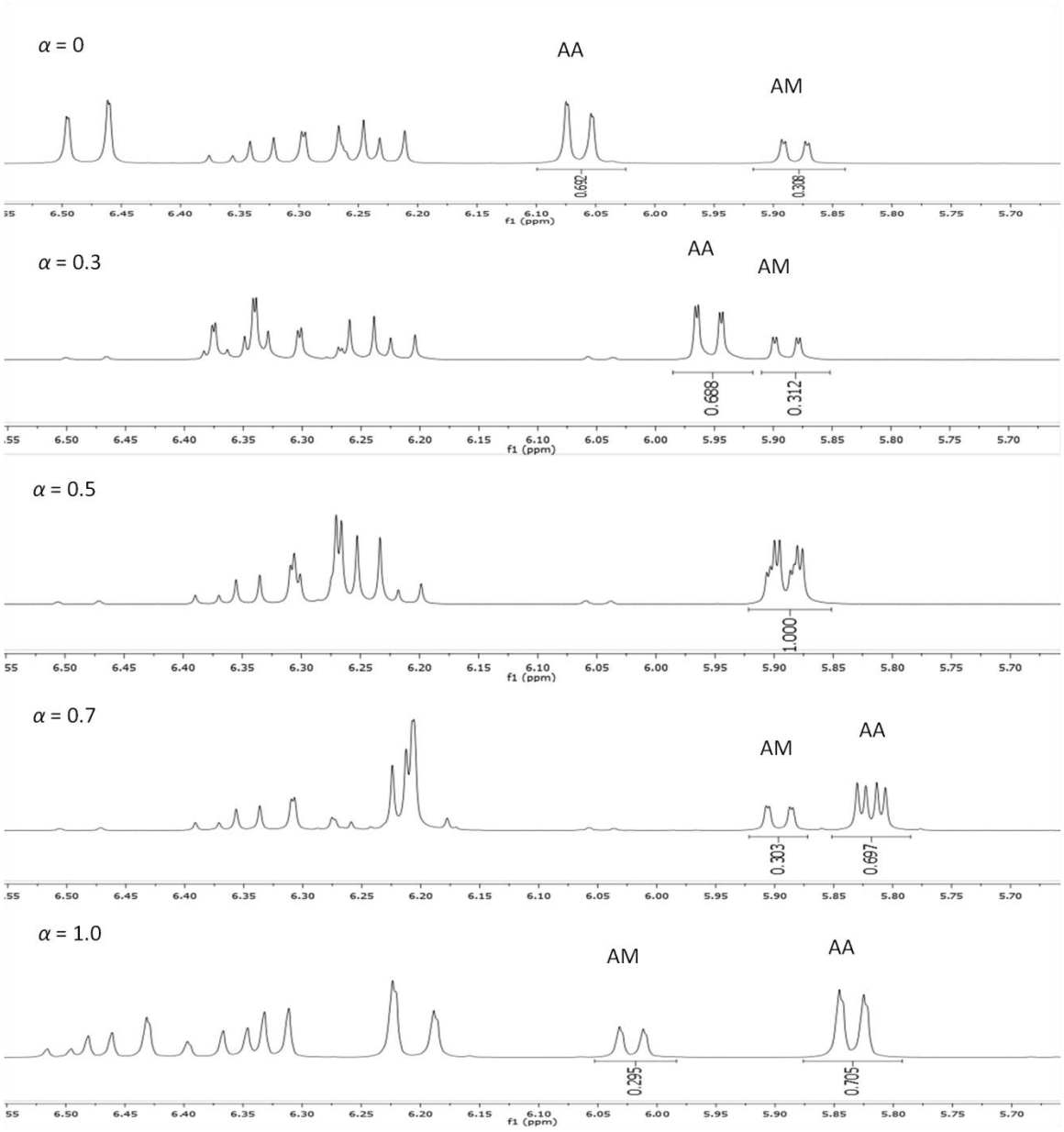

Figure 7.3 Comparison of monomer peak positions at f_{AM0} = 0.3 and 5 wt% monomer for varying degrees of ionization, as labeled in the figure. Only the monomer peaks used in the integration for the monomer composition and conversion calculation are labeled.

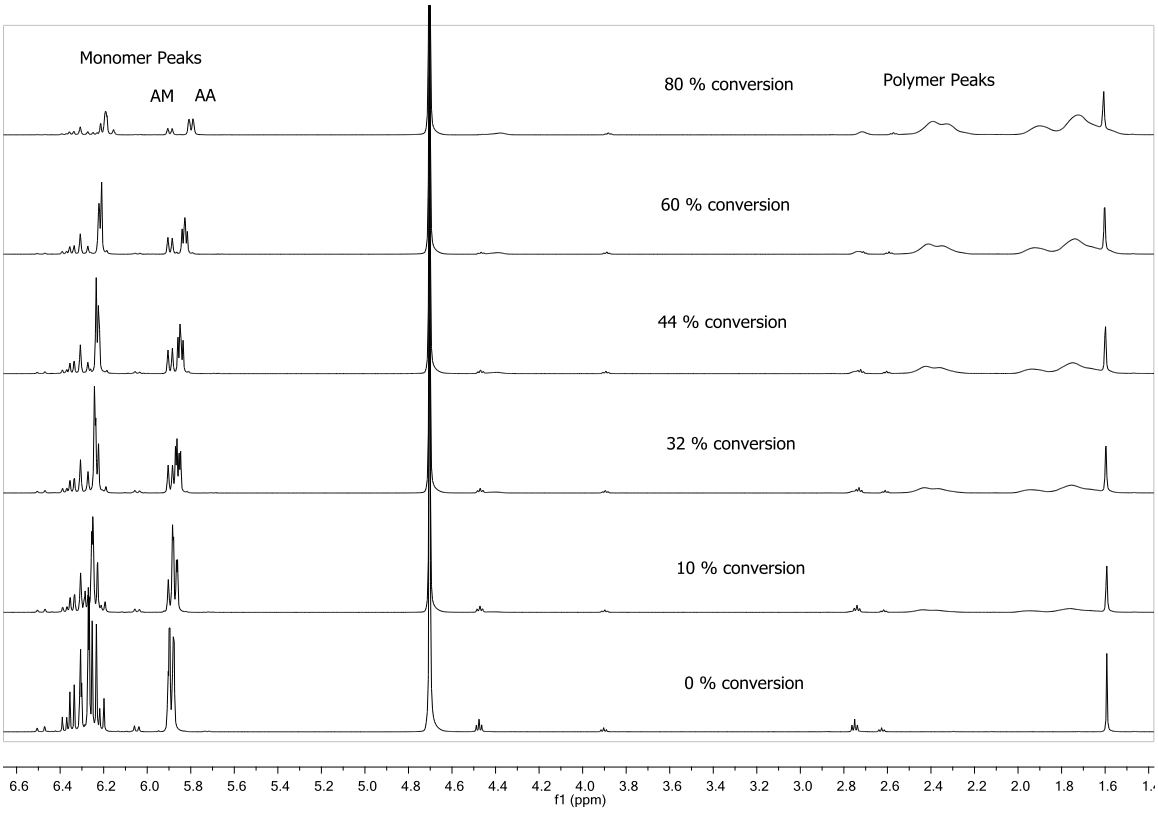

Figure 7.4 Evolution of the ^{1}H NMR spectra from low to high conversion for an experiment run at α = 0.5, f_{AM0} = 0.3, 5 wt%, 40 ^{o}C and 0.35 wt% V-50. The monomer peak overlap and separation as a function of conversion can be observed.

7.3 Design of experiments

Experiments were run at three degrees of ionization, α = 0.3, 0.5, and 0.7. In order to maintain consistency in the experimental design with the non- and fully ionized AA and AM copolymerization studies, the effect of initial monomer composition (f_{AM0} = 0.3, 0.5, 0.8) and concentration (5 to 40 wt%) was studied. In addition to these variables, the effect of ionic strength was also examined by manipulating initial conditions to maintain the same concentration of ionized AA (and therefore ionic strength) and initial monomer composition, while varying the overall monomer concentration and thus the degree of ionization of AA. The experimental monomer concentrations, ionic strength indicated by the weight fraction of ionized AA in the system, and the

monomer composition of all experiments run at degrees of ionization of α = 0.3, 0.5, 0.7, and 1.0 are graphically summarized in Figure 7.5. For easier comparison, the y-axes on all graphs have the same scale, allowing for an immediate visual comparison of the relative amounts of ionized AA at each experimental condition. As expected, the amount of ionized AA is highest at high degrees of ionization, total monomer content, and high AA monomer composition.

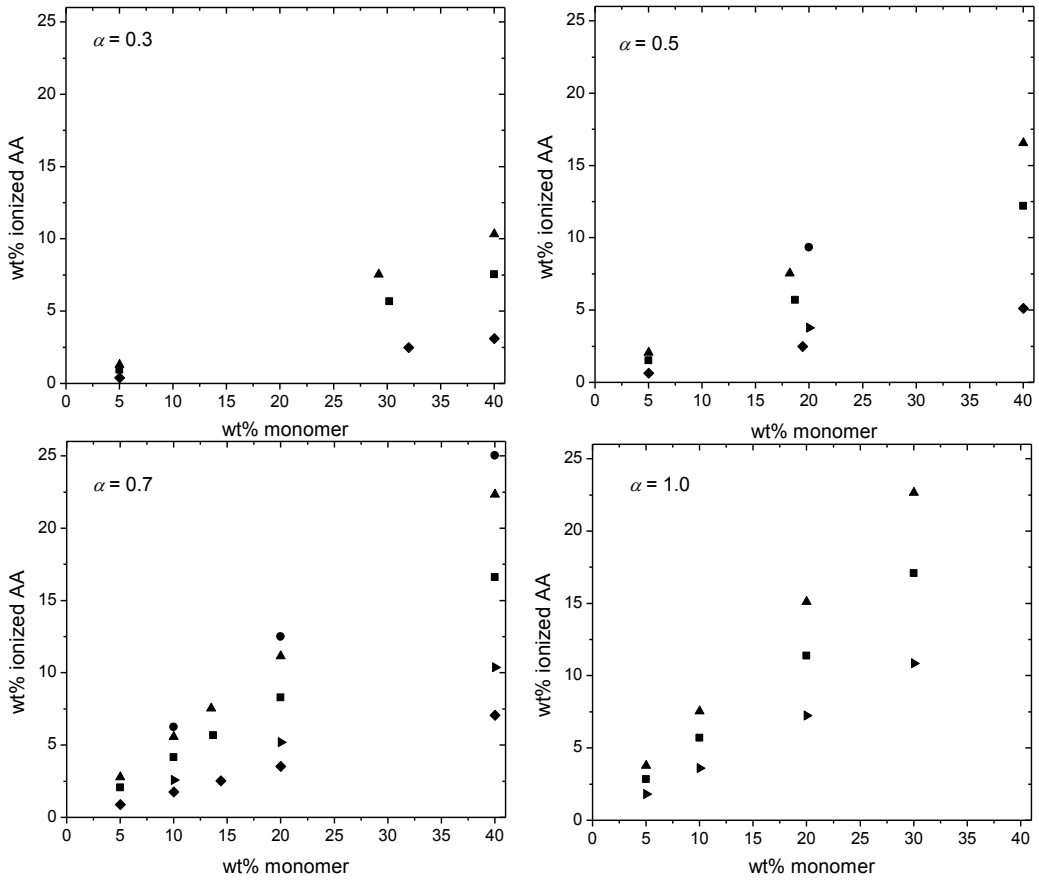

Figure 7.5 The weight % of ionized AA in aqueous solution is plotted as a function of the weight % of total monomer in solution for AA degree of ionization of α = 0.3 (top left), 0.5 (top right), 0.7 (bottom left), and 1.0 (bottom right) with initial monomer compositions of f_{AM0} of 0.2 (♦), 0.3 (▲), 0.5 (■), 0.7 (►), and 0.8 (●).

The temperatures and initiator contents used for the copolymerization experiments in this thesis project are summarized in Table 7.1. It would have been prudent to keep the initiator content and temperatures the same for all experiments; however NMR booking restrictions meant that the

majority of the reaction times were kept at 2 hours or less to allow for sufficient heating and cooling of the NMR machine and for unexpected complications. Therefore the temperature was increased from 40 to 50 °C for the fully ionized experiments, as the propagation rate coefficient of fully ionized AA is 10 times slower than that of non-ionized AA.[29] At degree of ionization of 0.7 the ratio of the ionized propagation rate coefficient to non-ionized rate coefficient is half,[29] leading to the required increase of initiator concentration from 0.20 to 0.35 wt% V-50. As a result, unfortunately, the conversion profiles for the entire data set cannot be directly compared. It is assumed that the monomer composition drift as a function of conversion can be compared regardless of temperature and initiator concentration, as the non-ionized copolymerization data collected at 40 and 70 °C showed no difference in the relative monomer consumption rates with conversion.

Table 7.1 Summary of temperature and initiator content for experiments run at different degrees of ionization.

Degree of ionization (α)	Temperature (°C)	Initiator content (wt% V-50)
0	40	0.22
0.3	40	0.22
0.5	40	0.22
0.7	40	0.35
1.0	50	0.22

In the interest in space and readability of the graphs, sometimes not all the available data are plotted. This mostly affects the conversion profiles at 10 wt% monomer and α = 0.7 and 1.0 as this monomer concentration was considered only for certain degrees of ionization. The data at 10

wt% is consistent with the trends observed with monomer concentration. The complete set of conversion profiles at α = 1.0 can be found in Chapter 6 and for α = 0.7 this can be found in Appendix B.

7.4 Discussion of monomer composition drift as a function of conversion

7.4.1 Effect of monomer concentration

Figure 7.6 plots the monomer composition drift as a function of conversion for experiments run at different initial monomer concentration at the initial degrees of ionization of 0.3, 0.5, 0.7, and 1.0. It can be observed in Figure 7.6 that for α = 0.3 the incorporation of AA is faster than AM, consistent with literature reactivity ratios estimated at pH = 3.6 (α = 0.2)[46,49] and as found for the copolymerization of non-ionized AA with AM. However, for higher values of α the relative reactivity of the two monomers is reversed: for α = 0.5 (pH = 4.3) the available monomer composition at high conversion and lower monomer concentration (5, 20 wt%) indicate a faster incorporation of AM relative to AA, consistent with the reactivity ratios determined by Rintoul and Wandrey at pH = 4.4 (α = 0.6).[46]

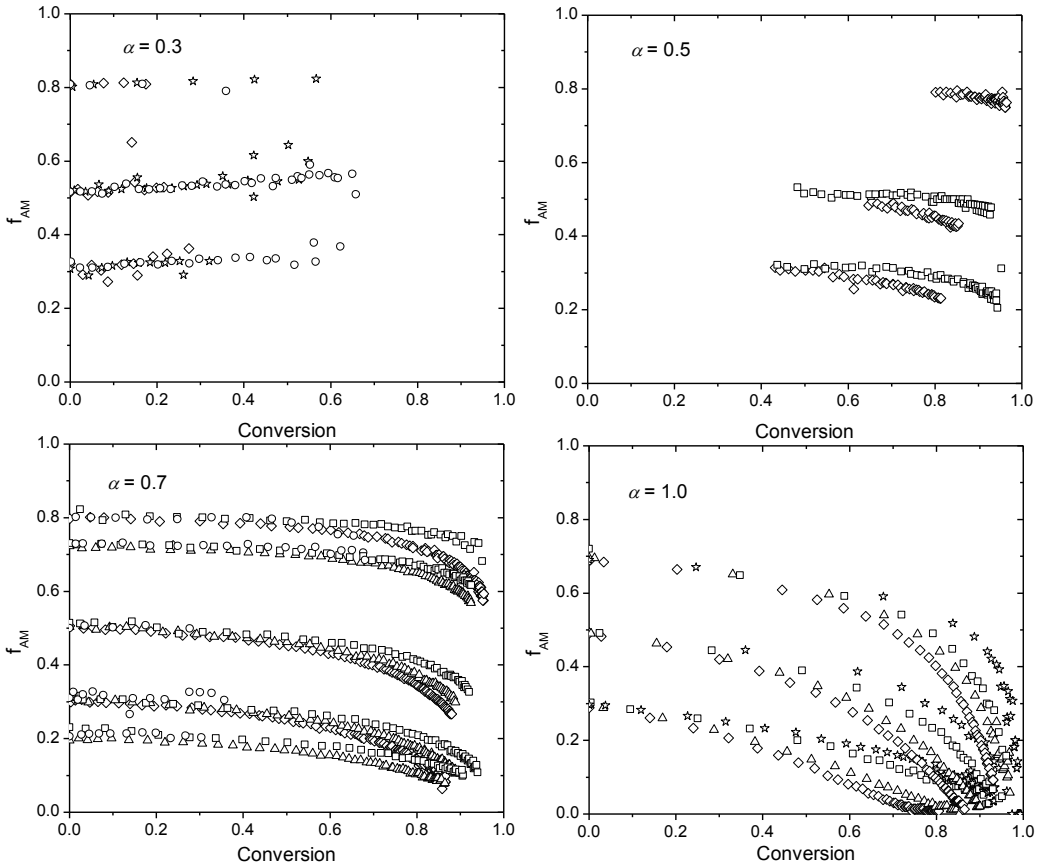

Figure 7.6 Acrylamide monomer composition drift plotted at initial degrees of ionization of α = 0.3 (top left) 0.5 (top right) 0.7 (bottom left) and 1.0 (bottom left). Experimental conditions were 40 ºC, 0.2 wt% V-50 for α = 0.3 and 0.5, 40 ºC and 0.35 wt% V50 for α = 0.7, and 50 ºC and 0.2 wt% V-50 for α = 1.0. Experiments were run at initial monomer concentrations of 5 (◇), 10 (△), 20 (□), 30 (☆), and 40 (○) wt%.

At α = 0.3 it is difficult to determine an effect on the monomer concentration on the composition drift. This is undoubtedly related to the lower concentration of ions in the system; recall that for the non-ionized system (Chapter 3 and Chapter 5) total monomer concentration had no influence on the composition drift. The effect of total monomer concentration on the composition drift increases with increasing α, with the largest influence observed for the fully ionized system. However, for α = 0.3, it is more difficult to observe the influence of total monomer

concentration due to the monomer peak overlap on the NMR spectra at high conversions. At these conditions some monomer concentration effect is anticipated, as it was observed by Paril et al. that the reactivity ratios were influenced by the total ionic strength for experiments run at pH = 3.6 (α = 0.2) with 3.5 wt% total monomer.[49] It is clear, however, that the effect of the monomer concentration at partially ionized conditions is diminished compared to the concentration effect at fully ionized conditions as a result of the lower total concentration of ionized AA units in the system (Figure 7.5).

The data collected at α = 0.7 and 40 wt% monomer also suffered from loss in the spectral quality, as observed by the extreme broadening of the solvent peak and large scatter in the data. Although this data is included in the plot and reactivity ratios are estimated for this condition, the estimated reactivity ratios should be considered unreliable.

7.4.2 Effect of degree of ionization and ionic strength

In the following plots (Figure 7.7, Figure 7.8, and Figure 7.9) the monomer composition drift as a function of conversion is compared at different initial degrees of ionization (alpha 0, 0.3, 0.5, 0.7, and 1.0) for the same initial total monomer concentration in aqueous solution. It was assumed that composition drift was independent of the initiator content and temperatures over the range of conditions examined. The data organized in this fashion clearly show that, for all initial monomer compositions and total monomer concentrations, the initial degree of ionization of AA leads to the overall difference in the incorporation of the monomer, thus controlling the reactivity ratios. As previously discussed, the effect of the degree of ionization on the reactivity ratios is largely explained by the changing rate coefficient for AA addition as a function of the degree of ionization (Figure 7.1).

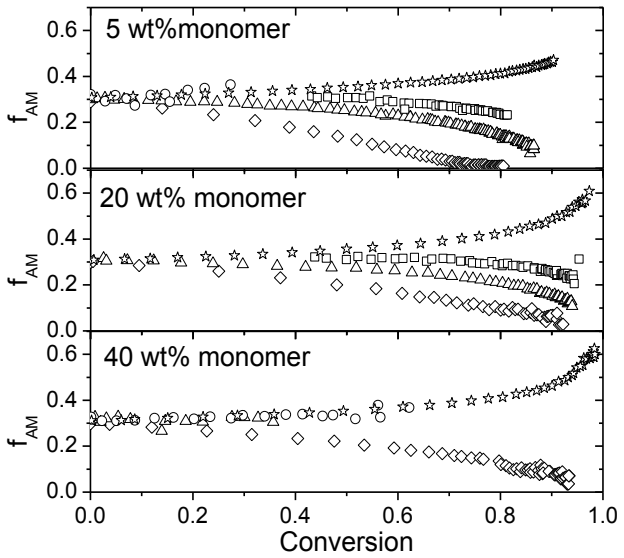

Figure 7.7 Experimental monomer composition as a function of conversion for f_{AM0} = 0.3 plotted at constant total monomer concentration of 5 (top), 20 (middle), and 40 (alpha = 1.0 at 30 wt%) (bottom) wt% monomer in aqueous solution, with degrees of ionization of AA at 1.0 (◇), 0.7 (△), 0.5 (□),0.3 (○), 0 (☆). (See Table 7.1 for full experimental conditions.)

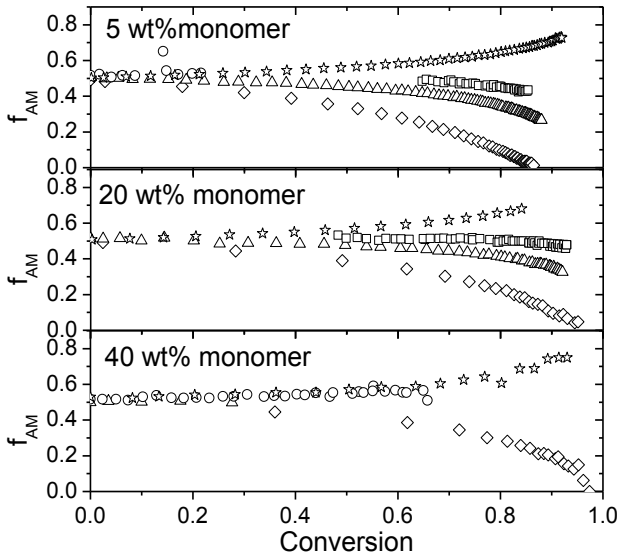

Figure 7.8 Experimental monomer composition as a function of conversion for f_{AM0} = 0.5 plotted at constant total monomer concentration of 5 (top), 20 (middle), and 40 (α = 1.0 at 30 wt%) (bottom) wt% monomer in aqueous solution, with degrees of ionization of AA at 1.0 (◇), 0.7 (△), 0.5 (□),0.3 (○), 0 (☆) conditions. (See Table 7.1 for full experimental conditions.)

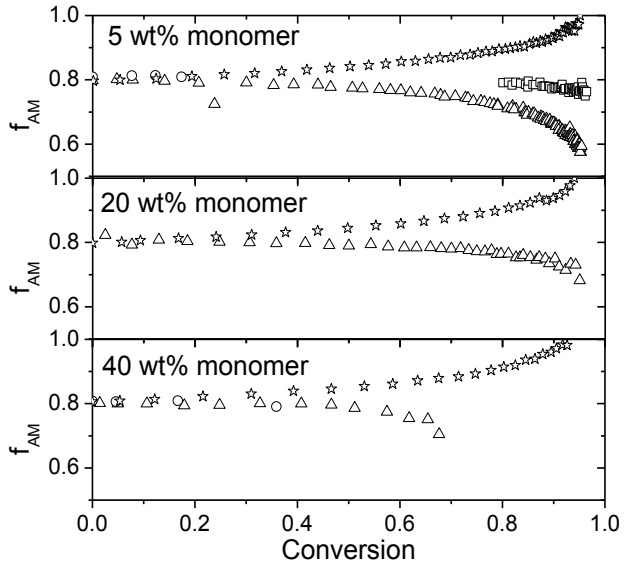

Figure 7.9 Experimental monomer composition as a function of conversion for f_{AM0} = 0.8 plotted at constant total monomer concentration of 5 (top), 20 (middle), and 40 (alpha = 1.0 at 30 wt%) (bottom) wt% monomer in aqueous solution, with degrees of ionization of AA at 1.0 (◇), 0.7 (△), 0.5 (□), 0.3 (○), 0 (☆). (See Table 7.1 for full experimental conditions.)

An important distinction must also be made at when discussing the influence of the degree of ionization and the ionic strength of the system. As shown in Figure 7.10, there are significant differences in the monomer composition drift for experiments run at different degrees of ionization and concentrations, while keeping the ionic strength the same. This result can be contrasted to that of Cuccato et al., who found that for the copolymerization of AM with DMAEA-Q, experiments run at differing monomer content but constant ionic strength (obtained by adding NaCl to the system) converged toward a single curve of monomer composition vs. conversion. The difference is undoubtedly due to the fact that DMAEA-Q carries a permanent charge, and thus it is not possible to vary the degree of ionization. For the AA/AM system, the degree of ionization of AA is the primary factor dictating the overall reactivity ratios, with the ionic strength (and/or total monomer concentration) a secondary, yet important, factor when considering monomer composition drift.

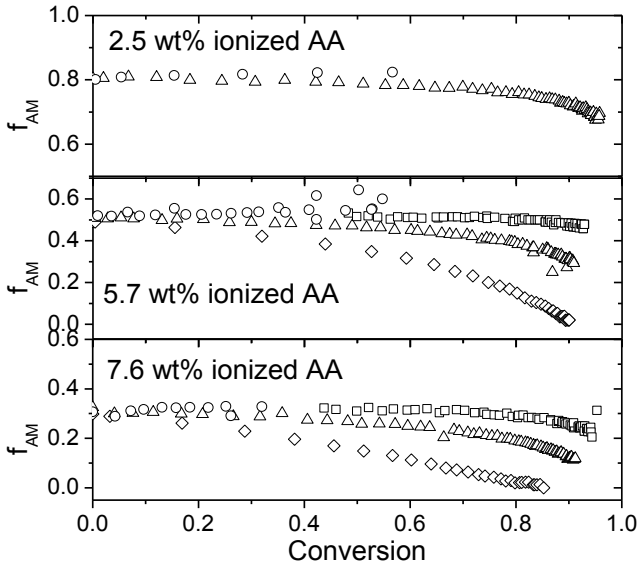

Figure 7.10 Experimental monomer composition as a function of conversion plotted at constant wt% of ionized AA of 2.5 (top), 5.7 (middle), 7.6 (bottom) in aqueous solution, with degrees of ionization of AA at 1.0 (◇), 0.7 (△), 0.5 (□), and 0.3 (○). The total monomer content is different for each experimental condition. (See Table 7.1 for full experimental conditions).

7.4.3 Determination of reactivity ratios for the partially ionized copolymerization of AA and AM

Monomer reactivity ratios were estimated individually at each initial total monomer concentration at each degree of ionization, following the strategy used for the fully ionized system (Chapter 6). Thus there are generally three experiments (with initial compositions f_{AM0} = 0.3, 0.5 and 0.8) used for each estimate of the r_{AA} and r_{AM} pair plotted in Figure 7.11. (The results for α = 1.0 are the same as presented in Chapter 6.) The fitting assumes that the system can be represented by the terminal model, and that the reactivity ratios do not vary with conversion; i.e., are only a function of the initial conditions of the batch system. The majority of the data follow a linear trend with increasing monomer concentration, with some outliers. This linear trend was also observed in the reactivity ratios estimated at the different monomer concentrations.[52]

The uncertainty in the reactivity ratios estimated at degrees of ionization α = 0.3 and 0.5 is high due to the lack of monomer composition data at all monomer compositions and concentrations, and for all conversions. This uncertainty is reflected in the error bars at α = 0.3. The reactivity ratio estimates at α = 0.7 and 40 wt% also has a high level of uncertainty associated with it, as data higher than 37% conversion is not available due to the loss of NMR spectral quality, as previously discussed. Due to these uncertainties, the values of the reactivity ratios estimated for these particular conditions were omitted from the linear fit.

In order to obtain a fit of the reactivity ratios valid at all monomer compositions and degrees of ionization, the values determined at degrees of ionization α = 0, 0.7, and 1.0 were linearized with respect to the intercept and slope, leading to the following expression:

$$r_{AA} = (1.287 - 1.105\alpha) + (-0.107 + 1.207\alpha)w'_{M0}$$
$$r_{AM} = (0.491 + 1.442\alpha) + (0.006 - 1.362\alpha)w'_{M0} \quad 7.3$$

where, α and w'_{M0} refer to the initial degree of ionization and total initial monomer weight fraction, respectively.

The resulting prediction of the reactivity ratios can be found in Figure 7.11 for ionized conditions, and in Figure 7.12 for non-ionized conditions. The representation captures the overall trends in the data, even at α = 0.3 and 0.5, which were excluded from the fit. The value of r_{AM} is not as well fit at α = 0.5 and 0.7 mainly because it was difficult to capture the inflection when the value of r_{AM} went from being smaller to greater than r_{AA} (between α of 0.3 and 0.5) as the degree of ionization increased. The reactivity ratios estimated by Rintoul and Wandrey suggest that the change in reactivity ratios in this region is sigmoidal, rather than linear (Figure 7.1).[46]

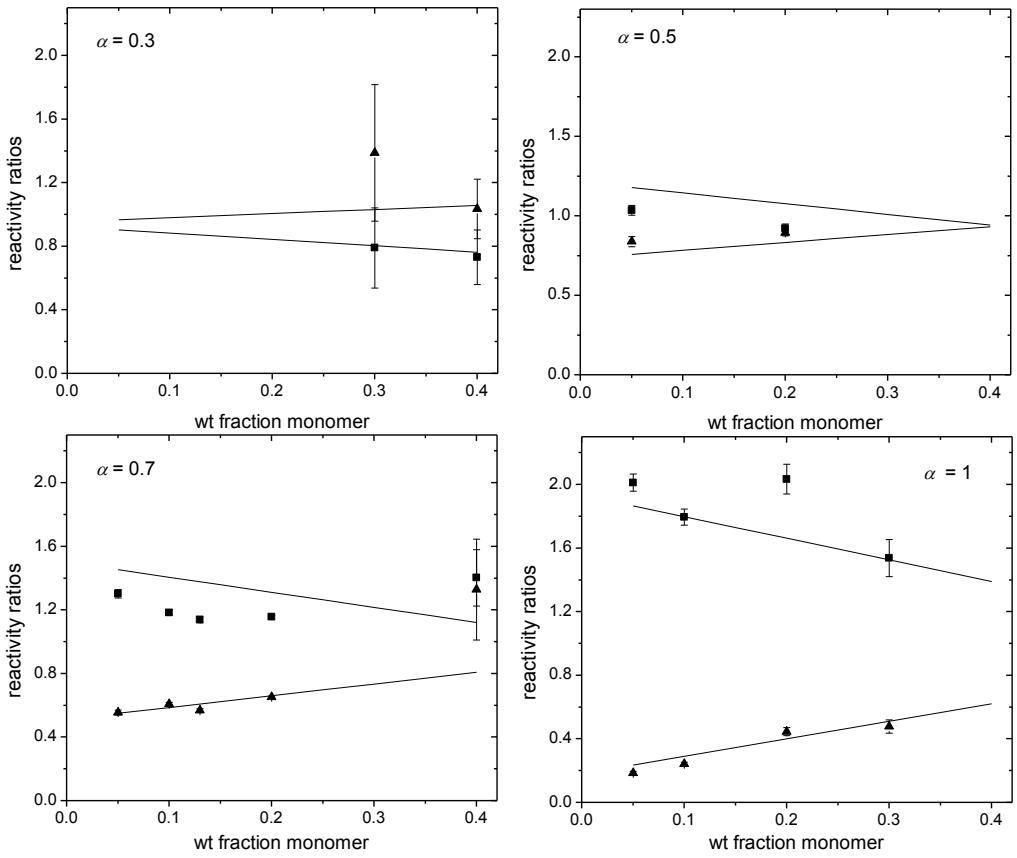

Figure 7.11 Reactivity estimates of r_{AM} (■) and r_{AA} (▲) obtained at each initial monomer concentration and the corresponding fit from Equation 7.3 for degree of ionization α = 0.3 (top left), 0.5 (top right), 0.7 (bottom left), and 1.0 (bottom right).

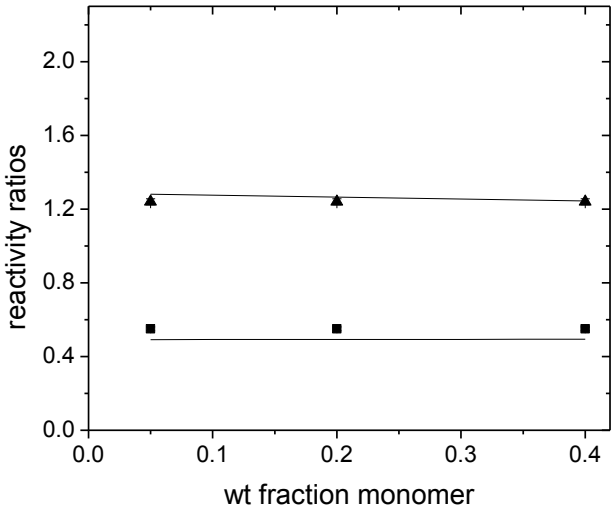

Figure 7.12 Reactivity estimates of r_{AM} (■) and r_{AA} (▲) at non-ionized conditions and the corresponding fit from Equation 7.3.

The predicted monomer composition drift calculated using the representation of reactivity ratios as a function of initial conditions expressed by Equation 7.3 are plotted in Figure 7.13 for ionized conditions and Figure 7.14 for non-ionized conditions. The degrees of ionization where the reactivity ratios were not as well fit (α = 0.5 and 0.7) are subsequently also not as well fit by the model, with the predicted drift in composition larger than what was measured experimentally. However, the general trends in the composition drift are well captured and for degrees of ionization of α = 0, 0.3, and 1.0, the ability of Equation 7.3 to represent the data is satisfactory. Overall, the representation gives a reasonable idea as to how the reactivity ratios change with the different experimental conditions, extending the empirical fit introduced in Chapter 6 to the complete range of degree of ionization.

The predicted reactivity ratios for the fully ionized conditions as presented in Chapter 6 are in good agreement with those with Equation 7.3, with the maximum absolute error in the reactivity ratios being 0.04 and 0.13 for r_{AA} and r_{AM}, respectively. Even with the slight deviations in the

reactivity ratios, the fit of the monomer composition drift is qualitatively equivalent for both expressions of the reactivity ratios.

For predicted reactivity ratios at non-ionized conditions, the r_{AM} predicted by Equation 7.3 is systematically lower at 0.49, compared to the value of 0.55 estimated previously.[23] This difference in r_{AM} leads to the slight misfit of the data at f_{AM0} of 0.5 and 0.8 (Figure 7.14). The monomer concentration term has little effect on the predicted reactivity ratios at non-ionized conditions; r_{AA} changes by 2.9 % and r_{AM} changes by 0.43 % between 5 and 40 wt% monomer.

Rintoul and Wandrey developed an expression to describe the reactivity ratios as a function of degree of ionization using a terpolymerization model, with the ionized and non-ionized AA each representing a species in addition to AM.[62] The reactivity ratios are estimated based on the predicted cross- and homopropagation rate coefficients and yield good predictions of the reactivity ratios and captures the sigmoidal change in the reactivity ratios with pH observed at the low monomer concentration conditions they examined experimentally.[62] This detail is not captured in by Equation 7.3 as a linear fit is implemented. The terpolymerization approach, however, does not consider the change in the reactivity ratios with monomer concentration.[62] Such a representation would not work over the range of conditions examined here, as monomer concentration has the greatest effect on rate coefficients for the non-ionized condition, where the reactivity ratios were observed to be independent of monomer concentration. The simpler and empirical Equation 7.3 developed in this work effectively describes the relative effects of the degree of ionization of monomer concentration on the reactivity ratios.

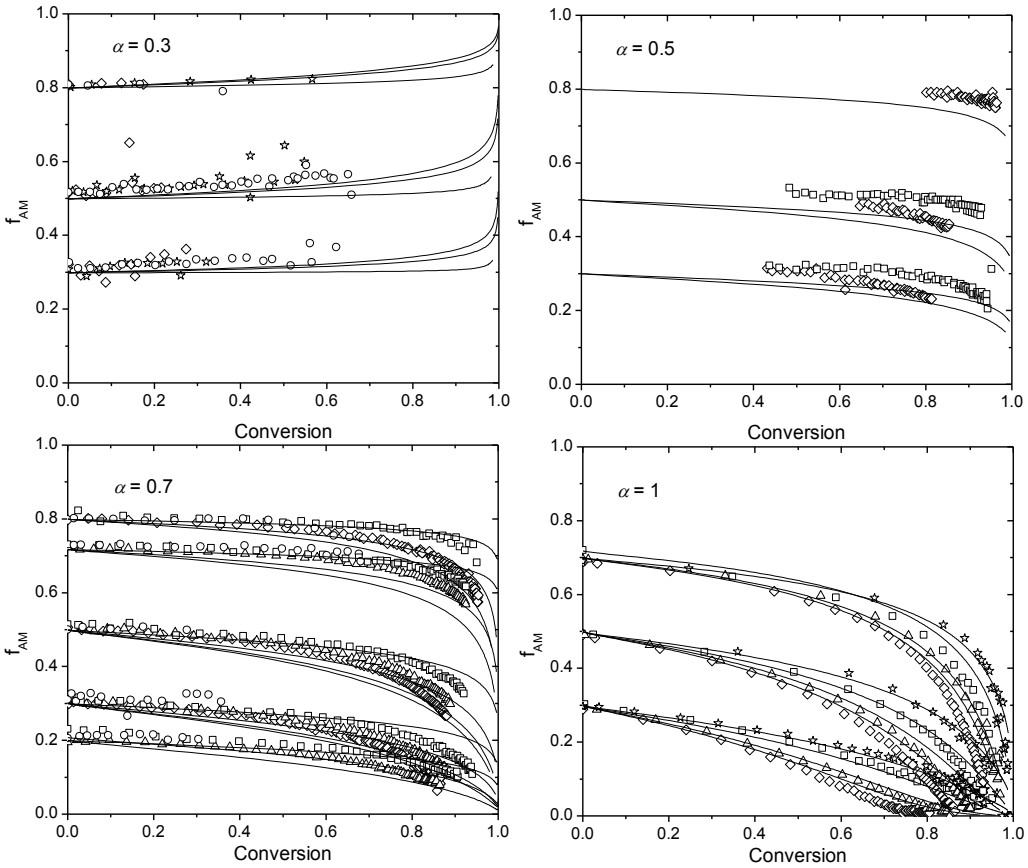

Figure 7.13 Acrylamide monomer composition drift plotted at degrees of ionization of α = 0.3 (top left) 0.5 (top right) 0.7 (bottom left) and 1.0 (bottom left). Experimental conditions were 40 ºC, 0.2 wt% V-50 for α = 0.3 and 0.5, 40 ºC and 0.35 wt% V50 for α = 0.7, and 50 ºC and 0.2 wt% V-50 for α = 1.0. Experiments were run at initial monomer concentrations of 5 (◇), 10 (△), 20 (□), 30 (☆), and 40 (○) wt%. The predicted monomer compositions (lines) as calculated using the reactivity ratios estimated by Equation 7.3 as a function of total monomer concentration and degree of ionization.

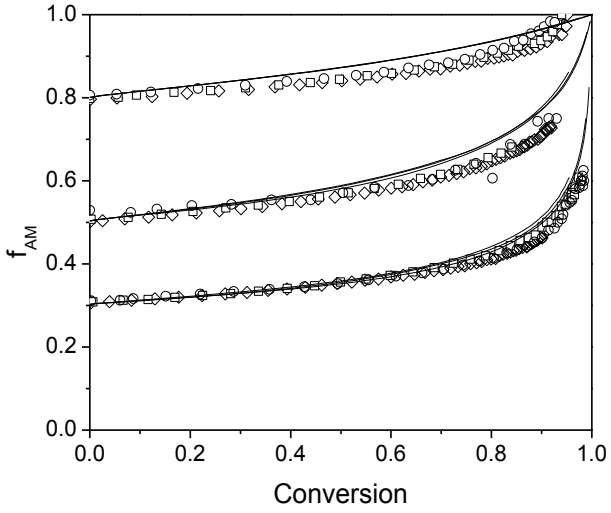

Figure 7.14 Acrylamide monomer composition drift plotted at non- ionized conditions polymerized at 40 ºC, 0.2 wt% V-50 and initial monomer concentrations of 5 (◇), , 20 (□), and 40 (○) wt%. The predicted monomer compositions (lines) as calculated using the reactivity ratios estimated with Equation 7.3 as a function of total monomer concentration and degree of ionization.

7.5 Discussion of monomer conversion profiles

7.5.1 Effect of monomer concentration and composition

Conversion profiles in Figure 7.15, Figure 7.16, and Figure 7.17 for initial monomer compositions f_{AM0} = 0.3, 0.5, and 0.8, respectively, are plotted as a function of monomer concentration at degrees of ionization of 0.3, 0.5, 0.7, and 1.0. (As no data was collected for the fully ionized conditions at f_{AM0} = 0.8, Figure 7.17 contains data collected at f_{AM0} = 0.7.) Data at 10 wt% monomer, which fit into the general trends with monomer concentration, was omitted to maintain readability of the plots; all experimental data at α = 0.7 can be found in Appendix B. At all degrees of ionization, increasing the monomer concentration leads to an increased conversion rate. As shown in previous modeling efforts for AA[21] and AM (Chapter 4) and their

copolymerization (Chapter 5, and Chapter 6), this behavior is explained by the presence of backbiting reactions for both AA and AM.

Although the influence of total monomer concentration is visible at all degrees of ionization, the magnitude of the effect varies with initial monomer composition. For example, at α = 0.5, the monomer concentration has little effect on the conversion profiles at the intermediate level of f_{AM0} = 0.5 (Figure 7.16), more so at f_{AM0} = 0.3 (Figure 7.15), and a major effect at f_{AM0} = 0.8 (Figure 7.17). This difference in the effect of the monomer concentration is surprising; more so as it does not show a consistent trend with AM content. Studies on the interaction of un-reactive pAA and pAM at various degrees of ionization indicate that as the degree of ionization increases, the interactions between the side groups decreases, due to shielding of the counterions.[108] The different total amount of ionized AA at each monomer composition shown in Figure 7.5 may lead to the different relative effect of monomer concentration at the different degrees of ionization.

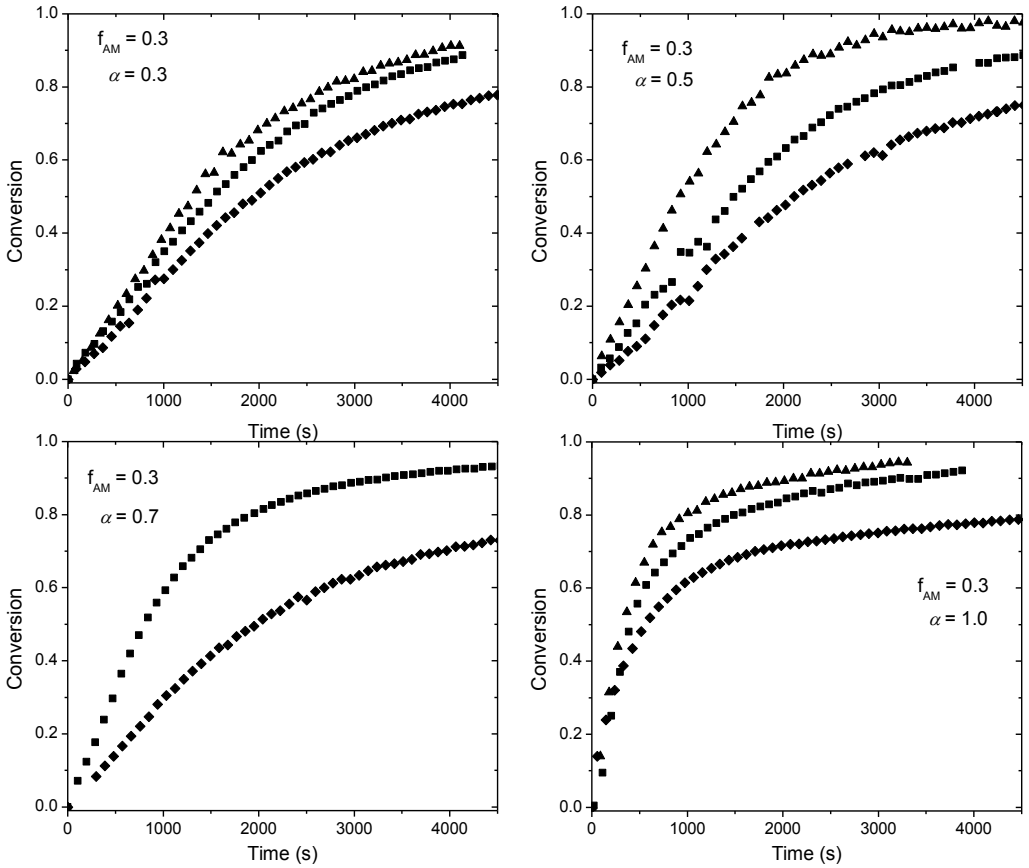

Figure 7.15 Experimental batch monomer conversion profiles collected with initial monomer composition f_{AM0} = 0.3 and degree of ionization α = 0.3 (top left) at 40 ºC, 0.2 wt% V-50 and 5 (♦), 30 (■) and 40 (▲) wt% monomer; α = 0.5 (top right) at 40 ºC, 0.2 wt% V-50 and 5 (♦), 20 (■) and 40 (▲) wt% monomer; α = 0.7 (bottom left) at 40 ºC, 0.35 wt% V-50 and 5 (♦), 20 (■) and 40 (▲) wt% monomer; and α = 1.0 (bottom right) at 50 ºC, 0.2 wt% V-50 and 5 (♦), 20 (■) and 30 (▲) wt% monomer.

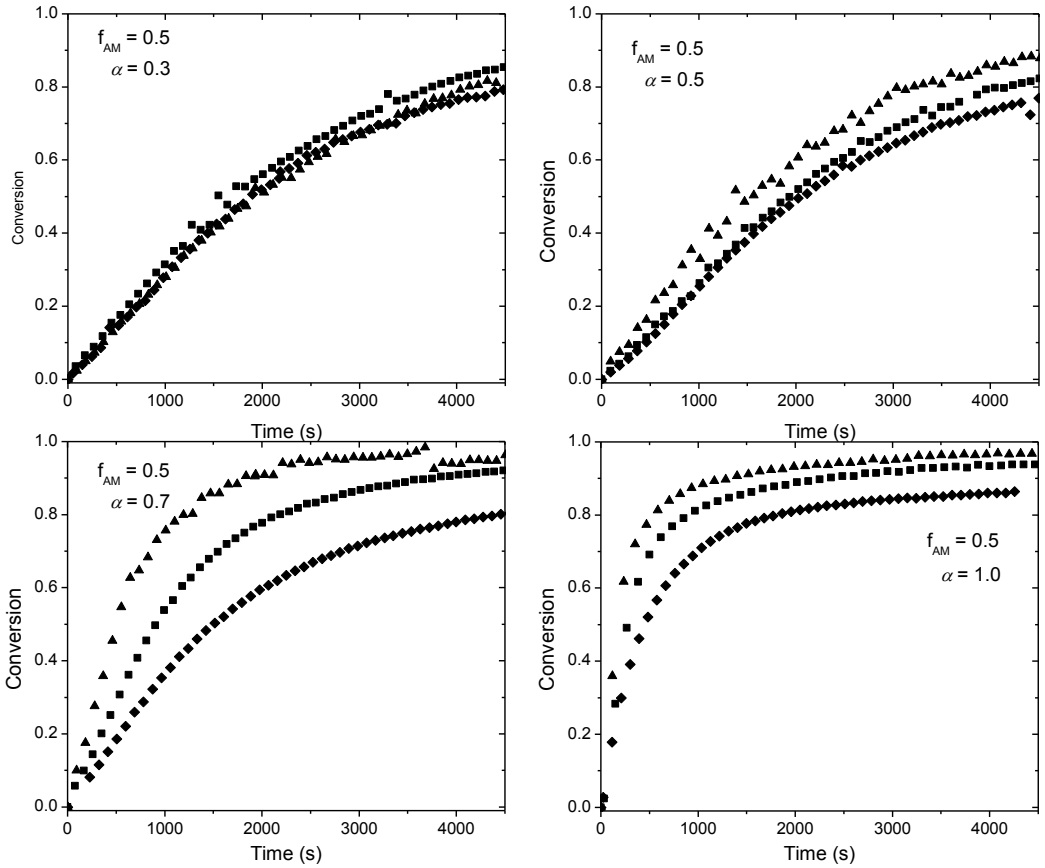

Figure 7.16 Experimental batch monomer conversion profiles collected with initial monomer composition f_{AM0} = 0.5 and degree of ionization α = 0.3 (top left) at 40 ºC, 0.2 wt% V-50 and 5 (♦), 30 (■) and 40 (▲) wt% monomer; α = 0.5 (top right) at 40 ºC, 0.2 wt% V-50 and 5 (♦), 20 (■) and 40 (▲) wt% monomer; α = 0.7 (bottom left) at 40 ºC, 0.35 wt% V-50 and 5 (♦), 20 (■) and 40 (▲) wt% monomer; and α = 1.0 (bottom right) at 50 ºC, 0.2 wt% V-50 and 5 (♦), 20 (■) and 30 (▲) wt% monomer.

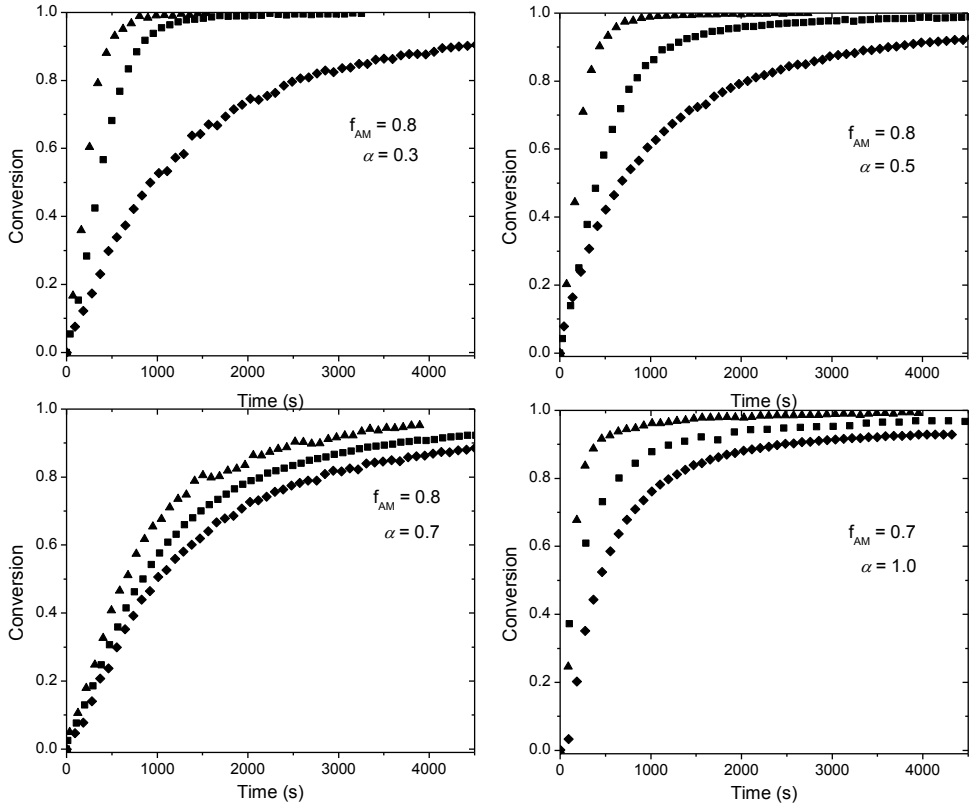

Figure 7.17 Experimental batch monomer conversion profiles collected with initial monomer composition f_{AM0} = 0.8 (f_{AM0} = 0.7 for α = 1.0) and degree of ionization α = 0.3 (top left) at 40 ºC, 0.2 wt% V-50 and 5 (♦), 30 (■) and 40 (▲) wt% monomer; α = 0.5 (top right) at 40 ºC, 0.2 wt% V-50 and 5 (♦), 20 (■) and 40 (▲) wt% monomer; α = 0.7 (bottom left) at 40 ºC, 0.35 wt% V-50 and 5 (♦), 20 (■) and 30 (▲) wt% monomer; and f_{AM0} = 0.7 and α = 1.0 (bottom right) at 50 ºC, 0.2 wt% V-50 and 5 (♦), 20 (■) and 30 (▲) wt% monomer.

7.5.2 Effect of the degree of ionization

Figure 7.18, Figure 7.19, and Figure 7.20 regroup the conversion profiles for initial monomer compositions of f_{AM0} of 0.3, 0.5, and 0.8, respectively, to show the effect of the initial degree of ionization of AA (α = 0, 0.3, and 0.5) at various monomer concentrations. Since the experiments for α = 0.7 and 1.0 were run at different initiator content and temperature, respectively, they are not included in this discussion. At f_{AM0} = 0.3 (Figure 7.18) the degree of ionization of the AA monomer has little effect on the monomer conversion rates, while at f_{AM0} = 0.5 the effect is

larger (Figure 7.19), but in both cases the degree of ionization of AA causes a decrease in the conversion rate, following the trends observed for AA homopolymerizations.[18,22] It is interesting that the degree of ionization of AA leads to a greater decrease in conversion rate at f_{AM0} = 0.5 compared to f_{AM0} = 0.3, with the effect becoming more pronounced with increasing monomer concentration (Figure 7.16).

At f_{AM0} = 0.8 (Figure 7.20) on the other hand, the degree of ionization of AA leads to an increase in the conversion rate relative to the non-ionized conditions (Figure 7.20). This result is surprising, as the rate coefficients of AM are thought to be independent of system pH and the rate coefficients of AA decrease with increase in the system pH. Therefore the enhancement of the conversion rate must stem from other phenomena. Perhaps it is related to the very small concentration of negatively charged AA in the reaction mixture that may promote the addition of monomer and/ or suppress the mechanism of backbiting, leading to the faster observed conversion rates.

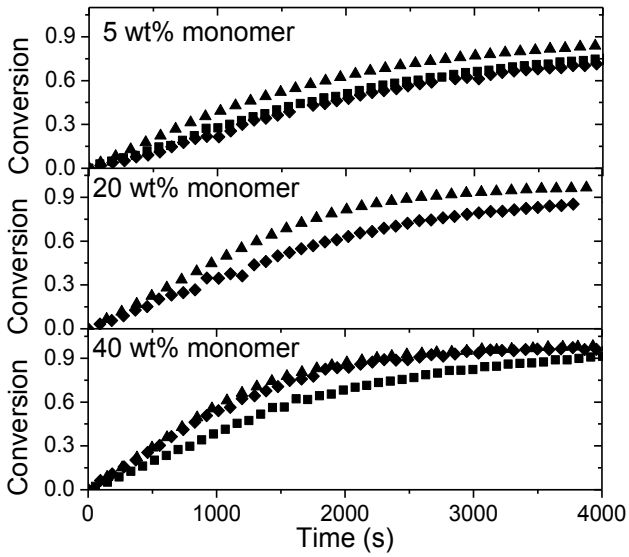

Figure 7.18 Experimental batch monomer conversion profiles collected with initial monomer composition f_{AM0} = 0.3 at 40 ºC and 0.2 wt% V-50 with 5 (top), 20 (middle), and 40 (bottom) wt% monomer in aqueous solution at degree of ionization α = 0 (▲), 0.3 (■), and 0.5 (♦).

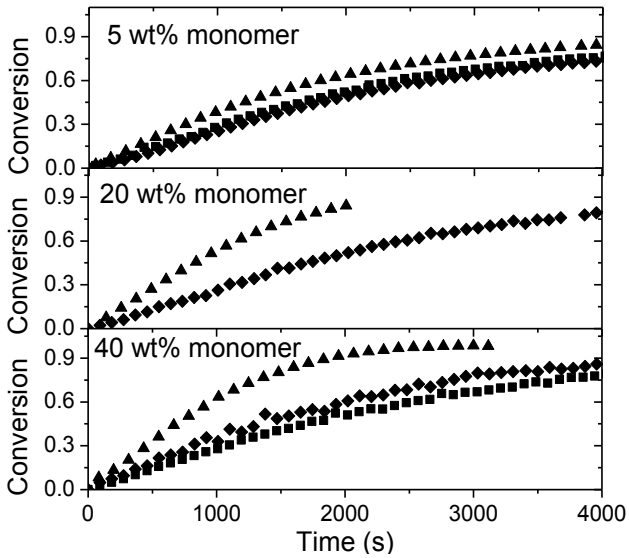

Figure 7.19 Experimental batch monomer conversion profiles collected with initial monomer composition f_{AM0} = 0.5 at 40 ºC and 0.2 wt% V-50 with 5 (top), 20 (middle), and 40 (bottom) wt% monomer in aqueous solution at degree of ionization α = 0 (▲), 0.3 (■), and 0.5 (♦).

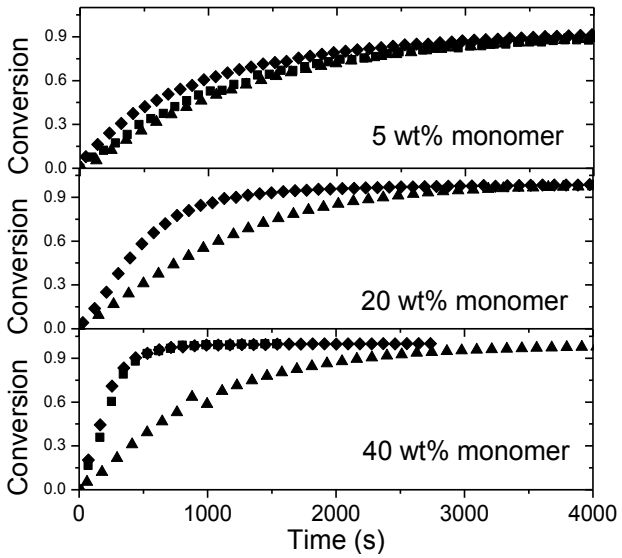

Figure 7.20 Experimental batch monomer conversion profiles collected with initial monomer composition f_{AM0} = 0.8 at 40 °C and 0.2 wt% V-50 with 5 (top), 20 (middle), and 40 (bottom) wt% monomer in aqueous solution at degree of ionization α = 0 (▲), 0.3 (■), and 0.5 (♦).

7.5.3 Effect of ionic strength

The data were also organized to compare conversion profiles collected at the same ionic strength but differing initial monomer concentrations and compositions. It has been shown that when the ionic strength alone is adjusted with salt, the conversion rates can be influenced for the polymerization of ionized AA alone[22] and for its copolymerization with AM.[51] Figure 7.21 compares the conversion rates of experiments run at full degree of ionization: even though the experiments were run at the same ionic strength, monomer concentration remains the dominant variable influencing the magnitude of the conversion rate. A similar observation can be made in Figure 7.22, where conversion profiles collected at α = 0.7 are compared at the same ionic strength, but different initial monomer compositions and concentrations. Therefore one can conclude that ionic strength alone does not dictate the overall conversion rate, a similar conclusion that was made about the monomer composition drift with conversion made earlier in this chapter.

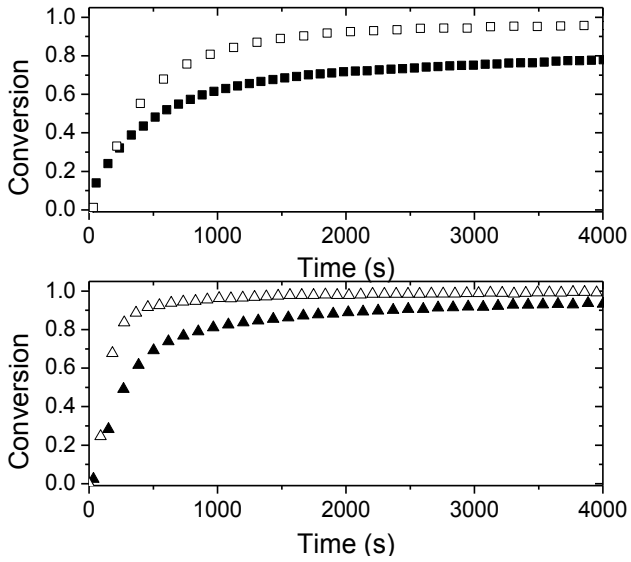

Figure 7.21 Experimental batch monomer conversion profiles collected at fully ionized conditions with (top) 3.6 wt% ionized AA at f_{AM0} = 0.3 and 5 wt% monomer (■) and f_{AM0} = 0.7 and 10 wt% monomer (□), and (bottom) 11 wt% ionized AA at f_{AM0} = 0.5 and 20 wt% monomer (▲) and f_{AM0} = 0.7 and 30 wt% monomer (△). All experiments were run at 50 ºC and 0.2 wt% V-50.

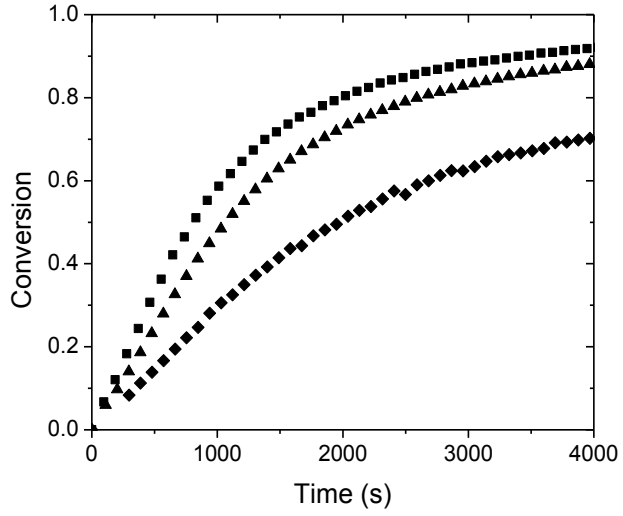

Figure 7.22 Experimental batch monomer conversion profiles collected at degree of ionization α = 0.7 with 2.6 wt% ionized AA at f_{AM0} = 0.3 and 5 wt% monomer (♦), f_{AM0} = 0.7 and 10 wt% monomer (▲), and f_{AM0} = 0.8 and 14.4 wt% monomer (■). All experiments were run at 40 ºC and 0.35 wt% V-50.

Interestingly however, when the monomer composition and the ionic strength are kept constant while the monomer concentration and degree of ionization are changed, the resulting conversion profiles overlap, as observed in Figure 7.23 and Figure 7.24. In Figure 7.23 it is striking that conversion profiles collected at 18.7 and 30.2 wt% monomer overlap, while in Figure 7.24 conversion profiles at 18.2 and 29.2 wt% monomer overlap. Going back to the monomer composition drift with conversion plotted with constant ionic strength (Figure 7.10), it was shown that the initial degree of ionization of the monomer, rather than ionic strength, was the dominant factor in determining the overall monomer composition drift. For experiments run at the same monomer composition however, the ionic strength appears to influence the overall conversion rate.

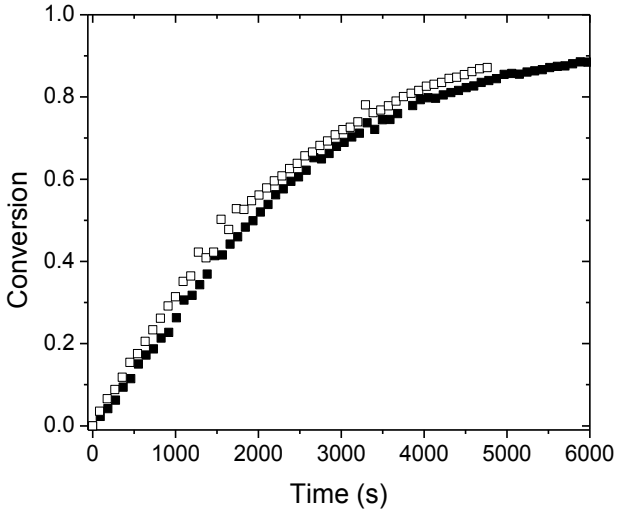

Figure 7.23 Experimental batch monomer conversion profiles collected with initial monomer composition f_{AM0} = 0.5 and 5.7 wt% ionized AA at α = 0.5 and 19 wt% monomer (■), and α = 0.3 and 30 wt% monomer (□). All experiments were run at 40 °C and 0.2 wt% V-50.

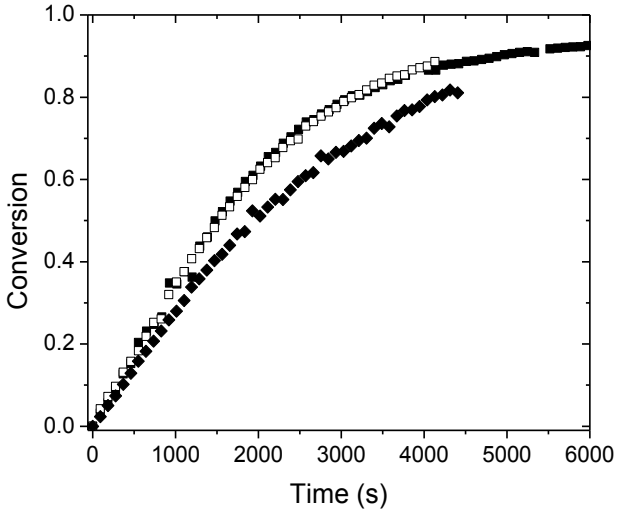

Figure 7.24 Experimental batch monomer conversion profiles collected with initial monomer composition f_{AM0} = 0.5 and 7.5 wt% ionized AA at α = 0.5, f_{AM0} = 0.3 and 18 wt% monomer (■), α = 0.3, f_{AM0} = 0.3 and 30 wt% monomer (□), and α = 0.3, f_{AM0} = 0.5 and 40 wt% monomer (♦). All experiments were run at 40 ºC and 0.2 wt% V-50.

7.5.4 Conclusions

This section examined the effect of monomer composition, monomer concentration, degree of ionization, and ionic strength on the conversion profiles. As conversion rates increase with increasing monomer concentration, it can be assumed that the backbiting mechanism is present in the partially ionized copolymerizations, consistent with the observations made for non-ionized and fully ionized conditions. For initial monomer compositions f_{AM0} = 0.3 and 0.5 the conversion rates decreased with increasing degree of ionization, as observed in AA homopolymerization.[22] As with the monomer composition drift with conversion, the ionic strength alone does not dictate the overall monomer conversion rate; the monomer composition and concentration are still the primary factors affecting the rate. For experiments run at the same initial monomer composition and ionic strength however, the conversion rates were similar.

7.6 Modeling Approach

Models to describe the copolymerization of AM with non-ionized and fully ionized AA were presented in the previous two chapters. For both cases, it was difficult to obtain a fit to the entire set of monomer conversion profiles. For the non-ionized system, the mismatch was hypothesized to be caused by the complexation of the AA and AM side groups on the polymer chains at 40 °C. For the fully ionized case, the unsatisfactory fit of the conversion profiles over the complete range of conditions was attributed to a lack of knowledge of the rate coefficients of fully ionized AA. Due to the difficulties in representing these limiting cases, a model for the copolymerization of partially ionized AA with AM was not formulated as part of this thesis. There is a lack of knowledge of the rate coefficients, including those for backbiting, for partially and fully ionized AA arising from the difficulty in studying this system with the PLP methods. Arguably the most important feature of such a complete model would be to include the equilibrium reactions between the charged monomer and polymer species. Due to the difference in the pK_a between the AA monomer and polymer,[29] the monomer is more likely to be in its ionized form relative to the polymer. This would lead to a change in the rate coefficients with conversion as a result of changing degrees of ionization and concentration.[34,107]

Another important consideration is how to treat the AA in its ionized and non-ionized form. One approach is to model the system as a terpolymerization, as in the work by Rintoul and Wandrey, where the reactivity ratios were represented as a function of pH.[62] For this approach only reactivity ratios at non- and fully ionized conditions would be considered and the behavior at partially ionized conditions would be calculated from the relative amounts of ionized and non-ionized AA monomer present during the reaction.

An alternate approach is to model the rate coefficients of AA in terms of the degree of ionization. For this case, the change in the rate coefficients would have to be explicitly known as both a function of the degree of ionization as well as monomer concentration, similar to the way

that reactivity ratios are represented by Equation 7.3. Due to the dearth of specific information about individual rate coefficients at partially ionized conditions, it would likely be easier to first implement a model as a terpolymerization model and focus on obtaining reliable rate coefficient data at fully ionized conditions for AA. Model implementation using the terpolymerization approach would show where additional data or kinetic understanding would be necessary.

7.7 Conclusions and recommendations for future work

This chapter focused on improving the understanding of the copolymerization of partially ionized AA with AM. A comprehensive set of experiments to study the effect of the degree of ionization (α = 0.3, 0.5, 0.7), monomer concentration (5 to 40 wt% monomer), monomer composition (f_{AM0} = 0.3, 0.5, 0.8), and ionic strength were examined. The monomer concentration drift was found primarily to be a function of the initial degree of ionization, but also influenced by initial monomer concentration, with the combined effect largest for highly ionized systems. A representation of the reactivity ratios was developed as a function of initial degree of ionization and total initial monomer concentration, greatly extending the representation of copolymer composition compared to previous studies.

The monomer conversion rate at all degrees of ionization increases with increasing monomer concentration, indicating that backbiting remains an important mechanism in this copolymerization. The degree of ionization, however, has a varying effect on the conversion rates and appears to be dependent on the monomer composition. Additionally, experiments run at the same monomer composition and ionic strength yield similar conversion rates even with very different monomer concentrations. Overall, the monomer concentration and composition have the largest effect on the monomer conversion profiles. The underlying mechanisms behind these trends are currently not understood, but could be related to the total amount of ionized AA in the system and to the interactions between the AA and AM side groups.

As several of these observations have not been previously observed in the literature, a study of these trends using different experimental methods, such as the ACOMP method,[48,49] gravimetry,[50–52] NIR, or Raman for example would be useful. Additional experiments to further study the combined effect of monomer composition and ionic strength on the conversion profiles would be helpful to further the kinetic understanding of this complex system, as would further studies into the interaction between the monomer and polymer at different compositions and degrees of ionization. Rate coefficient data from PLP studies would provide additional insight into the kinetics of this copolymerization, which would be well complemented with modeling efforts using a terpolymerization approach.

Chapter 8

Conclusions

8.1 Overall experimental contributions

An in-situ NMR technique was developed (Chapter 3) to study the aqueous phase free radical copolymerization of AM copolymerization with AA at varying degrees of ionization. This in-situ NMR technique allowed for the study of this system at much higher monomer concentrations (up to 40 wt% monomer) than previously reported in the literature. The motivation for this came from the knowledge that propagation and termination rate coefficients of water soluble monomers, of which AA and AM are no exception, are functions of monomer concentration. Quality of the NMR spectra was not significantly reduced due to the high viscosity of this water soluble polymerization, even at high monomer concentrations and allowed the tracking of monomer composition and conversion to high conversion.

The copolymerization of AM and AA was studied at a range of monomer concentrations (5 to 40 wt%), monomer compositions (always at least three intermediate monomer compositions), and degrees of ionization (non- to fully ionized). Secondary variables examined were temperature (40 to 70 ^{o}C for AM homopolymerization and non-ionized AA/AM copolymerization), and ionic strength (for fully and partially ionized AA/AM copolymerization).

The conversion rate for all polymerizations increased as the monomer concentration increased, despite the measured decrease in the propagation and termination rate coefficients using PLP techniques. This result was explained by the occurrence of backbiting reactions for both monomers, with the influence on rate confirmed by the modeling results.

The conversion rates decreased for monomer compositions of f_{AM0} = 0.3 and 0.5 with increasing degree of ionization; however, at f_{AM0} = 0.8 the ionized AA caused an increase in the conversion rate. The explanation for this surprising result is uncertain, as it was observed that any

degree of ionization will result in a decrease in the observed conversion rate for AA homopolymerization.

Monomer composition data collected up to high conversions over the complete range of experimental conditions gave insight into the combined effects of monomer concentration and degree of ionization on the composition drift. Reactivity ratios were estimated by implementing the differential monomer composition equation in Predici. The monomer composition drift at non-ionized conditions was independent of monomer concentration, indicating that the cross-propagation rate coefficients follow the same dependence on monomer concentration as homopropagation. At partially and fully ionized conditions however, as the total initial monomer concentration increased, the incorporation of AA increased, indicating that reactivity ratios needed to be estimated based on the initial monomer concentration and degree of ionization. The combined effect was captured in an expression valid for copolymerizations over the complete range of experimental conditions, with the resulting predictions of monomer composition drift as a function of conversion providing a good representation of the data obtained.

8.2 Modeling contributions

All of the modeling work was implemented in the Predici software package. The homopolymerization of AM (both rate and molecular mass data) was successfully modeled as a function of monomer concentration and temperature using rate coefficients collected by our collaborators. The model also predicts conversion profiles from literature that were collected using other experimental techniques and generated using other initiators.

A copolymerization model for non-ionized AA and AM was developed, using a penultimate model to represent propagation , based upon new data measured by our collaborators. Treatments for the termination and backbiting rate coefficients were developed. The model fit the experimental data at 70 ºC, but not at 40 ºC. A sensitivity analysis on the unknown rate coefficients did not yield a satisfactory fit at both temperatures. An influence of complexation between the AA

and AM side groups on the polymer chain, known to be strongly dependent upon temperature, on reactivity was proposed as the most likely reason for this discrepancy.

Available propagation rate coefficients for fully ionized AA homopolymerization are limited to low temperatures and monomer concentrations, with independent reliable measures of termination and backbiting rates not available. Additionally, all copolymerization rate coefficients were unknown, with the exception of the reactivity ratios estimated from this study. Despite these uncertainties, the model predictions matched the experimental data collected at 5 wt%; however as the monomer concentration increases, the ability of the model to capture the effect of monomer composition on the conversion profiles diminishes.

Due to the lack of rate coefficient data at partially ionized conditions for both AA homopolymerization and copolymerization rate coefficients, model was not developed.

8.3 Recommendations for future work - Experimental

The completed experimental work covered a broad range of experimental conditions in an attempt to fully understand the free radical aqueous phase copolymerization of AM with AA at varying degrees of ionization. The main focus of these experiments was to study the effect of monomer concentration, monomer composition, and the degree of ionization. As a result, the effect of temperature on the monomer composition drift and conversion rates was not studied for the partially and fully ionized cases. A comparison of monomer composition drift from the literature to our data, indicated no temperature effect on the monomer composition drift at temperatures close to ours (40 or 50 ^{o}C). This is in agreement with the monomer composition drift being independent of temperature between 40 and 70 ^{o}C for the non-ionized copolymerization. However, it is advisable to have monomer conversion profiles collected at different temperatures to validate the model over a broad temperature range.

The effect of controlling ionic strength by addition of NaCl was not studied in our work, which instead focused on industrial polymerization conditions. From an academic standpoint to

improve fundamental understanding, it would be of interest to extend the representation of the reactivity ratios, currently a function of initial total monomer concentration and degree of ionization, to include the effect of additional salt in the system.

8.4 Recommendations for future work - Modeling

The models developed should provide the framework to represent the copolymerizations of AM with both fully ionized and non-ionized AA. Further validation is limited due to unknown copolymerization propagation rate behavior, with the exception of the recent PLP measurements obtained at non-ionized conditions. Measurement of the rate coefficients for fully and partially ionized AA is ongoing by our collaborators, and will serve as the basis of improved rate coefficients for the homopolymerization system. However, the combination of low propagation and termination rate coefficients make PLP-SEC measurements over a range of monomer concentrations and compositions very challenging. Work is currently also ongoing to determine the fully ionized AA/ AM copolymer propagation rate coefficients as a function of monomer composition and temperature. Implementation of improved estimates for this rate coefficient may lead to better model predictions of how monomer composition affects rate for this system. Rate coefficients at the partially ionized conditions are also imperative in order to guide an appropriate modeling strategy for this copolymerization.

The poor model fit at 40 ^{o}C at non-ionized conditions is also an area for further study, as the hypothesis that complexation of the polymer side groups affecting the conversion rate must be validated. In-situ NMR experiments run at the intermediate temperature of 50 ^{o}C and experiments run with the addition of NaCl can give insight into this hypothesis, and lead to improved representation of the rate coefficients in the model.

^{13}C NMR is unable to give a good indication of the extent of backbiting in the copolymer system, due to the low levels of branching combined with possible peak overlap and broadening. Therefore alternate methods to determining branching levels and thus backbiting rate coefficients

would be useful. Possibly PLP-EPR experiments could give insight into the backbiting and termination rate coefficients of this copolymerization.

8.5 Publications on Thesis Work

Chapter 3 has been accepted and published in Macromolecular Symposia, **2013**, 333, 122 – 137.

Chapter 4 is being prepared for submission.

Sections from Chapters 5, 6, and 7 will be combined for a paper discussing the reactivity ratio estimation at different temperatures, degrees of ionization, and monomer concentration.

All papers are co-authored by Robin A. Hutchinson.

References

[1] R. A. Hutchinson, in: "*Handbook of Polymer Reaction Engineering"*, T. Meyer, J. Keurentjes, Wiley-VCH (Weinheim) **2005**, pp 153-211

[2] BASF, at <http://www.basf.com/group/corporate/en/>, accessed April 10, **2012**.

[3] D. R. L. Vedoy, J. B. P. Soares, *Can. J. Chem. Eng.* **2014**, *93*, 888.

[4] S. Beuermann, M. Buback, *Prog. Polym. Sci.* **2002**, *27*, 191.

[5] O. F. Olaj, I. Bitai, F. Hinkelmann, *Makromol. Chem.* **1987**, *188*, 1689.

[6] S. Beuermann, M. Buback, P. Hesse, R. A. Hutchinson, S. Kukučková, I. Lacík, *Macromolecules* **2008**, *41*, 3513.

[7] J. Barth, M. Buback, *Macromolecules* **2012**, *45*, 4152.

[8] J. Barth, W. Meiser, M. Buback, *Macromolecules* **2012**, *45*, 1339.

[9] F. D. Kuchta, A. M. van Herk, A. L. German, *Macromolecules* **2000**, *33*, 3641.

[10] I. Lacík, S. Beuermann, M. Buback, *Macromolecules* **2003**, *36*, 9355.

[11] S. A. Seabrook, M. P. Tonge, R. G. Gilbert, *J. Polym. Sci., Part A Polym. Chem.* **2005**, *43*, 1357.

[12] L. Učňová, A. Chovancová, M. Stach, I. Lacík, *Personal communications.*

[13] M. Stach, I. Lacík, D. Chorvát, M. Buback, P. Hesse, R. A. Hutchinson, L. Tang, *Macromolecules* **2008**, *41*, 5174.

[14] S. Santanakrishnan, L. Tang, R. A. Hutchinson, M. Stach, I. Lacík, J. Schrooten, P. Hesse, M. Buback, *Macromol. React. Eng.* **2010**, *4*, 499.

[15] M. Buback, P. Hesse, R. A. Hutchinson, P. Kasák, I. Lacík, M. Stach, I. Utz, *Ind. Eng. Chem. Res.* **2008**, *47*, 8197.

[16] N. F. G. Wittenberg, M. Buback, R. A. Hutchinson, *Macromol. React. Eng.* **2013**, *7*, 267.

[17] J. M. Asua, S. Beuermann, M. Buback, P. Castignolles, B. Charleux, R. G. Gilbert, R. A. Hutchinson, J. R. Leiza, A. N. Nikitin, J. P. Vairon, A. M. van Herk, *Macromol. Chem. Phys.* **2004**, *205*, 2151.

[18] S. S. Cutié, P. B. Smith, D. E. Henton, T. L. Staples, C. Powell, *J. Polym. Sci., Part B Polym. Phys.* **1997**, *35*, 2029.

[19] T. Ishige, A. E. Hamielec, *J. Appl. Polym. Sci.* **1973**, *17*, 1479.

[20] A. R. Mahdavian, M. Abdollahi, H. R. Bijanzadeh, *J. Appl. Polym. Sci.* **2004**, *93*, 2007.

[21] N. F. G. Wittenberg, C. Preusser, H. Kattner, M. Stach, I. Lacík, R. A. Hutchinson, M. Buback, *Macromol. React. Eng.* **2015**, doi:10.1002/mren.201500017.

[22] P. Drawe, M. Buback, I. Lacík, *Macromol. Chem. Phys.* **2015**, *216*, 1333.

[23] C. Preusser, R. A. Hutchinson, *Macromol. Symp.* **2013**, *333*, 122.

[24] C. J. Kim, A. E. Hamielec, *Polymer* **1984**, *25*, 845.

[25] H. Kattner, M. Buback, *Personal communications.*

[26] M. J. Roedel, *J. Am. Chem. Soc.* **1953**, *75*, 6110.

[27] T. Junkers, C. Barner-Kowollik, *J. Polym. Sci. Part A* **2008**, *46*, 7585.

[28] R. G. Gilbert, *Pure Appl. Chem.* **1992**, *64*, 1563.

[29] I. Lacík, S. Beuermann, M. Buback, *Macromol. Chem. Phys.* **2004**, *205*, 1080.

[30] I. Lacík, S. Beuermann, M. Buback, *Macromolecules* **2001**, *34*, 6224.

[31] P. Pascal, M. A. Winnik, D. H. Napper, R. G. Gilbert, *Macromolecules* **1993**, *26*, 4572.

[32] S. Beuermann, M. Buback, P. Hesse, I. Lacík, *Macromolecules* **2006**, *39*, 184.

[33] S. Beuermann, M. Buback, P. Hesse, S. Kukučková, I. Lacík, *Macromol. Symp.* **2007**, *248*, 41.

[34] I. Lacík, L. Učňová, S. Kukučková, M. Buback, P. Hesse, S. Beuermann, *Macromolecules* **2009**, *42*, 7753.

[35] V. F. Gromov, N. I. Galperina, T. O. Osmanov, P. M. Khomikovskii, A. D. Abkin, *Eur. Polym. J.* **1980**, *16*, 529.

[36] A. Chapiro, *Eur. Polym. J.* **1973**, *9*, 417.

[37] S. C. Thickett, R. G. Gilbert, *Polymer* **2004**, *45*, 6993.

[38] B. De Sterck, R. Vaneerdeweg, F. Du Prez, M. Waroquier, V. Van Speybroeck, *Macromolecules* **2010**, *43*, 827.

[39] G. Blauer, *Trans. Faraday Soc.* **1960**, *56*, 606.

[40] J. Barth, M. Buback, P. Hesse, T. Sergeeva, *Macromol. Rapid Commun.* **2009**, *30*, 1969.

[41] A. N. Nikitin, R. A. Hutchinson, M. Buback, P. Hesse, *Macromolecules* **2007**, *40*, 8631.

[42] M. Buback, P. Hesse, I. Lacík, *Macromol. Rapid Commun.* **2007**, *28*, 2049.

[43] A. N. Nikitin, R. A. Hutchinson, *Macromolecules* **2005**, *38*, 1581.

[44] J. Schrooten, M. Buback, P. Hesse, R. A. Hutchinson, I. Lacík, *Macromol. Chem. Phys.* **2011**, *212*, 1400.

[45] F. R. Mayo, F. M. Lewis, *J. Am. Chem. Soc.* **1944**, *66*, 1594.

[46] I. Rintoul, C. Wandrey, *Polymer* **2005**, *46*, 4525.

[47] W. R. Cabaness, T. Y. Lin, C. Párkányi, *J. Polym. Sci., Part A Polym. Chem.* **1971**, *9*, 2155.

[48] A. Paril, A. M. Alb, A. T. Giz, H. Çatalgil-Giz, *J. Appl. Polym. Sci.* **2007**, *103*, 968.

[49] A. Paril, A. Giz, H. Catalgil-Giz, *J. Appl. Polym. Sci.* **2013**, *127*, 3530.

[50] M. Riahinezhad, N. Kazemi, N. McManus, A. Penlidis, *J. Polym. Sci. Part A Polym. Chem.* **2013**, *51*, 4819.

[51] M. Riahinezhad, N. Kazemi, N. McManus, A. Penlidis, *J. Appl. Polym. Sci.* **2014**, *131*.

[52] M. Riahinezhad, N. McManus, A. Penlidis, *Macromol. React. Eng.* **2015**, *9*, 100.

[53] S. Ponratnam, S. L. Kapur, *Makromol. Chem.* **1977**, *178*, 1029.

[54] N. Kazemi, T. A. Duever, A. Penlidis, *Macromol. React. Eng.* **2011**, *5*, 385.

[55] V. E. Meyer, G. G. Lowry, *J. Polym. Sci. Part A* **1965**, *3*, 2843.

[56] R. Losada, C. Wandrey, *Macromolecules* **2009**, *42*, 3285.

[57] D. Cuccato, G. Storti, M. Morbidelli, *Macromolecules* **2015**, *48*, 5076.

[58] R. J. Minari, G. Caceres, P. Mandelli, M. M. Yossen, M. Gonzalez-Sierra, J. R. Vega, L. M. Gugliotta, *Macromol. React. Eng.* **2011**, *5*, 223.

[59] H. R. Lin, *Eur. Polym. J.* **2001**, *37*, 1507.

[60] F. S. Dainton, M. Tordoff, *Trans. Faraday Soc.* **1957**, *53*, 499.

[61] A. E. Hamielec, *Chem. Eng. Commun.* **1983**, *24*, 1.

[62] I. Rintoul, C. Wandrey, *Macromolecules* **2005**, *38*, 8108.

[63] J. Barth, M. Buback, *Macromolecules* **2011**, *44*, 1292.

[64] G. T. Russell, *Macromol. Theory Simul.* **1995**, *4*, 549.

[65] A. Giz, H. Çatalgil-Giz, A. Alb, J.-L. Brousseau, W. F. Reed, *Macromolecules* **2001**, *34*, 1180.

[66] S. S. Cutié, D. E. Henton, C. Powell, R. E. Reim, P. B. Smith, T. L. Staples, *J. Appl. Polym. Sci.* **1997**, *64*, 577.

[67] A. R. Mahdavian, M. Abdollahi, *J. Appl. Polym. Sci.* **2007**, *103*, 3253.

[68] A. R. Mahdavian, M. Abdollahi, L. Mokhtabad, H. Reza Bijanzadeh, F. Ziaee, *J. Appl. Polym. Sci.* **2006**, *101*, 2062.

[69] A. R. Mahdavian, M. Abdollahi, L. Mokhtabad, F. Ziaee, *J. Macromol. Sci., Pure Appl. Chem.* **2006**, *43*, 1583.

[70] M. Abdollahi, B. Massoumi, M. R. Yousefi, F. Ziaee, *J. Appl. Polym. Sci.* **2012**, *123*, 543.

[71] A. Hartwig, R. H. Brand, C. Pfeifer, N. Dürr, A. Drochner, H. Vogel, *Macromol. Symp.* **2011**, *302*, 280.

[72] A. L. Van Geet, *Anal. Chem.* **1968**, *40*, 2227.

[73] D. L. Pavia, G. M. Lampman, G. S. Kriz, J. A. Vyvyan, "*Introduction to Spectroscopy" (4th Ed)*, Brooks/Cole (Belmont) **2008**.

[74] J. Barth, M. Buback, G. T. Russell, S. Smolne, *Macromol. Chem. Phys.* **2011**, *212*, 1366.

[75] S. A. Seabrook, P. Pascal, M. P. Tonge, R. G. Gilbert, *Polymer* **2005**, *46*, 9562.

[76] J. Schrooten, *PhD Thesis, U. Göttingen* **2013**.

[77] K. Liang, R. A. Hutchinson, *Macromolecules* **2010**, *43*, 6311.

[78] V. F. Kurenkov, V. a. Myagchenkov, *Eur. Polym. J.* **1980**, *16*, 1229.

[79] C. Chachaty, A. Forchioni, *J. Polym. Sci., Part A Polym. Chem.* **1972**, *10*, 1905.

[80] D. Konkolewicz, S. Sosnowski, D. R. D'hooge, R. Szymanski, M.-F. Reyniers, G. B. Marin, K. Matyjaszewski, *Macromolecules* **2011**, *44*, 8361.

[81] M. Wulkow, *Macromol. Theory Simulations* **1996**, *5*, 393.

[82] A. N. F. Peck, R. A. Hutchinson, *Macromolecules* **2004**, *37*, 5944.

[83] W. Wang, R. A. Hutchinson, *Macromol. Symp.* **2010**, *289*, 33.

[84] G. Moad, D. H. Solomon, "*The Chemistry of Radical Polymerization"* (*2nd Ed*), Elsevier Ltd. (Oxford) **2006**, pp 251-263.

[85] A. N. Nikitin, R. A. Hutchinson, W. Wang, G. A. Kalfas, J. R. Richards, C. Bruni, *Macromol. React. Eng.* **2010**, *4*, 691.

[86] C. H. Bamford, R. W. Dyson, G. C. Eastmond, *Polymer* **1969**, *10*, 885.

[87] Wako Chemicals, at <*http://www.wako-chem.co.jp/specialty/waterazo/V-50.htm*>, accessed November 18, **2013**.

[88] M. W. Liberatore, S. Baik, A. J. McHugh, T. J. Hanratty, *J. Nonnewton. Fluid Mech.* **2004**, *123*, 175.

[89] N. M. Ahmad, F. Heatley, P. A. Lovell, *Macromolecules* **1998**, *31*, 2822.

[90] Sigma Aldrich, at <http://www.sigmaaldrich.com/content/dam/sigma-aldrich/docs/Aldrich/General_Information/thermal_initiators.pdf>, accessed August 24, **2015**.

[91] SciFinder, at <https://scifinder.cas.org>, accessed August 24, **2015**.

[92] G. Staikos, K. Karayanni, Y. Mylonas, *Macromol. Chem. Phys.* **1997**, *198*, 2905.

[93] G. A. Mun, Z. S. Nurkeeva, V. V. Khutoryanskiy, G. S. Sarybayeva, A. V. Dubolazov, *Eur. Polym. J.* **2003**, *39*, 1687.

[94] K. Sivadasan, P. Somasundaran, *J. Polym. Sci. Part A Polym. Chem.* **1991**, *29*, 911.

[95] K. Sivadasan, P. Somasundaran, N. J. Turro, *Colloid Polym. Sci.* **1991**, *269*, 131.

[96] D. Li, M. C. Grady, R. A. Hutchinson, *Ind. Eng. Chem. Res.* **2005**, *44*, 2506.

[97] W. Wang, R. A. Hutchinson, *AIChE* **2011**, *57*, 227.

[98] W. Wang, R. A. Hutchinson, *Macromol. React. Eng.* **2008**, *2*, 199.

[99] J. N. Atherton, A. M. North, *Trans. Faraday Soc.* **1962**, *58*, 2049.

[100] T. Fukuda, K. Kubo, Yung-Dae Ma, *Prog. Polym. Sci.* **1992**, *17*, 875.

[101] E. Merz, T. Alfrey, G. Goldfinger, *J. Polym. Sci.* **1946**, *1*, 75.

[102] D. Li, J. R. Leiza, R. A. Hutchinson, *Macromol. Theory Simulations* **2005**, *14*, 554.

[103] I. Degirmenci, T. F. Ozaltin, O. Karahan, V. Van Speybroeck, M. Waroquier, V. Aviyente, *J. Polym. Sci. Part A Polym. Chem.* **2013**, *51*, 2024.

[104] J. Loiseau, N. Doërr, J. M. Suau, J. B. Egraz, M. F. Llauro, C. Ladavière, J. Claverie, *Macromolecules* **2003**, *36*, 3066.

[105] K. Liang, R. A. Hutchinson, *Macromol. Rapid Commun.* **2011**, *32*, 1090.

[106] P. Drawe, M. Buback, *Personal communications.*

[107] N. F. G. Wittenberg, *PhD Thesis, U. Göttingen* **2013**.

[108] F. O. Garces, K. Sivadasan, P. Somasundaran, N. J. Turro, *Macromolecules* **1994**, *27*, 272.

[109] Y. Li, J. C. T. Kwak, *Langmuir* **2002**, *18*, 10049.

[110] K. D. Branham, H. S. Snowden, C. L. McCormick, *Macromolecules* **1996**, *29*, 254.

[111] A. Chapiro, *Eur. Polym. J.* **1989**, *25*, 713.

[112] H. Çatalgil-Giz, A. Giz, a. M. Alb, A. Öncül Koç, W. F. Reed, *Macromolecules* **2002**, *35*, 6557.

[113] C. De Stefano, A. Gianguzza, D. Piazzese, S. Sammartano, *React. Funct. Polym.* **2003**, *55*, 9.

Appendix A: Supporting Information for Chapter 4

Figure A.1 shows the model fit of conversion profiles collected at varying amounts of initiator. Following, are the conversion and molecular mass fits for data taken from Ishige (1973),[19] and Hamielec (1984)[24] with the model predictions for monomer conversion profiles and molecular masses. Finally, the plots for the standard error between the experimental and predicted conversion profiles are shown.

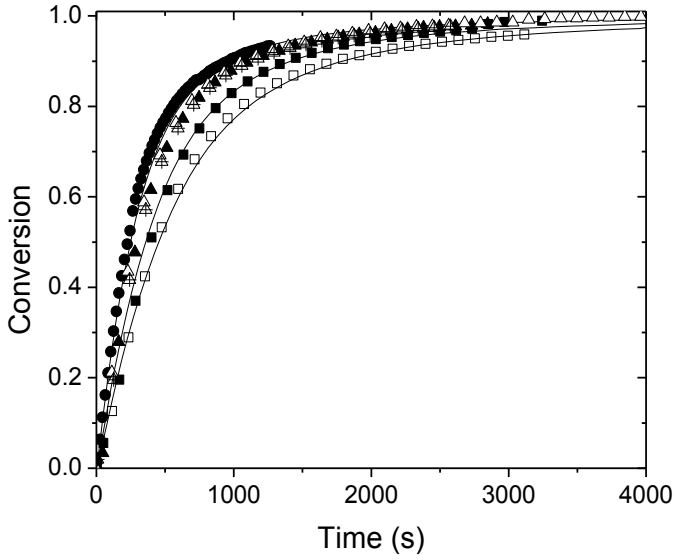

Figure A.1 Experimental batch monomer conversion data (symbols) and predictions (lines) at 50 ºC, 10 wt% AM for 0.08 (■), 0.14 (▲), and 0.27 (●) wt% V-50.

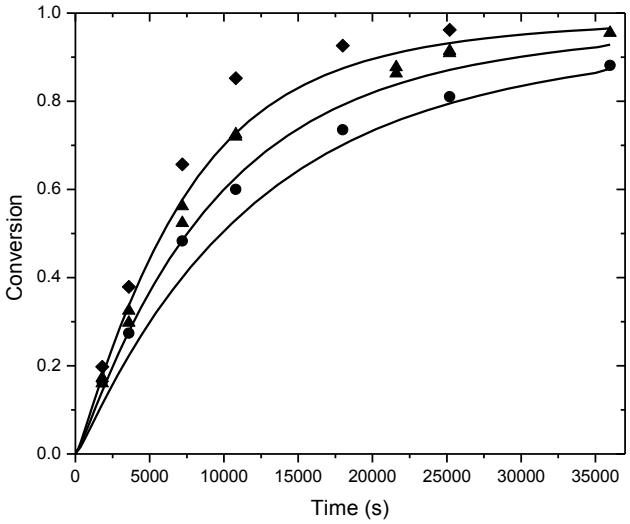

Figure A.2 Experimental data from Ref [19] plotted with the prediction from the model for the conversion profiles at 40 ºC and 0.02 wt% ACV at 4 (0.563 mol·L^{-1}) (●), 8 (1.126 mol·L^{-1}) (▲), and 16 (2.252 mol·L^{-1}) (♦) wt% AM.

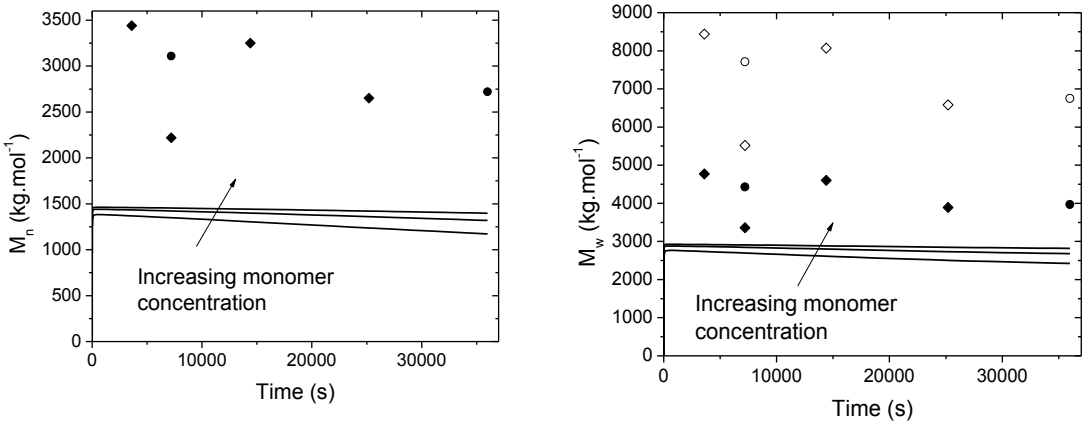

Figure A.3 Experimental M_n and M_w data from Ref [19] plotted with the prediction from the model for M_n (a) and M_w (b) at 40 ºC and 0.02 wt% ACV at 4 (0.563 mol·L^{-1}) (●), 8 (1.126 mol·L^{-1}) (▲), and 16 (2.252 mol·L^{-1}) (♦) wt% AM.

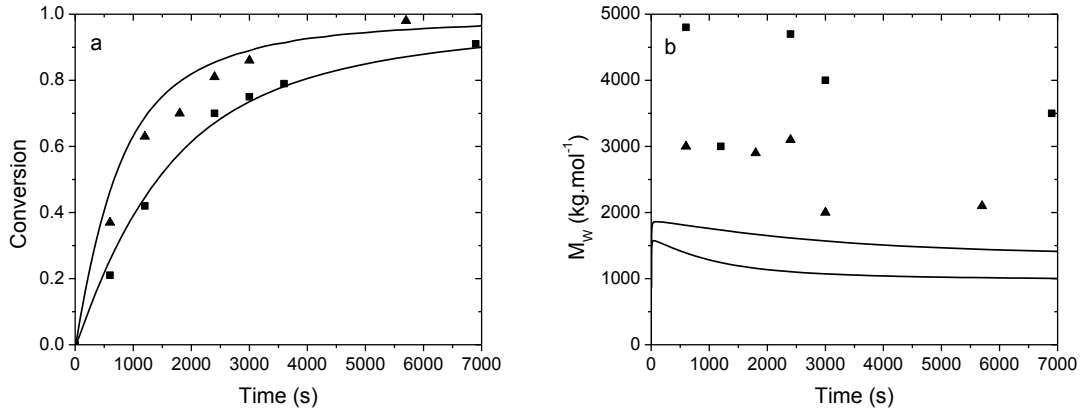

Figure A.4 Experimental data from Ref [24] (Figures 1 and 2) plotted with the prediction from the model for the conversion profiles (a) and M_w (b) at 70 ºC and 5.3 wt% (0.75 mol·L^{-1}) AM at 1.2×10^{-4} (■) and 5.2×10^{-4} (▲) mol·L^{-1} KPS.

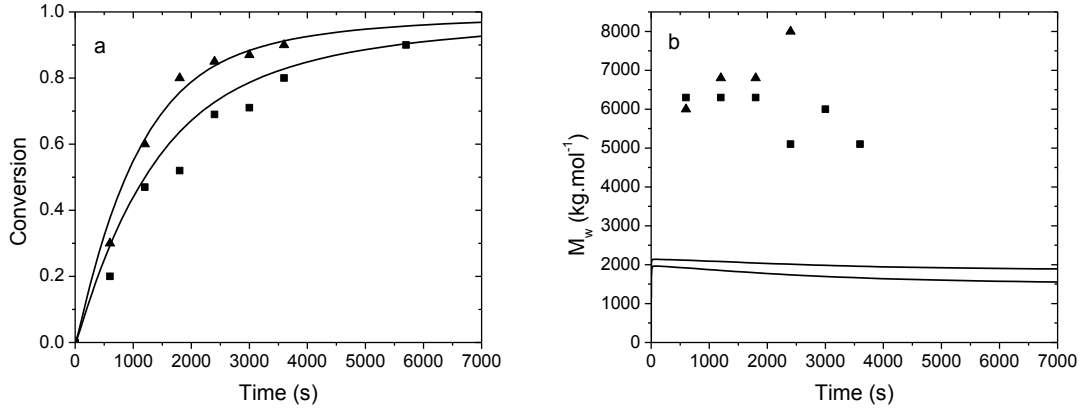

Figure A.5 Experimental data from Ref [24] (Figures 3 and 4) plotted with the prediction from the model for the conversion profiles (a) and M_w (b) at 70 ºC and 1.3×10^{-4} mol·L^{-1} KPS at 7.1 wt% (1 mol·L^{-1}) (■) AM and 15.6 wt% (2.2 mol·L^{-1}) (▲) AM.

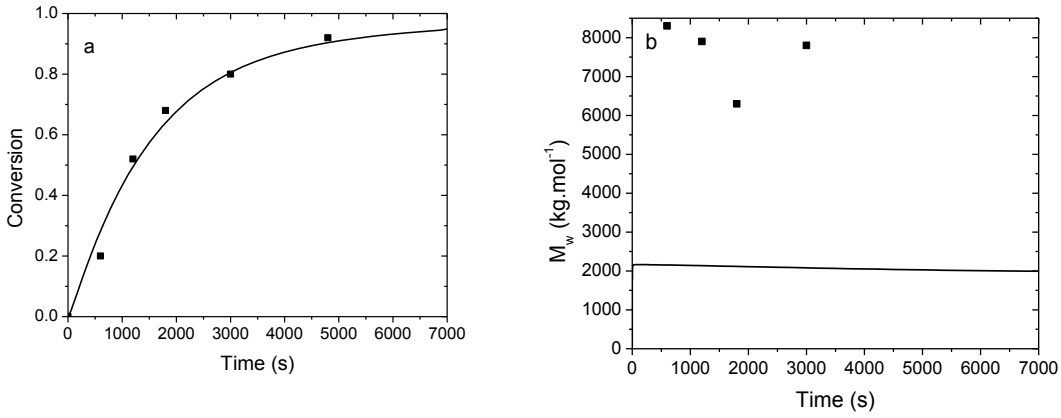

Figure A.6 Experimental data from Ref [24] (Figure 5) plotted with the prediction from the model for the conversion profile (a) and M_w (b) at 70 ºC and 0.65×10^{-4} mol·L^{-1} KPS at 15.6 wt% (2.2 mol·L^{-1}) AM.

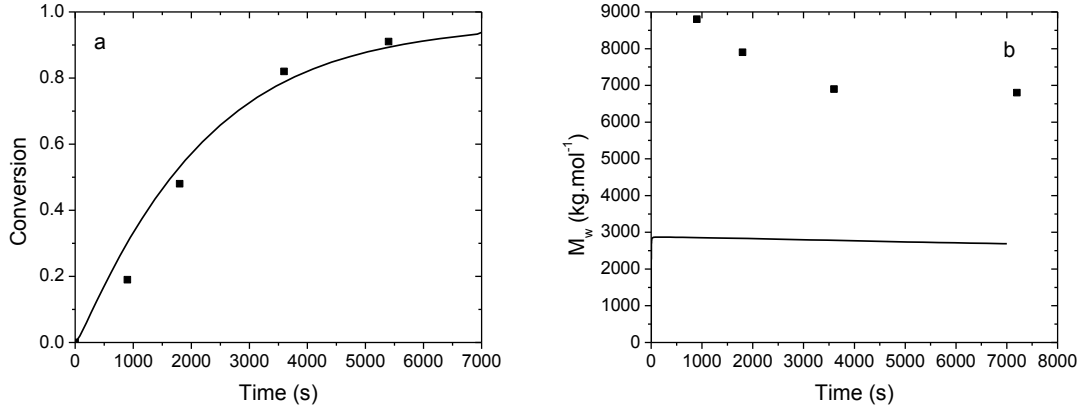

Figure A.7 Experimental data from Ref [24] (Figure 9) plotted with the prediction from the model for the conversion profile (a) and M_w (b) at 40 ºC and 3.3×10^{-4} mol·L^{-1} KPS at 17.8 wt% (2.5 mol·L^{-1}) AM.

Note: There is a typo in Ref [24] on Figure 9. The initiator concentration should read 3.3×10^{-4} mol·L^{-1} initiator, as otherwise the reaction takes place too fast. When it is reduced by a factor or 10, then the simulated conversion profile fits the experimental data well, as observed with all of the other conversion profiles.

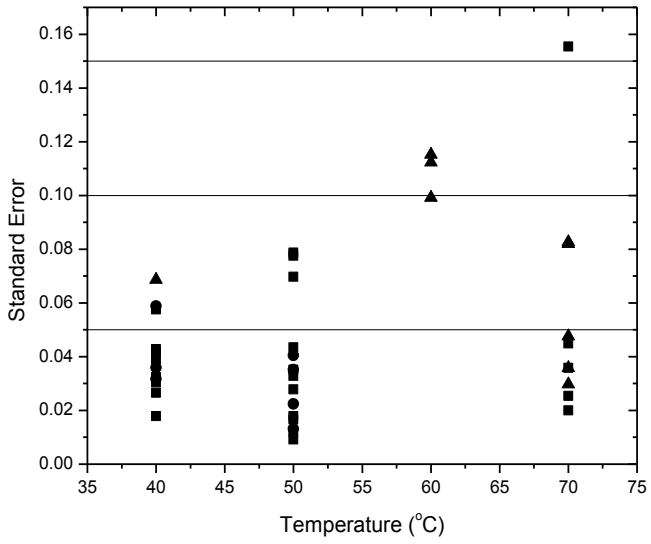

Figure A.8 Standard error of the conversion profiles as a function of temperature for the NMR data collected as part of this study (■), and published by Ishige (●)[19] and Hamielec (▲).[24]

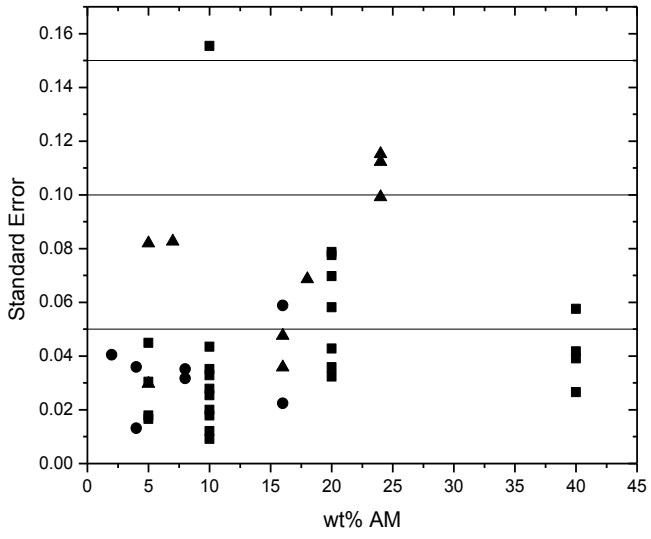

Figure A.9 Standard error of the conversion profiles as a function of wt% AM for the NMR data collected as part of this study (■), and published by Ishige (●)[19]and Hamielec (▲).[24]

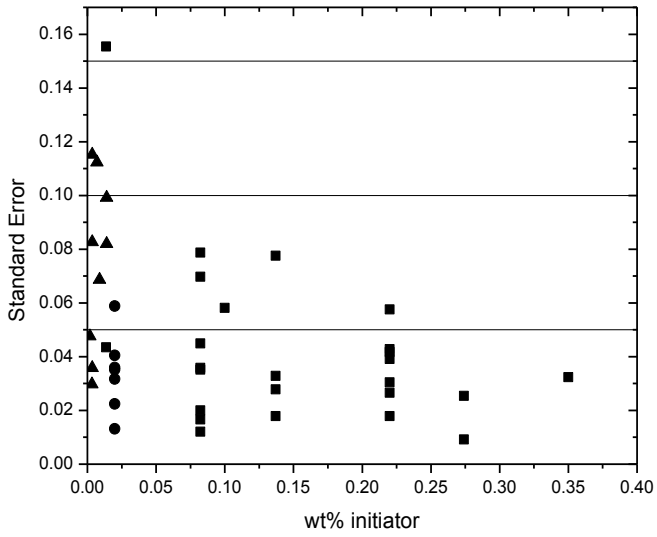

Figure A.10 Standard error of the conversion profiles as a function of wt% initiator for the NMR data collected as part of this study (■), and published by Ishige (●)[19] and Hamielec (▲).[24]

Appendix B: Additional Data for Chapter 7

This appendix shows the experimental conversion profiles not shown in Chapter 7. The data refers to conversion profiles collected at α = 0.7 at more monomer compositions and concentrations as discussed in the chapter. The extended set of experimental data was collected at this degree of ionization was to help validate the partially ionized model. However, due to the absence of available rate coefficients at partially ionized conditions, this model was not developed.

The experimental conversion data collected at initial monomer composition f_{AM0} = 0.2 and 0.3 suffered from a loss in the loss of the quality of the NMR spectra with conversion, indicated by the extreme broadening of the solvent peak and the scatter in the conversion and monomer composition data that is generally not observed with this in-situ NMR method. Re-runs at these conditions should be run to check whether the slow conversion rates and scatter are reproducible.

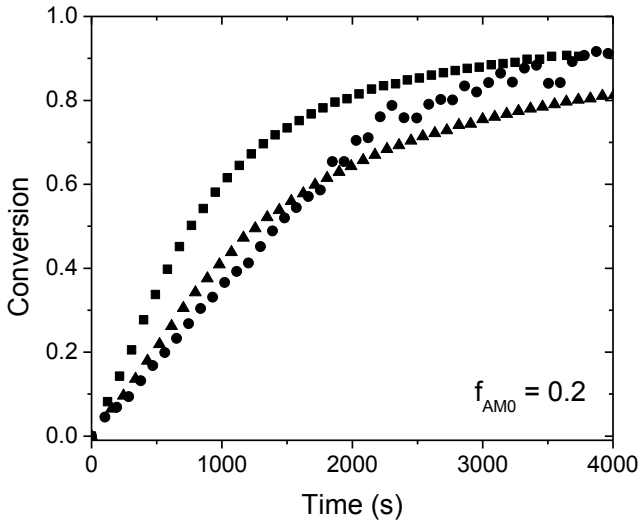

Figure B.1 Experimental batch monomer conversion profiles collected with initial monomer composition f_{AM0} = 0.2 and degree of ionization α = 0.7 at 40 ºC, 0.35 wt% V-50 and 10 (▲), 20 (■) and 40 (●) wt% monomer.

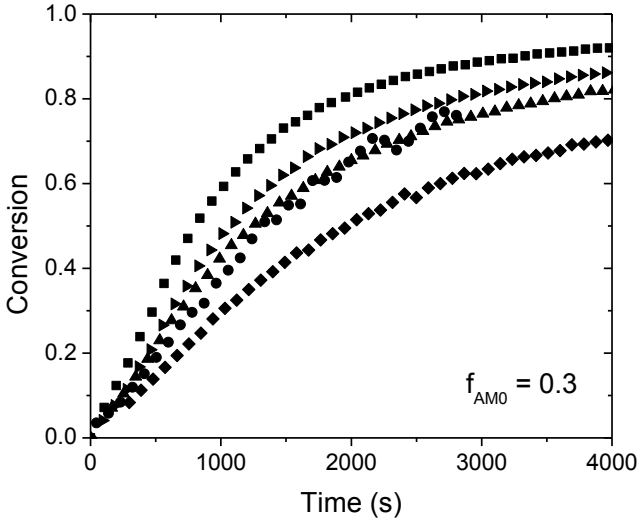

Figure B.2 Experimental batch monomer conversion profiles collected with initial monomer composition f_{AM0} = 0.3 and degree of ionization α = 0.7 at 40 ºC, 0.35 wt% V-50 and 5 (♦), 10 (▲), 13.5 (►), 20 (■) and 40 (●) wt% monomer.

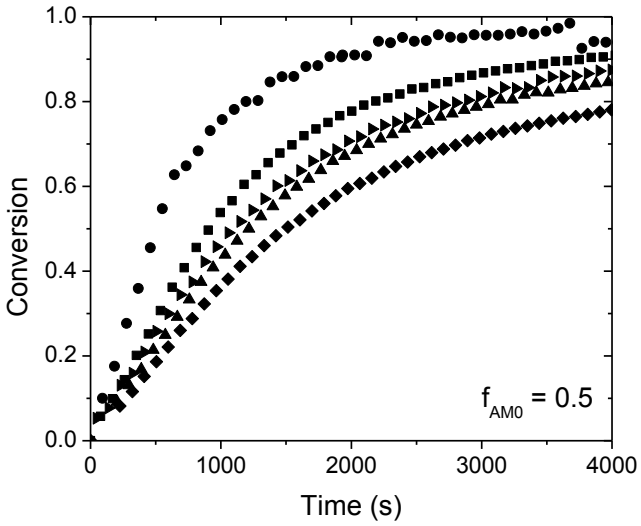

Figure B.3 Experimental batch monomer conversion profiles collected with initial monomer composition f_{AM0} = 0.5 and degree of ionization α = 0.7 at 40 ºC, 0.35 wt% V-50 and 5 (♦), 10 (▲), 13.7 (►), 20 (■) and 40 (●) wt% monomer.

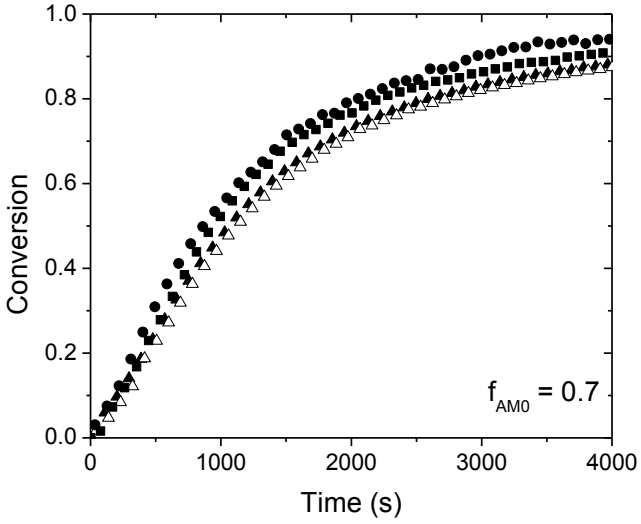

Figure B.4 Experimental batch monomer conversion profiles collected with initial monomer composition f_{AM0} = 0.7 and degree of ionization α = 0.7 at 40 ºC, 0.35 wt% V-50 and 10 (▲), 20 (■) and 40 (●) wt% monomer.

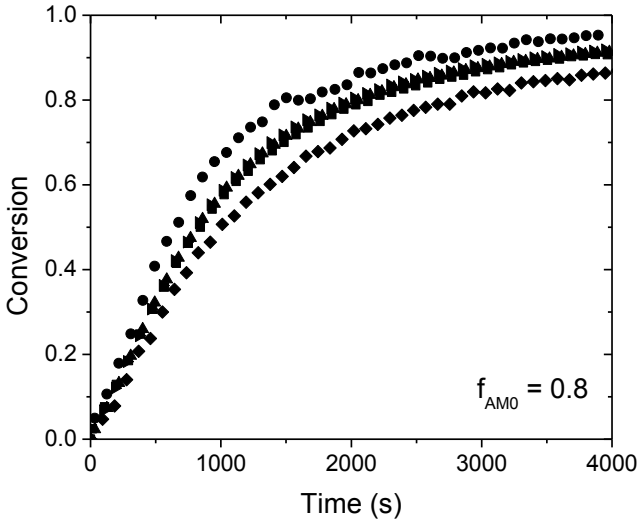

Figure B.5 Experimental batch monomer conversion profiles collected with initial monomer composition f_{AM0} = 0.8 and degree of ionization α = 0.7 at 40 ºC, 0.35 wt% V-50 and 5 (♦), 10 (▲), 14.4 (►), 20 (■) and 40 (●) wt% monomer.